

City Research Online

City St George's, University of London

Citation: Flint, O. (1971). Copper-plated carbon fibres. (Unpublished Doctoral thesis, The City University)

This is the accepted version of the paper.

This version of the publication may differ from the final published version. To cite this item please consult the publisher's version.

Permanent repository link: https://openaccess.city.ac.uk/id/eprint/38685/

Copyright and Reuse: Copyright and Moral Rights remain with the author(s) and/or copyright holders. Copies of full items can be used for personal research or study, educational, or not-for-profit purposes without prior permission or charge, unless otherwise indicated, provided that the authors, title and full bibliographic details are credited, a hyperlink and/or URL is given for the original metadata page and the content is not changed in any way. For full details of reuse please refer to City Research Online policy.

City Research Online: http://openaccess.city.ac.uk/ publications@citystgeorges.ac.uk

IN CONFIDENCE

Copper Plated Carbon Fibres

by

O. Flint

A thesis submitted for the degree of

Doctor of Philosophy

in the City University

1971

61823

"Ye shall no more give the people
straw to make bricks as heretofore:
let them go and gather straw for
themselves."

Exodus, V, 7.

Author's Note

The subject of carbon fibre fabrication and manipulation being relatively new has meant that the introduction to this work is necessarily rather long, in order to include the many descriptions and definitions needed in a new field, but it is felt that time spent here is well worth the effort.

Abstract

This thesis examines structure and strength of carbon fibres relative to other man-made filaments and associates variations in tensile strength with manufacturing and processing history. Methods of fibre identification using X-ray power diffraction techniques, etc. are given.

Metallic coating of fibre via vapour and liquid phases is shown to be unpromising and copper electrodeposition was chosen for close examination, the subject being introduced by description of theory and practice of fibre tensile testing, applied to bare and plated material.

Preliminary work revealed that high modulus, Type I fibres and acid electrolytes were unsuitable for production of high strength plated material and copper deposition from alkaline cyanide solutions is investigated, leading to results covering effects on tensile strength, of variations in temperature, current density, thickness of deposit and electrolyte with particular emphasis on the controlling influence of "free cyanide" concentration. Limits of stable deposition are outlined and an unfamiliar blue compound, formed during unstable conditions, is identified and synthesized.

Next, effects of fibre surface cleaning on plated finish and final strength are explored. Contrary to expectation, pre-wetting results in poor quality, low strength deposits, due to lack of fibre separation during plating, with consequent poor penetration of fibre bundle. The effect of annealing on plated fibre is also examined and no significant change in strength noted below 700^{o}C; above this temperature, strength loss is observed, associated with sintering. At this stage a specification for copper electrodeposition onto carbon fibre is presented.

On the basis of this work, and other reports, copper-carbon fibre composites are prepared and evaluated. Their low strength is associated with hot-pressing, fibre mis-alignment and thermal stress and equated to an overall damage factor.

In conclusion major variables affecting strength of carbon fibres, with and without copper deposits, are assessed in relation to results described. Further techniques leading to production of better composites are also discussed, a promising development involving chopped carbon fibre being mentioned.

Contents

		Page
Acknowledgements		
Chapter 1.	Introduction	1
1.1	Early work with fibres	1
1.2	Early carbon fibres	3
1.3	Strength of solids	5
1.4	Ideal strength of solids	7
1.5	Graphite structure	8
1.6	Structure of carbon fibre	9
1.7	R.A.E. Carbon fibre	10
1.8	Scope of present work	12
	a. The raw material	12
	b. The carbon fibre tow	12
	c. Preliminary work on metal deposition	14
	d. Copper deposits	14
	e. Tensile testing	15
	f. Surface activation	15
	g. Effect of annealing	15
1.9	Summing up of plated fibre results	16
1.10	Copper-carbon fibre composites	16
1.11	General discussion and conclusions	17
	References 1	
Chapter 2.	Graphite and the carbon fibre	18
2.1	The raw material	18
	a. X-ray diffraction analysis	18
	b. The temperature - 002 line width relationship	21
	c. Identification of carbon fibre by electrical linear resistance	22
	d. Relationship between tensile strength and fabrication history.	23

		Page
	e. Summary of results.	27
	References 2.	
Chapter 3.	Preliminary work on metal deposition by chemical reduction	28
3.1	Deposition from the vapour phase	28
3.2	Experimental detail	30
3.3	Results observed	30
	Run 1 Aluminium	30
	Run 2 75% aluminium + 25% zinc	31
	Run 3 Magnesium	31
	Run 4 25% Magnesium - 75% aluminium	31
	Run 5 50% Magnesium - 50% aluminium	31
3.4	Electroless deposition	32
3.5	Electroless plating results	33
	References 3.	
Chapter 4.	Whole tow testing	37
4.1	Introduction	37
4.2	Experimental detail	37
4.3	Evaluation of tensile test	39
	a. Elastic strain energy in tension	39
	b. Tensile strength of carbon fibre tows	41
4.4	Copper plated carbon fibre tows	43
	a. Thickness of deposit	43
	b. Composite density of fibre Part I	44
	" " " " Part II	45
	c. Composite modulus of plated fibre	46
	d. Tensile strength of plated fibre - sample calculation	47
	References 4.	

		Page
Chapter 5.	Preliminary work on copper electrodeposition	50
5.1	Historical background	50
5.2	Introduction	52
5.3	Experimental detail - acid electrolyte	53
5.4	Results - acid electrolyte	57
5.5	Experimental detail - alkaline electrolyte	58
5.6	Results - alkaline electrolyte	59
5.7	Discussion of results	60
	References 5.	
Chapter 6.	Copper deposition from the Rochelle salt-copper cyanide electrolyte	62
6.1	Introduction - the Rochelle salt-electrolyte	62
6.2	Experimental detail	63
6.3	Analytical control	65
6.4	Direct results	66
6.5	Analysis of tensile strength results	68
6.6	Identification of blue compound found at low free cyanide concentrations	70
6.7	Summary of results	72
	References 6.	
Chapter 7.	Effects of surface treatments and annealing on final strength	74
7.1	Introduction - surface treatments	74
7.2	Experimental detail	75
7.3	Surface treatment results	75
7.4	Identification of carbon fibre soot	77
7.5	Effect of annealing treatments on copper plated tows	78
	a. Experimental detail	78
7.6	Annealing results	79
7.7	Summary of results	80

Page

7.8 A specification covering the electrodeposition of Cu on carbon fibres. 80

References 7.

Chapter 8. Carbon fibre/copper composites 83

8.1 Introduction 83

8.2 Composite experimental detail 85

8.3 Cu/Cf composite tensile results 88

8.4 Quantitative analysis of copper on continuous tow, continuously plated 89

8.5 Discussion of Cu composite results 90

References 8.

Chapter 9. General assessment of results 94

9.1 Major variables affecting strength of PAN and unplated carbon fibre 94

9.2 Major variables affecting strength and quality of copper plated carbon fibre 96

9.3 General conclusions 103

References 9.

Appendices

1. The denier system of fibre classification

2. Calibration of Instron Universal Testing Machine

3. X-ray diffraction techniques

4. A powder pattern scanner

5. The 'cog-wheel' effect.

Acknowledgements

I would like to thank [redacted], without whose support this work would not have been possible.

To my supervisor, the late Dr. Howlett, must go posthumous thanks for the many hours he spared me for constructive criticism of this work.

Thanks too to [redacted] and his team for much discussion and their cooperative work with fibre composites. I would also like to thank [redacted] for their many helpful hints on fibre testing.

To Dr. Morris and Mr. Longstaff go thanks for the generous supply of carbon fibre material and to the A.E.R.E. Photographic Section for their X-ray positive photographs and enlargements.

Special thanks are also due to Mr. R. Shepherd of Instrument Services Section, for construction of the X-ray densitometer used in this work and to Mr. Baker for unrestricted use of his X-ray equipment.

Finally, I am indebted to Dr. Walter Marshall, Director, A.E.R.E., Harwell, for sponsoring this research.

CHAPTER 1

Introduction

1.1 Early work with fibres

Man has made use of natural fibre since the formation of his opposable thumbs. Cellulose fibres in his reed thatch and in the straw which gave strength to his sun-dried bricks, wood fibres in the wattle of his "wattle and daub" walls, cow's hair to stiffen the plasters, cotton or wool for cloth to keep him warm and collagen fibres in the leather of his harness, etc.

In the constant search for better, stronger, materials it is interesting to note that, as early as 1664, Dr. Robert Hooke[1] wrote, in his Micrographia, of how he had often thought that there might be a way

> "found to make an artificial glutinous composition much resembling if not fully as good as - nay better than - that exrement or whatever substance it be which the silk worm wire draws its claws."

In a sketch of the progress of man-made fibres Ironside[2], (1970) pointed out that Réaumur[3], (1720) also foresaw the production of artificial silk, and later in the 19th century a Swiss chemist patented a process for the manufacture of artificial silk from wood pulp, but the idea lapsed.

The first suggestion that carbon fibre filaments might be of use was made by J. W. Starr, 1822-47, in his patent for a platinum filament lamp and this lead was followed up by Swann[4], (1848), who produced the carbon filaments by carbonizing cellulose hydrate in the form of mercerized cotton thread. In parallel with this work Edison[5], (1840-1850), in America, produced after hundreds of trials, a carbon filament from carbonized bamboo. This filament, after litigation between the two, was incorporated in what is now known as the Ediswan incandescent lamp. [As a matter of interest an 8 micron carbon fibre was mounted on copper electrodes in a vacuum of 10^{-5} mm Hg (1 mm Hg ≡ 1 torr ≡ 133.3 Nm^{-2}) and gave about 20 candle power at 36 volts for several hours, during an early experiment in this work.]

Some years later Sir C. V. Boys[6], (Circa 1881), produced perhaps the first inorganic filament, for use in delicate instruments such as the torsion balance, microbalance etc., by firing from a little bow molten blobs of quartz attached to an arrow. Then came Swann's Patent[7], (1883), for producing fibres by forcing nitro-cellulose through a series of holes into acetic acid, but their potential was not fully exploited. Artificial silk was finally shown to the public in the Paris Exhibition when Chardonnet[8], (1889), displayed rayon, prepared from collodion, a solution of nitro-cellulose in alcohol or ether, and so-called because it was very shiny and seemed to give off rays of light. The material however was highly inflammable and became known as "mother-in-law silk", due to a sick joke of the times that "a rayon dress and a lighted match were ideal presents for a mother-in-law".

A much more stable rayon, called Viscose rayon, was patented by Cross, Bevan and Beadle[9], (1892), who prepared the fibre from cellulose xanthate made from a solution of cellulosic wood pulp in carbon disulphide and alkaline sodium xanthate. This fluid when squirted through a series of small holes into acetic acid forms artificial silk rayon fibre. A further important step was taken when it was found that stretching the viscose fibre whilst still plastic imparted greater strength; stretched material is known as Tenasco fibre (Bernthsen[10], 1942).

The molecular structure of the first fully synthetic fibre was "designed" by Carothers and Hill[11], (1932), and made by Carothers[11a], (1935), when he synthesized polyhexamethyleneadipamide - nylon 66 - from hexamethylene diamine and adipic acid, where the first digit in "66" indicates the number of carbon atoms in the diamine and the second digit the number of carbon atoms in the dibasic acid. The cold-drawn "66" fibres had a high tensile strength and elasticity, and the product now has innumerable uses.

Then came the discovery of Whinfield and Dickson[12], (1941), terylene, a synthetic polyester fibre made from ethylene glycol and terephthalic acid, derived from the oxidation products of p-xylene or oil of turpentine. Its uses are endless too, and like nylon it is thermoplastic and thus can be pleated or shaped.

Other synthetic fibres in daily use include stretchable elastomeric fibres, acrylic fibres, polyolefin, polyvinyl chloride, (P.V.C.), polystyrene, polytetrafluorethylene, (P.T.F.E.), and many others all practically "tailored" for the work required.

1.2 Early carbon fibres

As has been mentioned, carbonized fibre was used by Edison and Swann in their incandescent lamp.

Gibson et al[13], (1944), first produced "filamentous carbon" by "cracking" methane on an iron plate at 1000°C. The compound had an interlayer spacing of about 3.5Å with the 'c' axis perpendicular to the fibre axis, that is, the hexagon layer planes more or less parallel to the fibre axis, (30° maximum deviation), being an example of a fibre built up from lamellar units, of structure similar to graphite.

Bacon[14], (1960), reported the formation of graphite "whiskers" found at the center of a graphite "boule" or pear shaped drop grown from the vapour from carbon electrodes producing a D.C. arc under 92 atmospheres pressure of argon, at 3900°K. These whiskers also had the 'c' axis perpendicular to the 'whisker axis' and had a strength of 2.84×10^6 p.s.i., and a Young's modulus of 10.2×10^7 p.s.i., (1 psi ≡ 6894 Nm^{-2}).

Now Cahn[15], (1969), in a review of carbon forms, reports that the theoretical elastic modulus and breaking strength of the co-valent carbon-carbon bonds are of the order 15×10^4 and 15×10^3 N/mm^2, which is equivalent to 2.130×10^7 and 2.130×10^6 p.s.i., so that Bacon's graphite whiskers approach the ideal elastic restoring force of the c-c bond, and

have a greater value for the tensile strength, but the whisker length was limited to about 3 centimeters.

Cranch[16], (1961), produced a graphite cloth by heating woven fabric to 2700°C in an electric furnace. Individual fibres from this material were of low tensile strength between 50-100 kpsi.

We come now to the work of Shindo[17], (1961), who realized that carbon fibre could best be produced from an organic fibre which carbonized without melting, thus maintaining the original shape of the fibre. From a list of typical addition polymers, first classified by Carothers[18], (1929), he chose polyacrylonitrile fibre, now generally called PAN, as a precursor material with the most favourable characteristics for carbon fibre production. This fibre is now manufactured under the trade name PAN fibre, by Courtaulds, protected by their Patent No. 1,129,831.

PAN has a monomer $CH_2 = CH-CN$ with a repeating unit $- CH_2 - \underset{CN}{CH} -$ and Shindo found that strong carbon fibre could be prepared from PAN with a pre-oxidation treatment at 200°C in air, producing HCN and NH_3 as products of pyrolysis; followed by a carbonization in nitrogen at 1000°C, with further evolution of HCN.

Fibres produced in this manner had a tensile strength of up to 140 kpsi, (10,000 kg.wt./cm^2) and elastic modulus of (15-16) x 10^6 psi. He also found that with increasing temperature of carbonization the tensile strength of the carbon fibre was reduced and the elastic modulus increased. Examination of the micro-structure of such fibres led him to believe that a basic two-phase structure developed with crystallites parallel to the surface becoming increasingly more random in orientation the nearer the fibre center.

TABLE 1

Representative Tensile Strength of Fibrous Materials

Material	Tensile Strength psi x 10^6	Carbon fibres	Reference
Graphite whiskers (circa 1 μ)	up to 3.5		
Silica fibres	" 3.5	2.84	Bacon[14], (1960)
Alumina fibres	" 2.2		'Graphite whisker'
Iron whiskers	" 1.9		
Drawn Tungsten wire	" 0.55		
Ausformed Steel wire	" 0.45	0.4, Type II, 1000°C	Watt[29], (1969)
Piano wire	0.35	0.3, Type I, 2600°C	Watt[29], (1969)
Asbestos fibre	0.22		
Fibre glass	0.20		
Flux	0.16	0.14, 1000°C	Shindo[17], (1961)
Drawn Copper wire	0.08		
Nylon thread	0.08	0.07, 2500°C	Shindo[17], (1961)
Cotton	0.06		
Cat gut	0.06	0.05-0.1	Cranch[16], (1961)
Spider thread	0.027		
Hemp	0.015		
Hard wood, along grain	0.015		

(1 psi ≡ 6894.76 Nm^{-2})

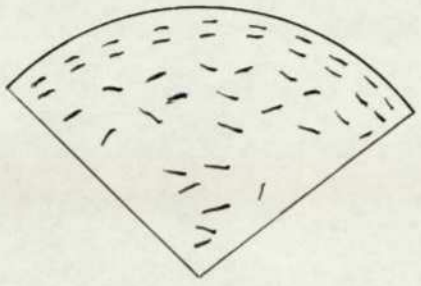


Fig. 1 Orientation of crystallites

In order that the relative strengths of the fibres discussed may be better appreciated, Table 1, based on work by Cottrell[19], (1964) is given, with the position of the various carbon fibres added.

1.3 Strength of solids

To understand the values quoted for tensile strength of solids in Table 1 it is necessary to consider the behaviour of solids in tension.

In 1678, Robert Hooke[20] wrote a Latin anagram to express the proportionality between stress and strain, thus:-

"cc iii no sss tt uu"

being probably expressed as an anagram for the same reasons that prompted Leonardo da Vinci, (1452-1519), to describe his work in short-hand mirror writing - to escape religious persecution.

Translated it becomes:-

"ut tensio sic uis"

or roughly:-

"The power of any spring is in the same proportion with the tension thereof."

Thus Hooke's experimental law may be given by the following equation:-

$$\delta = \frac{PL}{AE} \qquad \ldots (1)$$

where

P = force producing extension of bar

L = length of bar

A = cross-sectional area of bar

δ = total elongation of bar

and E = elastic constant of the material,

otherwise known as Young's modulus, after Thomas Young, (1773-1829), also famous for his translation of the Egyptian hieroglyphics on the Rosetta stone.

1.4 Ideal strength of solids

An estimate of the ideal strength of an elastic solid can best be made by the use of Cottrell's elegant work on the mechanical properties of matter[19], (1964), which is here quoted in full:

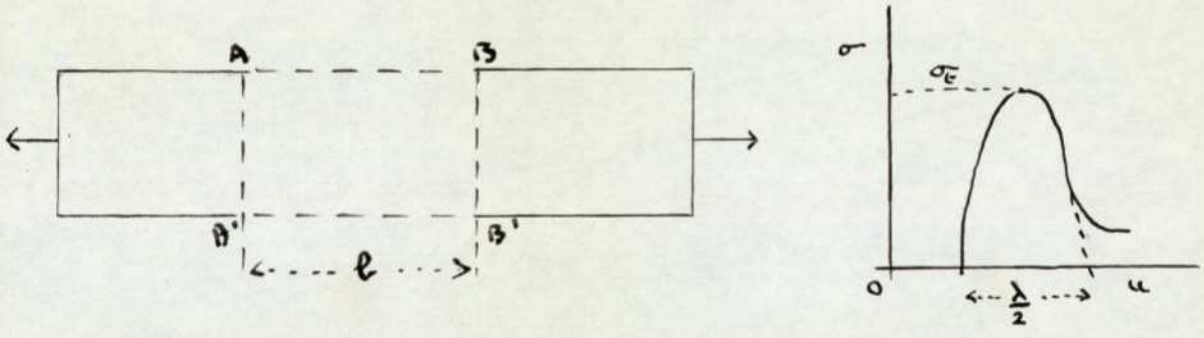


Fig. 2 Tensile fracture of a solid bar

"Suppose that we pull a cylindrical bar of unit cross-sectional area by a tensile stress σ. When σ reaches the ideal strength σ_t, the atomic bonds joining two neighbouring atomic planes such as AA' and BB' break. We approximate the atomic stress-strain curve of these bonds by a sine curve of wavelength λ, as shown in Fig. 2. This is reasonable provided we make its initial slope agree with Young's modulus 'E' of the material and make the area under it equal to 2γ, where γ is the surface energy. Thus

$$\sigma = \sigma_t \sin \frac{(2\pi u)}{\lambda} \qquad \ldots (2)$$

where 'u' is the displacement from the equilibrium spacing 'b'.

For infinitesimal strains this reduces to

$$\sigma = \sigma_t \frac{2\pi u}{\lambda} \qquad \ldots (3)$$

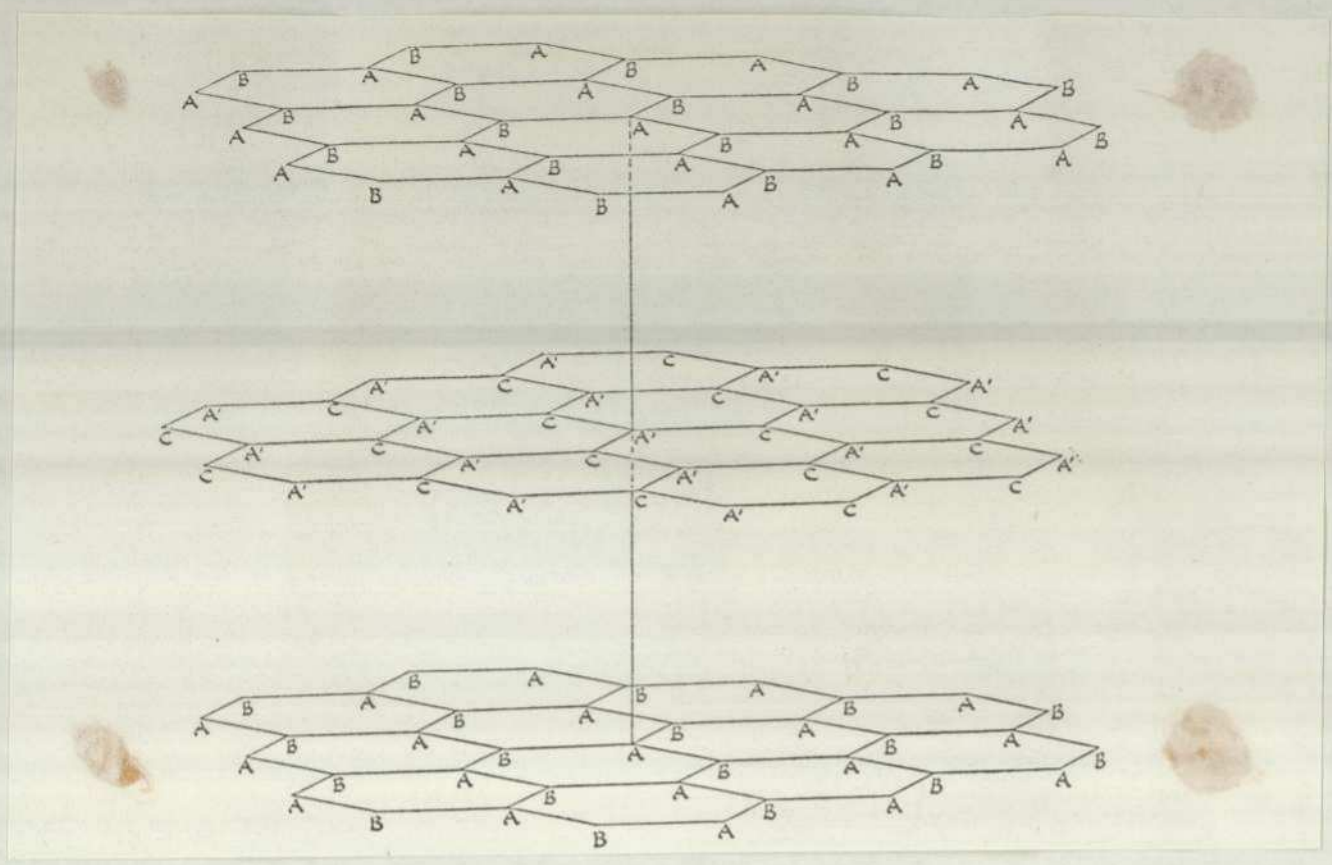


Fig. 3 The structure of graphite. (Bernal[22], 1924)

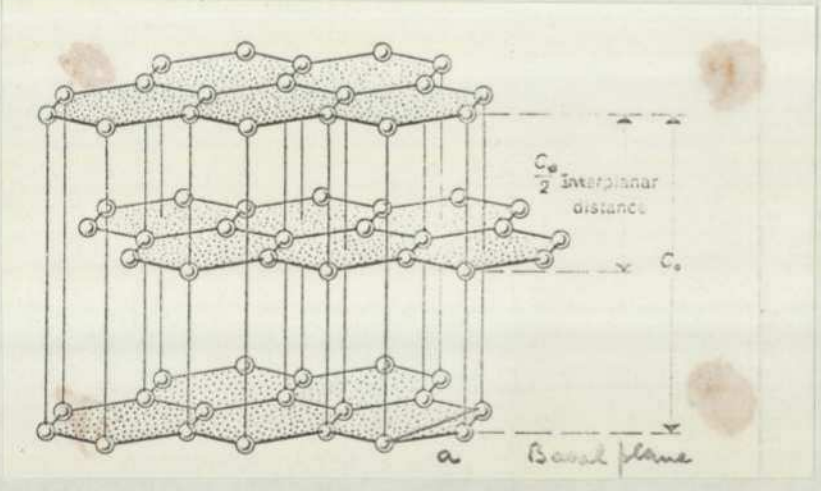


Fig. 4 Crystal structure of graphite. (Ubbelohde[24], 1965)

and hence from Hooke's law, ($\sigma = E \frac{u}{b}$)

$$\sigma_t = \frac{\lambda E}{2\pi b} \qquad \ldots (4)$$

The surface energy is given by

$$= \tfrac{1}{2} \int_0^{\frac{\lambda}{2}} \sigma_t \sin\left(\frac{2\pi u}{\lambda}\right) du$$

$$= \frac{\lambda \sigma_t}{2\pi} \qquad \ldots (5)$$

and hence

$$\sigma_t \simeq \sqrt{\frac{E\gamma}{b}} \qquad \ldots (6)$$

Broadly for most solids

$$\sigma_t \simeq \frac{E}{10} \qquad \ldots (7)$$

This high value indicates the high strength of atomic bonds."
Such high ideal strengths are rarely reached in practise due to the presence of minute surface cracks or flaws, both internal and external, which often reduce the tensile strength by two orders of magnitude, as was shown by Griffith[21], (1921), who demonstrated that ordinary glass will break at about 10^4 psi but freshly drawn threads of glass or silica broke at about 10^6 psi - almost the ideal strength. Such cracks or "stress-concentrators" have now become known as Griffith's cracks.

1.5 Graphite structure

We come now to the crystal structure of graphite since this is a principal component of carbon fibre and the mechanical properties both parallel and perpendicular to the basal plane are fundamental in this work. Fig. 3 shows the hexagonal lamellar structure of graphite as deduced by Bernal[22], (1924). He says:-

> "That the great difference between the mechanical properties of graphite and diamond is due to the fact that the atoms are linked closely in a two-dimensional net in the former and a three-dimensional lattice in the latter, and, in fact, graphite exhibits in the plane of the cleavage sheets considerable hardness and tenacity."

Indeed Williams et al[23], (1970), give tensile strengths as high as 3×10^6 psi and a Young's modulus of 148×10^6 psi for freshly prepared graphite whiskers, measured in the basal plane, (see Table 1).

Figure 4 is a picture of a cluster of unit cells in the graphite structure, due to Ubbelohde[24], (1965). Here the c-c bond distance between carbon atoms in the network, L_a in the basal plane, is 1.415Å ($1Å \equiv 10^{-10}$ m) and L_c, the distance between the 1st and 3rd layers is 6-7Å and the minimum distance between planes is never less than 3.35Å. The networks are accurately sited over one another in a staggered (hexagonal) sequence, ab ab ab. In a crystallite of graphite found in polycrystalline material there is a series of stacks of unit cell networks agglomerated so that their axes assume practically any orientation relative to one another. Such material has a very low strength, quoted by Nightingale[25], (1962), as about 3000 psi for near isotropic polycrystalline graphite.

1.6 Structure of carbon fibre

In the case of carbon fibre however the network stacks or crystallites are arranged so that, to a great extent, they are parallel to the fibre axis and with the 'c' axis perpendicular. They are however in turbostratic order which can best be understood by imagining the layer networks in Fig. 3. to be in the same planes, that is parallel, but in arbitrary azimuth, where the azimuth of a horizontal direction is defined as its deviation from the north or south. Such a structure, with the preferred orientation described, has a tensile strength some two orders of magnitude greater than a polycrystalline graphite, variations being due, in part, to the degree of parallelinity of the crystallites to the fibre axis, as shown by Shindo[17], (1961).

1.7 R.A.E. carbon fibre

The essential step in the production of very strong carbon fibre, which was missed by Shindo, is the application of tension during the pre-oxidation stage. This step was discovered by Watt, Phillips and Johnson[27], (1966) of the Royal Aircraft Establishment, and now covered by Patents 1,110,791 and 1,148,874.

During tension and oxidation of the PAN fibre the degree of preferred orientation already present in the precursor fibre is increased by further re-alignment of the crystallites with their stiff basal planes parallel to the fibre axis. This tension during formation results in a carbon fibre with an internal fibrous structure closely related to the precursor fibre, as described, but with a much higher degree of preferred orientation than was obtained by Shindo.

Watt et al also found that tensile strength decreased with increase in temperature of formation and that elastic modulus increased but for both parameters to a much greater extent than that previously reported, (see Table 1 and 2). Knibbs[28], (1969), confirmed Shindo's work on fibre structure showing that the orientation of the crystallite 'c' axis in the outside layer of R.A.E. fibre is radial, an effect increasing with residence time (in the furnace) at temperature. Kearsey et al[30], (1969), showed that oxidation of PAN was an exothermic reaction and Bromley[31], (1969), has suggested that the two-phase structure reported by Shindo[17], (1961), and since by Knibbs[28], (1969) and Macphail[32], (1969), is due to thermal gradients in the furnaces produced by such energetic oxidation during bulk production of fibre. It is to be noted that all phenomena quoted here lead to variations in the final tensile strength of the product.

It is of interest to note that Griffith[21], (1921), who also worked at the R.A.E., when elaborating his theory of rupture, stated that:

TABLE 2

Fibre Properties

(From Watt et al[29], 1969)

Properties	U.K. Carbon Fibres		U.S. Carbon Fibres eg Thornel	Boron Fibres	Single Crystal Aluminium Oxide Fibres
	High Strength Type II	High Modulus Type I			
Diameter (microns) (1 micron ≡ 10^{-6}m)	8.0	7.5	6.6	100	250
Specific Gravity	1.8	1.95	1.63	2.5	4.0
Young's Modulus (psi)	36×10^6	60×10^6	50×10^6	60×10^6	67×10^6
Tensile Strength (psi)	400×10^3	300×10^3	285×10^3	400×10^3	300×10^3
Electrical Resistivity (ohm cm)	1.3×10^{-3}	0.3×10^{-3}	-	-	1×10^{16}
Thermal conductivity at room temperature (cal/cm/degC/s) (1 cal/cm/degC/s ≡ 4.1868 w/cm. deg.C)	about 0.5 - 0.1		0.03	-	about 0.1

(1 p.s.i. ≡ 6894.76 Nm^{-2})

"If a wire is required to withstand a simple tension, it seems that the best arrangement is that in which the strongest directions of all the molecules are parallel to the axis of the wire. This is equivalent to making the wire out of a single crystal. The theoretical tenacity would not be obtained, however, if the gliding planes made with the axis, angles other than 0^{o} and 90^{o}, as yield would occur."

Further variations in carbon fibre structure and strength etc., revealed by other work, will be mentioned later in the thesis.

1.8 Scope of present work

a. The raw material

In this work various forms of graphite, the original Courtauld PAN fibres and carbon fibres, produced from this material in various ways, are examined physically by X-ray powder diffraction techniques etc., to establish quality, type and structure; also to determine the effect variations in fabrication techniques, geometry, history etc., have on tensile strength and elastic modulus of individual fibres, and those fibres chosen at random from various batches of material. As a result of this work a relationship between 002 line width and graphite formation temperature will be described, enabling rapid identification of fibre types. Results of many tensile tests reported in the literature are collated to reveal the general experimental scatter to be expected.

b. The carbon fibre tow

Throughout the main work on copper deposition, standard 14 inch carbon fibre tows were used as a substrate. The tow, hank or bundle is nominally here described as having 10,000 fibres of 7-8 microns diameter, (1 micron $\equiv 10^{-6}$ m) 1.8-2.0 gms/ml density, of high modulus, Type I, or high strength, Type II, respectively (see Table 2); other types of tow can be made to order.

Now although fibre may be extruded through plates having 10 x 10 spinarettes or holes during preparation of PAN, due to subsequent diameter reduction by further stretching, to increase strength, (Moreton[34], 1969), handling at all stages and inevitable breakages due to flaws etc., the exact

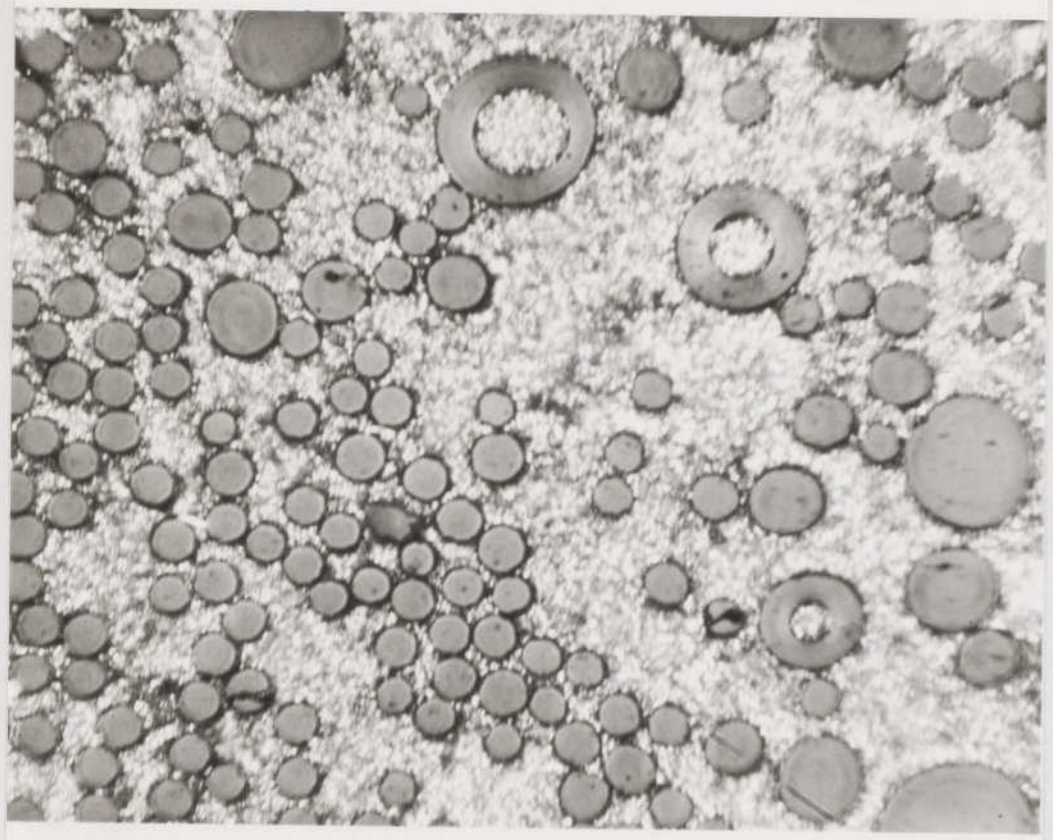


Fig. 5 Variations in fibre cross-section. X750



Fig. 5a Ellipsoidal fibre shapes, cut at an angle to fibre axis X750

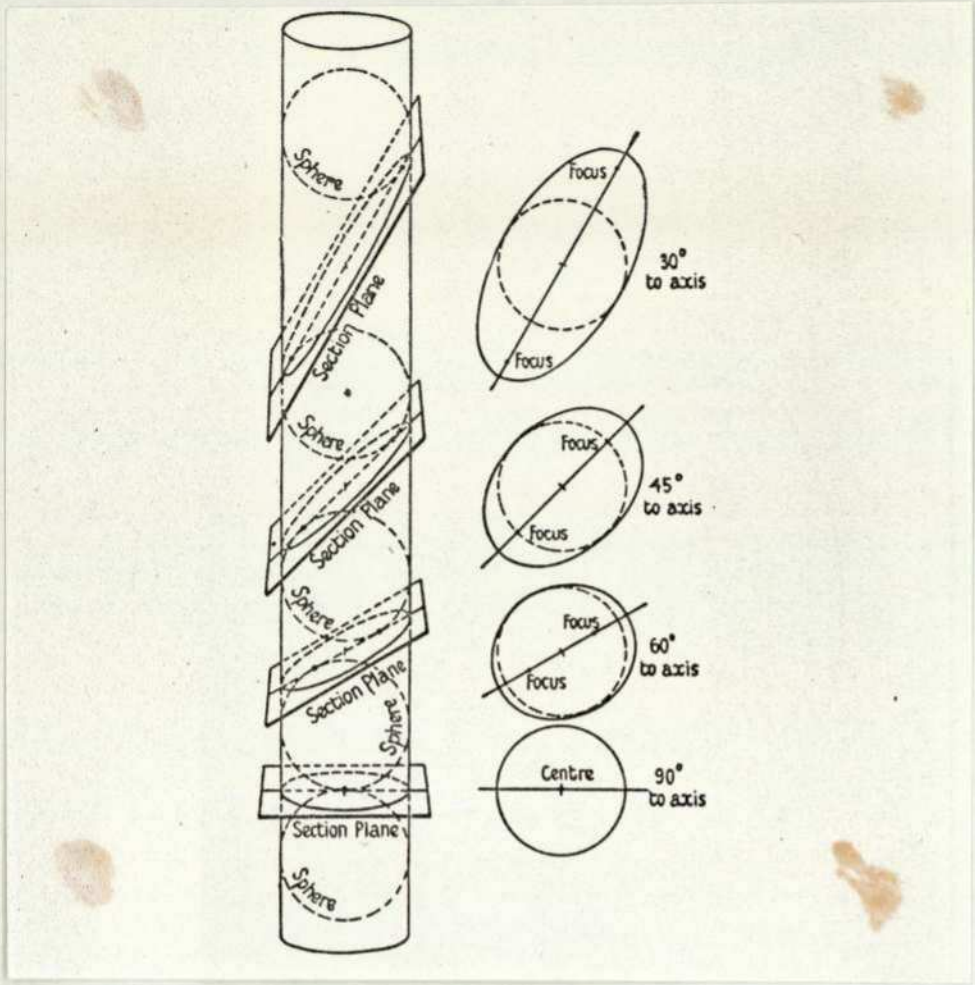


Fig. 6 Relation between angle of section and sectional shape

number of fibres per final bundle, before experimental work begins, is never known.

The thickness which varies along the fibre length, from fibre to fibre and from batch to batch, is frequently quoted in deniers, which is a unit of fineness originally borrowed from the silk industry and means, loosely, the weight in grains or grams of 9000 meters of a single fibre, but as a measure it is meaningless unless it is related to fibre cross-section or density; information which is frequently omitted in the literature. A short account of the denier is given in Appendix 1. Similar variations to those seen with fibre diameter, are recorded for the density of the material, due to temperature variations during manufacture etc., mentioned in Section 1.7.

Finally, since the evaluation of current densities employed, tensile strengths and elastic moduli measured etc., depend on an accurate knowledge of surface areas or areas of cross-section one would hope that the cross-section under examination were always at right angles to the fibre axis and were circular, but this is not always so, as seen in Figs. 5 and 5a, where hollow, oval, and ellipsoidal fibres (due to poor mounting), together with diameter variations can be clearly seen. Even bean shaped Acrilan fibres have been reported! (Johnson and Thorne,[35] 1969).

A further point to remember is that in order to determine the cross-sectional shape exactly it is necessary to prepare a mounted section such that the polished surface is at right angles to the fibre axis, which is difficult with such thin 8μ fibre. Also one cannot be sure at what angle to the fibre axis the section under examination has been made. Now Archimedes, (287-212 BC), and Apollonius, (200-30 BC), in their work on conic sections showed that a cylinder can be sectioned so that an elliptical or circular section results, depending on the angle of section. This is clearly seen in Fig. 6, taken from Singer's[36] "History of Science",



Fig. 7 Carbon fibre surface after sodium hypochlorite clean. (Bromley(31), 1969). Circa X50,000

(1959). Thus the geometrical and cross-sectional area of single fibres is difficult to determine with accuracy and a glance at Fig. 7, due to Bromley[31], (1969), will show the wide difference between relative and real fibre surfaces. For these reasons measurements in this work are presented as means of many single fibres or of whole tows and are comparative, relative etc., but never absolute.

As a consequence of the many variables noted, one might fairly be excused if one concluded that a fit and proper definition for a carbon fibre tow was identical to that given in the Times[37], (1969), for the human foot:-

> "The foot, as one writer on the shoe business has put it, is a technological nightmare."

c. Preliminary work on metal deposition

Metal deposition from the vapour phase, (Flint[38], 1963), onto carbon fibre is briefly described and reactions with aluminium, zinc and magnesium are explored. Metallurgical examination of the deposits together with the limitations imposed by the method of deposition are reported. Similarly the technique of electroless deposition, (Brenner[39], 1954), of both copper and nickel is investigated together with the effect of annealing on both deposits. As a result of this work it was decided to examine in depth the electro-deposition of copper on to carbon fibre.

d. Copper deposits

Copper plating from both acid and alkaline electrolytes was examined and preliminary tensile tests quickly showed that Type I fibres and acid electrolytes were unsuitable, due to poor adhesion of deposits.

As a result of this early work the well tried, currently used, Rochelle salt-copper cyanide electrolyte, exhaustively investigated by Graham and Read[40], (1937), was adopted as a standard and variations in the deposit due to temperature, current density, "free-cyanide" concentration, thickness of Cu, etc., were examined; the program being

monitored by repeated tensile tests of the plated tows on an Instron Tensile Testing apparatus, the lengthy calibration of this unit being given in Appendix 2. A standard test set of plated finishes was collected and from the tensile results an experimental test block of fibre tows plated at five current densities and five different temperatures was prepared for rapid comparison.

e. Tensile testing

It is necessary to note here that information on the calibration of the Instron for tensile testing is rarely given in the literature, indeed out of over 100 reports surveyed only two hinted at a mechanical "slackness factor" or load-cell error and none described the method of calibration employed in their work. In view of the inherent slackness of the 10,000 fibre tow itself it is not difficult to estimate the importance of this further variable.

f. Surface activation

The work on plating standardization was followed by a survey of the common surface activating pre-treatments and their effects on subsequent copper deposits but it was found, contrary to expectation, that the extra efficiency due to thorough wetting of the tow caused individual fibres to stick together with a corresponding lack of penetration and consequent coverage of fibre surfaces with copper.

g. Effect of annealing

It is known that carbides of many metals may form quite readily. For example

$$3\langle Fe\rangle + \langle C\rangle \rightleftharpoons \langle Fe_3C\rangle \qquad \ldots (8)$$

where $\Delta G_{1115-1808^{\circ}K} = + 2{,}475 - 2.43T$ kilo cals/mole

or

$$3\langle Ni\rangle + \langle C\rangle \rightleftharpoons \langle Ni_3C\rangle \qquad \ldots (9)$$

where $\Delta G_{298-1000^{\circ}K}$ = + 8,110-1.70 T kilo cals/mole

and $$\frac{4}{3}\langle Al\rangle + \langle C\rangle \rightleftharpoons \frac{1}{3}\langle Al_4C_3\rangle \quad \ldots (10)$$

where $\Delta G_{298-1000^{\circ}K}$ = - 11,700 + 1.0 T kilo cals/mole

(where 1 kilo calorie ≡ 4186.8 Joules)

from Richardson[41], (1953).

Whilst it is appreciated that these reactions will only occur at elevated temperatures because of their positive or low free energies of formation, some surface reactions may take place. Jackson and Marjoram[42], (1970), for example, report that with nickel plated carbon fibre, the fibres undergo structural recrystallization, at temperatures of about 1000-1100°C, by a dissolution/diffusion/reprecipitation mechanism.

Now copper does not form carbides, also copper and carbon are immiscible but the effect of heat on plated copper fibre is not known and could well be important. Therefore annealed plated samples were examined using the 5x5 test block of plated specimens to cover the range of current densities and annealing temperatures involved.

1.9 Summing up of plated fibre results

At this stage results were reviewed and a fibre plating specification drawn up.

1.10 Copper-carbon fibre composites

As a final step in the evaluation of the plating process batches of fibre were plated to various thicknesses of copper by both laboratory and production techniques. These were then compacted with pressures between 5-10 tons per square inch, (1 ton per sq. in. ≡ 15.44 MN m^{-2}) at about 850°C, in an argon flow. Dog-bone specimens were machined from this material and tensile tested. The results were analysed on the basis of theoretical work by McDanels et al[43], (1960), and Kelly[44], (1964).

The results observed, stressed the true importance of fibre alignment in the compact, as was stressed by Cottrell[45], (1964), in his article "Strong Solids", (written before carbon fibre was manufactured), by Kelly[44], (1964), in his theoretical survey and by Bhatacharyya et al[47], (1970) in their work on tungsten/silver composites.

1.11 General discussion and conclusions

Finally a survey of the work of the thesis, as a whole, is made and conclusions are drawn as to the practicability of the processes examined and their probable applications, bearing in mind those structural restrictions imposed by a tensile strength of only about 3,000-6,000 psi (1 psi = 6894 Nm^{-2}) at right angles to the carbon fibre axis and discussed by Pearce[48], (1969), in his article on designing with carbon fibre reinforced plastics.

References 1

1.1 Dr. Robert Hooke, Micrographia, 1664.

1.2 Ironside, J., Sunday Times Magazine, Aug. 16th, 1970.

1.3 Réaumur, A. F. de René, 1720, Williams, T. I., Dictionary of Scientists, Adam and Charles Black, 1969.

1.4 Swann, J. W., 1848, Book "Sir J. W. Swann", Swann, M. E., and Swann, K. R., 1929.

1.5 Edison, T. A., Ganots' Elements de Physique, Longmans, Green, 1898.

1.6 'Sir C. V. Boys', 1881, Paget, R. A. S., Proc. Phys. Soc., 56, 397, 1944.

1.7 Swann, J. W., 1883, See ref. 1.4.

1.8 Chardonnet, L. M. H. B., 1889, "The Flash of Genius", Garrett, A. B., Van Nostrand, 1963.

1.9 Cross, C. F., Bevan, E. J., and Beadle, C., 1892, J. Chem. Soc. 1337, 1935.

1.10 Bernthsen, A., Organic Chemistry, Backie, 1942.

1.11 Carothers, W., and Hill, J. W., J. Am. Chem. Soc. 54, 1579, (1932).

1.11a Carothers, W., 1935, See Ref. 1.8.

1.12 Whinfield, J. R., and Dickson, J. T., See ref. 1.2.

1.13 Gibson, J., Riley, H. L., and Taylor, J., Nature, 154, 544, 3913, 1944.

1.14 Bacon, R., J. Appl. Phys., 31, 283, 1960.

1.15 Cahn, R. W., and Harris, B., Nature, 221, 132, 1969.

1.16 Cranch, G. E., Proc. 5th Carbon Conf., Pennsylvania, State Univ., Vol. 1, June, Pergamon, 1961.

1.17 Shindo, A., Govt. Ind. Res. Inst. Osaka, No. 317, 1961.

1.18 Carothers, W. H., J. Am. Chem. Soc., 51, 2548, 1929.

1.19 Cottrell, A. H., The Mechanical Properties of Matter, John Wiley, 1964.

1.20 Robert Hooke, De Potentia Restitutiva, London, 1678.

1.21 Griffith, A.A., Phil. Trans. Roy. Soc., CCXXIA, 163, 1920-21.

1.22 Bernal, J. D., Proc. Roy. Soc., 106, 749-773, A742, 1924.

1.23 Williams, W. S., Steffens, D. A., and Bacon, R., J. App. Phys., 41, 12, 4893, 1970.

1.24 Ubbelohde, A. R., Endeavour XXIV, No. 92, p.63, May, 1965.

1.25 Nightingale, R. E., Nuclear Graphite, Academic Press, 1962.

1.26 Shindo, A., See ref. 1.17.

1.27 Watt, W., Phillips, L. N., and Johnson, W., The Engineer, 221, 5757, 815, 1966.

1.28 Knibbs, R. H., H.C.F.W.P., (69), P7, 1969.

1.29 Watt, W. and Johnson, W., New Scientist, 398, Feb. 1969.

1.30 Kearsey, H. A., Chidley, B. E., and Hornby, J., A.E.R.E., R6222, 1969.

1.31 Bromley, J., Private Communication, 1969.

1.32 Macphail, I., A.E.R.E., R6168, 1969.

1.33 Griffith, A. A., 1921, See ref. 1.21.

1.34 Moreton, R., R.A.E. Technical Report, 69114, 1969.

1.35 Johnson, J. W., and Thorne, D. J., Carbon, No.6, Vol. 7, 659-661, 1969.

1.36 Singer, C., A Short History of Scientific Ideas, Clarendon Press, 1966 (Paperback).

1.37 The Times, Wednesday, November 12, 1969.

1.38 Flint, O., Deposition of Metals from the Vapour Phase, Res. Dip. R.I.C. Thesis, 1963.

1.39 Brenner, A., Metal Finishing, Westwood, N. J., Nov.-Dec., 1954.

1.40 Graham, A., and Read, J., Metal Industry, p.559, Nov. 1937.

1.41 Richardson, F. D., J. Iron and Steel Inst., 175, (3), 33, 1953.

1.42 Jackson, P. W., and Marjoram, J. R., J. Mat. Sci., 9-23, 5, 1970.

1.43 McDanels, D. L., Jech, R. W., and Weeton, J. W., Metals Progress, 78, (6), 118, 1960.

1.44 Kelly, A., Fibre Reinforcement of Metals, H.M.S. Office, 1965.

1.45 Cottrell, A. H., Proc. Roy. Soc., 282A, pp. 2-9, 1964.

1.46 Haynes, W. M., and Tolbert, T. L., J. Composite Mat., Vol. 3, p.709, Oct. 1969.

1.47 Bhattacharyya, S. and Parikh, N. M., Met. Trans., Vol. 1, No.5, 1437, 1970.

1.48 Pearce, D. G., A.E.R.E., Eng. Review, Vol. 8, No. 5, May 1969.

Fig. 8 Diamond

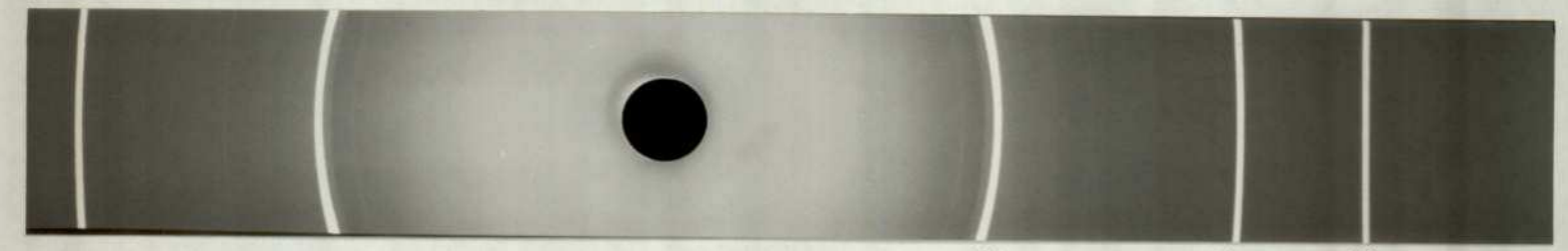


Fig. 9 Ceylon Graphite

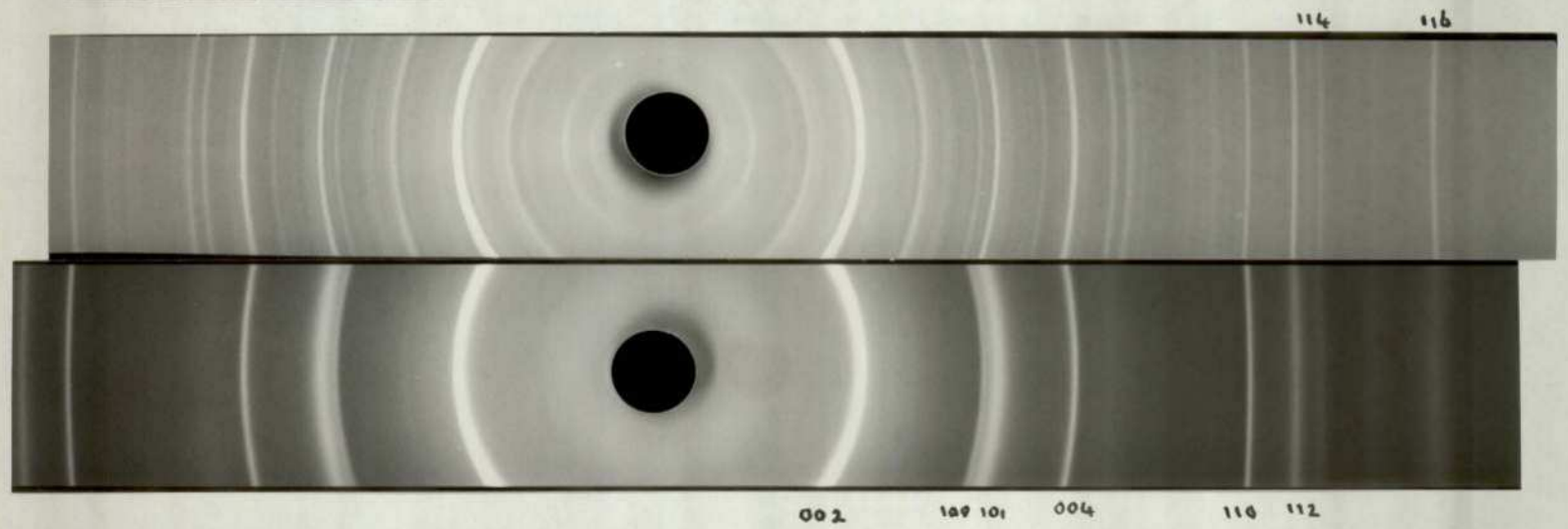


Fig. 10 Graphitized diamond

TABLE 3

Powder Pattern Data for Diamond and Graphite

a. Diamond (Cubic)

dÅ	I/I_1	h k l
2.060	100	1 1 1
1.261	27	2 2 0
1.0754	16	3 1 1
0.8916	7	4 0 0
0.8182	15	3 3 1

b. Synthetic Graphite (Hexagonal)

3.37	100	0 0 2
2.132	2	1 0 0
2.036	3	1 0 1
1.682	8	0 0 4
1.541	2	1 0 3
1.232	2	1 1 0

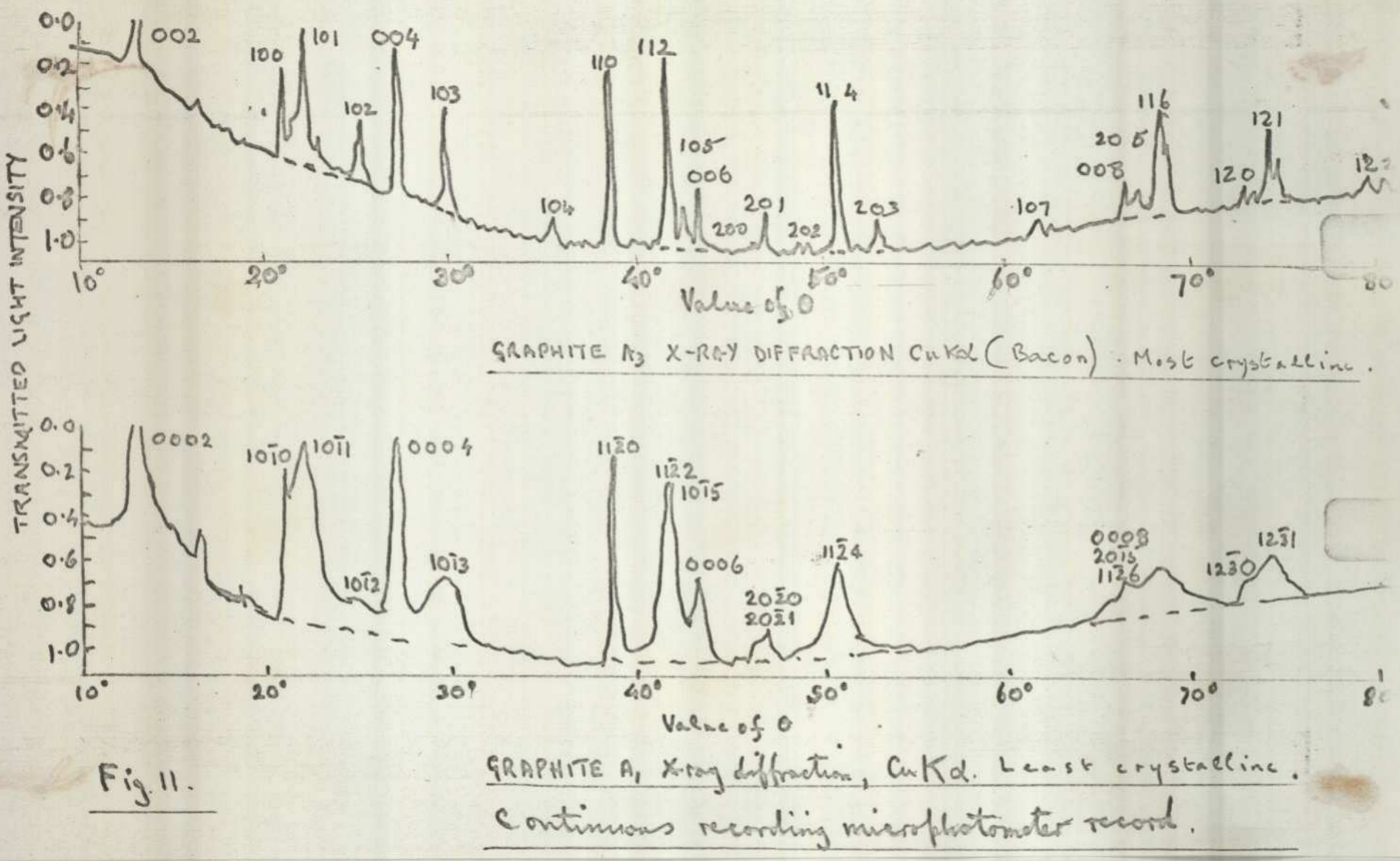


Fig. 11 Continuous recording microphotometer record

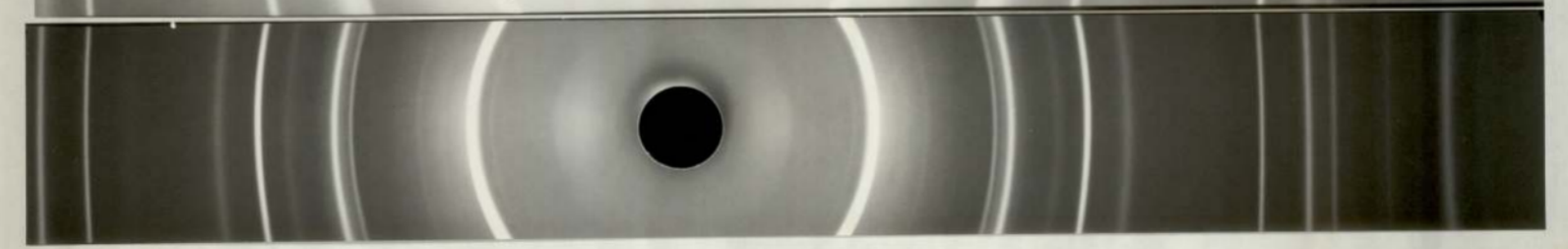
Fig. 12 Petroleum coke, 1100°C



Fig. 13 Petroleum coke, 2000°C



Fig. 14 Petroleum coke, 3000°C



CHAPTER 2

Graphites and the Carbon Fibre

2.1 The raw material

a. X-ray diffraction analysis

Samples of diamond powder, of 15-30 micron (1 micron ≡ 10^{-6} m) particle size, petroleum coke pyrolysed at various temperatures, and nuclear graphites etc., were examined, using the techniques of Debye-Scherrer X-ray crystallography and powder analysis, as fully discussed in a paper by Flint[1], (1966), given in Appendix 3.

Figures 8, 9 and 10 show X-ray diffraction powder patterns, using a Cu target, for diamond, Ceylon graphite and diamond which has been graphitized at about 2000°C. In Fig. 8, for the diamond, the tetrahedral cubic or adamantine lattice is seen, (Beynon[2], 1946), while Figs. 9 and 10 show a comparison of Ceylon natural graphite and graphitized diamond. Correspondence between the 002 lines will be noted and between the main hexagonal structure lines. Table 3 from the ASTM Index[3], (1960), gives interplanar spacings and relative intensities for the two materials. It will be noted that only six lines are given for synthetic graphite whilst 23 can be identified in Fig. 11, which is a micro-photometer record of a natural graphite pattern from Bacon's extensive work on the subject[4], (1958), where he also showed that many extra lines were due to SiO_2 and micaceous impurities.

Figs. 12, 13 and 14 show petroleum coke which has been heated from about 1000°-3000°C. The amorphous structure with foggy 002 and 100 lines, just forming in the low temperature example in Fig. 12, shows very little graphite structure but it is evident from the comparison between cokes heated to 2000°C and 3000°C in Figs. 13 and 14 that the graphite structure appears with rise in temperature. Franklin[5], (1951), also Fair and Childs[6], (1961), report that the interlayer spacing also decreases with

Fig. 15 Carbon fibre, 1000°C, Type II



Fig. 16 Nuclear graphite

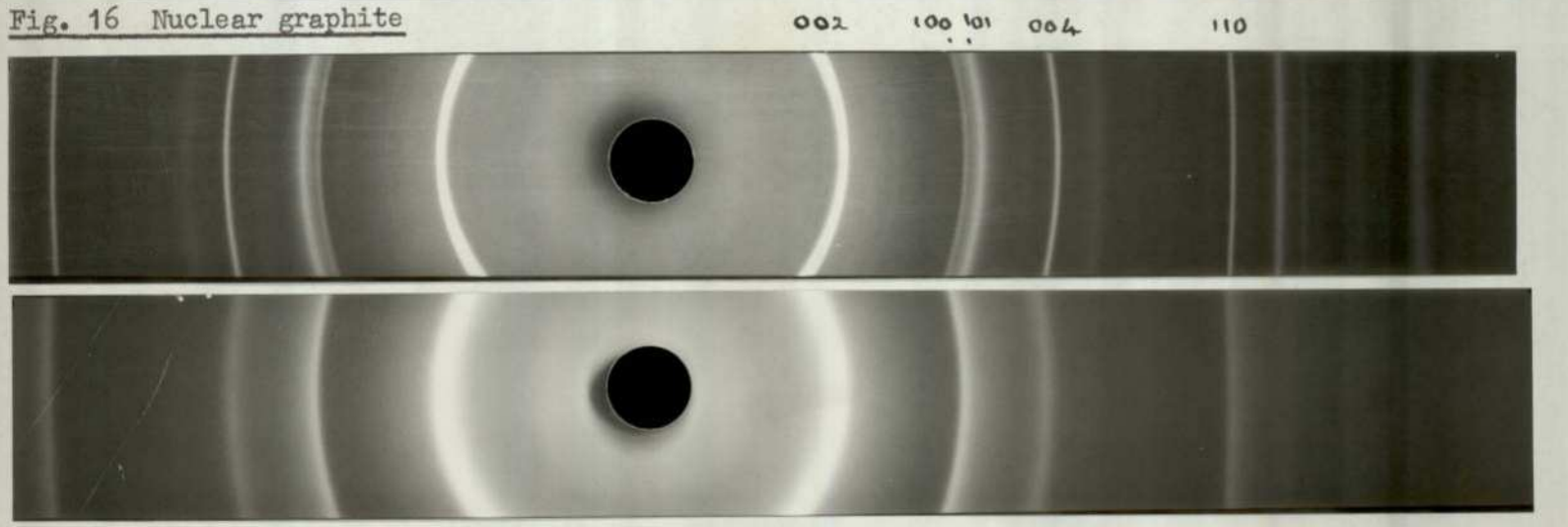


Fig. 17 Carbon fibre, 2600°C, Type I

Fig. 18 Raw PAN fibre





Fig. 19 Preferred orientation in Type I carbon fibre

residence time in the furnace at temperature, whilst Tarpinian[7], (1961), reports the same effect in binder-free petroleum coke. Most synthetic graphites are made from petroleum cokes bound together with a coal-tar pitch filler, (Nightingale[7a], 1962).

A similar sequence of events occurs when carbon fibre is prepared at increasing temperatures. Figs. 15, 16 and 17 show carbon fibre manufactured at 1000°C, known as Type II, and a comparison between nuclear graphite and carbon fibre manufactured at 2600°C, known as Type I. The similarities between the powder patterns for petroleum cokes and carbon fibres are striking.

Finally, to demonstrate that some degree of preferred orientation exists in the precursor PAN material and in carbon fibre, samples of both were X-rayed in a powder camera with bundles of the material held in such a manner that the fibre axes were at right angles to the beam. This was accomplished by filling the wide end of powder capillary tubes with lengths of fibre and mounting these in the usual way, (see Appendix 3). Figures 18 and 19, of raw PAN fibre and 2600°C, Type I, carbon fibre respectively, show in the first case some sign of preferred orientation in the central broadening of the two lines and in Fig. 19, the typical pattern of broadening due to preferred orientation of the fibre crystallites, parallel to the fibre axis, can be seen.

It is important to remember here that since the degree of preferred orientation is related to the final fibre strength, a further increase in orientation with furnace residence time at temperature, already mentioned, could explain variations in tensile strength recorded from batch to batch of similar material. Such variations in residence time could occur during variable furnace heat up and cooling times, which are a function of furnace heat capacity and design.

b. The Temperature-002 line width relationship

To facilitate the investigation of fibre properties a standard set of fibres has been prepared at Harwell incorporating fibre tows pre-oxidized at 220°C for 5 different periods, up to 7 hours and heat treated at 5 different temperatures up to 2600°C. Powdered samples from this experimental block of 5x5 test specimens were X-rayed to examined structural changes at various manufacturing stages. Again the graphite structure gradually appeared as both pre-oxidation times and heat treatment temperatures increased, and as a point of interest practically no structure could be seen in the powder pattern from a 1 hour oxidation - 1000°C sample. It was also noted that the breadth of the 002 line, which as has been said, is a relative measure of the degree of preferred orientation of the crystallites parallel to the fibre axis, appeared to decrease with increase in temperature. Watt et al[8], (1966), report that the width of the 002 line decreases with increase of Young's modulus, which also increases with temperature.

With a view to possible rapid identification of fibre types it was decided to examine the variation of 002 line width for various graphites and fibres. As commercial X-ray densitometer units are very expensive, in the order of £1500 plus, a small experimental densitometer was made. A 6 volt, 30 watt, light source was focussed onto a powder pattern film to give a spot of light 1 mm diameter, at the film center. The film, held in a rigid jig on a rack and pinion, was then traversed, horizontally, along its length, such that two centimeters per minute travel matched 2 inches of chart speed on a Honeywell recorder connected to the output of a barrier layer Evans electroselenium cell, with a 1 mm Perspex cone tip to focus the light beam coming through the film. The film traverse was arranged to give approximately 10 inches of travel, (25.4 cms), to cover the relevant detail. This unit if commercially produced would cost about £100, without the recorder.

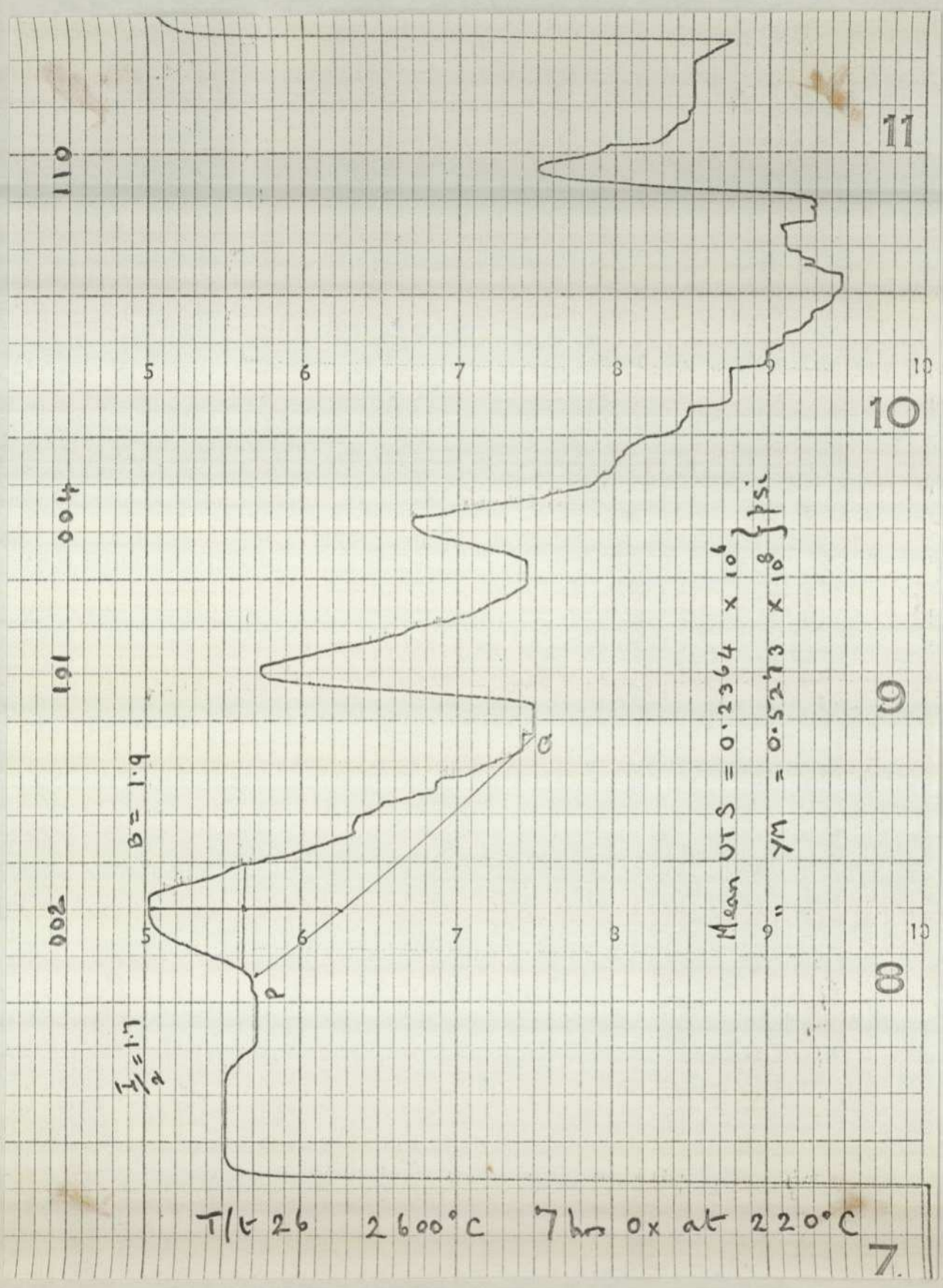


Fig. 20 Photometric trace of X-ray powder pattern

Relationship between breadth of 002 line and temperature of graphitization.

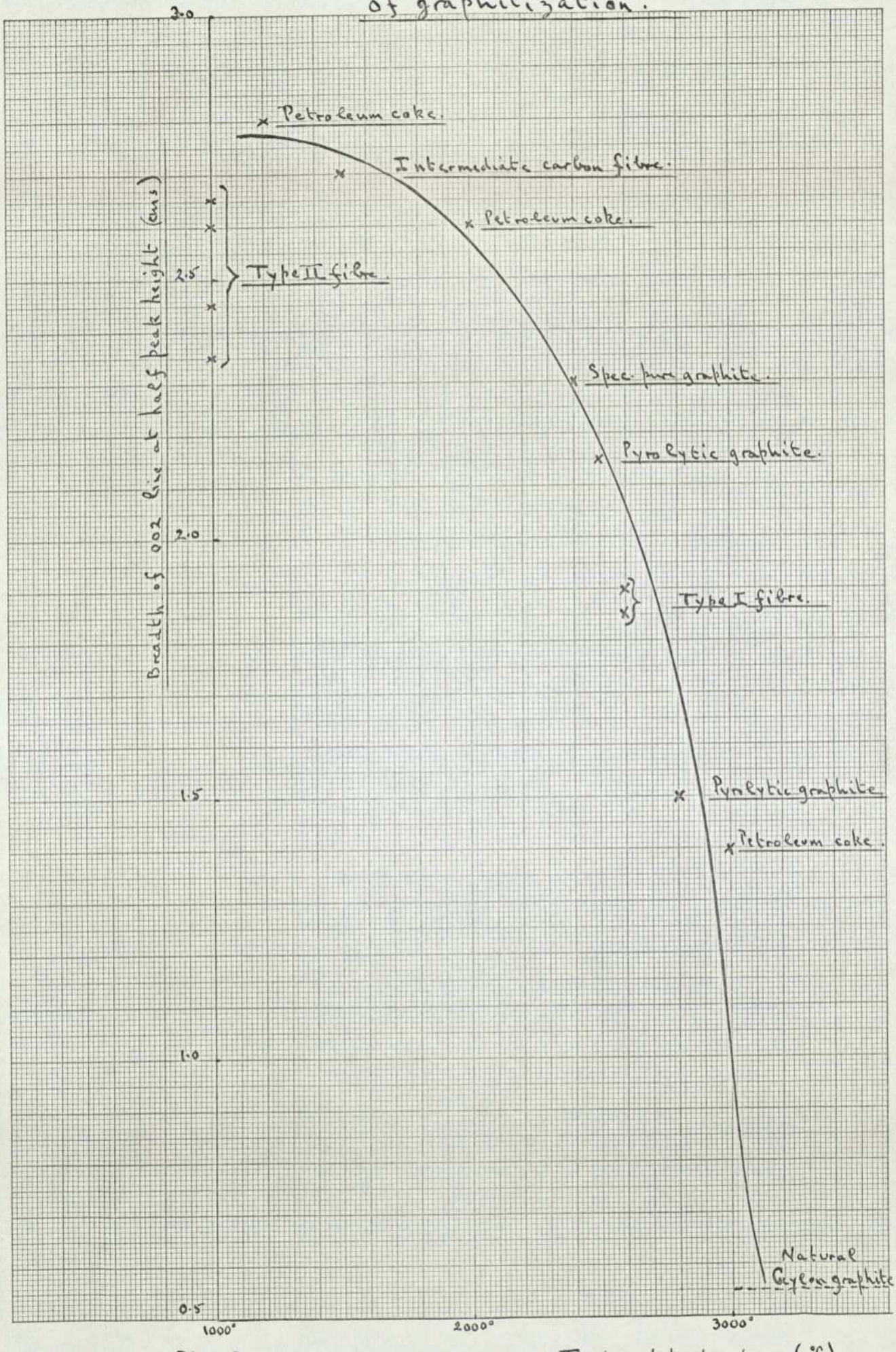


Fig. 21

It is of course appreciated that such an instrument can only be used for relative measurement and film exposure conditions must be kept constant, since a variation here, such as too great an exposure, would lead to a low signal level across the low impedance required to retain linear response. Linear accuracy of film traverse was found to be $\pm$ 0.1 mm.

Fig. 20 shows a trace of variations in light intensity through a powder pattern film of Type I carbon fibre, produced by the instrument described. Well defined peaks as light intensity decreased at 002, 101, 004 and 110 interplanar spacings, can be seen with the base line, of course, representing maximum light intensity through the film. To measure the 002 line width, the breadth of the line is defined here as the breadth B at half peak height I, where I is a line dropped from peak center to the line PQ joining the background curves on either side of the line. Then the area above the line PQ is proportional to the intensity of reflection corresponding to the 002 line.

The procedure described to estimate the 002 line width was followed for the various samples of graphitic materials and fibres available and a plot of 002 line width versus temperature of formation is given in Fig. 21. The relationship between line width and temperature is quite clear, one might say parabolic, and the two types of carbon fibre, now commonly in use, stand off the curve, but in correct relative position with respect to temperature. This is to be expected as the carbon fibre is not fully graphitized and not polycrystalline. It is also clear from Fig. 21 that differentiation between types of carbon fibre, should identification be lost, would be possible with this technique.

c. Identification of carbon fibre by electrical linear resistance

A more rapid separation of Type I from Type II fibre can be carried out by measurement of the resistance of a length of tow. Fig. 22 shows a

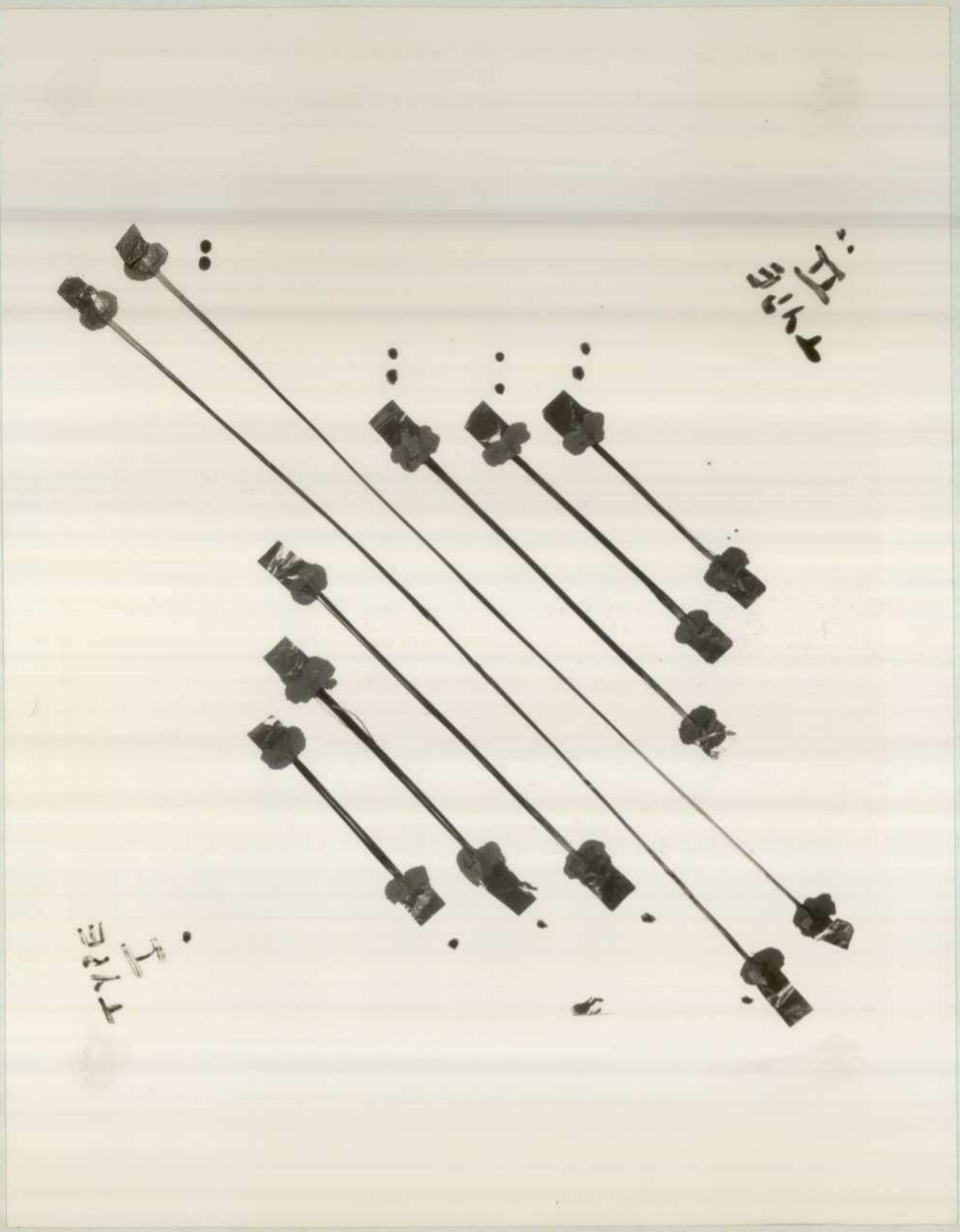


Fig. 22 Measurement of fibre linear resistance

TABLE 4

Resistance of Carbon Fibre Tow

No.	Length		Type I		No.	Length		Type II	
	Inches	Cms.	R/in	R/cm		Inches	Cms.	R/in	R/cm
1	13.7	34.8	0.44	0.17	5	13.6	34.5	0.92	0.36
2	5.6	14.2	0.45	0.18	6	5.5	14.0	0.91	0.36
3	3.4	8.6	0.47	0.19	7	3.5	8.9	0.97	0.38
4	2.3	5.8	0.43	0.17	8	2.5	6.4	1.00	0.39
Aver-age			0.45	0.18				0.94	0.37

set of lengths of carbon fibre tow, of both types, attached to copper tags at each end of the tow by means of alcohol DAG, (Deflocculated Acheson Graphite), the whole set on an insulating Perspex sheet. Linear resistances were taken with an Avometer, Model 7; at first through the copper end tags. These results however were very erratic and it was realized that resistances were taken, from the copper through the DAG seal to the fibre tow thus recording the resistance of the DAG seals.

Values taken by laying the probe direct to the surface at each end of a fibre tow, gave the readings shown in Table 4. These results give resistance per foot and per metre of Type I fibres as 5.4 Ω/ft and 18 Ω/meter respectively and for Type II fibre we have 11.3 Ω/ft and 37 Ω/meter. Thus a Type I carbon fibre is roughly twice as conductive as Type II, and such a difference is to be expected since Type I material is much more graphitic, and hence more conductive.

Owston[9], (1970), gives for single fibres, Type I 137 kΩ/meter and Type II, 691 kΩ per meter, or about a factor of 5 difference. He suggests that the high resistance recorded might be due to poor contact between the fibrils. Similarly for the rapid test given, variable contact between fibres may account for the lower factor of X2 difference between fibre types and could be due to test conditions which give a high resistance along fibre length, if out of contact with other fibres, or a reciprocal value for touching fibres throughout the 10,000 fibre bundle.

d. Relationship between tensile strength and fabrication history

From results collated from routine carbon fibre tests Goggin[10], (1968), using 20-25 single fibres per tow, measured the tensile strength and elastic modulus of single fibres and whole tows on an Instron Tensile Tester. He could find no relationship between tensile strength and weight per unit length, density or fibre diameter. His results are given in Table 5.

TABLE 5

Comparison of Tensile Strengths of Carbon Fibres

Number	Whole Tow Test Tensile Strength (psi x 10^3)	Single Fibre Test Tensile Strength (psi x 10^3)
1	245	237
2	275	236
3	262	198
4	241	161
5	244	198
6	192	217
7	300	304
8	177	262
9	274	207
10	216	195
11	252	195
12	162	191
13	220	195
14	181	156
15	163	208
Arithmetic Mean	224	211
Standard deviation	40.4	36.3
% Deviation from the Mean	18%	17%

For conversion to SI units 1 psi ≡ 6894.76 N/m^2

Effect on U.T.S. of Types I and II fibres, of oxidation time during fibre preparation. Single fibre tests.

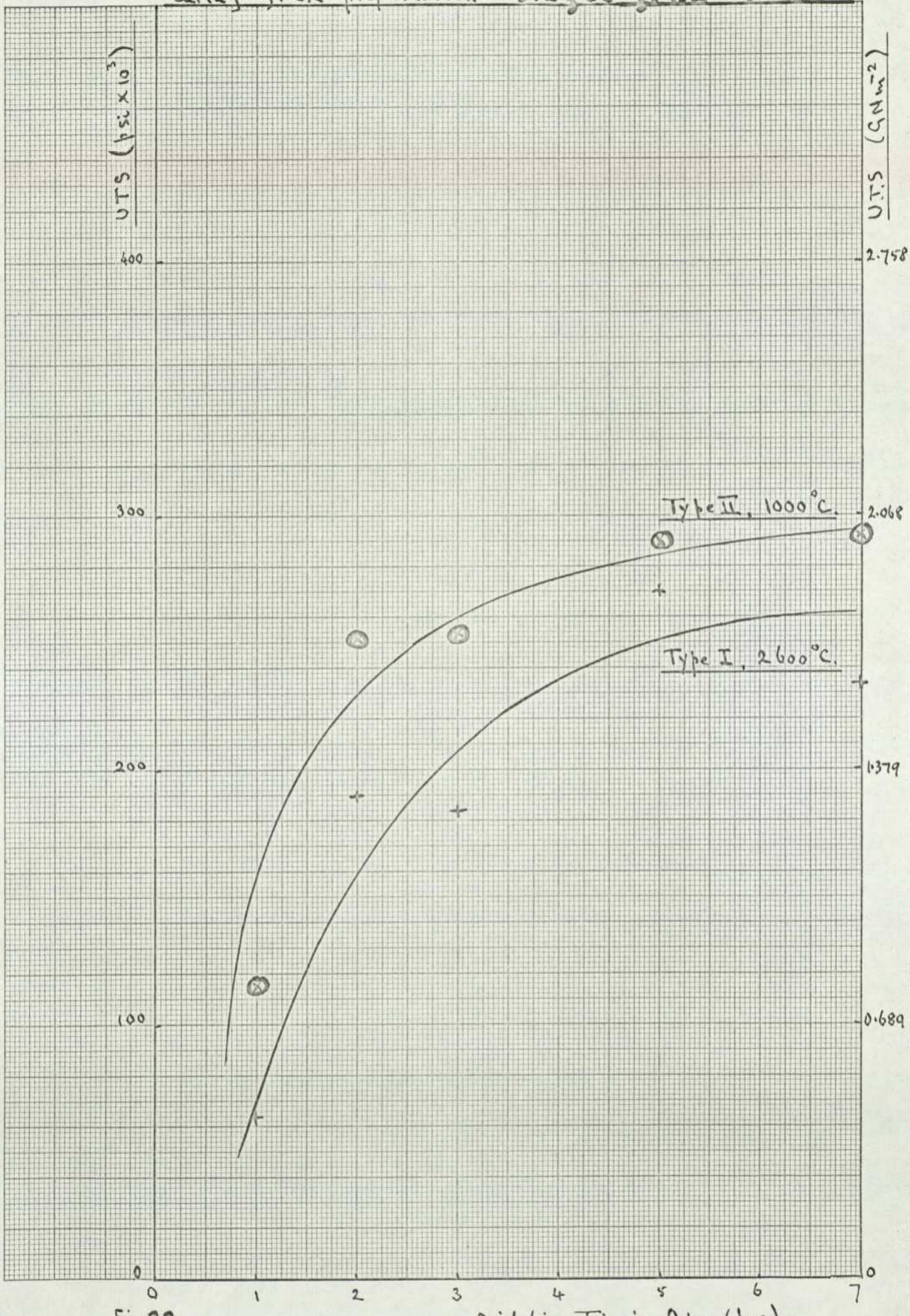


Fig 23

Effect on U.T.S of Type II fibre, of oxidation time during fibre preparation, showing single fibre test scatter.

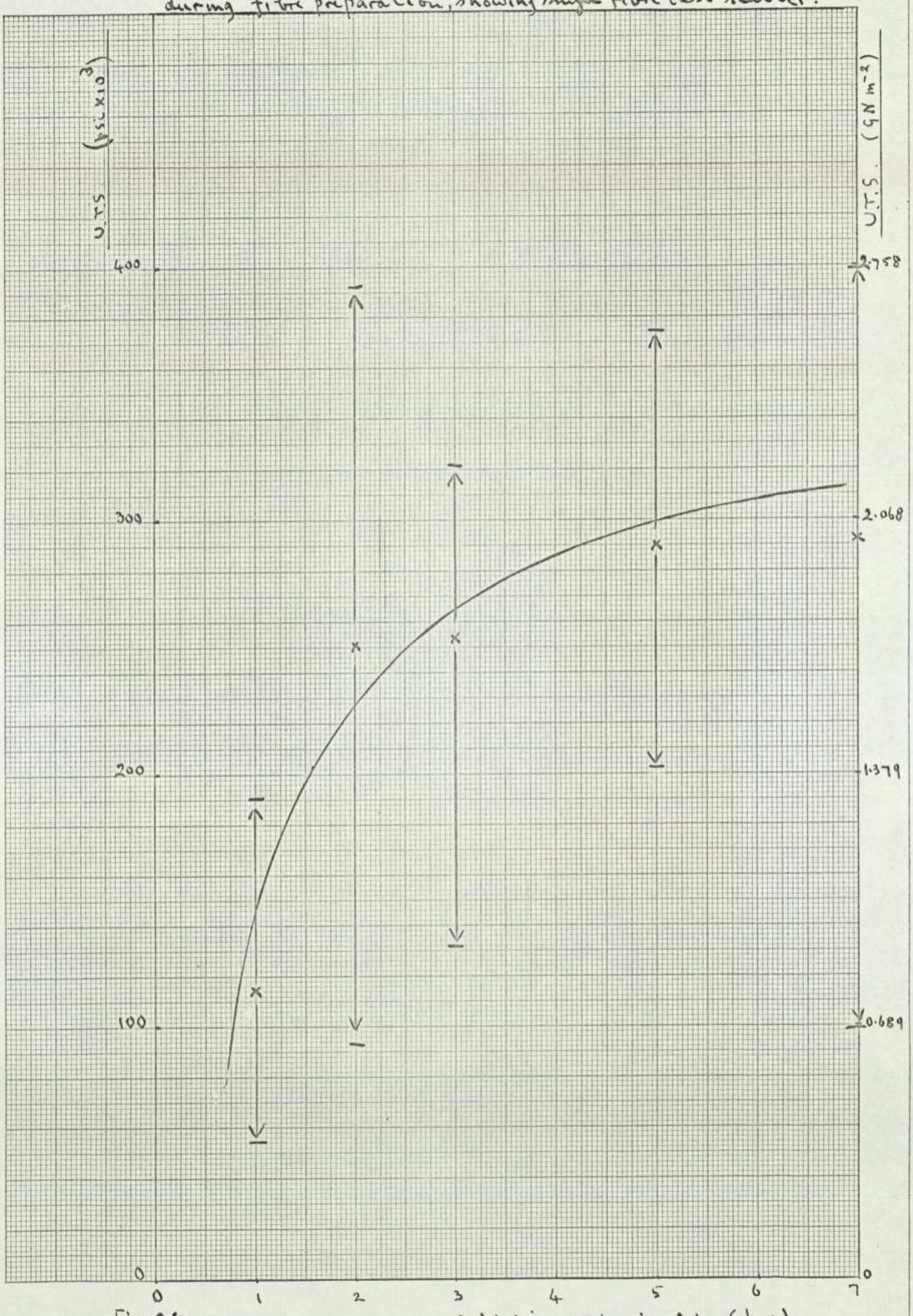


Fig. 24

Variation of U.T.S and Young's Modulus with temperature of fibre formation. Single-fibre tests

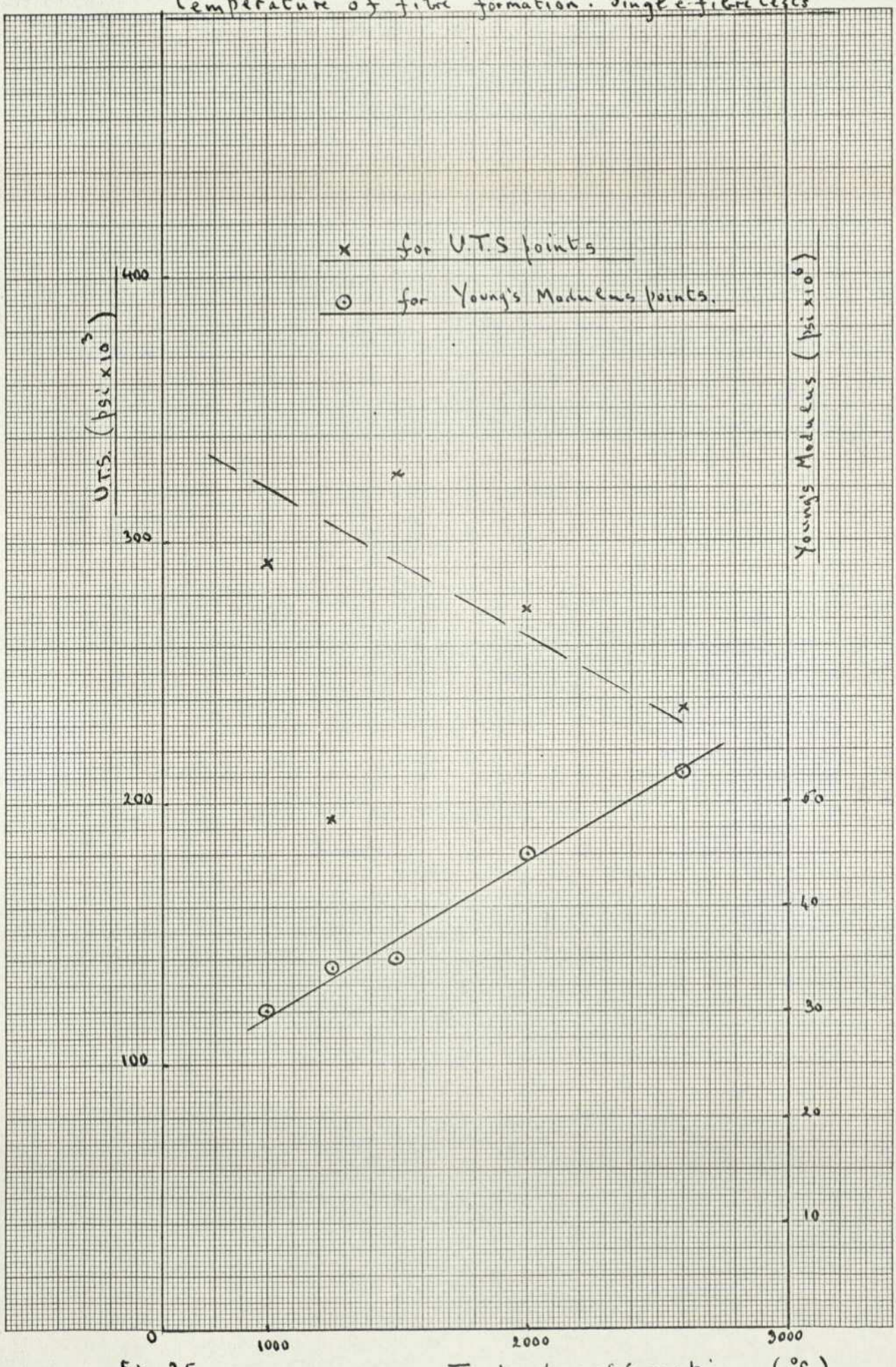


Fig. 25.

From these results Goggin concluded that whole tow testing was permissible and considerably faster than single fibre tests. This type of test has been adopted in this work.

From the test results on the standard test block of 5x5 carbon fibre specimens, also tested as single fibres by Goggin, (using 22-25 single fibres to strike a mean), a series of curves was drawn to show the effect of fibre fabrication history on the tensile strength and elastic modulus. Fig. 23 shows the trend of the variation of tensile strength with pre-oxidation time in air at 220°C, for both types of fibre, showing that increase of strength with oxidation time approaches constant values after about 7 hours.

Fig. 24 showing the variation of tensile strength with pre-oxidation time, for Type II again, highlights the high degree of scatter to be expected from individual single fibre test results, when samples are taken from batch to batch. If, however, the deviation of 20 tests from a single tow is studied we find that with single fibre testing the percent deviation from the mean is not more than 3% and for whole tow tests, from the same batch, the corresponding figure can vary from 5-15%.

Figure 25 shows tensile strength and elastic modulus measured for single fibres, as a variation of temperature of formation, after a fixed 7 hr. pre-oxidation treatment. The tensile strength is vaguely decreasing but a definite positive increase of modulus with temperature is clear. Reasons for the poor definition of the tensile strength curve may well be due to variations in cross-sectional area, density, gauge length etc., as given in Section 1c. An average value of Young's modulus can be taken direct from the curve, with a correction for machine "softness factor" as described in Appendix 2. Further causes of variations in both parameters will be discussed later.

Some idea of the probable thickness variations likely to occur along the length of any carbon fibre is given in Fig. 26 which shows representative

Fibre profiles, assuming spherical cross-section.

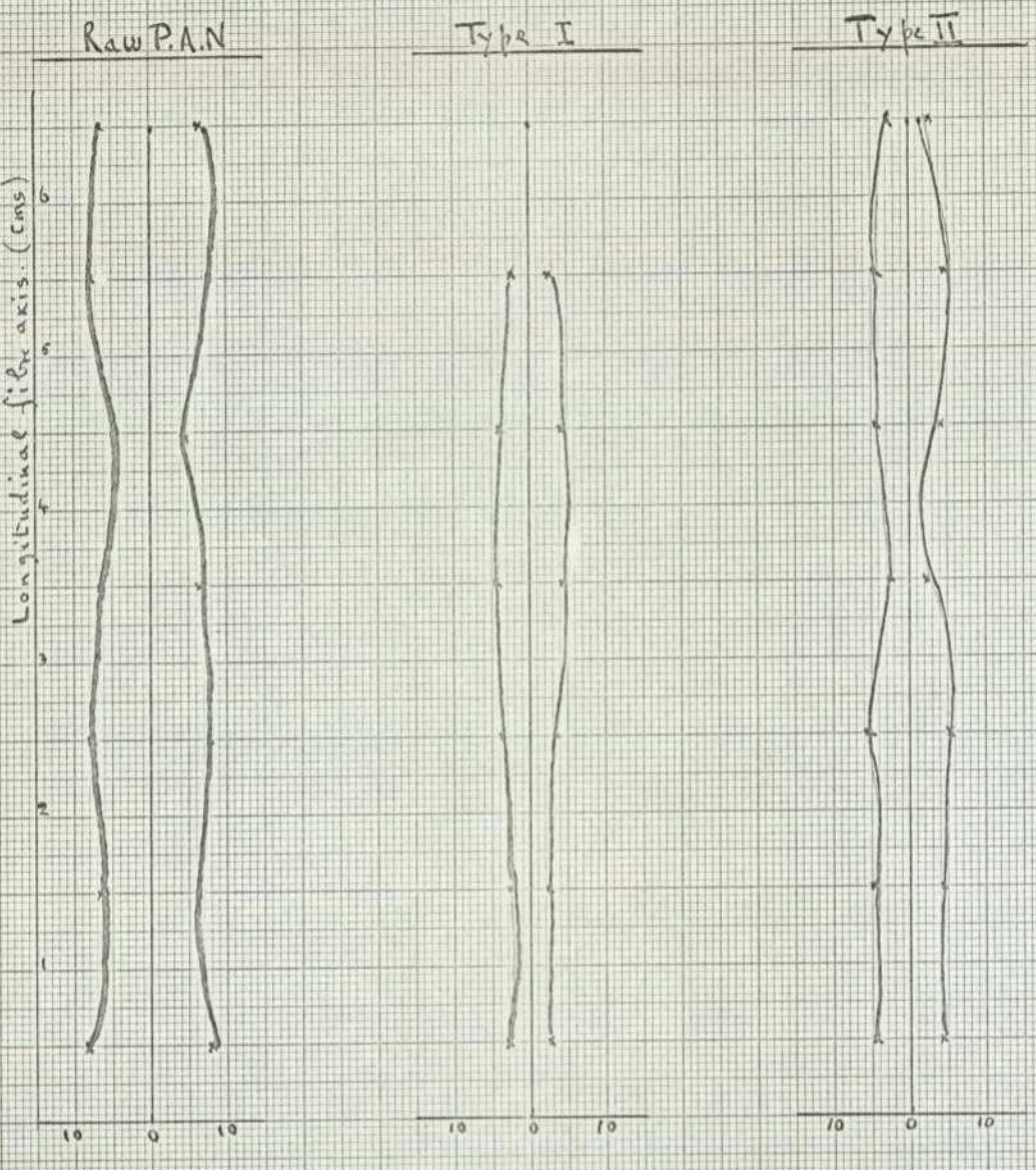


Fig. 26.

profiles of fibre diameter at any given point. For comparison similar variations in Courtauld PAN fibre are given.

e. Summary of results

After comparison of the structure of the various materials the increase in graphitization with temperature is shown. Methods are given for estimation of 002 line width by simple X-ray densitometry and these results are correlated with temperature of formation of graphitic material. They also provide means of fibre type identification as do the electrical resistance measurements given, showing Type I, the higher temperature fibre, with a linear resistance smaller by a factor of 2 than the low temperature fibre, Type II. Finally comparisons are made between effects of history of formation of fibre with strength and modulus.

References 2

2.1 Flint, O., AERE Report 5171, 1966.

2.2 Beynon, C. E., The Physical Structure of Alloys, Edward Arnold, 1946.

2.3 A.S.T.M. Indis, X-Ray Powder Data File, 1960.

2.4 Bacon, G. E., AERE M/R 2702, 1958.

2.5 Franklin, R. E., Roy. Soc. Proc. 209A, 196-218, 1951.

2.6 Fair, F. V., and Collins, F. M., Proc. 5th Carbon Conf. Pen. State Univ. Vol, June Pergamon, 1961.

2.7 Tarpinian, A., Tech. Rep. No. W.A.L.T.R. 825, 5/1, Watertown Arsenal, Waterbury, Mass., 1961.

2.7a Nightingale, 1962. See Ref. 1.25.

2.8 Watt et al, (1966), See Ref. 1.27.

2.9 Owston, C. N., J. Phys. D., Vol. 3, No. 11, Nov. 1970.

2.10 Goggin, P. R., H.C.F.W.P.(68), P.11, 1968.
and Wells, H., Colclough, W. J. and Goggin, P. R., A.E.R.E. R-6149, 1969.

CHAPTER 3

Preliminary work on metal deposition by chemical reaction

3.1 Deposition from the vapour phase

The deposition of metals by processes which depend ultimately on the production of a vapour phase at the substrate metal surface, has been carried out for many years. An early example of deposition from a metal vapour, used in industry, was that of Michelin[1], (1911), who coated iron with zinc by heating the basis metal to about 400°C in contact with a reducing mixture of zinc oxide, carbon and an alkaline carbonate, to act as a flux:

$$2\langle ZnO\rangle + \langle C\rangle \rightleftharpoons 2\langle Zn\rangle + \langle CO_2\rangle \qquad \ldots (11)$$

With reference to the transport of solids by vapour phase reactions, Mandel[2], (1961), in a review article, states:-

> ".... it has been shown by Schafer et al[3], (1956), that various solid substances, e.g. Cu, Cu_2O, Fe_2O_3, Ge and Si, may be transported through the vapour phase in the presence of a temperature gradient under relatively mild conditions provided that a reactive gas such as a halogen or hydrogen halide is present. It was suggested by these authors that the basis for this transport was the rapid establishment of an equilibrium between the solid substance and the reactive gas, hereafter referred to as a 'vapour solvent', e.g:
>
> $$\langle Cu_2O\rangle_s + 2(HCl)_g \rightleftharpoons 2(CuCl)_g + (H_2O)_g \qquad \ldots (12)$$
>
> Diffusion of the gaseous reaction products into a temperature region in which the equilibrium constant for the above reaction was lower than at starting point then results in deposition of the solid substance: Cu_2O in the above example. Thus if the net enthalpy change is ΔH and positive, it would be expected that transport would proceed from the hotter zones to the colder ones, and vice-versa."

The mass transfer for the reaction given in Eqn. (12) may be better understood if the free energy of the reaction is considered in relation to both a temperature gradient and the geometry of the system.

Consider a reaction tube having a rising temperature gradient in the direction A → B and consider zone A containing solid Cu_2O and HCl gas:

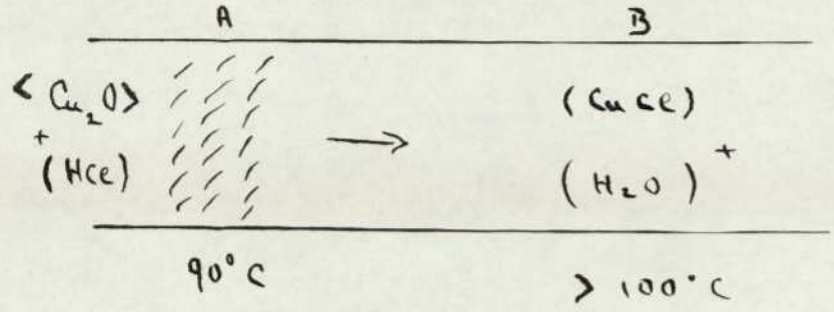


Fig. 26a

Then, at A, below 100°C solid CuCl and liquid H_2O would be formed since, as a first approximation, the free energy change ΔG in the reaction shown by Eqn. (12) would be -23 kilocals/mole and the reaction would be:

$$<Cu_2O> + 2(HCl) \longrightarrow 2<CuCl> + (H_2O)$$

As the temperature at A rises, above 100°C, the solid CuCl formed would become gaseous and so would the water and these would diffuse outwards along the tube to the increasingly hotter zone B, but ΔG for these products, when gaseous, is +76 kilo cals/mole and the reaction therefore would reverse thus:

$$<Cu_2O> + 2(HCl) \longleftarrow 2(CuCl) + (H_2O)$$

with deposition of solid Cu_2O in the hotter zone B.

(For conversion to SI units 1 kilo cal/mole is equivalent to 4186.8 Joules/mole.)

Deposition of Cu, in the presence of a halogen was confirmed by Flint[4], (1963), provided that reactants are at the appropriate concentrations:

$$2<CuO> + 4(HBr) \rightleftharpoons 2(CuBr_2) + 2(H_2O) \quad \ldots (13)$$

$$(CuBr_2) \rightleftharpoons <Cu> + (Br_2) \quad \ldots (14)$$

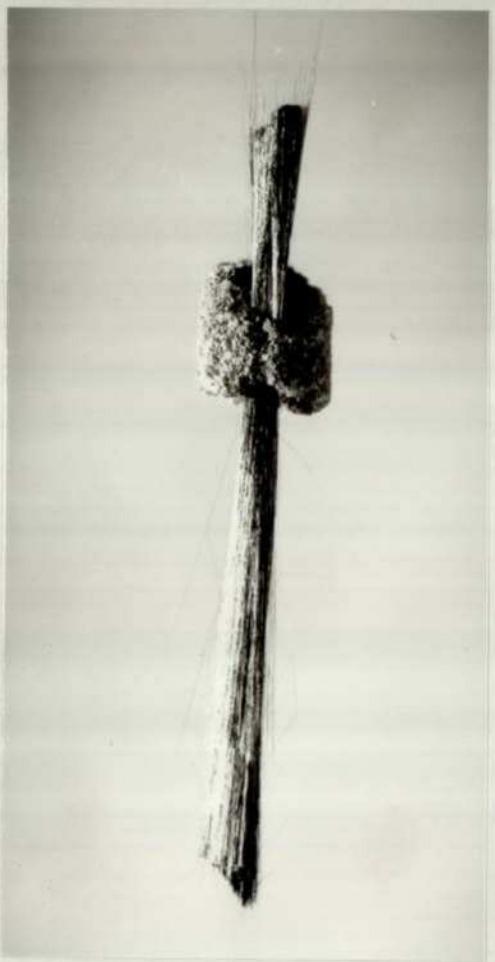


Fig. 27 Sintered aluminium powder on carbon fibre tow. X3

Although it was realized that carbon fibre was likely to play little or no chemical part in any vapour phase reaction, as would, say, a reactive metal surface, the fibre surface might provide a reducing zone and allow metals in the vapour phase to nucleate, for example on an initial layer of the appropriate carbide.

3.2 Experimental detail

Samples of carbon fibre were encapsulated in an 18" long, $\frac{1}{2}$" diameter Pyrex tube, with 1% by weight of $CuBr_2$ to provide a source of clean, dry bromine, as in equation 14, and covered with various metal powders, viz:

1. Aluminium
2. 75% aluminium + 25% zinc
3. Magnesium
4. 25% magnesium + 75% aluminium
5. 50% magnesium + 50% aluminium

These tubes were evacuated to a pressure of 10^{-5} mm Hg (1 mm Hg ≡ 1 torr ≡ 133 Nm^{-2}) and heated to 500°C, for 4 hours, in a furnace, with 9" of tube exposed to the air to provide a thermal gradient. Any deposits found were mounted in Bakelite mounting powder, ground and polished under paraffin, to avoid electrochemical action, which would take place if water were the lubricant, photographed and examined.

3.3 Results observed

Run 1. Aluminium

No coverage of fibre with Al took place, which was to be expected since the vapour pressure of aluminium is < 10^{-11} mm Hg at 500°C, but active bromine might have penetrated the thick oxide skin always present on Al powder, and allowed some transport to take place but no reduction of the $AlBr_3$ would occur due to carbon. The Al powder did however sinter, as can be seen in Fig. 27, but with no adhesion to the fibre bundle, which could be pulled out of the metal pack with ease. Fig. 28, a micro-section of the pack, shows holes in the Al sinter due to this pull-out.

Vapour phase deposits on carbon fibre

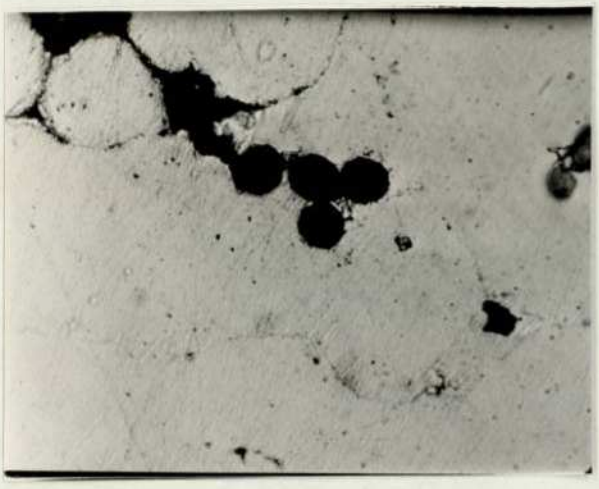


Fig. 28 Aluminium. X750



Fig. 29 Al, 75%-Zn, 25%. X750

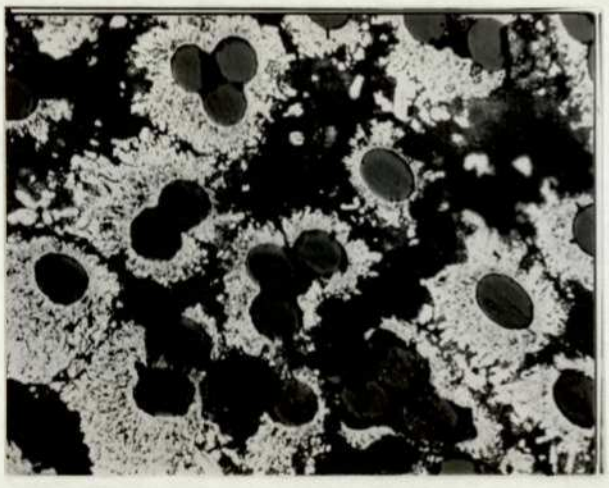


Fig. 30 Magnesium. X750



Fig. 31 Magnesium, showing corrosion spots upper left. X750



Fig. 32 Magnesium. X750

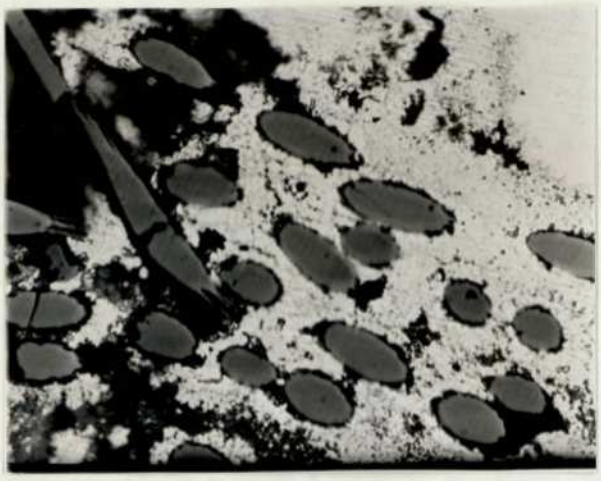


Fig. 33 25% Magnesium - 75% aluminium (w/w). X750



Fig. 34 Al/Mg, 50-50 mixture X750

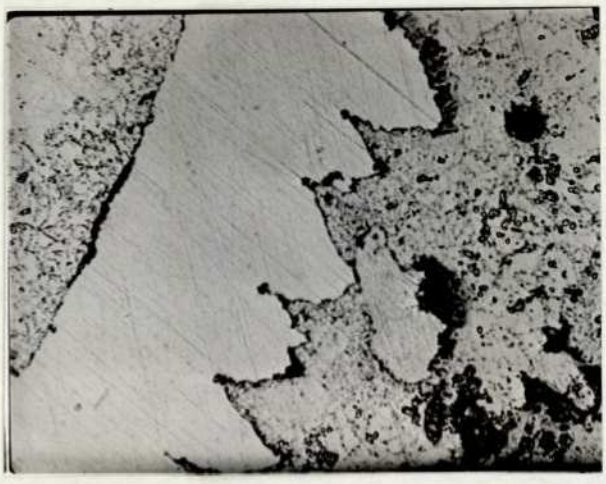


Fig. 35 Structure of Al/Mg alloy X1250

Run 2. 75% aluminium - 25% zinc

In this case a few outside fibres in the tow were covered with a metal deposit of some indeterminate alloy but there was no deposition in depth. Fig. 29 shows a few isolated fibres in the alloy deposit.

Run 3. Magnesium

Here 0.1 ml of the volatile organic chloride in the form of CCl_2-C-HCl, trichlorethylene was also added to the reaction tube, to promote the reaction. Some coverage, of a powdery nature took place, as can be seen in Fig. 30. The deposit, however, was so reactive, being a galvanic couple of carbon with magnesium i.e. elements at opposite ends of the electromotive series; that rapid corrosion occurred whilst taking the polished specimen to the microscope, due to reaction with the natural humidity of the air. The polished surface could be seen to effervesce under the heat of the microscope lamp system. Fig. 31 shows corrosion vacancies in the upper left of the picture, also ellipsoidal fibres due to an acute angled section to the fibre axis. Fig. 32 shows a magnesium deposit from a run using only one halide, $CuBr_2$, and although a little coverage can be seen, most of the tow remained unplated.

Run 4. 25% Magnesium + 75% aluminium

In this run too much aluminium powder was used and only a powdery sinter was formed. Fig. 33 shows the sinter and it can also be seen that the metals never quite touch the fibre.

Run 5. 50% magnesium + 50% aluminium

Here some alloying took place but deposition was poor, as can be seen in Fig. 34. That alloying occurred can be seen in Fig. 35, which at higher magnification shows the growth of a band of magnesium rich material with a saw-toothed edge into the sinter pack. That the material was Mg rich was indicated by the more vigorous corrosion observed in this area. In all cases both adhesion and coverage was poor, whilst the corrosion of the magnesium deposits was excessive, estimated at an order of

magnitude greater than for Mg alone. It has been reported by Peakall[5] et al, (1970), that aluminium/carbon fibre composites also had a corrosion enhancement, by a factor of 3-6, over and above the pure metal.

In view of these results it was felt that further work on deposition from the vapour phase would be unprofitable. It must be pointed out however that very good deposits of aluminium, from tri-isobutyl aluminium, can be made, (Holmes et al[6], 1969), using a process described by Crosby[7], (1962).) Here triisobutyl aluminium is decomposed thermally, carried by a stream of argon over the substrate:

$$Al(C_4H_9)_3 \overset{260^oC}{\rightleftharpoons} Al + 1\tfrac{1}{2}\,H_2 + 3C_4H_8 \qquad \ldots (15)$$

The aluminium compound however is toxic, carcinogenic, pyrophoric and explosive and should be treated with great respect.

3.4 "Electroless" deposition

Nickel and cobalt can be deposited in coherent films on non-conductors or chemically inert surfaces, by chemical reduction, as was discovered by Roux[8], (1916), and developed by Brenner[9], (1954). The principal reaction in the process is the reduction of the appropriate chloride with sodium hypophosphite, under pH control:-

$$NaH_2PO_2 + H_2O \rightleftharpoons NaH_2PO_3 + H_2 \qquad \ldots (16)$$

$$NiCl_2 + NaH_2PO_2 + H_2O \rightleftharpoons Ni + 2HCl + NaH_2PO_3 \qquad \ldots (17)$$

Surface activation by pre-dipping in a solution of 10% $SnCl_2$ + 5% HCl may be necessary to start the deposition process.

Copper may be deposited by reduction of ammoniacle copper sulphate with hydrazine sulphate, a process used for coppering mirrors and glass Dewar vessels, discovered by Eyber[10], (1927). The reaction depends on the powerful reducing properties of the hydrazines:

Fig. 36 Electroless nickel plated carbon fibre

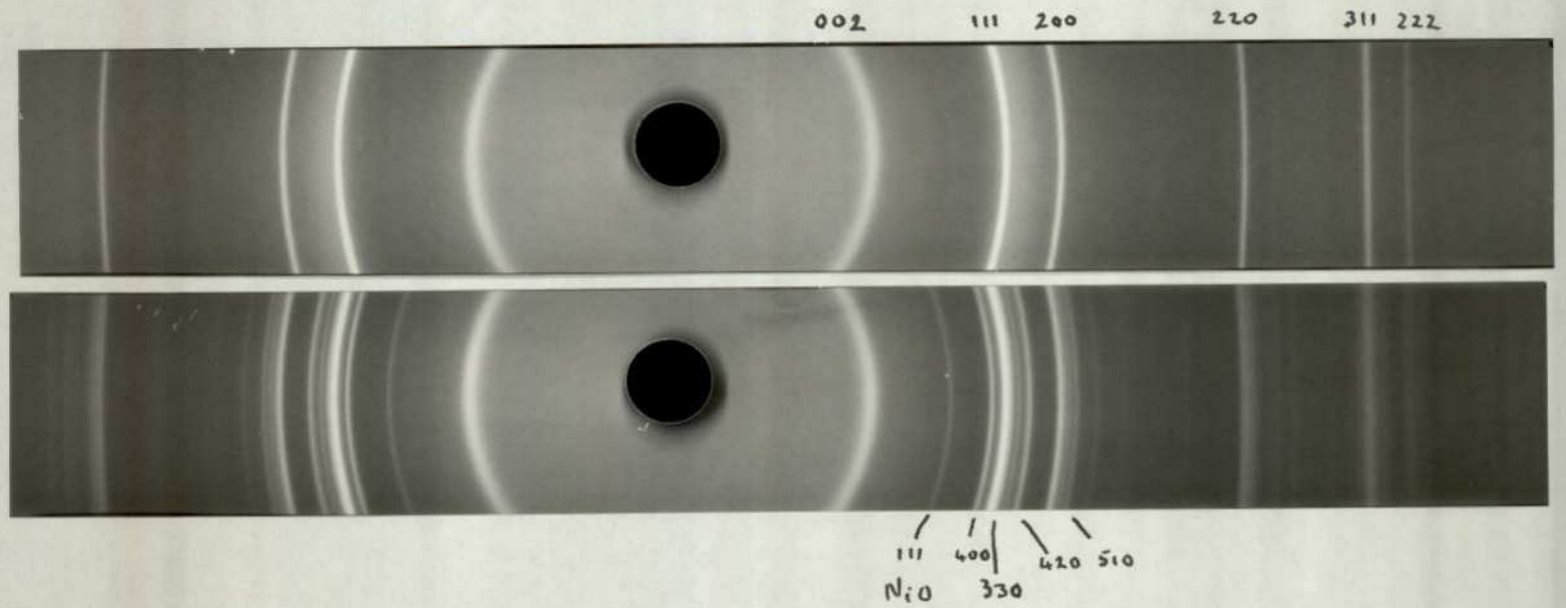


Fig. 37 Annealed electroless nickel plated carbon fibres

$$N_2H_4 + 2HX \rightleftharpoons N_2H_4HX + HX$$

$$\rightleftharpoons N_2H_5^{\cdot} + H^{\cdot} + 2X' \quad \ldots (18)$$

$$4CuO + N_2H_4 \rightleftharpoons 2Cu_2O + 2H_2O + N_2 \quad \ldots (19)$$

$$2Cu_2O + N_2H_4 \rightleftharpoons 4Cu + 2H_2O + N_2 \quad \ldots (20)$$

Both nickel and copper were deposited by Brenner's "electroless" technique, as described by Flint[11], (1964), a copy of the relevant report being included, as Appendix 5. For comparative purposes samples of tow were also electroplated for 30 mins at 2.2A/sq.dcm ($A/10^{-2}m^2$), 60° in a Watts nickel bath and a copper sulphate batch. The "electroless" nickel and copper deposits and the electroplated controls were also annealed at 700°C, for 4 hours in argon, to determine whether their relevant X-ray powder patterns showed a state of stress and whether this was relieved by subsequent annealing.

After these treatments the plated fibre tows were ground to a powder and X-ray powder diffraction pattern photographs taken. (See Appendix 3). These were compared with powder patterns of their respective metals. To relieve the eyestrain which invariably accompanies the analysis of large numbers of X-ray powder pattern negatives, a powder pattern scanner, described in Appendix 4, was used.

3.5 "Electroless" plating results

A comparison between a powder photograph of "electroless" nickel and the annealed deposit on carbon fibre is shown in Figs. 36 and 37. Fig. 36 shows five of the characteristic lines for nickel with the strong 002 line for the carbon fibre substrate. After annealing, these lines again appear, together with the 111 line for nickel oxide, as seen in Fig. 37 and the 400, 330, 420 and 510 lines for nickel phosphide, Ni_7P_3,

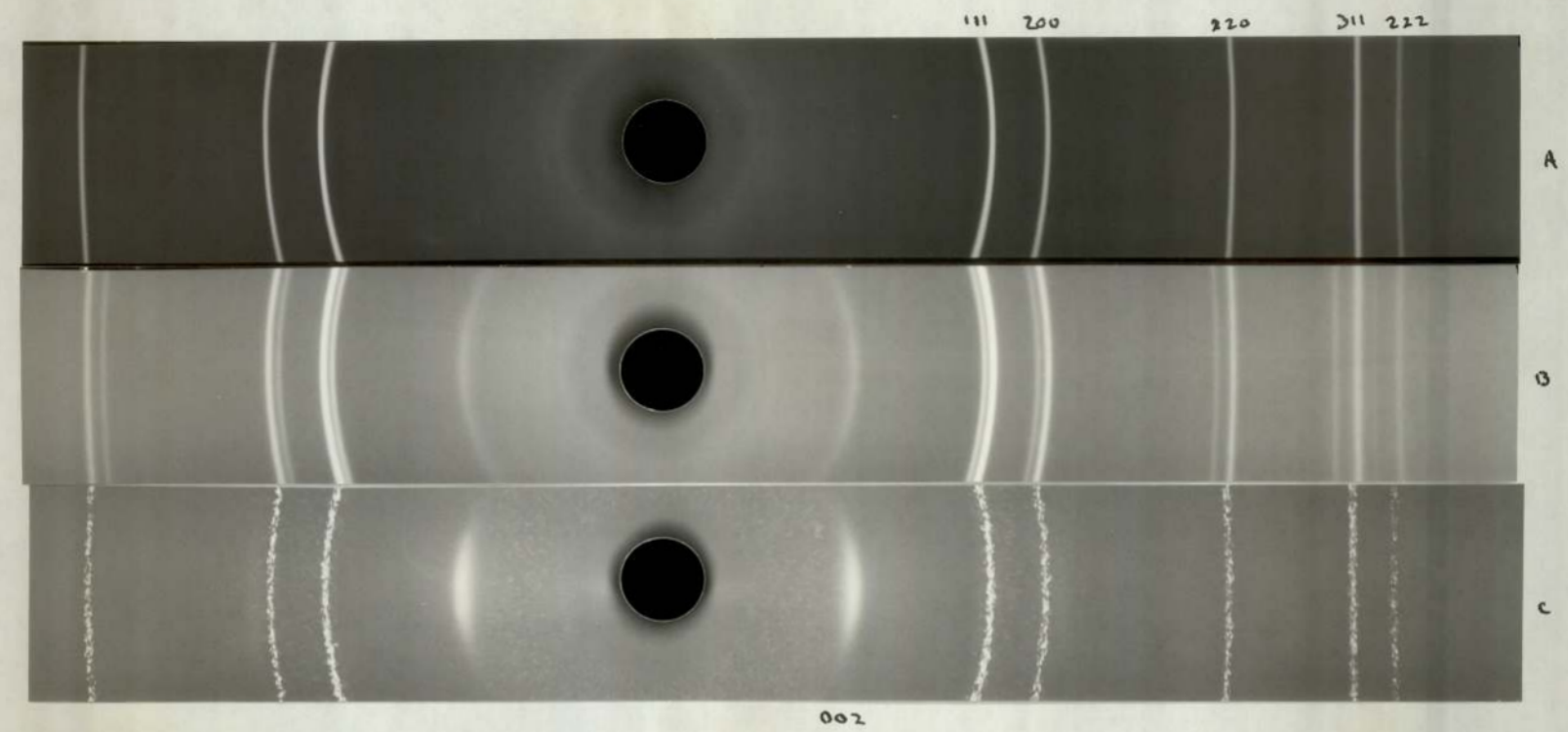


Fig. 38 Powder patterns of A, nickel, B, nickel plated carbon fibre, and annealed nickel plated carbon fibre (longitudinal)

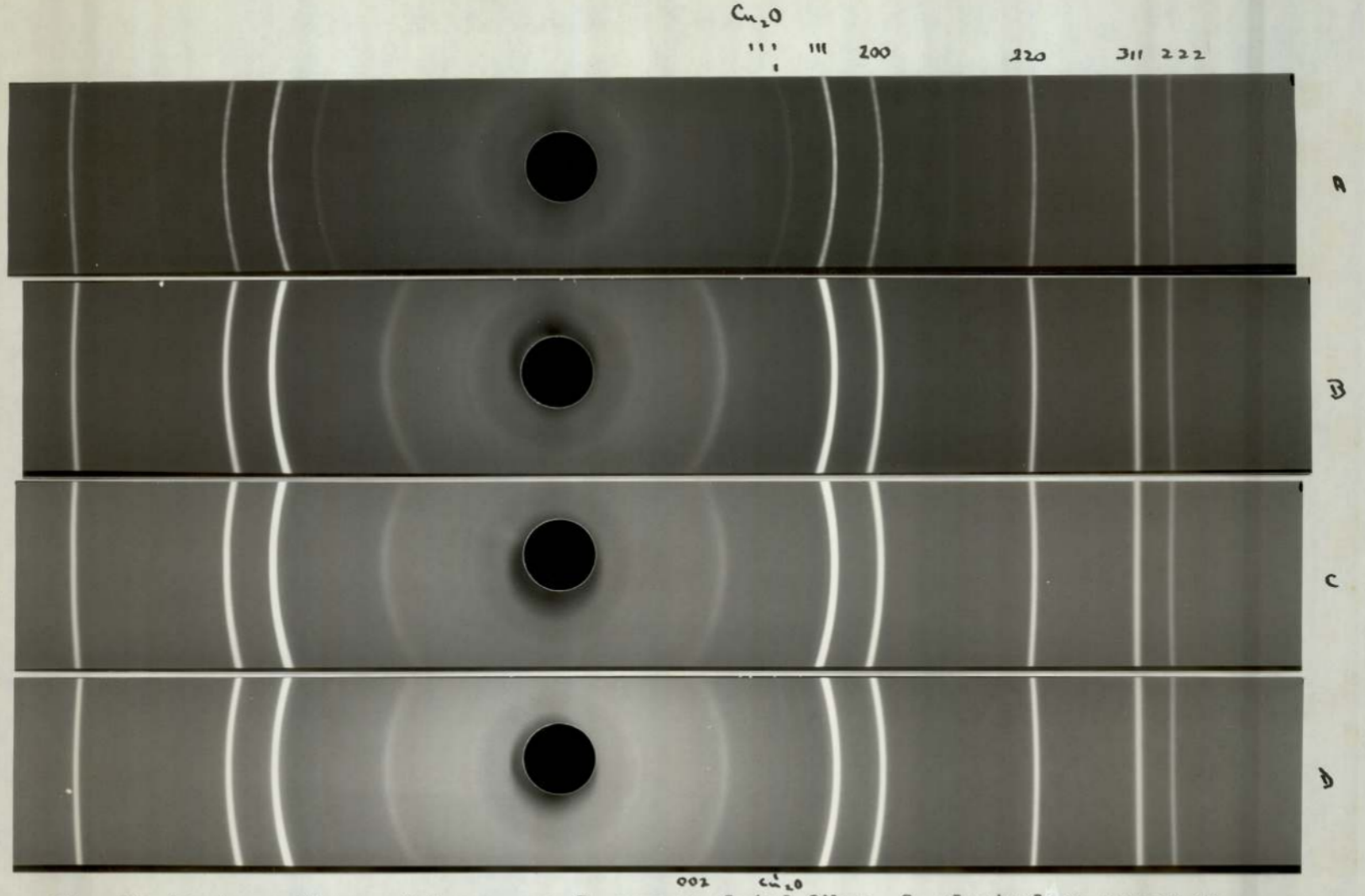


Fig. 39 Powder patterns of A, copper, B, copper plated fibre, C, electroless copper on fibre and D, annealed electroless copper on fibre.

(see Table 6), which precipitates from solid solution on annealing.

The appearance of the phosphide is to be expected since chemical analysis of the deposit shows up to 8% phosphorus; a strong line for nickel oxide, after thermal treatment, is also quite reasonable.

Fig. 38 shows a comparison between the powder patterns of close packed hexagonal nickel powder (by chemical reduction), A, nickel plated carbon fibre, B, and the annealed plated fibre. No sign of stress is shown by displacement of the nickel lines in B, but C shows that recrystallization of the deposit took place during annealing at 700°C with the formation of large grains, giving the characteristic granular pattern. The duplex pattern in B is due to the close juxtaposition of the background lines of the fibre substrate.

In the case of the copper deposits, shown in Fig. 39, no significant difference can be seen between the face centered cubic pattern of powdered copper and the electro-plated, "electroless" plated or annealed "electroless" deposit other than the appearance of the 002 carbon fibre substrate line and the Cu_2O, 111 line in the powder pattern of both the elemental copper and the annealed "electroless" deposit. This is quite normal since in the first case copper powder is always heavily oxidized and in the second case some oxidation may take place during annealing.

During "electroless" plating of fibre, the very vigorous effervescence, of either hydrogen or nitrogen (as the hypophosphite or hydrazine reduces the nickel or copper salts respectively), leads to massive tangling of the fibre tow, (as it moves about in the solution) and for this reason, although penetration and coverage is good, the process cannot be used since subsequent tensile testing becomes impossible, there being no portion of the fibre tow left straight enough for even a short gauge length.

TABLE 6

Data for Nickel Phosphide Powder Pattern

Cubic	Ni_7P_3	FeK_α
dÅ	I_1/I_o	h k l
3.06	40	2 2 0
2.73	40	3 1 0
2.31	60	3 2 1
2.16	70	4 0 0
2.04	60	3 3 0
1.93	70	4 2 0
1.84	100	3 3 2
1.70	40	5 1 0
1.53	20	4 4 0
1.37	20	6 2 0
1.28	60	6 3 1
1.22	60	5 5 0
1.20	80	6 4 0
1.14	60	7 3 0
1.10	100	7 3 2
1.08	60	8 0 0
1.07	80	8 1 1

Because of these results it was decided to investigate thoroughly the more controllable process of electro-deposition of copper onto carbon fibre, since the physical parameters and plating variables for this metal are quite well known.

References 3

3.1 Michelin, A. J., British Patent 16294, 1911.

3.2 Mandel, G. J., Phys. Chem. Solids, Vol. 23, 587-598, June, 1962.

3.3 Schafer, H. et al. Z. Anorg. Chem., 286, 27, 1956.

3.4 Flint, O., 1963 See Ref. 1.38.

3.5 Peakall, A. K., and Antill, J. E., AERE R-6364.

3.6 Holmes, E., Harris, S. J., Baker, A. A., Carbon Fibre Meeting, Univ. Nottingham, October 1968.

3.7 Crosby, J. J., Tech. Proc. Am. Electroplaters Soc., 49, 133-9, 1962.

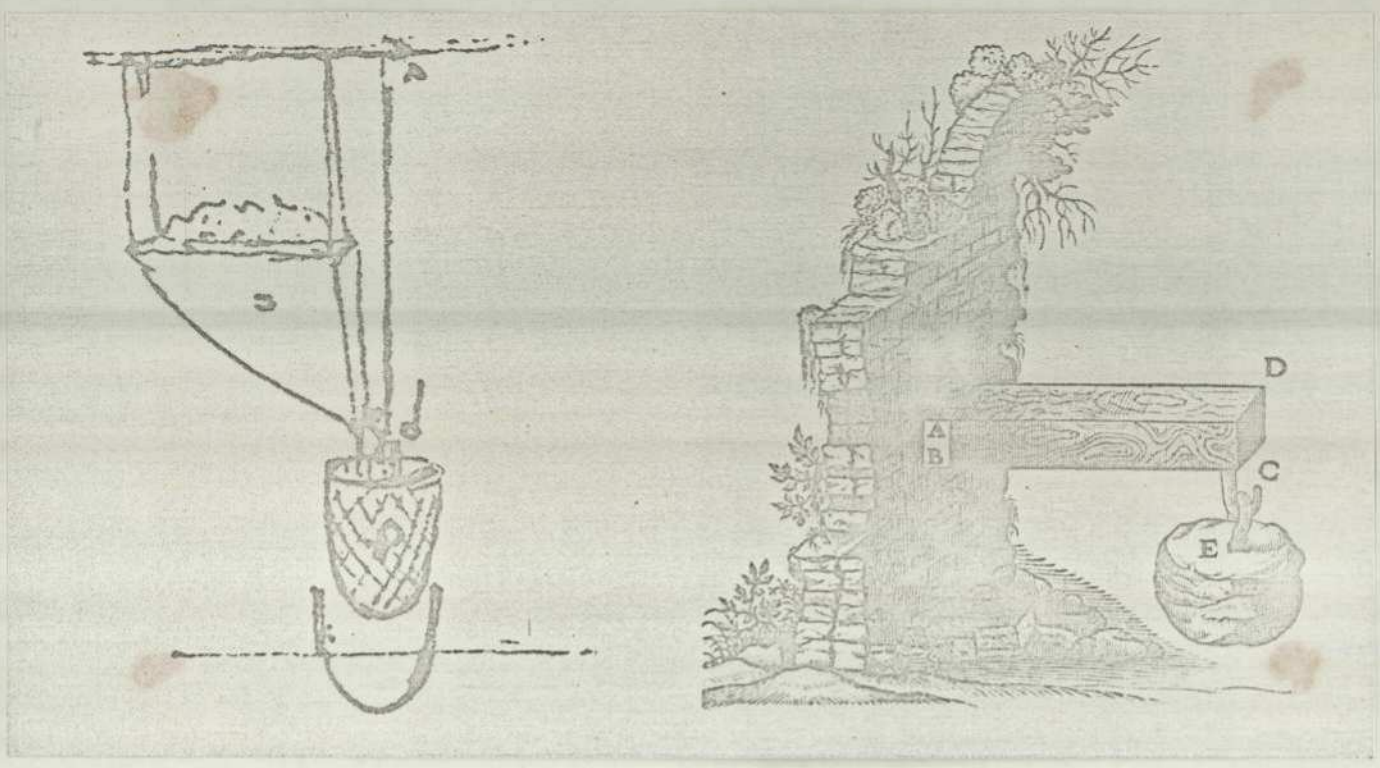
3.8 Roux, F. A., U.S. Patent 1, 207, 218, 1916.

3.9 Brenner, A., Metal Finishing, Westwood, N. J., Nov-Dec., 1954.

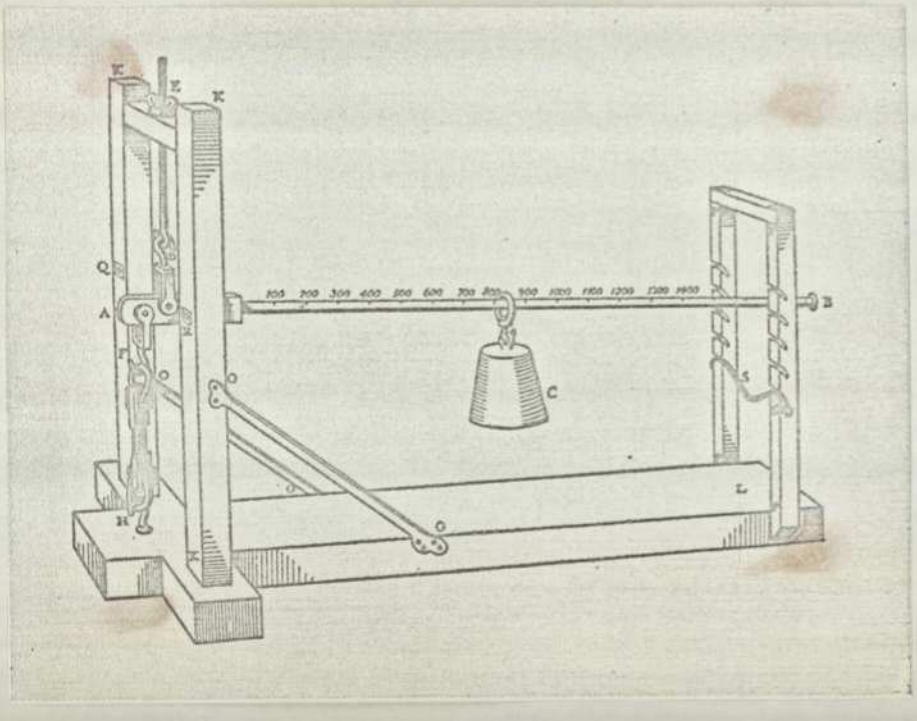
3.10 Eyber, G. Chem. Ztg, 51, 4, 1927.

3.11 Flint, O., A.E.R.E. M1508, 1964.

3.12 Flint, O., A.E.R.E., M2063, 1968.



A B



C

Fig. 39a Tensile testing - old style

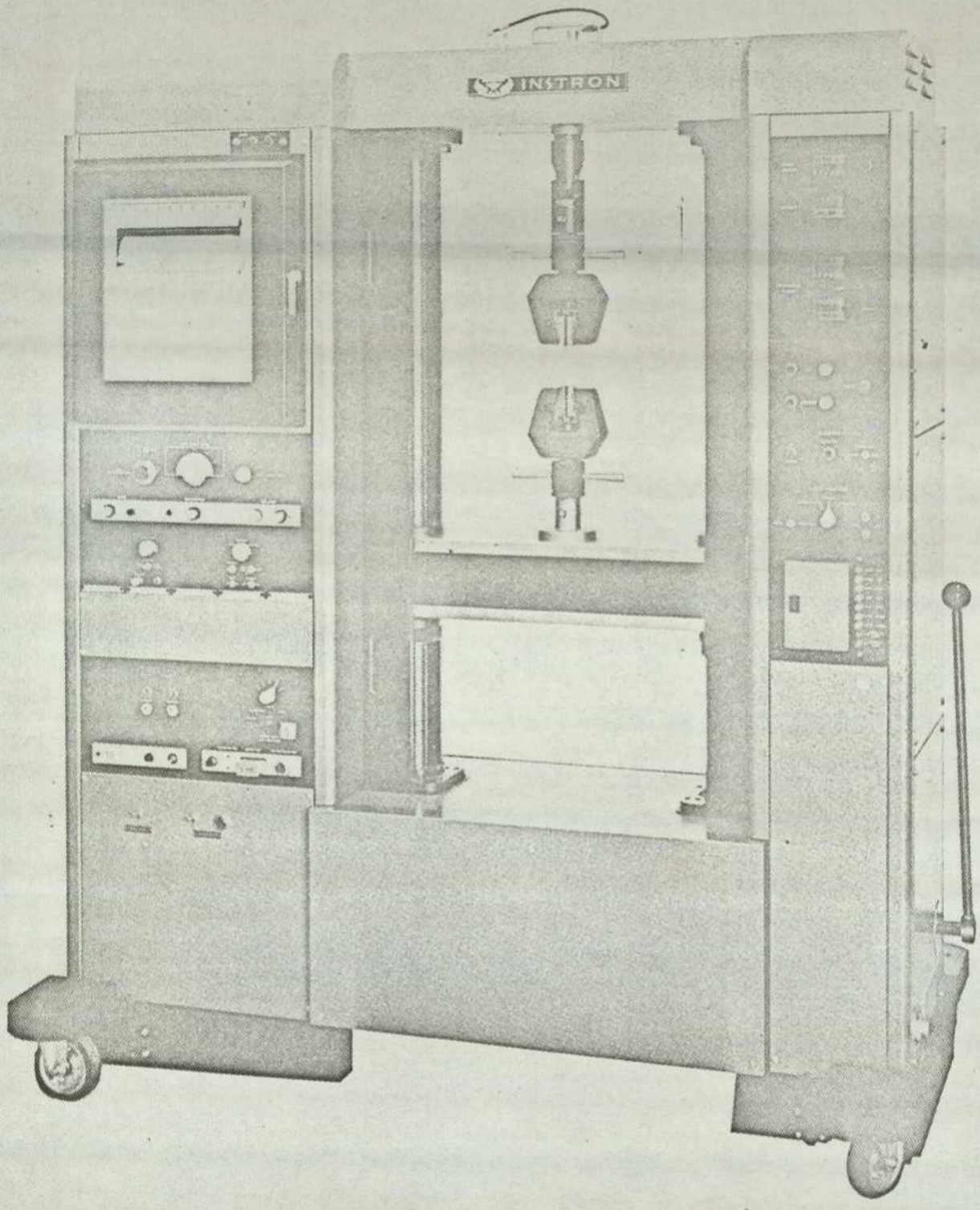


FIGURE 4-- Instron Universal Testing Instrument, floor-model (TT-D)

CHAPTER 4

Whole Tow Tensile Testing

4.1 Introduction

In order to measure the strength of the plated material and so monitor one's progress it is necessary, of course, to have an instrument, apparatus or machine stronger than the specimens, with the technique quantized in some manner. Leonardo da Vinci[1], (1452-1519), solved this problem, for wire testing, by the sand-hopper technique, shown in Fig. 39a,A and Galileo Galilei[2], (1638), treated the strength of materials mathematically, evolving 17 propositions relating to the fracture of beams etc., (Fig. 39a,B).

Later, after Robert Hooke's work on elasticity, Pieter van Musschenbroek[3], (1729), tested the cohesion of solid bodies on the tensile testing machine shown in Fig. 39a,C.

It was from these lines of thought that the modern tensile testing machine has evolved.

4.2 Experimental detail

To follow the progress of experimental work on copper electrodeposition onto the carbon fibre tow, in a quantitative manner, it was decided to measure the tensile strength of the plated tow on an Instron machine, as shown in Fig. 40.

To determine whether such an instrument would be suitable for test pieces of bundled material rather than the traditional "dog-bone" test piece used for solid materials, several bundles consisting of 2, 3, 5 and 10 copper wires of the same gauge were placed between the jaws and pulled to fracture. In each case, after the initial straightening and ductile period, the wire bundles fractured at stress intervals roughly corresponding to the number of wires in the bundle.

Fig. 41 shows a stress/strain plot of a five wire bundle pulled to fracture, and five interruptions in the continuity of the curve are seen.

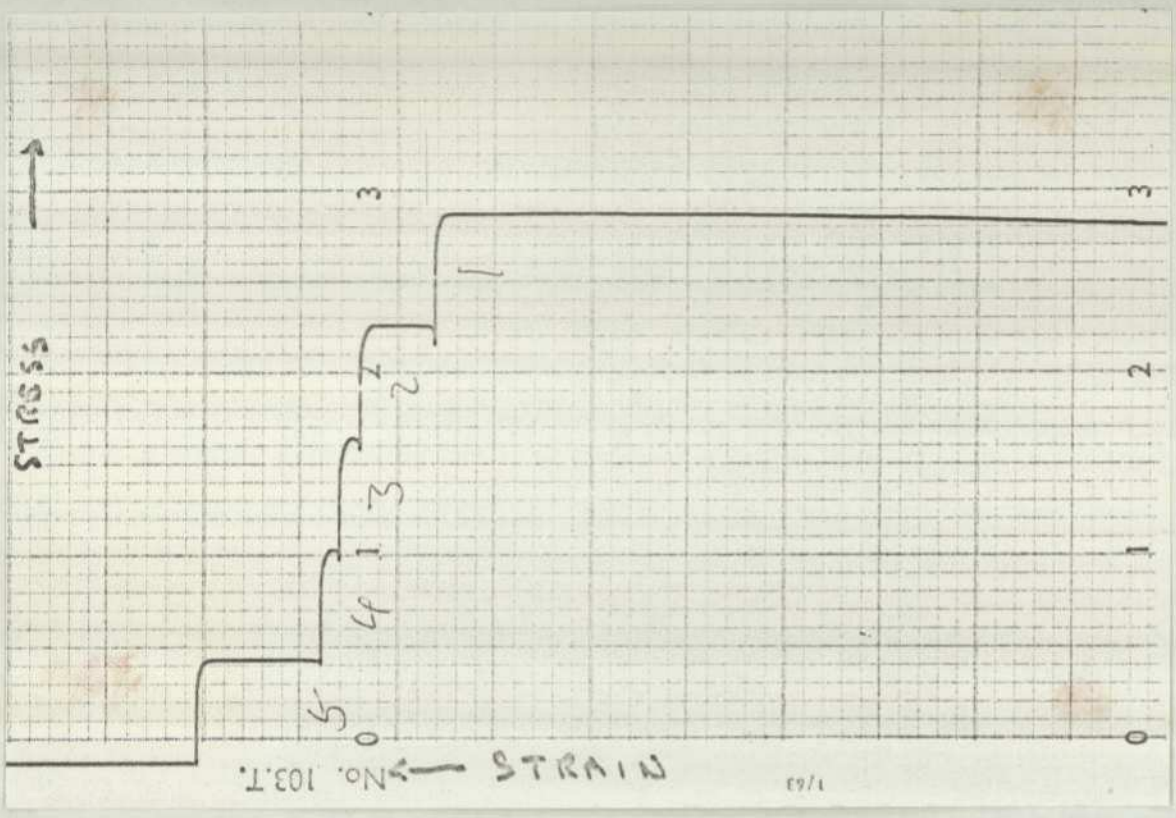


Fig. 41 Failure of a 5 wire copper bundle



Fig. 42 Tensile test of unplated tow. X $\frac{1}{2}$.



Fig. 43 Carbon fibre tow pulling out of resin bed. X6.

The total area under the curve represents the work to fracture the bundle i.e. from the start of the test to failure of the last wire. The elastic energy released as each wire snaps is absorbed to some extent by the other components so that total collapse does not take place with the first fracture. This effect would be minimal in a ten thousand fibre bundle until practically all components had fractured.

Attempts were made to determine the tensile strength of unplated fibre tows by pulling them mounted in Araldite, as shown in Fig. 42. But at failure it was seen that adhesion of the whole tow to the resin had not taken place and Fig. 43 shows the tow pulling out of the resin bed. This problem was later solved by plating both ends of a tow with copper from the cyanide electrolyte, to be described later, and pulling it with the plated ends mounted in a lead foil sheath so that the copper cold welded to the lead, on clamping the jaws, thus avoiding slip. As a cross-check, comparisons were made with tensile strength values found by the Carbon Fibre Section at A.E.R.E. who employ an Araldite vacuum impregnation technique for mounting the fibre tow, as described by Goggin[4], (1968), in which each fibre is bonded to the resin throughout the bundle.

For the experimental work to be described, the Instron was set to a strain rate or cross-head speed of 0.005"/min. with a chart speed of 1 inch, min. and full scale deflection, (F.S.D.), of 100 lbs or 10 lbs/inch of chart, the stress applied at any time then being the load divided by the total cross-sectional area of a ten thousand fibre bundle. (The Instron employed in this work was calibrated in inch-lb-minute units.)

Figures 44 and 45 are typical examples of stress/strain diagrams from an Instron for copper deposits on a Type II fibre tow, (see Table 2, Chapter 1), from sulphate and cyanide baths respectively. The area under the curve represents the work to fracture and this is measured by tracing the border with the tracing point of a planimeter, the area concerned

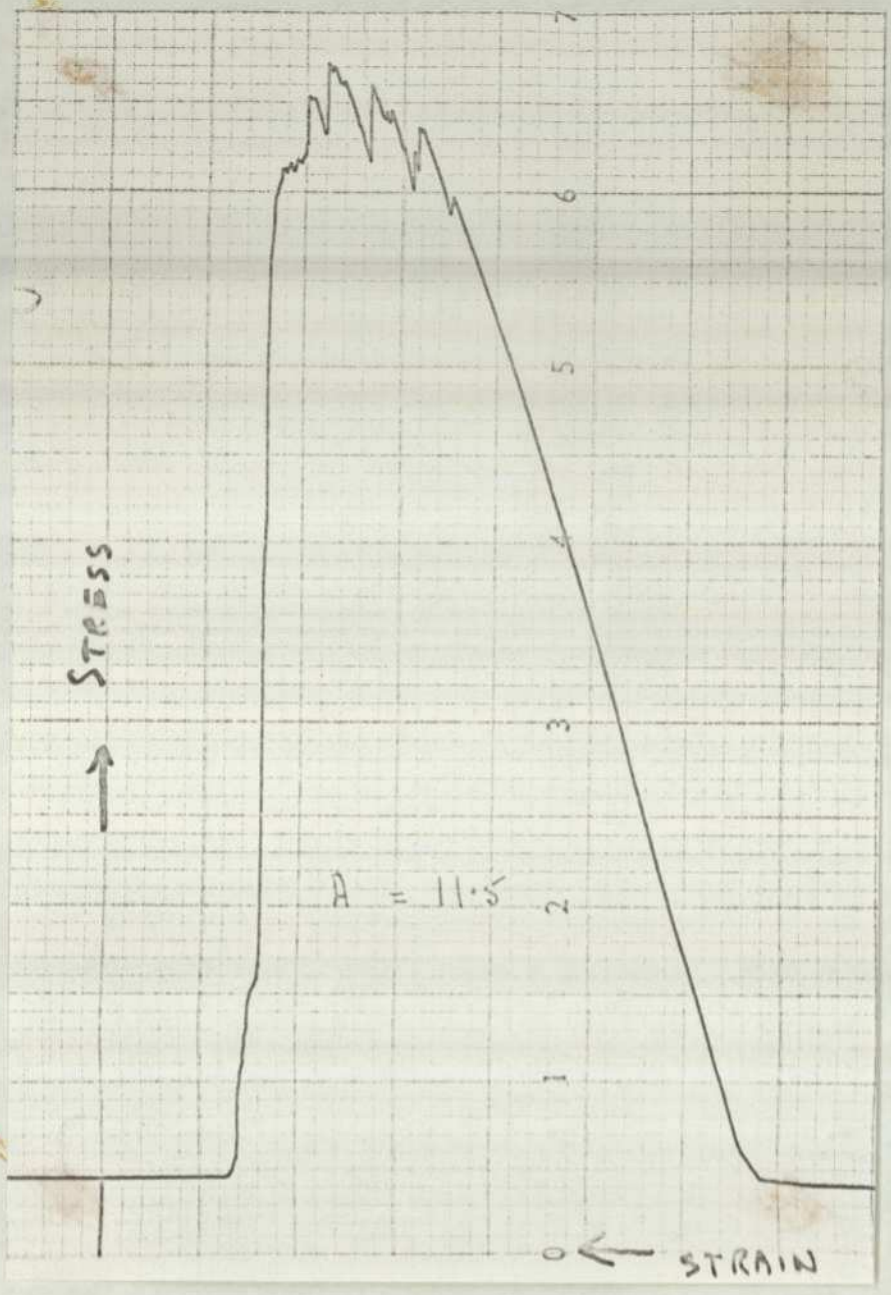


Fig. 44 Stress/strain diagram for Sulphate copper deposit on Type II carbon fibre.

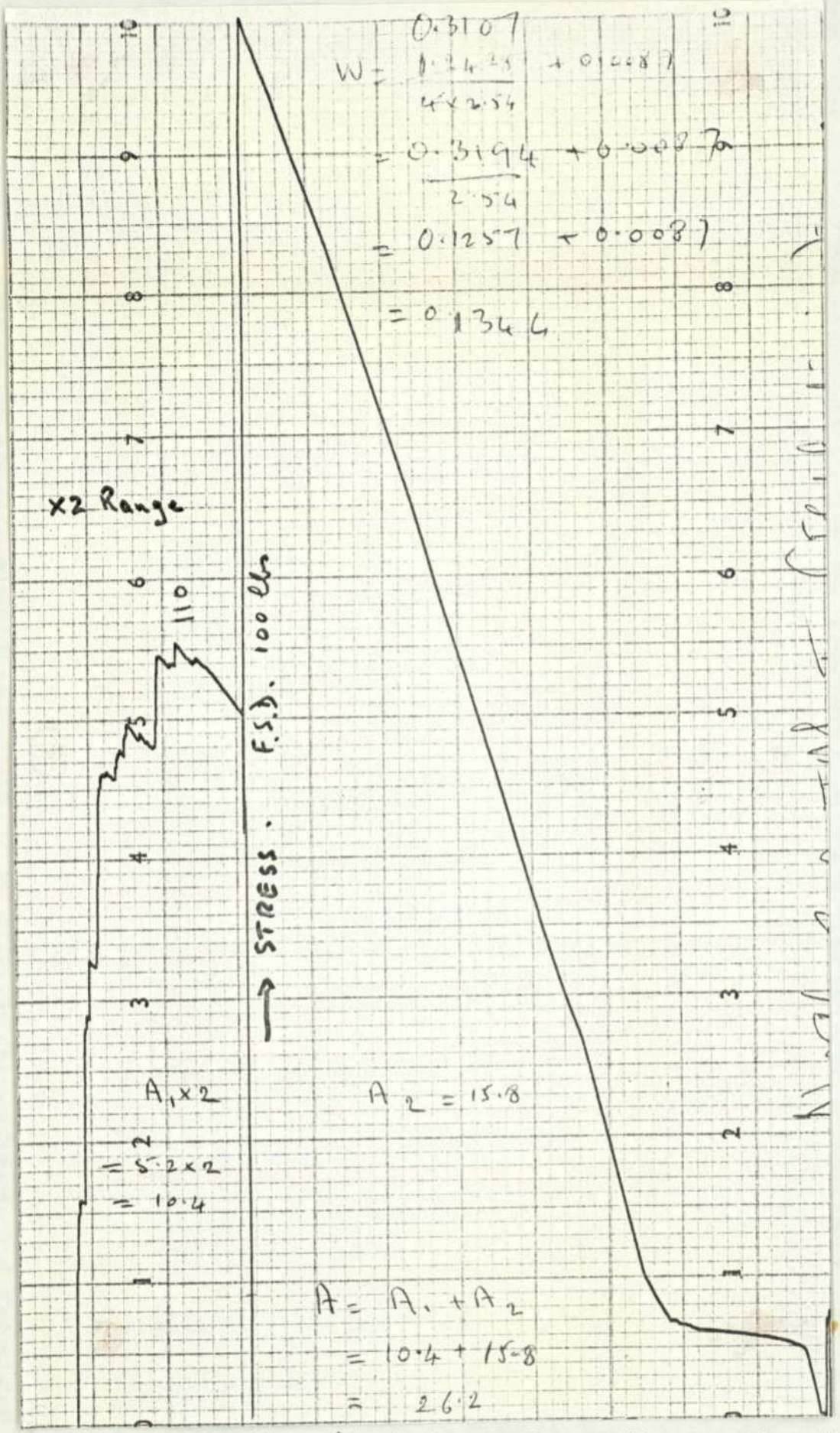


Fig. 45 Stress/strain diagram for cyanide copper deposit on Type II carbon fibre.

being shown as a constant, times the distance travelled by the wheel, where, with the Instron set in the ranges described, an area of 1 square inch on the chart is equivalent to:

$$5 \times 10^{-3} \times 10 \text{ inch lbs.}$$

$$\equiv \frac{5}{12} \times 10^{-2} \text{ ft.lbs.}$$

It can be seen from a study of the design of the machine seen in Fig. 40 that there are many places where mechanical slackness could exist. Also in operation, both the vertical and horizontal members bow, to some extent, however massive they may appear, and there is, of course, an in-built error in the load-cell. The guage length or length of the specimen under test can be measured from jaw end-face to jaw end-face but a correction must be made here since the jaws are chamfered at the face for about a distance of 0.1 inch each and thus clamping is not obtained along the whole of the inner jaw faces, the gauge length of say, a nominal 1" being therefore 1.2". This correction is of great importance since 0.2" in a 1" length is 20% of test specimen length, and a 1" gauge length was taken as a standard in this work.

Apart therefore from the regular daily calibration of the load cell, recommended by the makers, a lengthy full calibration of the instrument must be made before a run of tests, to establish what is known as the "slackness factor", which of course will be different with every instrument and vary with any load cell change made. (See Appendix 2).

4.3 Evaluation of tensile test

a. Elastic strain energy in tension

Using the argument propounded by Timoshenko[5], (1950), we consider the case of a bar in tension and assume that during tension all longitudinal fibres of the bar have the same elongation and the cross-section of the bar, originally plane and perpendicular to the axis of the bar,

remains so after extension, then if the strain in the bar remains within the elastic limit, the work done will be recovered during unloading the bar.

If the final load is P and the elongation produced δ, the tensile test diagram will be as in Fig. 46. P_1 represents an intermediate value of the load and δ_1 the elongation due to it. An increase dP_1 in the load causes an increase $d\delta_1$ in the elongation. The work done by P_1 during this elongation is $P_1 d\delta_1$ for a very thin element of area as shown in the shaded area abcd. The total work done in increasing the load from 0 to P is the sum of such elements of area given by Δ OAB.

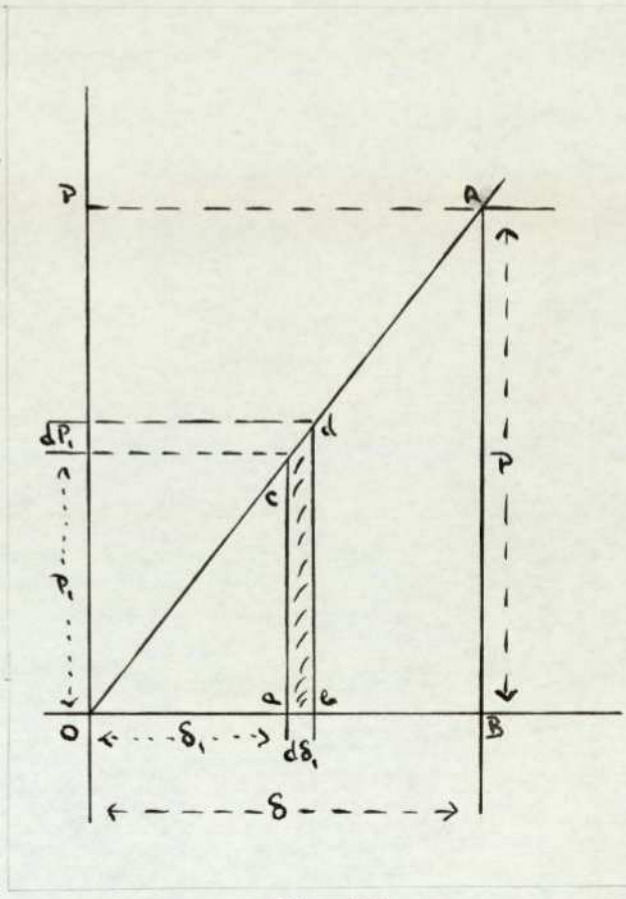


Fig. 46

This represents the total energy U stored in the bar during strain. Then

$$U = \frac{P\delta}{2} \qquad \ldots (21)$$

since area Δ OAB is $\frac{1}{2}$ base δ x height P. By the use of Hooke's law given in Section 1.3 the elongation

$$\delta = \frac{Pl}{AE} \qquad \ldots (1)$$

Thus two expressions for the strain energy in the bar can be obtained, viz:-

$$U = \frac{P^2 l}{2AE} \qquad \ldots (22)$$

and

$$U = \frac{\delta^2 AE}{2l} \qquad \ldots (23)$$

For practical applications the strain energy, ω, per unit volume, is

$$\omega = \frac{U}{Al} = \frac{\sigma^2}{2E} \qquad \ldots (24)$$

where σ is the force per unit area, $\frac{P}{A}$, or tensile stress.

b. Tensile strength of carbon fibre tows

As a first approximation with a carbon fibre tow, ω, the work to fracture is the total work done (in the tensile test diagram) to fracture, represented by the area under the curve OPA in Fig. 47 and from equation (24)

$$\omega = \frac{\sigma^2}{2E}$$

where here ω = work to fracture per unit volume of whole carbon fibre tow, and σ is the ultimate tensile stress or σ_u for whole tow. In single fibre tests

$$\sigma_u = P/A$$

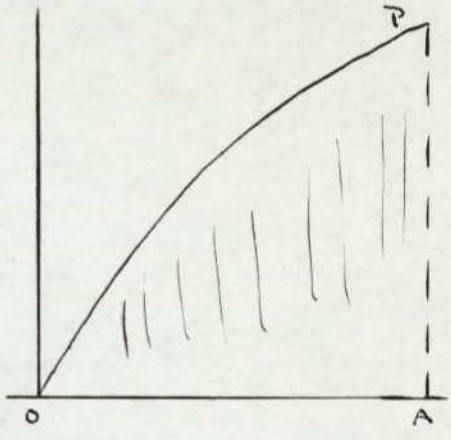


Fig. 47

Now in a carbon fibre tow let

A_x = area under stress/strain curve = work to fracture rr

D = average diameter of fibres

N = no. of fibres per tow

GL = l = gauge length or length of specimen under test

W = weight of tow per unit length

R = average density of carbon fibres

and E = modulus of elasticity.

From equation (24) we have

$$\sigma_u^2 = \omega\, 2E \qquad \ldots (25)$$

Now the volume of one fibre in gauge length l of tow is

$$V = \pi r^2 l \qquad \text{(assuming fibre has a cylindrical shape)}$$

$$= \pi \frac{D^2}{4} l \qquad \ldots (26)$$

Hence $$\omega = \frac{A_x}{\pi \frac{D^2}{4} l} \quad \text{for 1 fibre} \qquad \ldots (27)$$

where ω = (work to fracture per unit volume).

$$= \frac{A_x}{\pi \frac{D^2}{4} Nl} \quad \text{for a tow of N fibres} \qquad \ldots (28)$$

Substituting in equation (25)

$$\sigma_u^2 = \frac{2 A_x E}{\pi \frac{D^2}{4} Nl} \qquad \ldots (29)$$

$$= \frac{8 A_x E}{\pi D^2 Nl} \qquad \ldots (30)$$

a formula given in Goggin's paper on whole tow testing, (1968).

Now W the weight per unit length of tow =

$$RV \text{ (where V = vol. of fibres)} = R\pi \frac{D^2}{4} N \qquad \ldots (31)$$

or $$N = \frac{W}{\pi \frac{D^2}{4} R} \qquad \ldots (32)$$

Substituting for N in equation (30) we have

$$\sigma_u^2 = \frac{8 A_x E}{\pi D^2 Nl} \qquad \ldots (30)$$

$$= \alpha \frac{8 A_x E}{\pi D^2 \cdot \frac{W}{R\pi \frac{D^2}{4} \cdot l}} \qquad \ldots (33)$$

$$= \frac{8 A_x E R \pi \frac{D^2}{4}}{\pi D^2 W l} \qquad \ldots (34)$$

$$= \frac{2A_x ER}{W1} \qquad \ldots (35)$$

an equation also given in Goggin's report. Thus equations (30) and (35) enable us to determine the tensile strength σ_u of a carbon fibre tow either in terms of diameter and number of fibres per tow or in terms of average fibre density and weight per unit length of tow, either case involving an assumption of E, the modulus of elasticity, N the number of fibres per tow and D their average diameter or of E and R the average fibre density.

4.4 Copper plated carbon fibre tows

a. Thickness of deposit

Consider first the thickness t of a copper deposit on a carbon fibre of length l, shown in Fig. 48.

Then $t = r_2 - r_1 \qquad \ldots (36)$

The cross-sectional area of the copper deposit, A, is

$$\pi(r_2^2 - r_1^2) \qquad \ldots (37)$$

$$= \pi(r_2 + r_1)(r_2 - r_1) \qquad \ldots (38)$$

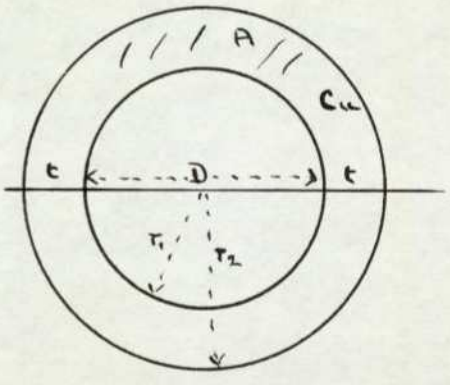


Fig. 48

and from equation (36)

$$A = \pi t(r_2 + r_1) \text{ for one plated fibre} \qquad \ldots (39)$$

which is numerically equal to the volume of the deposit if l = one.

But $r_2 = r_1 + t$

$$\therefore \quad V = \pi t(t + 2r_1) \text{ for one fibre} \qquad \ldots (40)$$

$\therefore$ For one tow

$$\Sigma V = N\pi t(t + 2r_1) \qquad \ldots (41)$$

where N = No. of fibres per tow.

Fig 49 Relationship between thickness t and weight of Cu deposit per unit length of plated tow.

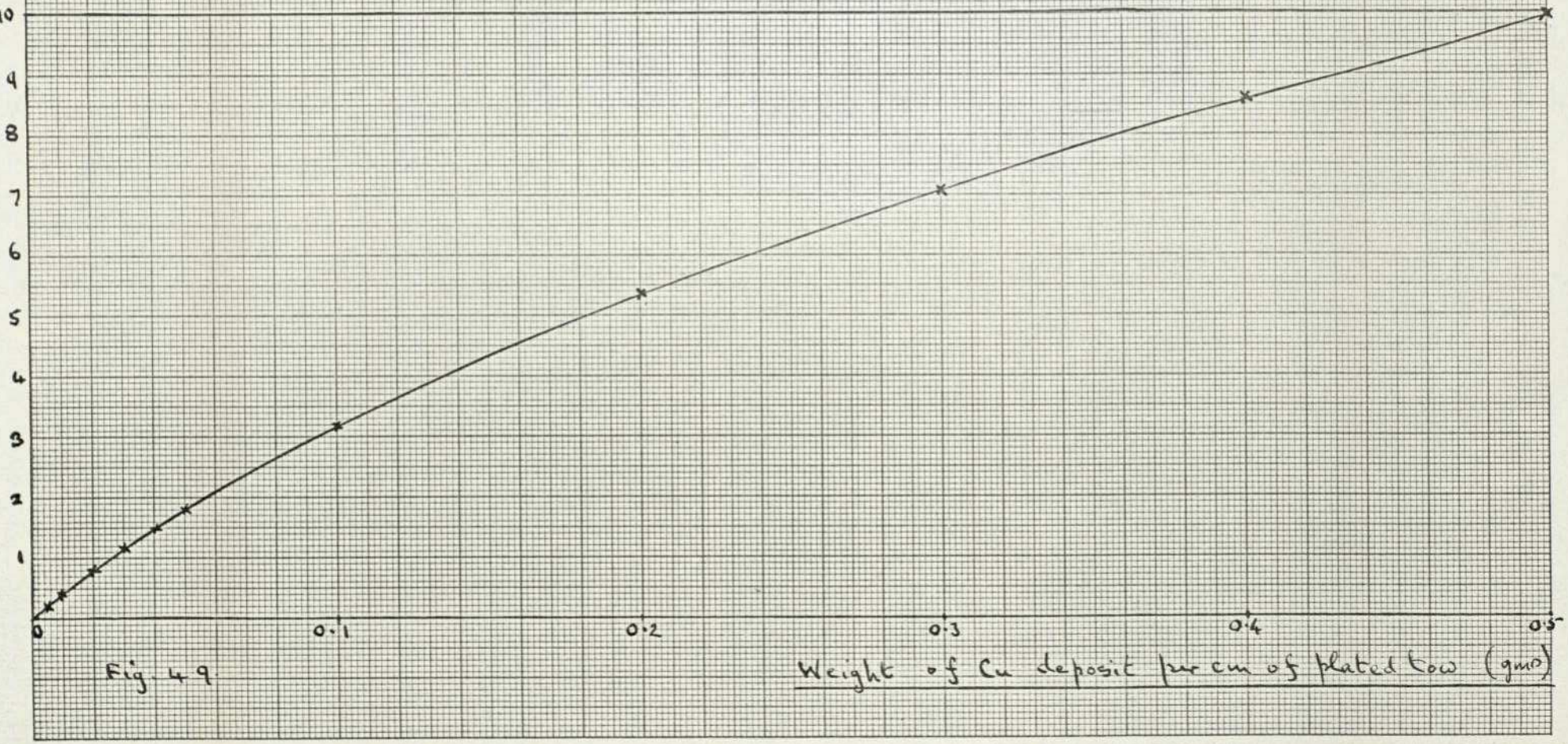


Fig. 4 9

Since weight = volume x density, the weight of copper deposit per unit length of plated tow

$$W_{Cu} = NR_{Cu}\,\pi t(t + 2r_1) \qquad \ldots (42)$$

where R_{Cu} is the density of copper

or $$NR_{Cu}\,\pi t^2 + NR_{Cu}\,\pi t.2r_1 - W = 0 \qquad \ldots (43)$$

and

$$t = \frac{-NR_{Cu}\,\pi 2r_1 \pm \sqrt{(NR_{Cu}\pi 2r_1)^2 - 4(NR_{Cu}\pi)(-W)}}{2NR_{Cu}\pi} \qquad \ldots (44)$$

Values of t_1 the thickness of copper deposit per unit length of plated tow calculated from equation (44) plotted against W_{Cu} the weight per unit length of the copper deposit on the tow, give the parabolic/weight relationship shown in Fig. 49, derived from experimental observations.

b. Composite density of plated fibre

When evaluating the tensile strength of copper plated tows it must be remembered that the values of R the average density and E, the Young's modulus used in equations (30) and (35) now become composite values depending on the volume fraction of carbon to copper present. To estimate these values use is made of what is known as the "Law of Mixtures", given by Mellor[6], (1946) as:

> "If a mixture of two substances contains x fractional parts of a substance of specific gravity S, it will contain 1-x parts of the other substance of specific gravity S_2. Then if S be the specific gravity of the mixture,
>
> $$xS_1 + (1-x)S_2 = S."$$

One of the first, modern, reported uses of such a concept was that of Lord Rayleigh and W. Ramsay[7], (1895), in their investigation of the mixture of argon, nitrogen and oxygen in the atmosphere.

Part 1. Taking unit length of copper plated fibre as shown in Fig. 50. By the "Law of Mixtures" quoted

$$R_{(Cu+f)} = aR_f + bR_{Cu} \quad \ldots (45)$$

where 'a' and 'b' are the respective volume fractions of the whole, thus

$$R_{(Cu+f)} = aR_f + (1-a)R_{Cu} \quad \ldots (46)$$

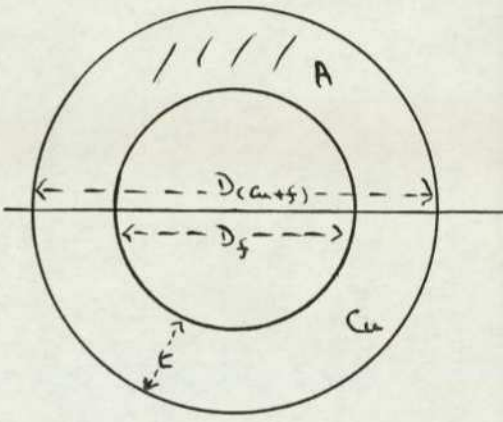


Fig. 50

From Fig. 50 the $V_{(Cu+f)}$ or volume per unit length of the composite =

$$\pi\left(\frac{D_{(Cu+f)}}{2}\right)^2$$

and that of the fibre is $\pi\left(\frac{D_f}{2}\right)^2$

Thus $$a = \frac{\pi\left(\frac{D_f}{2}\right)^2}{\pi\left(\frac{D_{(Cu+f)}}{2}\right)^2} = \frac{(D_f)^2}{\left(D_{(Cu+f)}\right)^2} \quad \ldots (47)$$

and $$b = 1-a \quad \ldots (48)$$

Whence values of $R_{(Cu+f)}$ can be found by substitution in equation (46).

Part 2. Alternatively if 't' the thickness of deposit is known then weight per unit length

$$W_{(Cu+f)} = W_{Cu} + W_f \quad \ldots (49)$$

But W = density x volume.

Therefore

$$W_{(Cu+f)} = R_{(Cu+f)}V_{(Cu+f)} = R_{Cu}V_{Cu} + R_fV_f \quad \ldots (50)$$

where R is the symbol for average density.

Now

$$V_{(Cu+f)} = \pi \left(\frac{D_{(Cu+f)}}{2} \right)^2 \quad \ldots (51)$$

and $$V_{Cu} = \pi \left[\left(\frac{D_{(Cu+f)}}{2} \right)^2 - \left(\frac{D_f}{2} \right)^2 \right] \quad \ldots (52)$$

Therefore

$$V_{Cu} = \pi \left[\frac{D_{(Cu+f)}}{2} + \frac{D_f}{2} \right] \left[\frac{D_{(Cu+f)}}{2} - \frac{D_f}{2} \right] \quad \ldots (53)$$

and $$V_f = \pi \left(\frac{D_f}{2} \right)^2 \quad \ldots (54)$$

Hence by substitution equation (50) becomes

$$R_{(Cu+f)} \pi \left(\frac{D_{(Cu+f)}}{2} \right)^2 = R_{Cu} \pi \left[\frac{D_{(Cu+f)} + D_f}{2} \right] \left[\frac{D_{(Cu+f)} - D_f}{2} \right]$$

$$+ R_f \pi \left(\frac{D_f}{2} \right)^2 \quad \ldots (55)$$

or

$$R_{(Cu+f)} = \frac{R_{Cu} \left[D_{(Cu+f)} + D_f \right] \left[D_{(Cu+f)} - D_f \right] + R_f D_f^2}{\left(D_{(Cu+f)} \right)^2} \quad \ldots (56)$$

giving the composite density in terms of the density of copper and carbon fibre, the diameter of the plated fibre and that of the fibre alone.

c. Composite modulus of plated fibre

By a similar argument to that given in Section 4.4b the composite elastic modulus, $E_{(Cu+f)}$, for the plated fibre is also given by the "law of mixtures": thus

$$E_{(Cu+f)} = aE_f + (1-a)E_{Cu} \quad \ldots (57)$$

where

$$a = \frac{(D_f)^2}{\left[D_{(Cu+f)} \right]^2} \qquad \ldots (47)$$

d. Tensile strength of plated fibre - Sample calculation

Taking observed values from Run 216, a tow plated at $0.1A/10^{-2}m^2$, $40^{\circ}C$, for one hour, in a copper cyanide electrolyte:

Instron settings

1" of chart ≡ 0.005"/min. cross-head movement.

1"/min. chart speed

Area under curve, Δ PBC = 41.7 sq. inches, by planimeter reading.

No. of fibres per tow, $N = 10^4$.

Thickness of copper deposit, from Fig. 49, $t = 1.7\mu$.

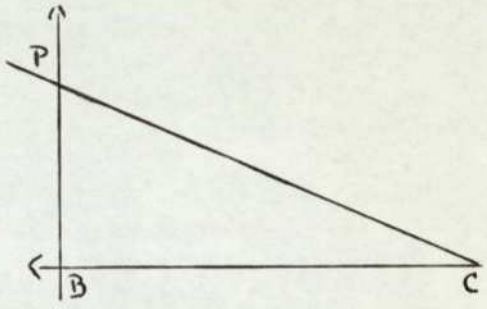


Fig. 51

Fibre diameter, $D_f = 8\mu$.

Weight of (fibre + copper) per unit length

$$W = 0.0456 \text{ gms.}$$

Gauge length l = 2.54 cms.

Plated fibre diameter = 8 + 2t = 11.4μ.

Average fibre density = 1.8 = R_f.

Average copper density = 8.95 = R_{Cu}.

Young's modulus for Type II fibre = 36×10^6 psi.

Young's modulus for copper = 18.83×10^6 psi.

Then evaluating the various components of Equation (35), we have:

1. Composite density

$$R_{(Cu+f)} = \frac{1.8 \times 64 + 8.95[19.4 \times 3.4]}{(11.4)^2}$$

$$= 5.43 \text{ gms/cc.}$$

2. Composite Young's modulus

From equation (57):

$$E_{(Cu+f)} = 10^6(36 \times 0.492 + 18.83 \times 0.508)$$

$$= 27.28 \times 10^6 \text{ psi}$$

$$\equiv 27.28 \times 6.8947 \times 10^{10} \text{ dynes/cm}^2.$$

3. Work to fracture

From the Instron curve

$$A_x = 41.7 \left[\frac{0.005}{12} \times 10\right] 1.356 \times 10^7 \text{ ergs.}$$

4. Tensile strength

$$\sigma_u = \sqrt{\frac{2A_x E_{(Cu+f)} R_{(Cu+f)}}{Wl}} \qquad \ldots (35)$$

or

$$\sigma_u = \sqrt{\frac{2x41.7x\frac{0.005}{12} x10x1.356x10^7x27.28x6.8947x10^{10}x5.43}{0.0456 \times 2.54}}$$

$$= 2.015 \times 10^{10} \text{ dynes/cm}^2.$$

But since 1 psi = 6.895×10^4 dynes/cm^2

$$\sigma_u = 0.2922 \times 10^6 \text{ psi.}$$

This, corrected for a "machine slackness" factor given in Appendix 2 as 3.256, becomes

$$0.0897 \times 10^6 \text{ psi.}$$

(where 1 psi ≡ 6894 Nm^{-2}, for conversion to SI units).

Of course, the value of the tensile strength σ_u can be obtained by direct measurement of $D_{(Cu+f)}$, the diameter of the plated fibre, if you are sure you can isolate only one fibre plated with copper from the tow, without involving the calculated thickness t, of the copper deposit.

It is realised that the term "ultimate" is one of convenience, permitted by common usage, and does not imply absolute values of tensile strength.

Factors controlling variations in values obtained will be discussed in a later Chapter, since all values quoted are the means of many experiments.

References 4

4.1 Leonardo da Vinci, (1452-1519), Holliday, L., Scientific America, Vol. 222, No. 5, May, 1970.

4.2 Galileo, G., (1638) Ibid.

4.3 Musschenbroek, P., (1729), Ibid.

4.4 Goggin, P. R., 1968, See Ref. 2.10.

4.5 Timoshenko, S., Strength of Materials, Pt. 1, Van Nostrand, 1950.

4.6 Mellor, J. W., Treatise on Inorganic and Theoretical Chemistry Vol. 1 Longmans, 1946.

4.7 Lord Rayleigh and Sir. W. Ramsay, Argon, a New Constituent of the Atmosphere Proc. Roy. Soc. (Lond) 57, 265-286, 1894-95.

CHAPTER 5

Preliminary work on copper electro-deposition

5.1 Historical background

The first reported electrolytic separation of copper from copper sulphate solution is to be found in the work of Wollaston[1], (1801), who discharged an electrostatic machine through two thin silver wires immersed in acidulated copper sulphate solution. He found that copper deposited on both electrodes and thus, unwittingly, was also the first man to employ a periodic reverse plating technique! Faraday[2], (1832-3), was not satisfied with the quality or quantity of copper produced in this way and using a modification of Volta's Pile[3], (1800), consisting of 2000 copper/zinc pairs, (Vinal[4], 1950), in sulphuric acid, as a source of direct current, deposited copper quantitatively from acid copper sulphate, during his work on the "Laws of Electrolysis", (Williams[5], 1965).

The first technical report on copper electrodeposition was made by Warren de la Rue[6], (1836), who when only 21, invented a modification of the Daniell cell[7], (1836), and used it to electroform articles in copper, so that even "scratches in the surface of the mould were faithfully reproduced". This was followed by the work of Jacobi[8], (1840), on electrotyping, in St. Petersburg, Russia, and reported independently in England by Spencer[9], (1840), who both described a commercial process for producing images in copper of ceramic and plaster moulds, (coated with powdered graphite, to carry the current) and plated in a copper sulphate electrolyte, to form what were then called galvanoplastic replicas. In this way the electrodeposition of copper from acid solutions gradually became a commercial enterprise but unfortunately ferrous articles could not be plated as described, since iron displaces copper, chemically, from the electrolyte.

Chemical displacement of metals, particularly of copper by iron had

been reported by the Greek alchemist Zosimus[10], (250-300 A.D.), who recorded, in 28 volumes, what was then known about chemical processes. In 1775, Bergmann[11] noted that:

> "If iron is put into a solution of vitriol of copper the solution is soon observed to be covered with cupreous pelliculae but this does not happen if ochre be added." Ochre = iron oxide.

In further work he noted the order of displacement of metals from their salts[12], (1788).

> "Zinc over iron, iron over lead, lead over tin, tin over copper, copper over silver, silver over mercury."

Also Scheele[13], (1783), in his work "De Materia tingente coerulei Berolinensis", reported that the cyanides prevented precipitation of copper by iron.

One of the first reports of a copper cyanide electrolyte being used for plating iron was made by E. Davy[14], (1831) (not Sir Humphrey), and this was followed by the extensive work of J. Wright[15] which resulted in the well known Elkington electroplating Patents, (1836-1840)[16]. Wright, after the Patents were well established, published in 1882. At about the same time Weil[17], (1870), to overcome the obnoxious cyanide fumes developed an alkaline copper bath containing tartates, which he used to electroplate with copper, the metal aluminium, a rarity in those days, produced by Bunsen[18] or Deville's[19], (1854) fused salt processes carried out by the electrolysis of fused sodium aluminium chloride with carbon electrodes. Deville, who prepared electrolytic Al in France at the same time as Bunsen, also used this cell to electrodeposit copper, from the fused salts.

The coupling of tartrates with the cyanide electrolyte was reported by Watts[20], (1915), in his "cleaning and coppering" process where he stated that anode corrosion or depolarization was improved by the addition of tartrates.

Further improvement of anode performance was made by McCullogh and

Gilchrist[21], (1932), who employed Rochelle salt, sodium potassium tartrate, $NaKC_4H_4O_6$, as an addition to their cyanide bath.

This work was followed by Pan's[22][23] report on a concentrated copper cyanide electrolyte, (1933-5), where he stated that a cathode/anode efficiency of 80% was attained in 1 molar copper cyanide solutions. Pan's deposits however were dull and rough, even at 1 mil thickness, and polarization was still a problem.

The first commercially successful high efficiency bath, incorporating the anode depolarizing Rochelle salts, was introduced in 1938, (Bair and Graham[24], 1942). Later, to increase conductivity and improve anode corrosion Wernlund et al[25], (1942) added alkali and this was followed by Jernstedt's periodic reverse plating process[26], (1948), which served to increase still further the efficiency of the modern plating bath, since the anode, during any negative cycle, depolarizes electrolytically as well as chemically.

5.2 Introduction

The copper sulphate/sulphuric acid electrolyte produces coarse crystalline deposits at normal plating current densities, the rate of deposition being about 1 mil at 2.2 A/sq.dcm, (20 A/sq.ft., or 20 $A/10^{-2}m^2$) in one hour at 20°C. Bancroft[27], (1905), and Blum[28], (1919), both ascribe this coarseness of deposit to impurities in the electrolyte and recommend a higher current density to reduce crystal size.

If the temperature and current density are lowered, the crystallinity of the deposit increases and at about 0.1-0.2 $A/10^{-2}m^2$, 10°C, single crystals of copper sometimes form, as can be seen in Fig. 52. These crystals grew in 72 hours, under the conditions described.

The coarseness of the deposit may be refined to a great extent by mechanically rotating the cathode, when the brightness of the deposit, so found, was described by Hughes[29], (1921), as being due to the "smallness of the grains". The same effect can also be produced chemically

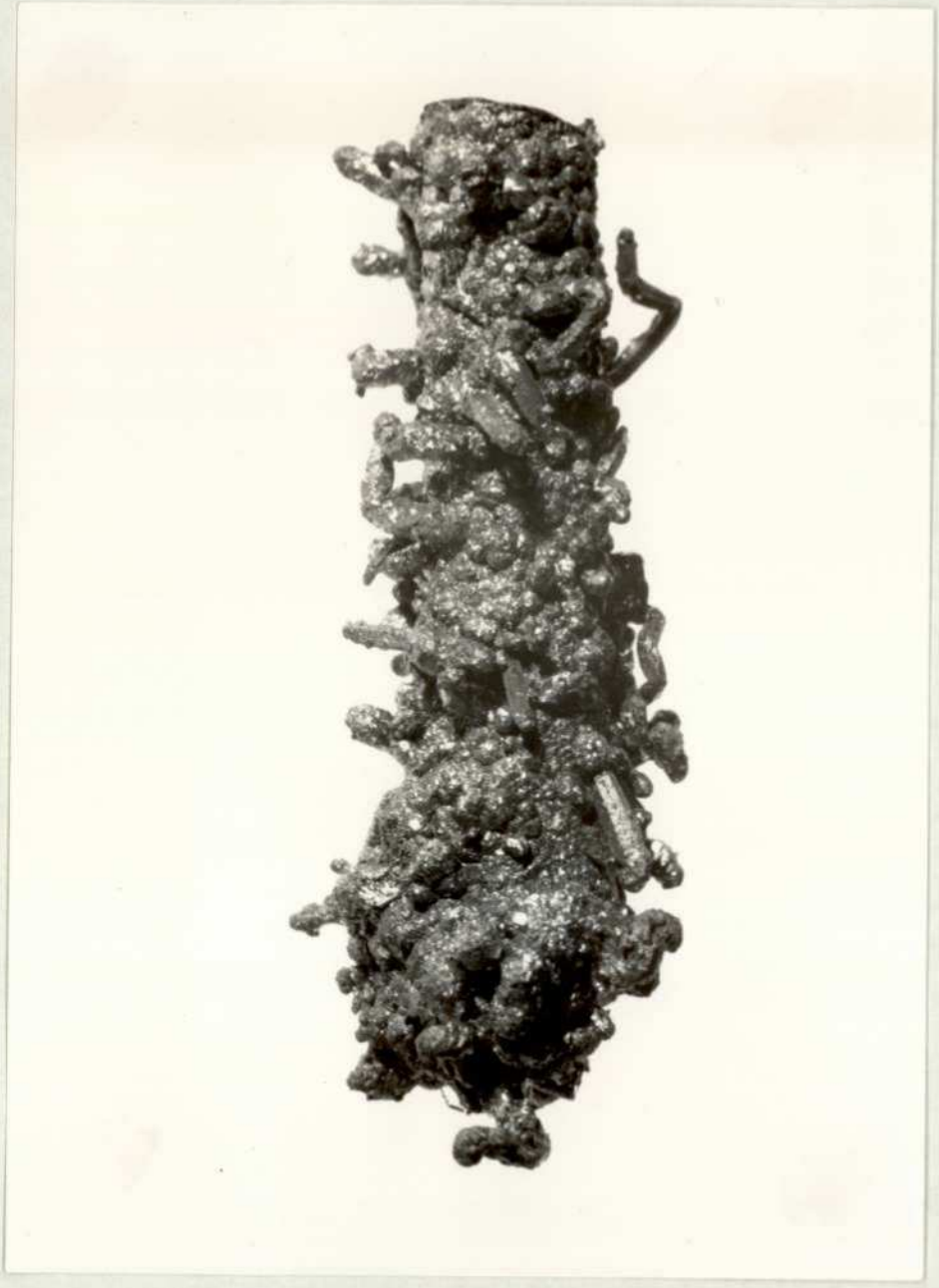


Fig. 52 Single crystals of copper. X4.

by addition of aluminium sulphate to the electrolyte. Such an addition gives rise to salmon pink, satin smooth, matte copper deposit at 2.2 A/ $10^{-2}m^2$.

Vagramyan et al[30], (1956) report that when Al ions are present in a sulphate bath the internal stresses in the deposit are increased and hence grain size is decreased. But they do not explain why this effect on the lattice parameter should take place and their explanation leaves the mechanism of Al grain refinement of the sulphate copper deposit still obscure.

5.3 Experimental detail - acid electrolyte

After cutting the standard 4" length chosen for this work, the experimental tow was weighed. In order to plate the carbon fibre it has to be supported or "racked" and must be "ballooned out" a little to ensure penetration. The method used is clearly seen in Fig. 52a a diagram of the loaded $\frac{1}{8}$" copper wire rack.

The "ballooned" tow is lightly squeezed between two Cu wire loops, held in position by spring clips and 1" glass tube spacers, 'g'.

The whole is immersed in the electrolyte until the level is half way up the glass tubes. This technique eliminates weight loss errors which would occur if copper deposits were allowed to form on the rack. The tow must be cut on a cutting board, with a razor, to obtain a clean end cut, as scissors produce ragged edged cuts due to fibres slipping along each other. Both types I and II fibre were used in these initial runs.

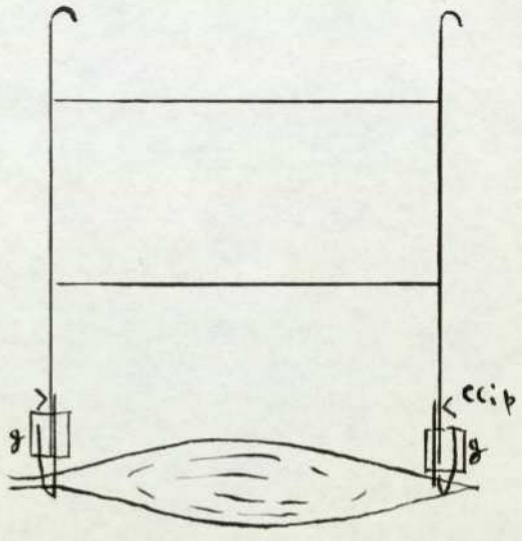


Fig. 52a

TABLE 7

Carbon Fibre Mensuration

	Length		Superficial Surface Area	
	ins.	cms.	Sq.ins.	Sq.cms.
Unit length of tow	1	1	9.9	63.8 25.1
Experimental tow length	4	10.2	39.5	255.2
Production tow length	14	35.6	138.3 or 0.96 sq.ft.	893.2 or 0.0893 m^2

TABLE 8

Current Density Ranges

Amps/cm length	0.025	0.05	0.1	0.15	0.20
Amps/4" length	0.25	0.5	1.0	1.5	2.0
Amps/sq.ft.	0.909	1.818	3.637	5.455	7.274
Amps/sq.decimeter ($A/10^{-2}m^2$)	0.1	0.2	0.4	0.6	0.8
Coulombs/60 minutes	900	1800	3600	5400	7200
Theoretical weight of Cu in 1 hr in gms. $CuSO_4 \longrightarrow Cu^{\bullet\bullet} + SO_4^{--}$	0.296	0.592	1.184	1.776	2.368
Theoretical weight of Cu in 1 hr in gms. $Cu(CN)_2^{-} \longrightarrow Cu^{\bullet} + 2CN^{-}$	0.592	1.184	2.368	3.546	4.738

The D.C. current used throughout this work came from an A.C. supply, through a Variac transformer control to an eliminator constructed from selenium rectifiers, to give full wave rectification, and heavy duty transformers, chokes and mica condensers in the circuit, to give a smoothed current, with no A.C. ripple detectable on a cathode ray oscillograph. This eliminator, with the plating circuit, is given in Fig. 53.

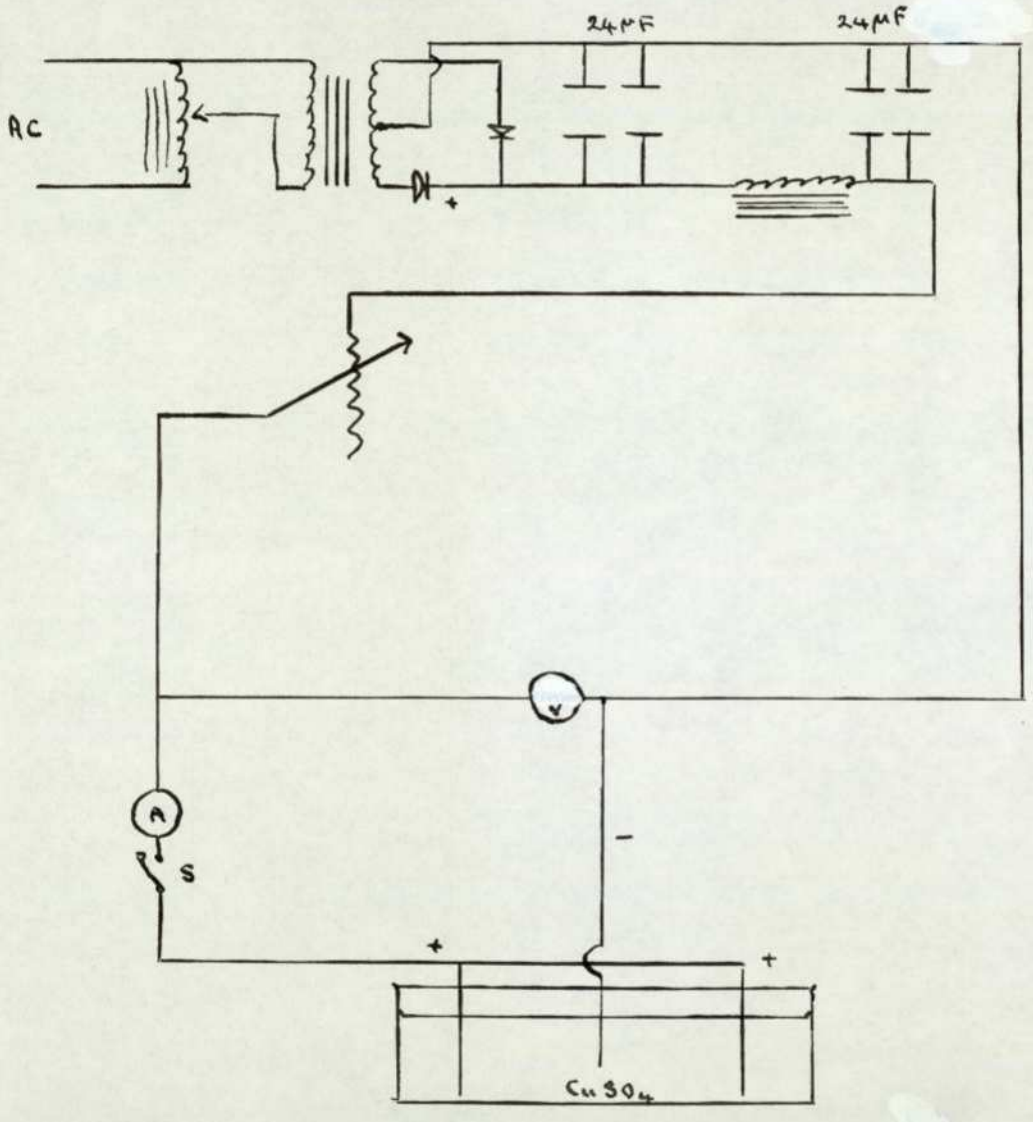


Fig. 53 Current supply and plating circuit diagram

Attempts to use Variac control without the variable rheostat, gave coarse control only, and corresponding lack of efficiency.

Tables 7 and 8 give data for calculation of fibre superficial surface areas, current densities, the range used in this work, together with

TABLE 9

Plating detail

Vessel	Pyrex glass dish, 2000 ml
Anodes	Two 7.5 x 7.5 cm electrolytic copper sheets, or 112.5 sq.cms facing cathode.
Electrode spacing	Not less than 5 cms
Electrolyte	200 g/l copper sulphate, $CuSO_4$, $5H_2O$ 48 g/l sulphuric acid, H_2SO_4, 1.84 S.G. 26 g/l aluminium sulphate, $Al_2(SO_4)_3$, $18\ H_2O$
Electrolyte volume	1500 ml
pH	Between 1.0 and 2.0
Agitation	Glass paddle
Temperature	$20^{\circ}C$
Ageing of electrolyte	None

quantity of copper to be expected, if deposition were carried out under ideal theoretical conditions, with 100% anode/cathode Faraday efficiency. Table 9 gives plating detail for deposits formed in this preliminary work. Concentration polarization, a common feature with this electrolyte since H_2 is not evolved at the cathode, was counteracted by the use of paddle agitation.

A standard plating time of one hour was chosen for the whole of the work described in this report, since it was felt that any anomalies encountered would be seen in this period.

The plated tows were washed in distilled water and dried in a 4" diameter vacuum drying tube coupled to an Edwards Highvac backing pump. This reduced the pressure to 10^{-2} mm Hg (1 mm Hg ≡ 133.3 Nm^{-2}), leaving an untarnished, salmon pink tow, which was weighed and tensile tested in the manner described in Chapter 4. It is of interest to note here that when rubber bungs, instead of Quick-fit joints, were used in the vacuum drying apparatus, all tows tarnished badly due to volatile sulphur compounds in the rubber.

5.4 Results - acid electrolyte

It was quickly realized that Type I, high modulus, carbon fibre was quite unsuitable for electrodeposition trials, since tensile tests gave strengths well below 30,000 psi, the UTS of pure annealed copper itself. Results of the order of 10-15,000 psi were common and difficult to reproduce. Type I fibre when plated, gave 95-100% Faraday cathode efficiency with good tow coverage and stress/strain diagrams similar to that of Fig. 44, Chapter 4, but anodes polarized with the formation of a black film as their effective surface area was less than half the superficial cathode area.

Fig. 54 shows a plot of tensile strength of sulphate copper deposits against volume fraction of fibre, compared with results from cyanide copper deposits formed at the same temperature, to be described later. These

Deposits from CuCN and CuSO4 electrolytes, at 20°C.

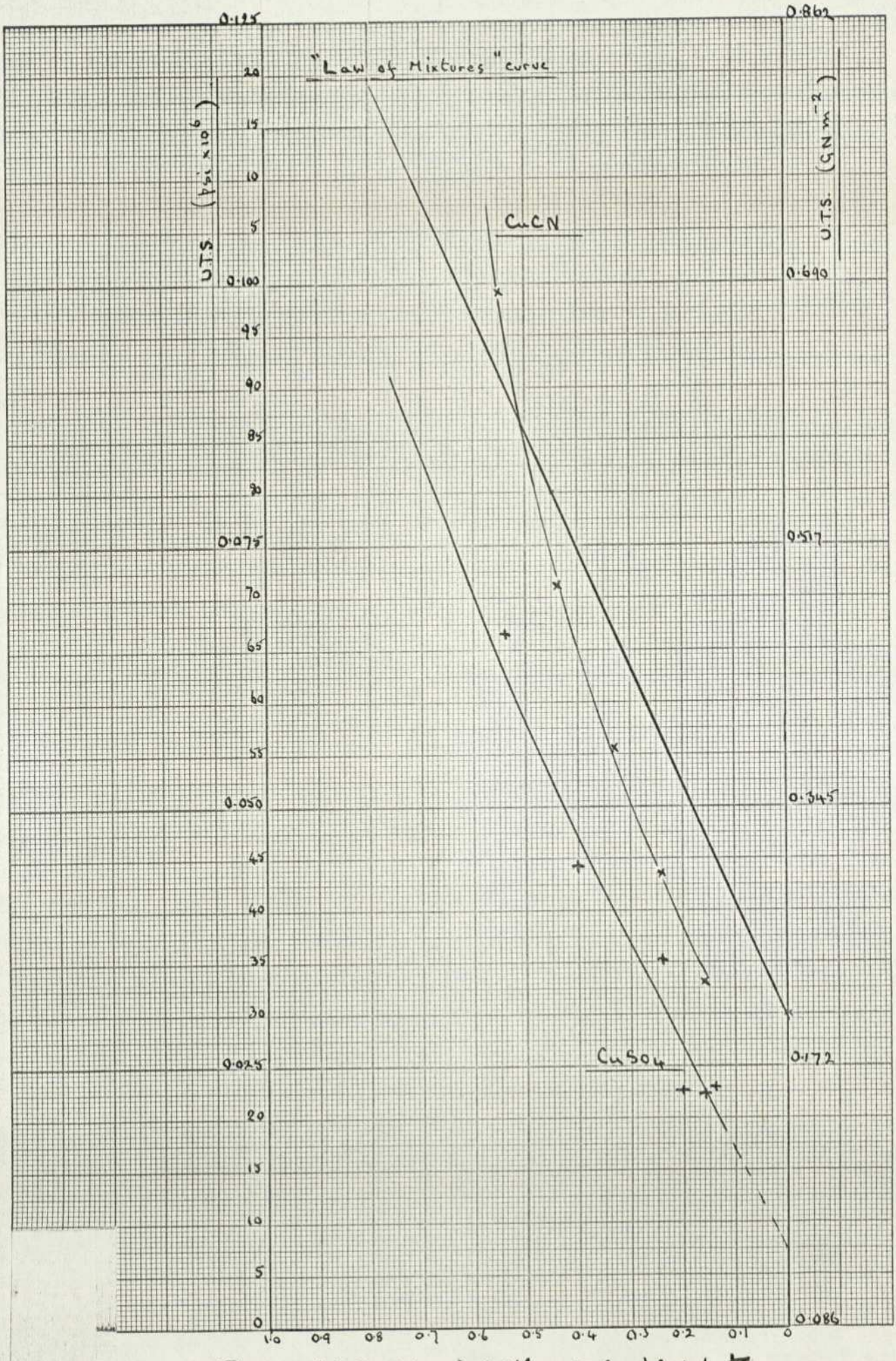


Fig 54 Vol fraction of C fibre in Cu plated tow.

Type I or II ?

results are also compared with the theoretical "law of mixtures" curve for UTS against volume fraction, which is constructed by drawing a line through the point 0.030×10^6 psi, the UTS of pure annealed copper, at zero fibre concentration, to the point 0.142×10^6 psi, the UTS of Type II carbon fibre at 100% concentration.

It will be noted that the UTS of the batch of Type II untreated carbon fibre, used throughout this work, was 142,000 psi, a very low value when compared with 300-400,000 psi values commonly quoted. The result given for this poor quality material was the mean of twelve whole tow tests, with a standard deviation of 13,000 psi and a percent deviation from the arithmetic mean of 9%.

It can be seen in Fig. 54 that the curve formed in the acid electrolyte is well below both the cyanide copper and theoretical curves. This difference can be regarded as a function of the decreased adhesion of such acid deposits on carbon fibre, which during test often pulled out of the copper envelope.

5.5 Experimental detail - alkaline electrolyte

During plating from the sulphate solution it was noticed that unless tows were well "ballooned" out on racking, they became covered with an envelope of copper before full penetration of the metal deposit throughout the tow. It was thought that this defect might be overcome by the use of an electrolyte from which hydrogen, as well as copper, was liberated at the cathode. A simple cyanide solution was chosen for this purpose, with a 5-10 gm/l "free cyanide" concentration: the term "free cyanide" being defined as the quantity of sodium cyanide in solution over and above that required to dissolve copper cyanide, CuCN (1.1 gm NaCN/1.0 gm CuCN). A solution given in Metal Finishing[31], (1947), was made up with twice the recommended concentration of "free cyanide" to reduce rate of Cu deposition, in the hope that penetration would occur before encapsulation

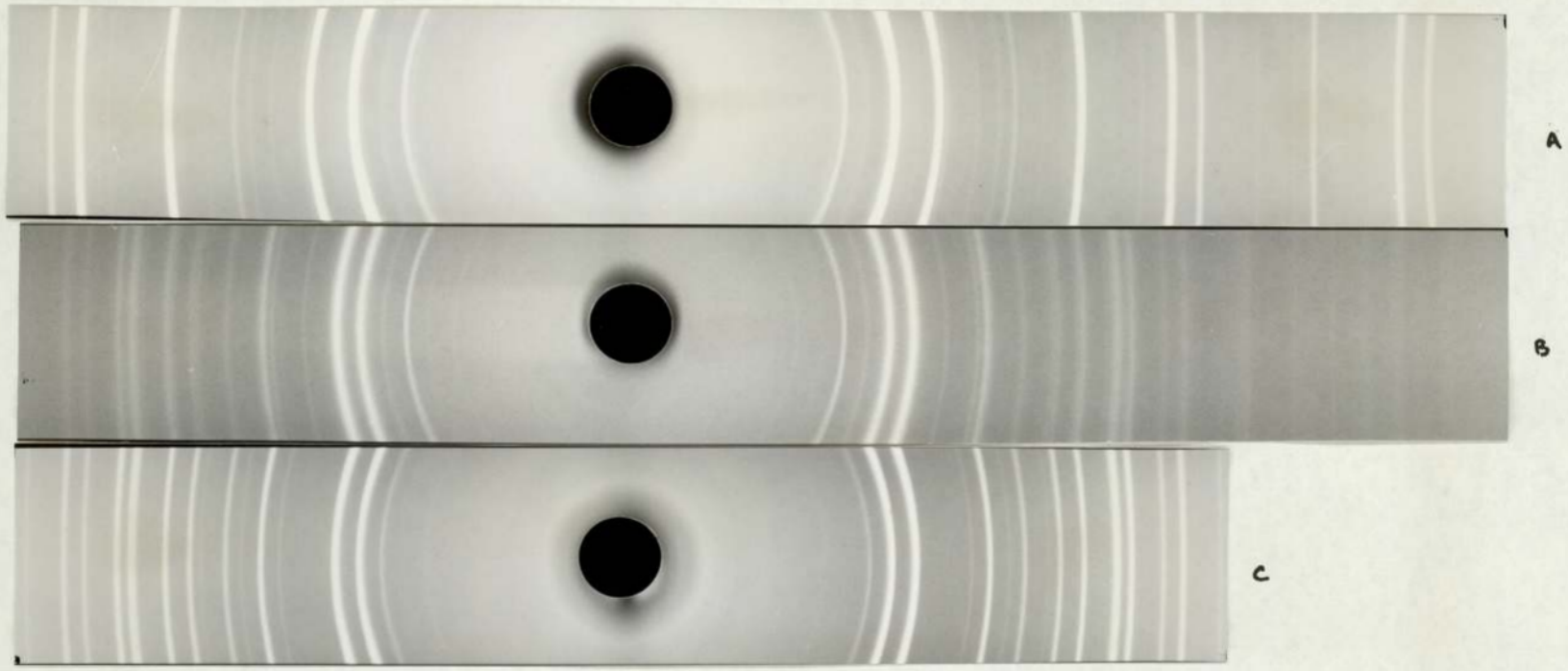


Fig. 55 Comparison between cuprous oxide, A, black anode slime, B, and cupric oxide, C.

of the tow, due to increased evolution of hydrogen and oxygen taking place in high free cyanide bath.

The formula was:

CuCN	18.7 g/l
NaCN	28.0 g/l
Na_2CO_3	12.8 g/l
Free NaCN	7.5 g/l

Operating this electrolyte at 40°C, in the manner described in Section 5.3, the carbon fibre was plated under conditions which gave rise to vigorous effervescence of hydrogen at the cathode.

In practice this electrolyte gave good penetration of Type II tows due to initial "ballooning" and H_2 agitation but the anodes polarized badly, even though their effective area was increased from the sulphate area of 112 sq.cms. to >250 sq.cms. They became covered with a thick black deposit and the cathode efficiency, from tow to tow, for a given current density, was so erratic that effective control was impossible. Doubling the concentration of "free cyanide" did not remove this defect.

To determine the composition of the polarizing anode film, a washed anode was dried, the film removed and powdered for X-ray analysis.

5.6 Results - alkaline electrolyte

Fig. 55 shows a comparison of the X-ray powder patterns of cuprous and cupric oxide with that of the black anode deposit. It will be seen that four strong lines in the cuprous oxide pattern, A, and eleven in the cupric oxide pattern, C, coincide with lines in the anode deposit pattern, B. Thus the major component in the anode deposit is cupric oxide.

Reduction in deposition rate and erratic results from anodes covered with cupric oxide are to be expected since the specific resistance or resistivity of CuO is 400 ω compared with copper at 0.000017 ohm/cms. (Mellor[32], 1946) and Streintz[33], (1902), has said that powdered CuO is a non-conductor. In practice, in such a cell, the voltage rises, current density drops, and deposition rates decrease, sometimes to zero.

5.7 Discussion of Results

These preliminary experiments demonstrated that plating trials with Type I, high modulus fibre, gave unsatisfactory, erratic stress/strain curves and results well below the tensile strength of copper. This material was therefore rejected for further work.

Acid copper sulphate electrolyte gave good deposits on Type II material with such a high plating rate, that a tow often became encapsulated in Cu before penetration of the bundle in depth. Also the tensile strength of the plated fibres was well below that indicated by the "law of mixtures", for a given volume fraction of fibre, indicating poor adhesion, which was confirmed by "pull-out" during test.

It is of interest that Lamb and Valentine[34], (1966), in a review article on the mechanical properties of electrodeposited copper from the sulphate solution, give 26 reported values of tensile strength, with no correlation between any of the plating parameters, apart from a trend of increased strength with increase of sulphuric acid concentration. The arithmetic mean of values quoted was 34,800 psi which compares well with 30,000 psi for pure annealed Cu, when it is remembered that a little copper oxide may well co-deposit with Cu, under laboratory plating conditions; with a resultant increase of tensile strength, as observed.

The reproducibility of values quoted by Lamb et al, was low, varying from 20,000-60,000 psi. Contrary to the general belief that copper sulphate electrolytes were elementary, Shreir[35], (1951), has shown this is not the case and that due to polarization effects of impurities on the nucleation of the deposit, fine grained or coarsely crystalline deposits may be formed in a most erratic manner.

It is also of interest to note that Lamb et al, when considering suitable parameters to monitor, in order to assess the effects of variables during deposition, rejected hardness because of the low correlation of this parameter with other properties, resistivity because of too little

variation and polarization measurements, (which should theoretically serve the purpose), as being too impracticable because of time and effort required to check reliability and reproducibility. Finally they chose tensile strength measurements as the most satisfactory monitor of reliability and reproducibility of baths and deposits.

The almost complete polarization of the anode in a simple copper cyanide electrolyte, due to the formation of a film largely composed of cupric oxide - not hydroxide as one might expect - rules out use of such a solution, even though the low deposition rate of 0.0006 inch/hr (0.0015 cms/hr) might solve the encapsulation problem.

It must be mentioned here that green basic copper hydroxide would form on an anode, effectively polarizing the circuit, if the "free cyanide" concentration was allowed to fall below the minimum set limit.

Further work, with the standard, more rapid, Rochelle salt/cuprous cyanide electrolyte, was carried out and is reported in Chapter 6.

References 5.

5.1 Wollaston, W. H., Phil. Trans., 427ff, 1801.

5.2 Faraday, 1832, "Michael Faraday", by L. P. Williams, Chapman and Hall, 1965.

5.3 Volta's Pile, 1840 Phil. Trans. Roy. Soc. 90, 1800.

5.4 Vinal, G. W., "Primary Batteries", John Wiley, 1950.

5.5 Williams, 1965, see Ref. 5.2.

5.6 Warren de la Rue, London and Edinburgh Phil. Mag., 9, 484, 1836.

5.7 Daniell, J. F., Phil. Mag. III, 8, 421, 1836.

5.8 Jacobi, M. H., British Patent, 8610, 1840.

5.9 Spencer, T., Jahrb. Min., 230, 1840.

5.10 Zosimus, 300 BC, Bibliographical Encyclopaedia of Science and Technology, Ed. I. Asimov, George Allen and Unwin, 1964. Mellor, J. W., Vol. 3, p.14, Longmans, 1946.

5.11 Bergmann, T., De Attractionibus electivis, Upsala, 1775.

5.12 Bergmann, T., Opuscula physica et chemica, Lipsiae, 2, 349, 1788.

5.13 Scheele, C. W., De Materia tingente. Coerulei Berolinensis 1783. Opuscula chimnia et physica, Lipsiae, 1, 148, 1788.

5.14 Davy, E., Phil. Trans., 121, 147, 1831.

5.15 Wright, J., Phil. Mag. 5, 13, 265, 1882.

5.16 Elkington, G. R., and Elkington, H., British Patents Nos. 7134, 7304, 7496 of 1836-8 and 8447 of 1840.

5.17 Weil, F., Compt. Rendu, 70, 997, 1870.

5.18 Bunsen, R., Pogg. Ann., 92, 648, 1854.

5.19 Deville, H. St.C., Ann. Chim. Phys. 3, 43, 5, 1854.

5.20 Watts, O. P., Trans. Am. Electrochem. Soc. 27, 141, 1915.

5.21 McCullogh, J. F. K., and Gilchrist, B. W., U.S. Patents, 1, 863, 869, 1932.

5.22 Pan, L. C., Metal Cleaning and Finishing, 5, 112, 152, 166, 1933.

5.23 Pan, L. C., Trans. Electrochem. Soc., Vol. LXVIII, 471, 1935.

5.24 Bair, R. R. and Graham, A. K., Modern Electroplating, Ed. Lowenstein, F. A., John Wiley, 1942.

5.25 Wernlund, C. J., Benner, H. L. and Bair, R. R., U.S. Patent, 2, 287, 654, 1942.

5.26 Jernstedt, G. W., U.S. Patents, 2, 451, 340 and 2, 451, 341, 1948.

5.27 Bancroft, W. D., Journ. Phys. Chem., 9, 277, 1905 ib., 12, 75, 1908 and Trans. Amer. Electrochem. Soc. 6, 27, 1904 ib., 23, 261, 1913.

5.28 Blum, W., ib., 36, 213, 232, 1919.

5.29 Hughes, W. E., Journ. Phys. Chem. 25, 495, 1921.

5.30 Vagramyan, A. T., and Tsareva, Yu S., Zhur. Fiz. Khim. 29, 185, 1956.

5.31 Metal Finishing Guide Book, Metal Industry Pub. Co. N.Y., 1947.

5.32 Mellor, J. W., Vol. 3, Longmans, 1946.

5.33 Streintz, F., Annal. Physik, (4), 9, 864, 1902.

5.34 Lamb, V. A., and Valentine, D. R., AES Research Project No. 21, I, 1289-1311, 95, Plating, December, 1965.

5.35 Shreir, L. L., J. Electrochem. Soc., 98, 193, 1951.

CHAPTER 6

Copper deposition from the Rochelle Salt - Copper cyanide electrolyte

6.1 Introduction - the Rochelle salt electrolyte

The standard Rochelle salt - copper cyanide solution, now in general use, was chosen to overcome the excessive anode polarization experienced while plating carbon fibre tows in the simple unbuffered copper cyanide electrolyte, described in Chapter 5.

This electrolyte was first fully investigated by Graham and Read[1-6], (1938), and in six reports, they made the salient points that:-

a. Anode and cathode efficiency were fairly constant between the pH range 10.5-12.2, as can be seen in Fig. 56, based on their figures.

b. Cathode efficiency is independent of pH, in the presence of sodium carbonate.

c. The limiting current density was about 24 amps/sq.ft. or 2.5 amps/$10^{-2}m^2$, for all pH values, before inhibiting polarization set in, as can be seen in Fig. 57.

d. Above pH 13.3 the anode operated at only 1.5% efficiency and was virtually insoluble, again indicated in Fig. 56.

e. Anode area should be twice cathode area.

f. Cathode efficiency was constant over wide range of copper and Rochelle salt concentrations.

g. The "free cyanide" concentration was critical and required constant analytical control.

With these points as guide lines, the electrolyte was prepared and controlled as suggested.

Unfortunately, however, the data of Graham and Read is not tied to any quantitative data associated with the deposit, only a qualitative colour/surface appearance table being given in their report for any set of variations. In this work an estimation of the tensile strength of plated tows has been chosen as a monitor to evaluate the effect of the many variables investigated.

Fig. 56 Electrode Efficiency in Standard Rochelle Salt Bath.

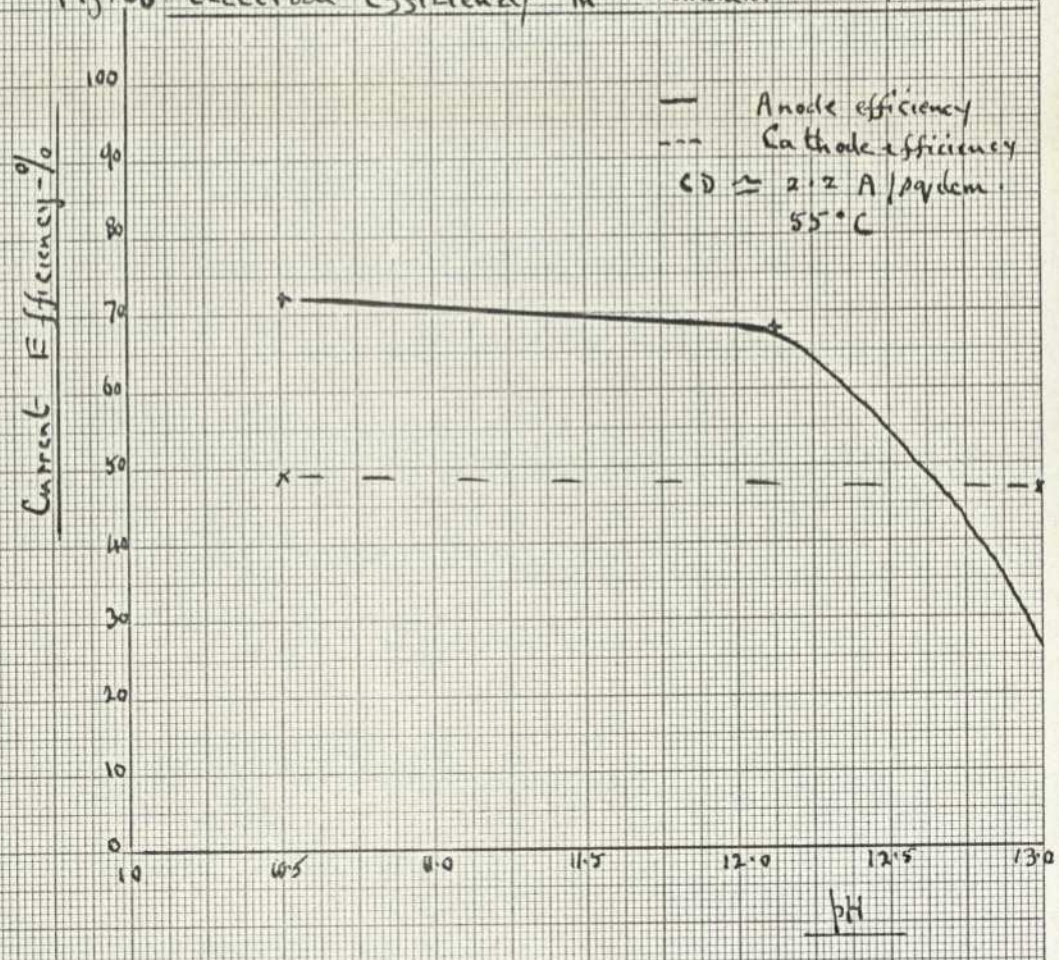


Fig. 57 Anode Polarization.

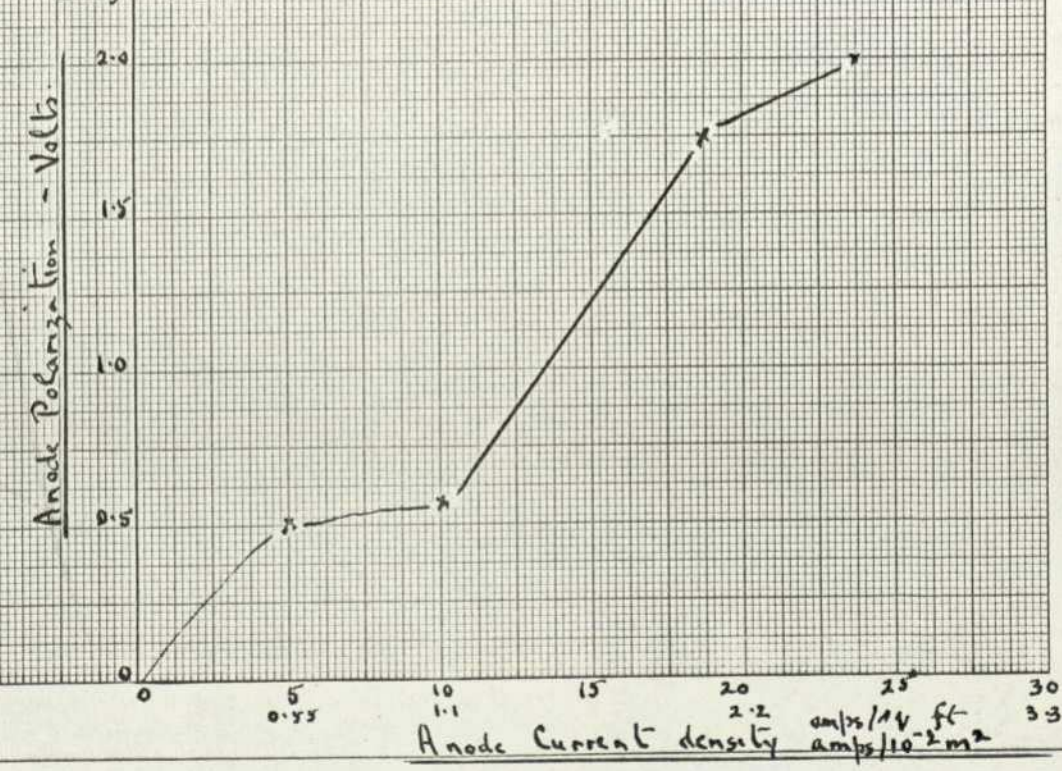


TABLE 10

Plating detail

Vessel	Pyrex dish, 2000 ml.			
Anode	Copper, cylindrical, 25 x 10 cms immersed, or 250 sq. cms. facing cathode.			
Electrode spacing	9 cms. radial			
		g/l	oz/gel	Formula
Electrolyte	Copper cyanide	21.9 (20-25)	3.5	CuCN
	Sodium cyanide (total)	28.8 (25-30)	4.6	NaCN
	Free cyanide	6.0 (4 - 8)	1.0	NaCN
	Rochelle salt (sodium potassium tartrate)	50 (40-50)	8.0	$NaKC_4H_4O_6$
	Sodium carbonate	25 (20-40)	4.0	$Na_2CO_3 10H_2O$
	Sodium hydroxide to pH 12.6 (12.2 - 12.8)			
Electrolyte volume	1500 ml			
Agitation	Glass paddle			
Ageing	None			
Plating time	1 hour			

6.2 Experimental detail

Standard 4" tows of Type II fibre were weighed, racked and plated at controlled current densities in the manner described in Section 5.3.

For the temperature range 20-50°C investigated, 1500 ml of electrolyte in a Pyrex 2000 ml circular dish, was immersed to solution level in a thermostatically controlled water bath maintained at the chosen temperature to within ± 1°C by means of a Techne Tempunit control unit, and the electrolyte was stirred with a glass paddle operated by a Townson and Mercer compressed air motor.

Two litres of electrolyte were prepared for each temperature run, the residual 500 ml being used to make up volume after each analysis. Evaporation losses were made up to the fixed mark with distilled water.

To determine the life of the cyanide bath and the plating range in which good deposits were formed, runs were made to show the variations of the Faradaic efficiency with free cyanide concentration and to delineate the relationship between free cyanide content and total current passed.

Finally a set of specimens was plated over an experimental test block of 5x5 temperature/current density ranges, taking three 4" specimens from each standard 4" tow, making 75 specimens in the complete comparison plating range prepared.

The plating details are given in Table 10 and after plating, all tows were washed, vacuum dried and weighed, as described in Section 5.3 and subsequently tensile tested, as described in Chapter 4.

To determine the distribution of copper throughout the fibre tow, specimen segments from the center to the periphery of sample tows, from each current density range, were mounted in a Millen mounting press with the fibre axis at right angles to the die surface, in a thermosetting Bakelite compound, at 140°C under a pressure of 3000 p.s.i. The mounted specimen was then ground, (under paraffin to avoid galvanic attack,) on silicon carbide impregnated papers of grit grades 240, 320, 400 and 600 mesh.

Relationship between "Free cyanide" concentration and titration reading.

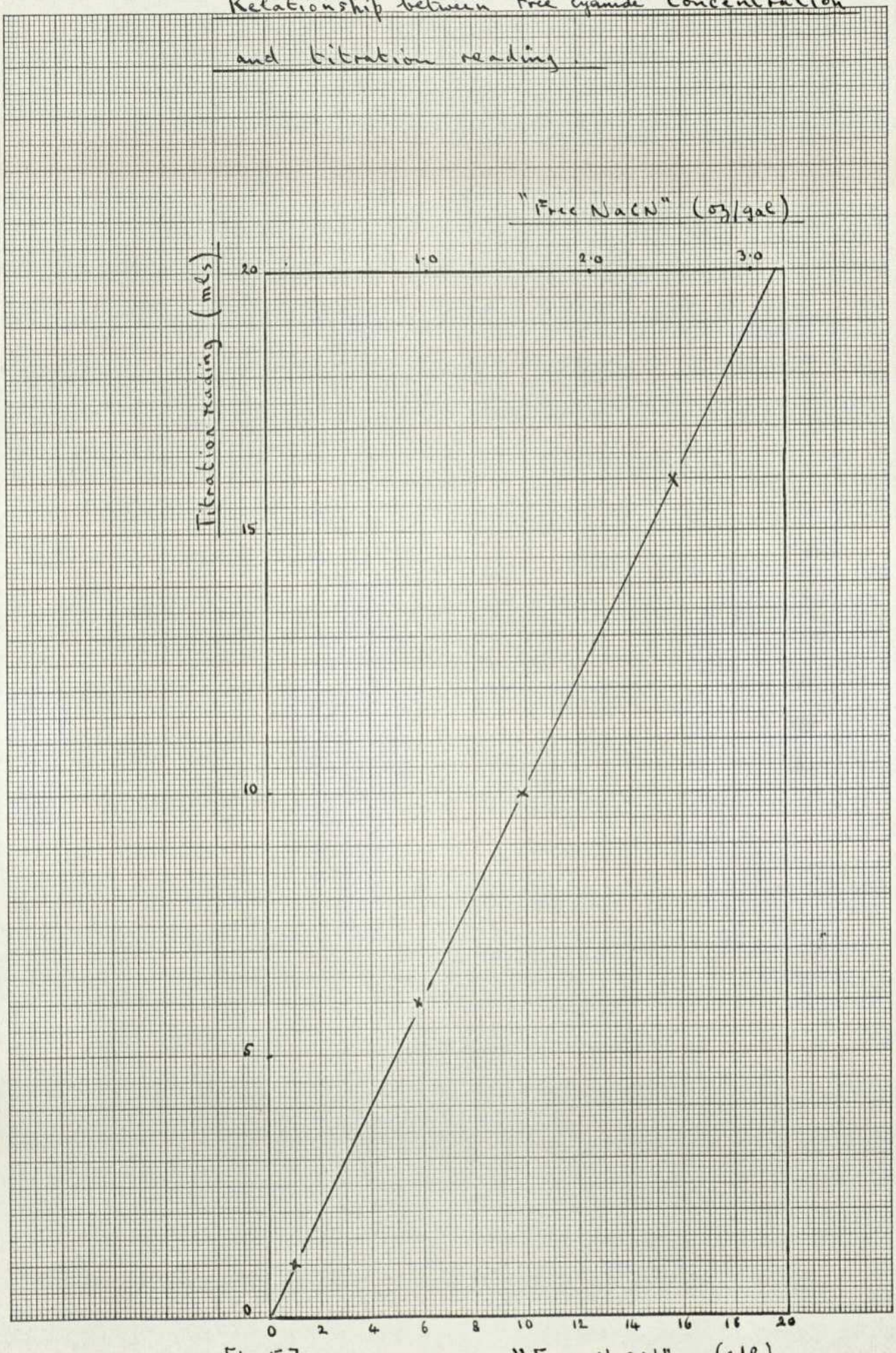


Fig. 57a

They were then finished on Jackson polishing wheels covered with Selvyt cloth impregnated with Hyprez diamond grease compound, in particle size stages from 8, 6, 1 and $\frac{1}{4}$ micron. A final polish on a Selvyt cloth, with MgO, producing a mirror surface.

6.3 Analytical control

The concentration of free cyanide in the stock solution was determined initially and then before each run, using a modification of the analytical technique described by Thompson[7], (1931).

Thus, a 10 ml sample of the electrolyte, taken with a rubber syphon safety 'Propipette', (a proprietary name for a pipette with a rubber bulb) was titrated with N/10 silver nitrate, until faint turbidity, using 1 ml of a 10% potassium iodide indicator.

Then

$$TR \times 0.0098 \times 100 = g/l \text{ free } NaCN,$$

where T.R. = titration reading.

A graphical representation of this titration is given in Fig. 57a, for convenience.

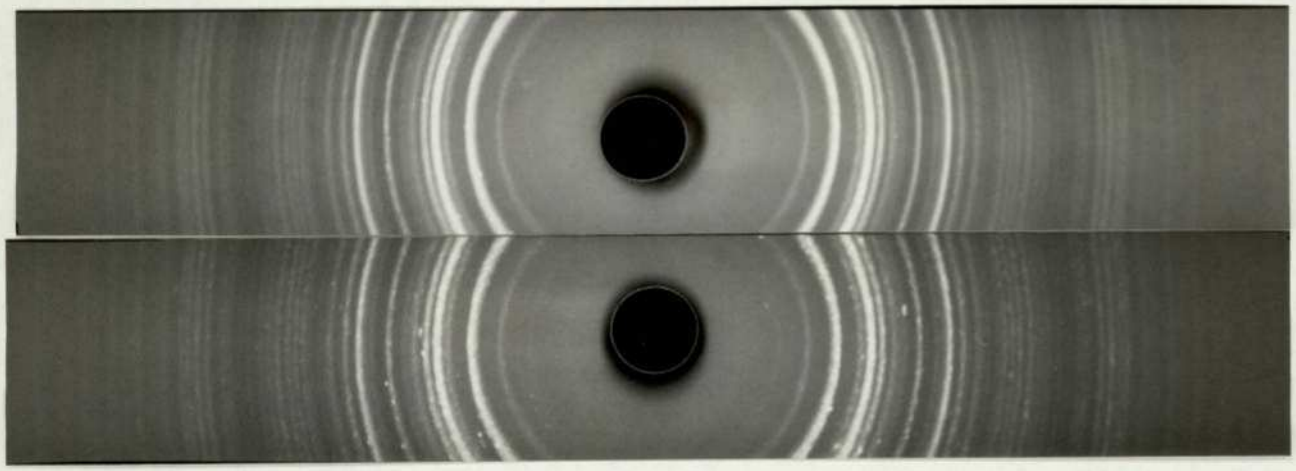
Stock solutions

A.R. silver nitrate, $AgNO_3$, N/10, 17 g/l.
A.R. potassium iodide, KI, 100 g/l.

The 10 ml sample removed for each test was replaced, in the main body of the electrolyte, from the 500 ml of stock solution. The pH of the electrolyte was taken with a glass electrode on a Model 23, direct reading pH meter by Electronic Instruments Ltd.

As a quality control on the B.D.H. copper cyanide used in this work, samples of fresh powdered cyanide, A, were compared with the industrial product, B, by X-ray powder diffraction techniques since the industrial cyanide sample, by chance, happened to be 25 years old, offering an ideal opportunity to look for degradation with time.

A. Laboratory quality, B.D.H. copper cyanide.



B. Industrial quality copper cyanide

Fig. 57b Comparison between laboratory and industrial copper cyanide

Variation of Faraday efficiency with "Free Cyanide" concentration.

at the Cathode, at 45°C.

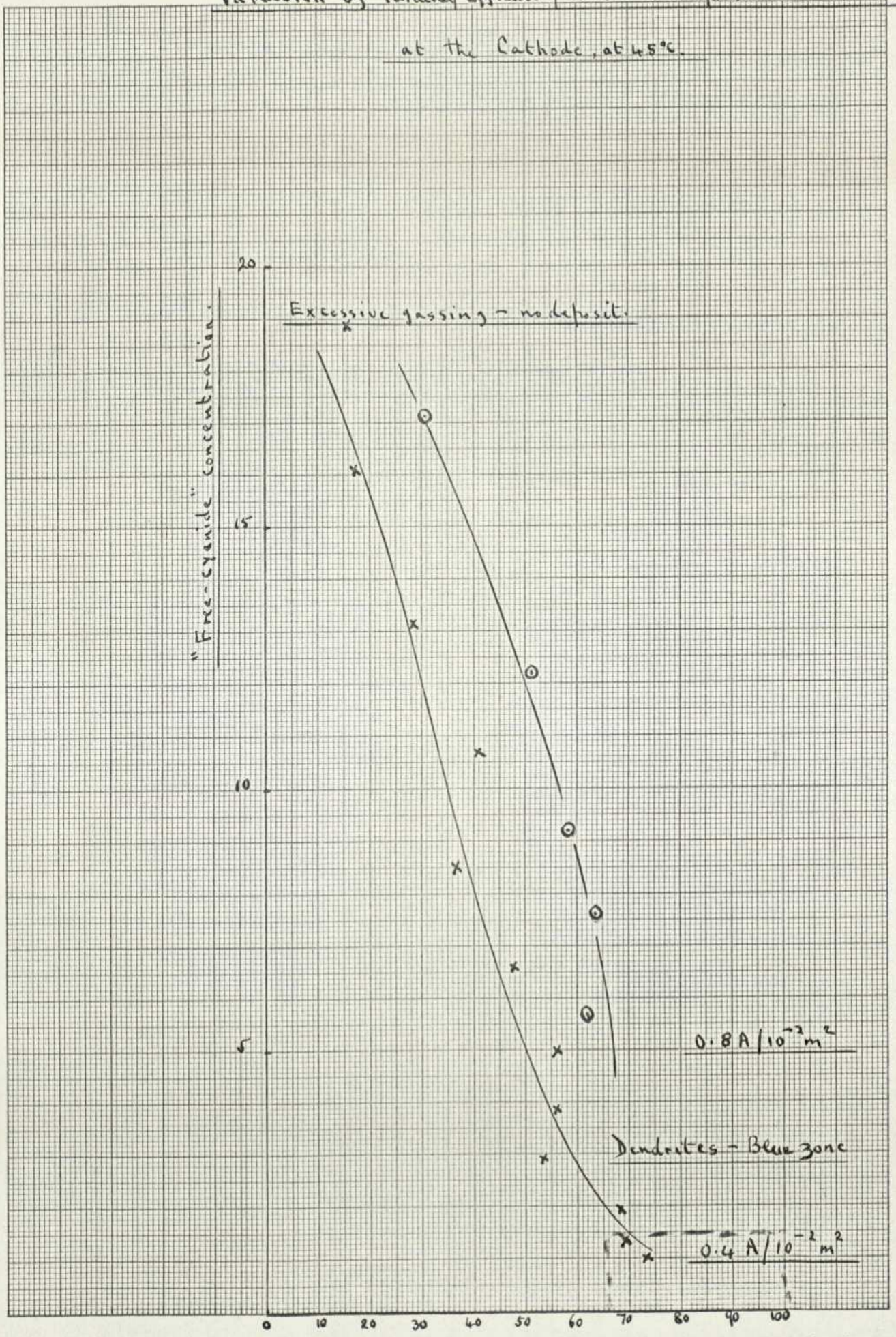


Fig. 58



Fig. 59 Dendritic fern growth on single carbon fibre. X4.

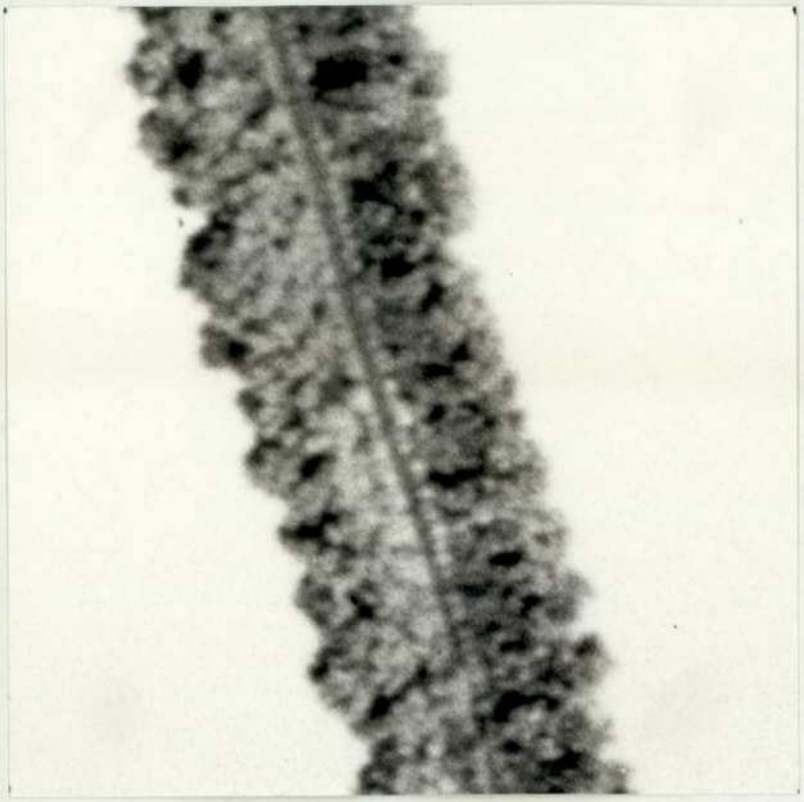


Fig. 60 Close up of dendrite structure on single carbon fibre. X1000.

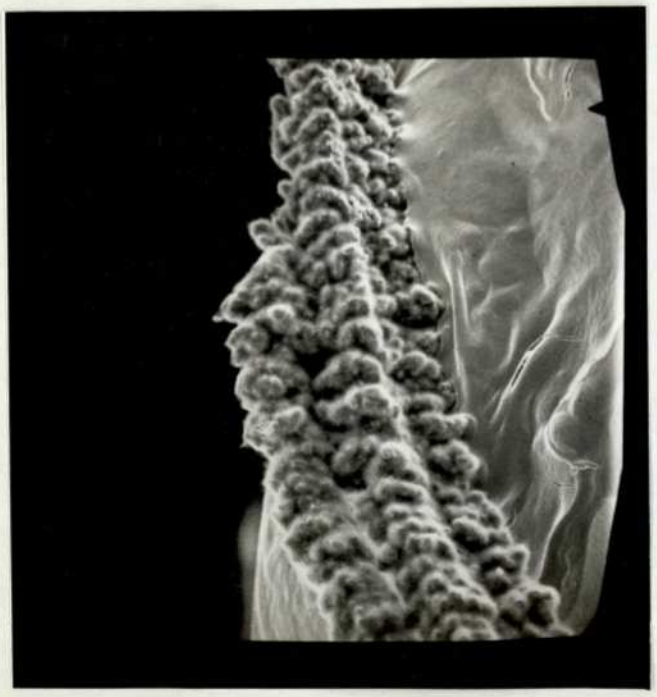


Fig. 61 Graphite whisker. X75.
(After Bennett[9], 1970)

Decrease in "free cyanide" concentration with passage of current, at 45°C

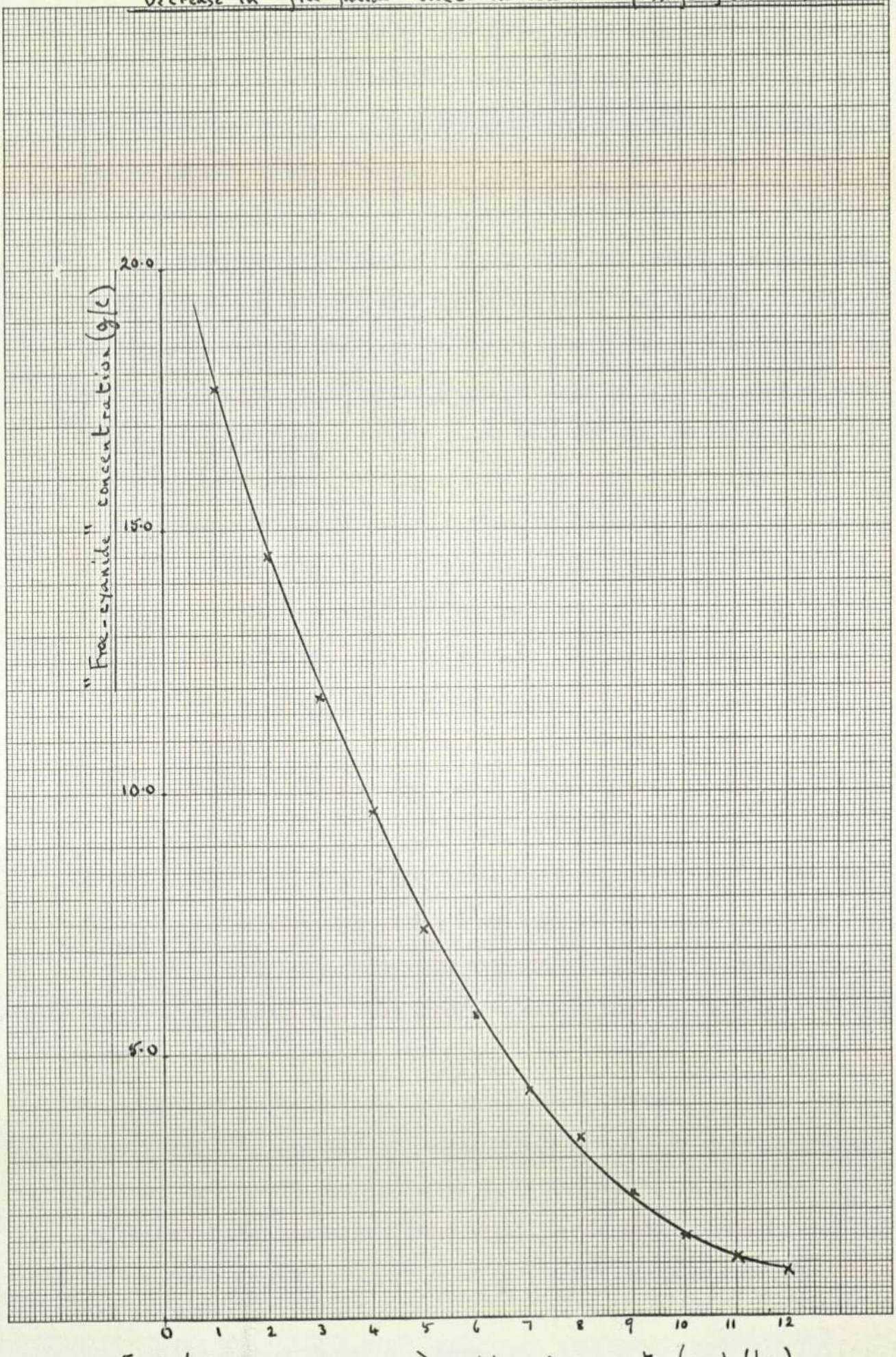


Fig. 62

Variation of U.T.S. with "free Cyanide" concentration.

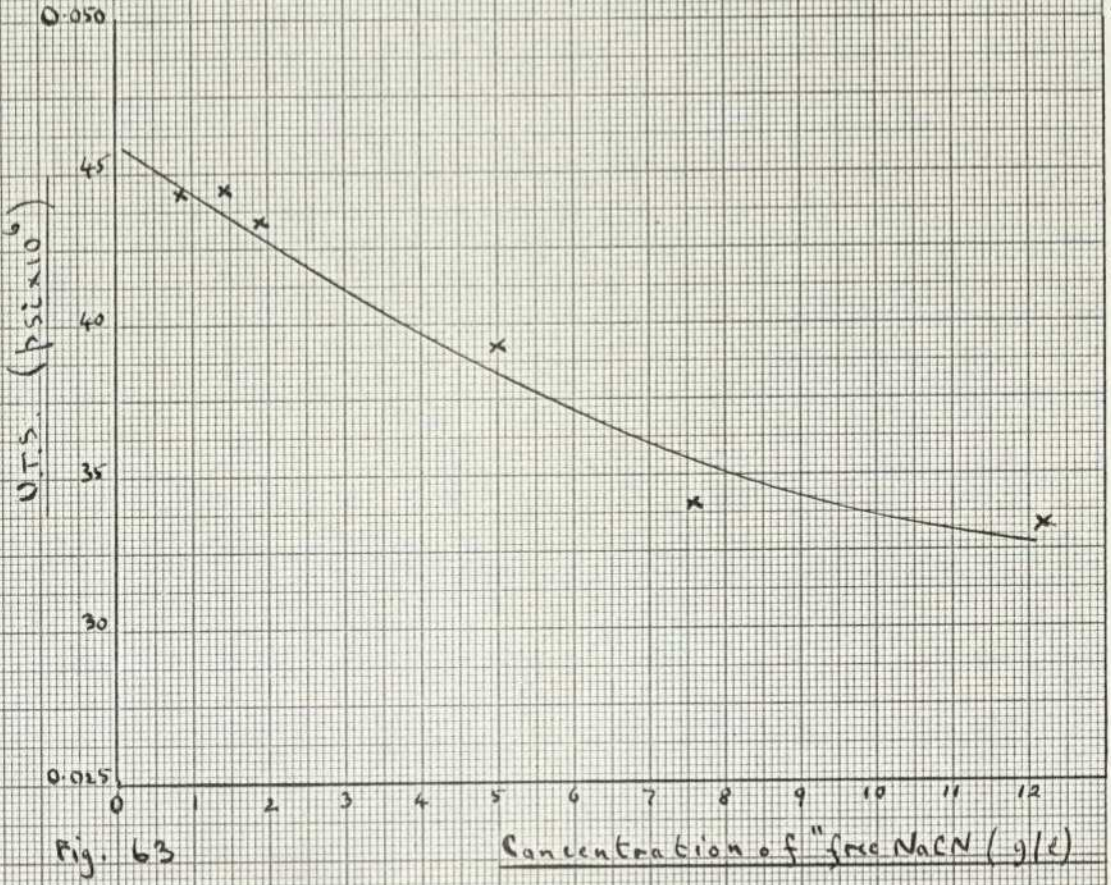


Fig. 63

Table II Variation of U.T.S. of Cu plated Type II fibre with various parameters, calculated from direct weight of Cu.

	0·1 A/10^{-2} m^2				0·2 A/10^{-2} m^2				0·4 A/10^{-2} m^2				0·6 A/10^{-2} m^2				0·8 A/10^{-2} m^2			
Deposition Temparature	No.	U.T.S (psi x 10^6)	F_f	1-F_f	No.	U.T.S (psi x 10^6)	F_f	1-F_f	No.	U.T.S (psi x 10^6)	F_f	1-F_f	No.	U.T.S (psi x 10^6)	F_f	1-F_f	No.	U.T.S (psi x 10^6)	F_f	1-F_f
	197	–			200	0·0740	0·50	0·50	203	–										
20°C	198	0·0925	0·61	0·39	201	–			204	0·0583	0·32	0·68	95	0·0458	0·24	0·76	95	0·0331	0·16	0·84
	199	0·1002	0·63	0·37	202	0·0671	0·49	0·51	205	0·0530	0·32	0·68								
Arithmetic Mean		0·0964	0·62	0·38		0·0706	0·50	0·50		0·0557	0·32	0·68								
Standard Deviation		3840 psi.	% S.D. = 4·0			3450 psi	% S.D. = 4·9			2650 psi	% S.D. = 4·8									
	185	0·0972	0·60	0·40	209	0·0577	0·41	0·59	212	0·0536	0·27	0·73								
30°C	207	0·0936	0·58	0·42	210	0·0580	0·39	0·61	213	–										
	208	–			211	0·0678	0·39	0·61	214	0·0512	0·25	0·75								
A.M.		0·0954	0·59	0·41		0·0612	0·40	0·60		0·0524	0·26	0·74								
S.D.		2359	% S.D. = 2·5			4692	% S.D. = 7·7			1200	% S.D. = 2·3									
	215	–			218	0·0715	0·39	0·61	221	0·0471	0·24	0·76	224	0·0433	0·18	0·82	227	0·0422	0·13	0·87
40°C	216	0·0907	0·50	0·50	219	0·0666	0·37	0·63	222	0·0462	0·27	0·73	225	0·0361	0·18	0·82	228	0·0418	0·14	0·86
	217	0·0943	0·54	0·46	220	0·0732	0·35	0·65	223	0·0512	0·24	0·76	226	–			229	0·0477	0·17	0·82
A.M.		0·0925	0·52	0·48		0·0704	0·37	0·63		0·0485	0·25	0·75		0·0397	0·18	0·82		0·0439	0·15	0·85
S.D.		1800.	% S.D. = 1·9			2798.	% S.D. = 4·0			2642.	% S.D. = 5·4			3600.	% S.D. = 9·1			2693.	% S.D. = 6·1	
	230	0·0819	0·51	0·49	233	0·0587	0·36	0·64	236	0·0484	0·25	0·75	239	0·0420	0·23	0·77	242	–		
45°C	231	0·0830	0·50	0·50	234	0·0538	0·37	0·63	237	0·0465	0·23	0·77	240	0·0358	0·19	0·81	243	0·0340	0·15	0·85
	232	–			235	0·0675	0·33	0·67	238	0·0477	0·21	0·79	241	–			244	0·0330	0·15	0·85
A.M.		0·0825	0·51	0·49		0·0600	0·35	0·65		0·0475	0·23	0·77		0·0389	0·21	0·79		0·0335	0·15	0·85
S.D.		550.	% S.D. = 0·7			5668.	% S.D. = 9·4			778.	% S.D. = 1·6			3100.	% S.D. = 8·0			500.	% S.D. = 1·5	
	245	0·0714	0·44	0·56	248	0·0514	0·34	0·66	251	0·0449	0·20	0·80	254	0·0398	0·16	0·84	257	0·0312	0·12	0·88
50°C	246	0·0774	0·48	0·52	249	0·0561	0·35	0·65	252	0·0405	0·22	0·78	255	0·0349	0·16	0·84	258	0·0316	0·12	0·88
	247	0·0751	0·46	0·54	250	0·0543	0·32	0·68	253	0·0426	0·21	0·79	256	0·0340	0·16	0·84	259	0·0312	0·12	0·88
A.M.		0·0746	0·46	0·54		0·0539	0·34	0·66		0·0427	0·21	0·79		0·0369	0·16	0·84		0·0313	0·12	0·88
S.D.		2472.	% S.D. = 3·3			1936.	% S.D. = 3·6			1450.	% S.D. = 3·4			2368	% S.D. = 6·4			20.	% S.D. = 0·06	

concentration change is not so rapid. For example, under the laboratory conditions described, the total available free cyanide would be about 10 gms, for each solution volume of 1500 mls whereas the total available free cyanide in 1000 gallons of electrolyte at 1 oz/gal concentration, would be 62.5 lbs or about 28,313 gms.

The variation of tensile strength of plated tow with free cyanide concentration, for any given run is shown in Fig. 63. There is a reduction in strength with increased cyanide content but the problem is made complex by the fact that tensile strength will also vary with thickness of deposit which also increases for a given increase in current density, and this problem must therefore be reviewed when more facts are available.

Results for the standard experimental test block of 5x5 temperature/ current density ranges are shown in Table 11 and they provide indications of trends of variations of tensile strengths with temperature and current density and they also provide a check on the progress of experimental accuracy, during the long runs involved.

For example, any violent fluctuation in the arithmetic meanof any three samples would show poor experimental control, any deviation from the mean, above 10%, would also indicate indifferent technique. In fact the per cent variation of the standard deviation was, in this series, never as high as 10% and on average, over the whole period of 75 hours plating time, only 4.3%. This compares favourably with the 9% deviation from the mean, quoted in Section 5.4, for unplated whole tow tensile tests.

It is realized, of course, that a true standard deviation for any set of samples, cannot be calculated from a comparison of three units, but this method of assessment of results was chosen to reveal gradual deterioration of experimental control of the very fragile 10,000 fibre tows used in this work, and as can be seen the per cent standarddeviations from the mean of the last three runs, of three units, were 3.4, 6.4 and 0.6%, showing

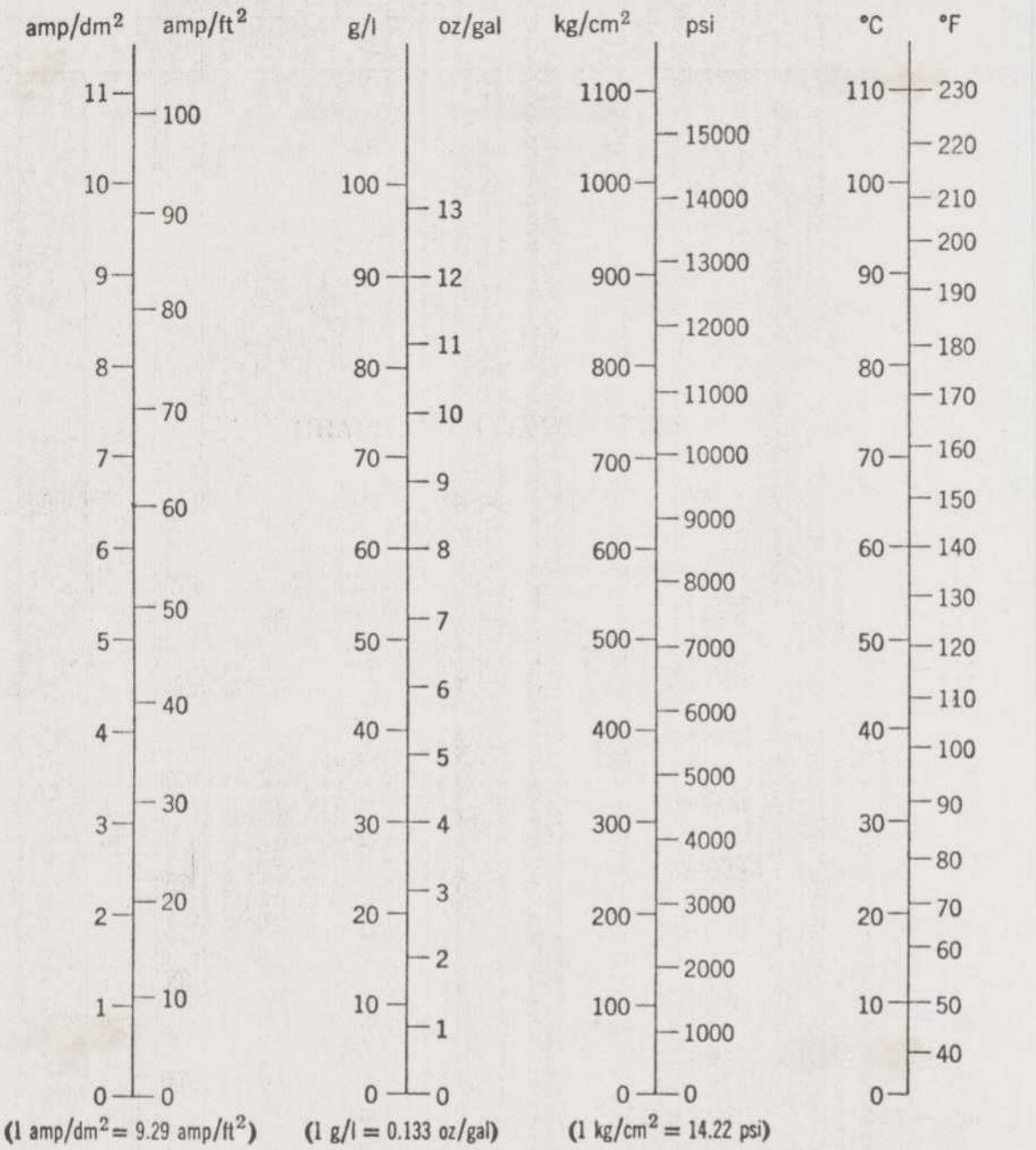
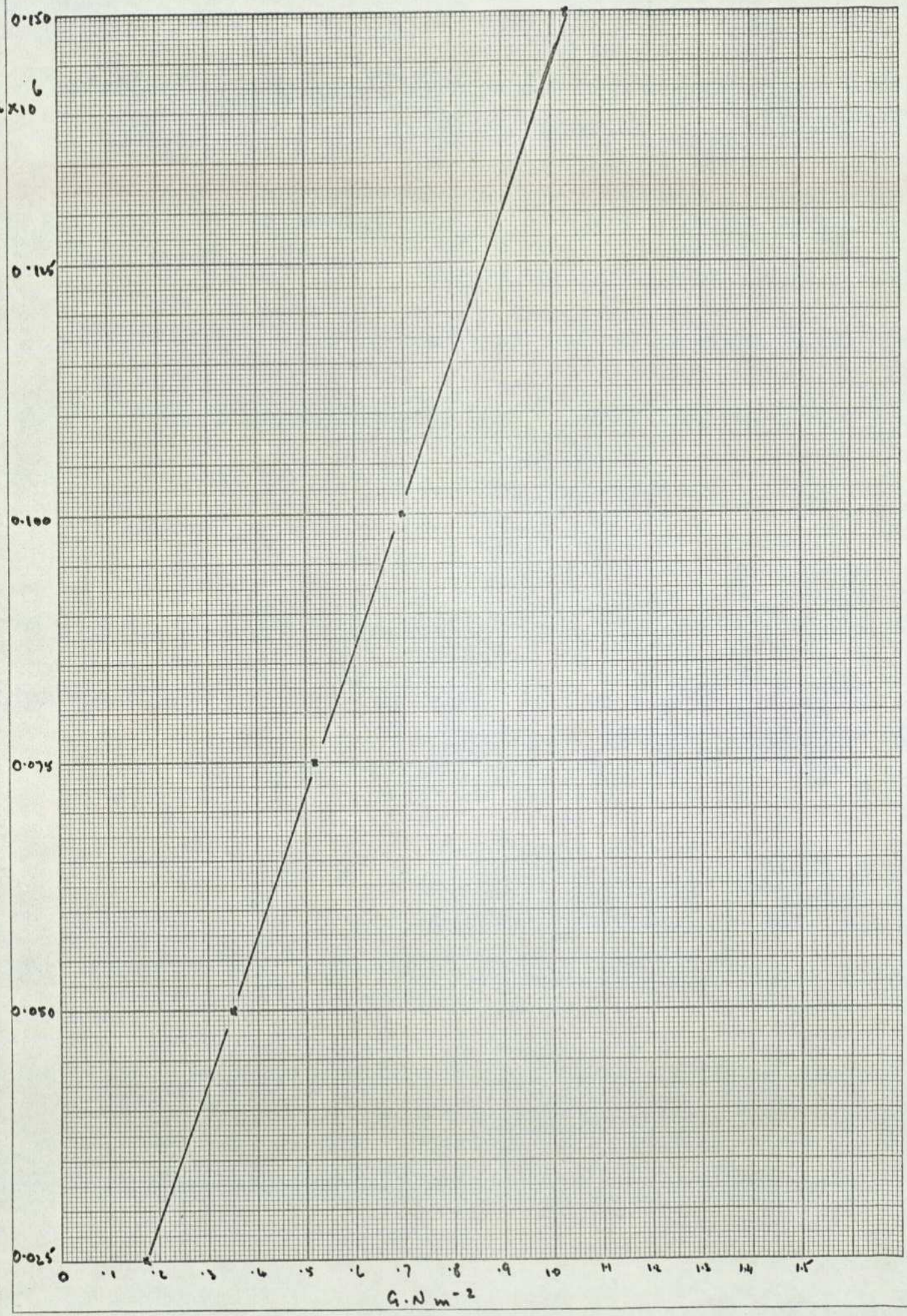


Table 12. Graphical Conversions

Fig. 66. Conversion from p.s.i. to $G\,N\,m^{-2}$.



Experimental scatter in 45°C Standard Cu CN run.

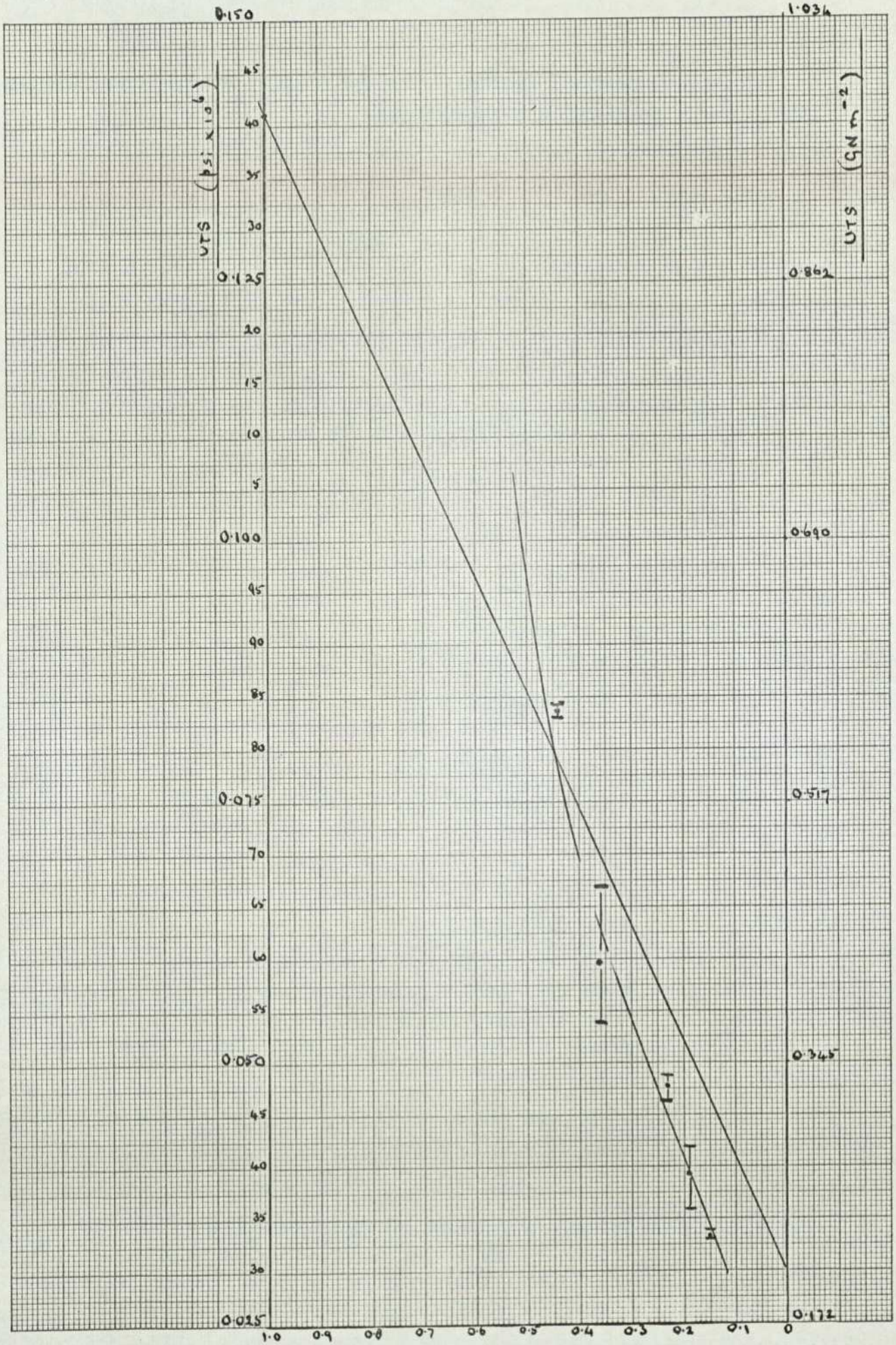


Fig. 65 Vol. fraction of C fibre in Cu plated tow.

Variation of U.T.S with temperature.

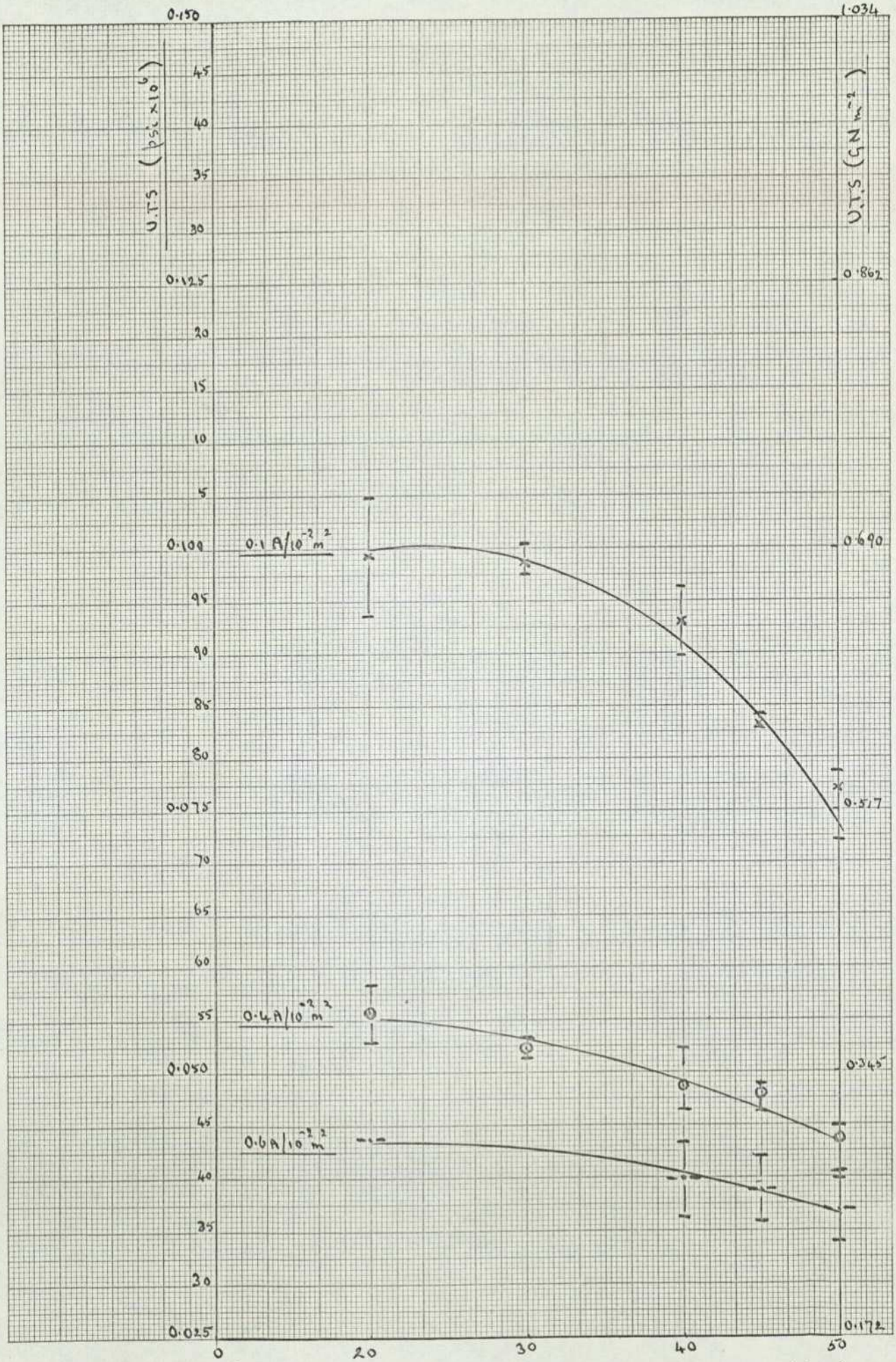


Fig. 66

Variation of

U.T.S. with vol. fraction of C fibre in plated tow, at various temperatures.

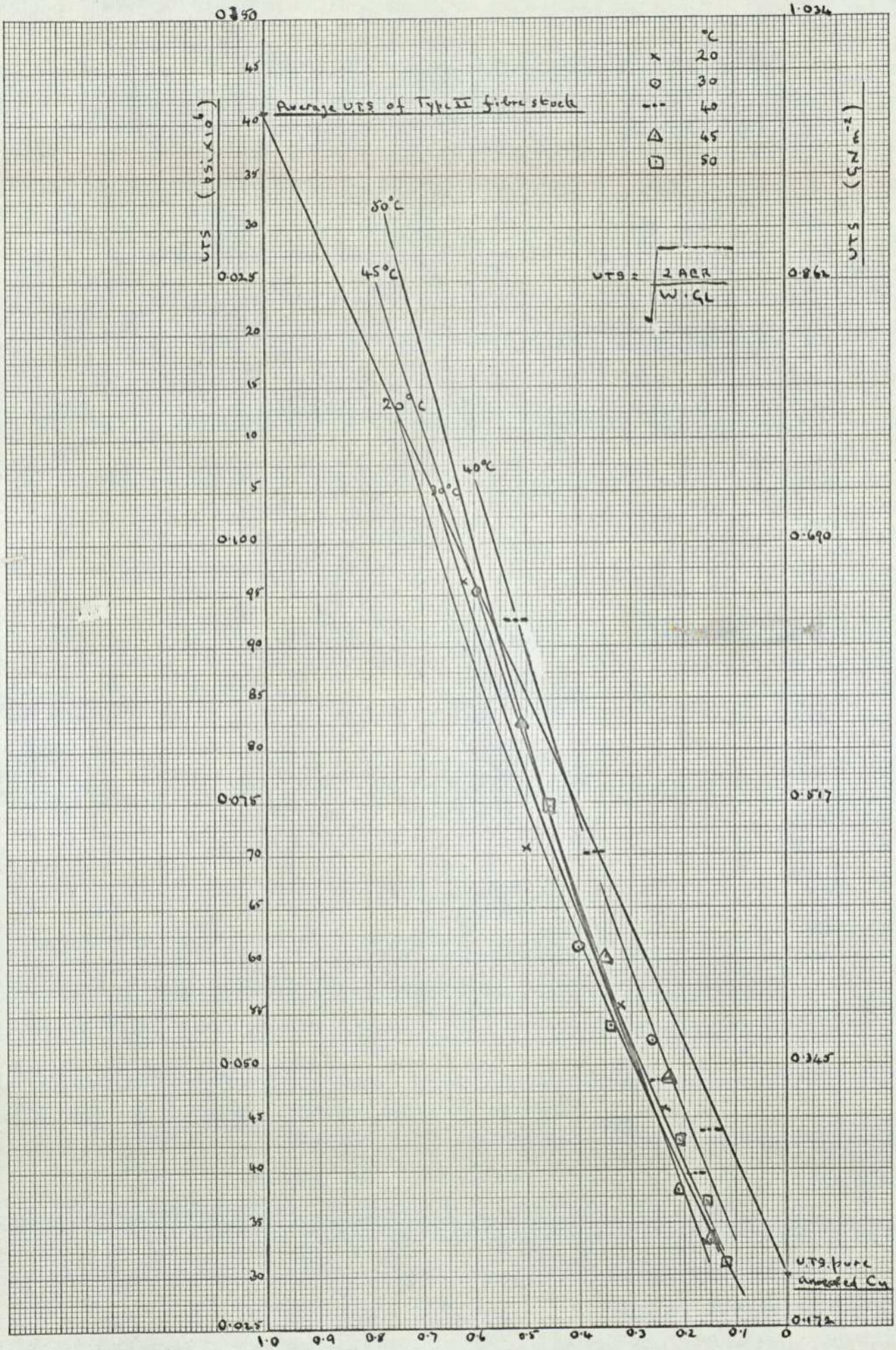


Fig. 67 Vol. fraction of C fibre in Cu plated tow.

that control had not become lax.

6.5 Analysis of tensile strength results

An analysis of the important variations of tensile strength with the variables studied is given below. To assist in the evaluation of these results, Lowenheim's[10], (1942) conversions from sexagesimal to metric and then on to SI units for tensile results are given in Table 12 and Fig. 64.

From the results of the tensile strengths of Cu plated tows shown in Table 11, a plot of the variation of strength with volume fraction of carbon fibre is given in Fig. 65, for deposits made at 45°C. The experimental scatter is shown and was some 3-4 times less than that shown by the general unplated carbon fibre tests given in Fig. 24, Chapter 2. This is to be expected since all results in this work are from a single batch of fibre and not from a random selection of tows from random batches of material. It should also be noted that these results are near but not quite equal to those given by the calculated values, using the "law of mixtures" as control, and the thinner the deposit, that is to say the greater the volume fraction of carbon fibre, the nearer the match to the calculated strength.

Fig. 66 shows a comparison of tensile strengths of fibres plated at various temperatures and current densities. As can be seen, the strength falls with rise in temperature the highest value of UTS being at about 30°C and rises with fall in current density, or in other words the thinner the deposit the stronger the plated composite, bearing in mind that all deposits formed in this work were plated for the constant time of one hour. Fig. 67 however shows that when all the tensile results for each temperature are plotted against volume fraction of carbon fibre in the composite, then, within the large experimental scatter associated with this work, there is no significant differences between deposits plated at various temperatures other than their deposit thicknesses, of course.

Relationship between thickness of deposit and vol. fraction of C fibre.

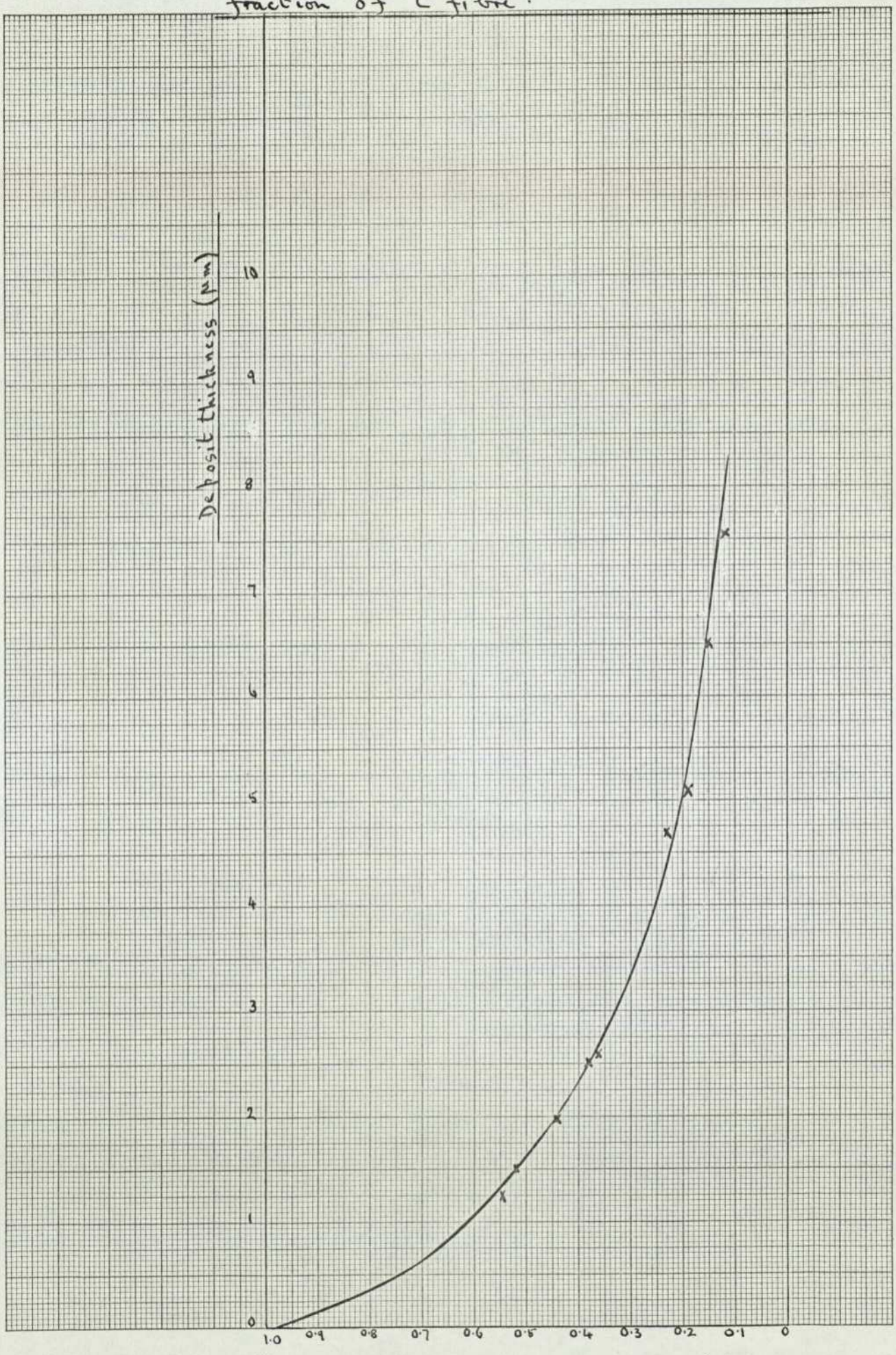


Fig 68 Vol. fraction of C fibre in Cu plated tow

Relationship between UTS and thickness of Cu deposit

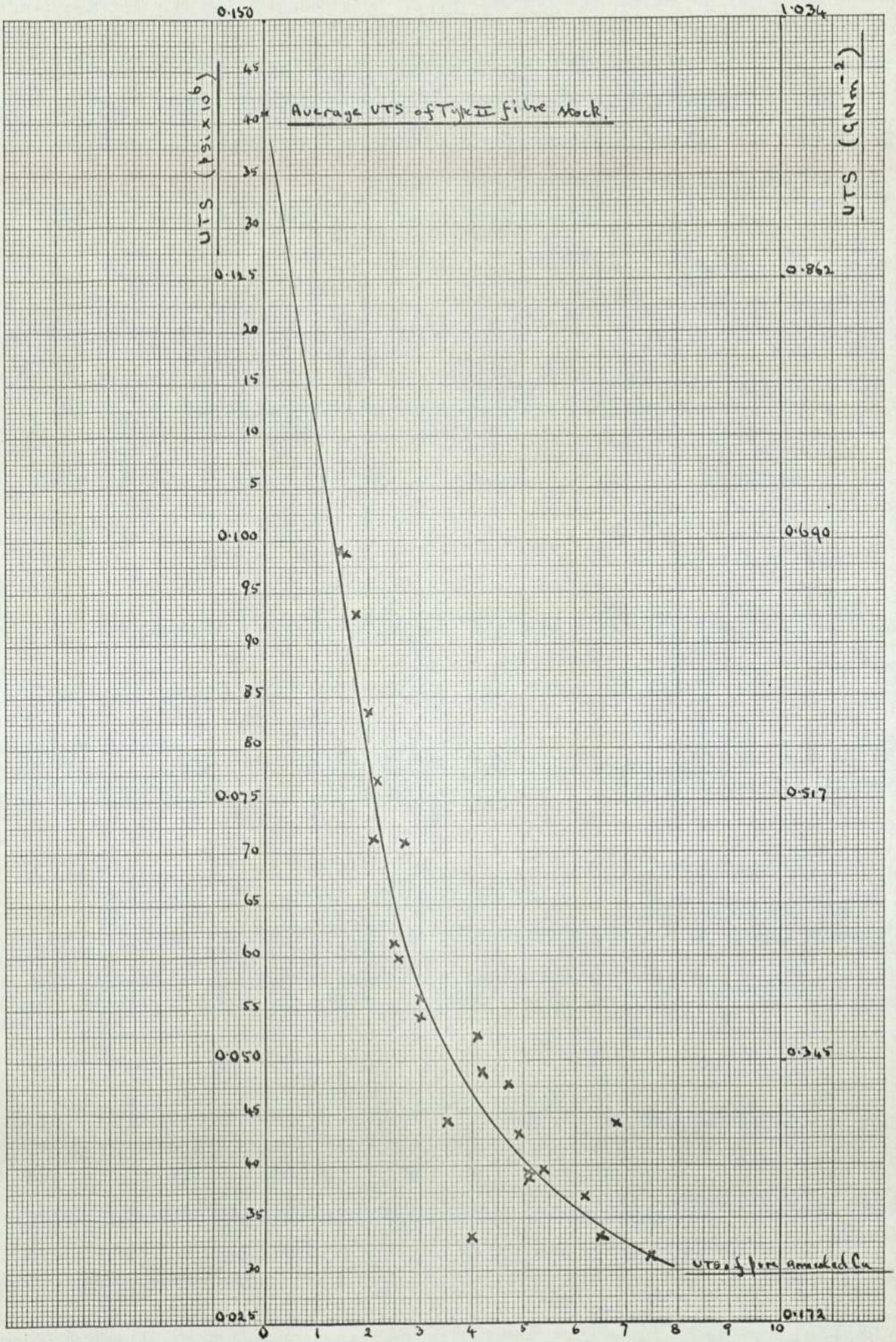


Fig. 69

Random variation of diameter of plated fibre selected at random from plated tow. (10 mins at $0.4 A/10^{-2} m^2$)

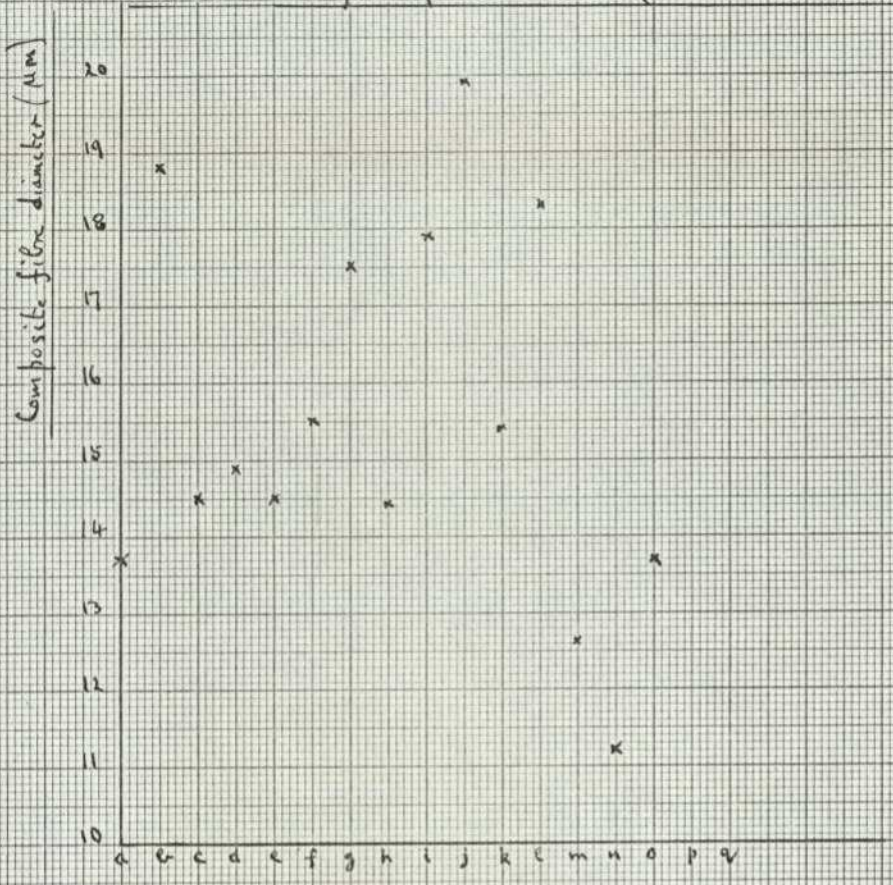


Fig. 70

Mass profile of Cu plated tow, along tow length, plated for 5 M, at $(0.4 A/10^{-2} m^2)$.

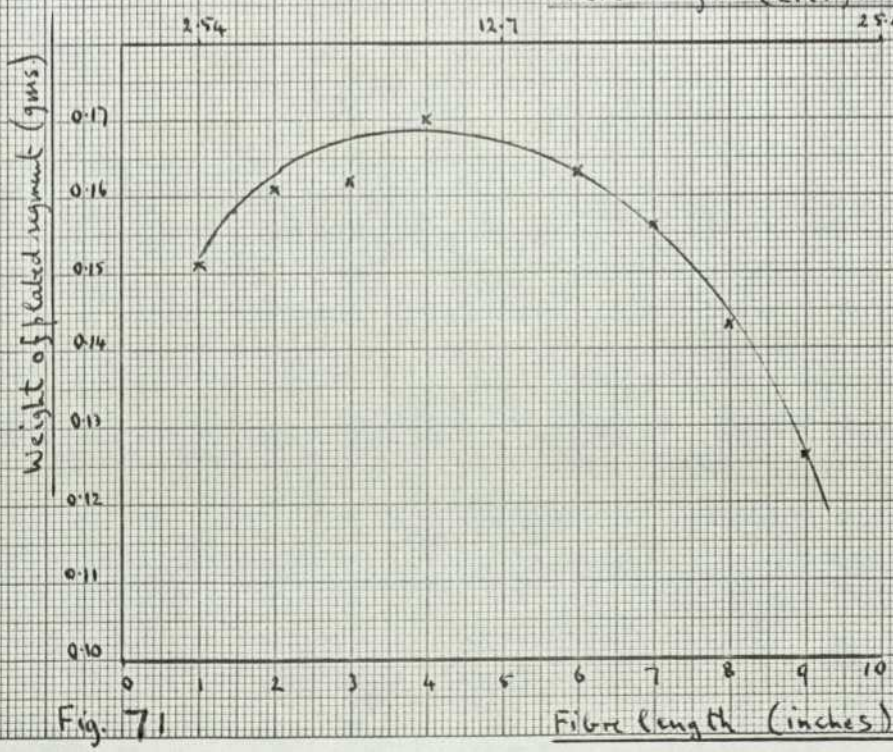


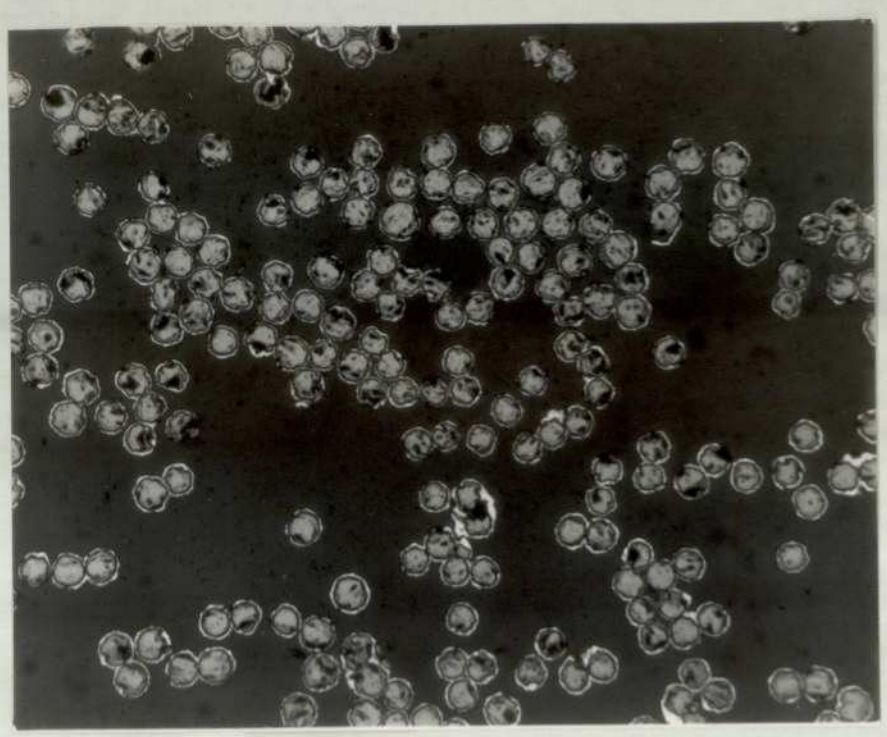
Fig. 71

To appreciate fully the significance of these results one should examine them with the assistance of Fig. 68 which shows the calculated relationship between the thickness of copper deposited on a carbon fibre and the volume fraction of fibre present, taking a Type II, 8 micron, 1.8 density fibre as standard.

Fig. 69 shows the overall relationship of 24 tensile tests, (taken at random from the work described), to the thickness of the copper deposit. The fit to the point of 100% fibre, at 142,000 psi and 100% Cu, at 30,000 psi, is very good, as is the fit of those points at thicknesses of less than 4 microns.

Finally composite Cu/C fibre diameters, of single plated fibres chosen at random from a tow, are shown diagrammatically in Fig. 70. This picture demonstrates the wide variations experienced and it can be seen that attempts to determine absolute values would be difficult, a mean of a large number of results being obviously necessary. To emphasize this point, Fig. 71 shows a mass profile of a plated tow, taking one inch sections along the length of a 14" plated standard bundle. This distribution of copper along the length can be better understood when it is remembered that due to the plating technique of "ballooning" the tow, the center is much nearer the anode than are the ends and of course not so restricted. A further inherent factor of the plated deposit is the distribution of copper throughout the tow. Figures 72-76 show the plating thicknesses on outer and center fibres, at each current density chosen for the experimental test 5x5 block. In each case the outer fibres are substantially thicker than those at the center, a fact which makes the taking of mean values in this work imperative, since no practical method of fibre arrangement would result in even metal distribution, whilst retaining appropriate tensile strengths. The plating thickness distribution revealed by these micro-sections also make it plain that single fibre testing is not practicable.

a. Centre fibres



b. Outer fibres

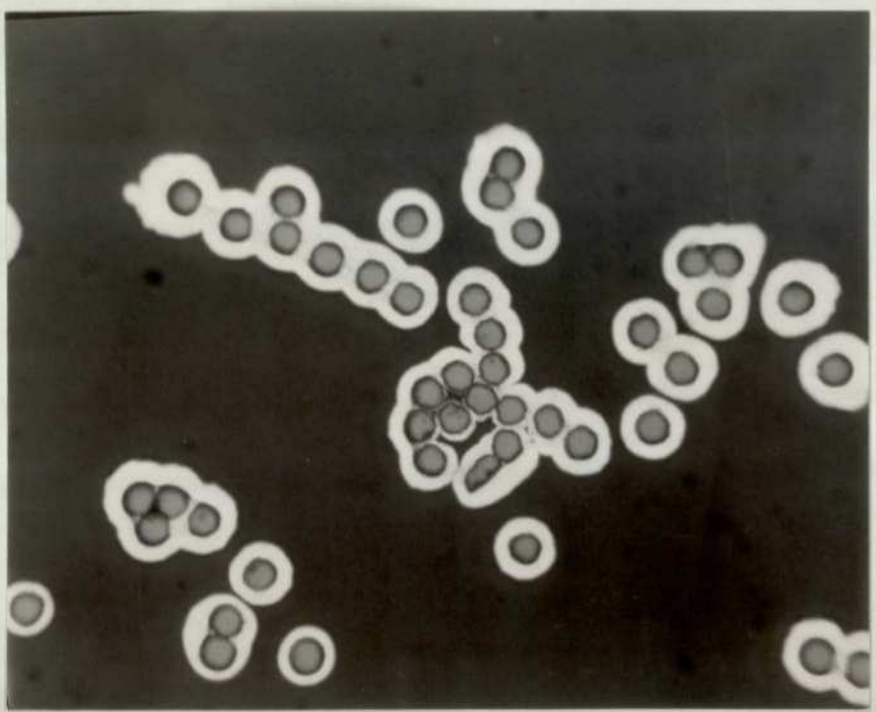
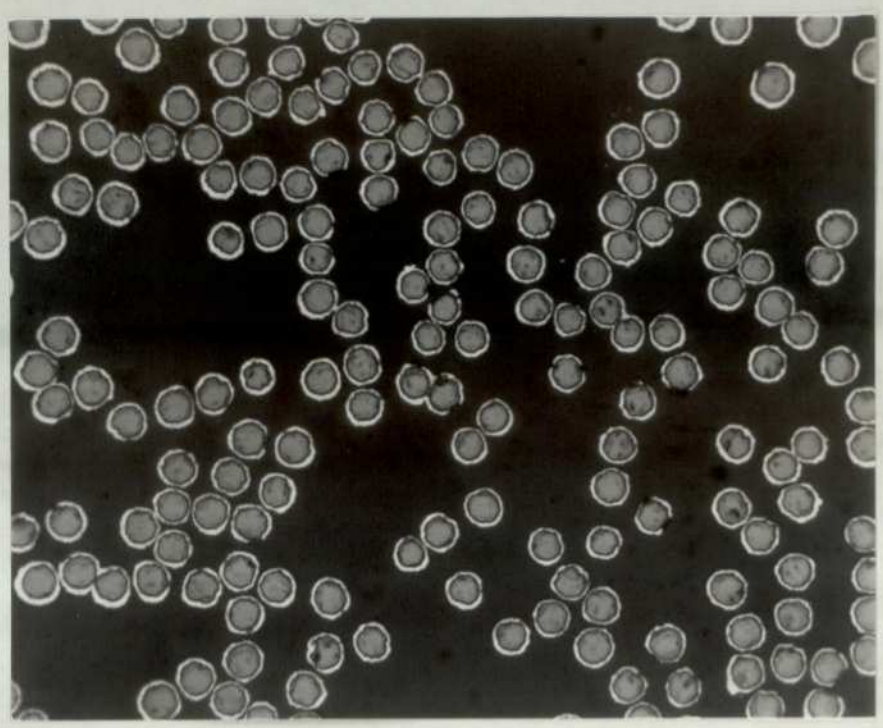


Fig. 72 Distribution of Cu on plated tow 45°, 0.1 A/10^{-2} m^2, 60M, Average volume fraction - 0.56. X500.

a. Centre fibres



b. Outer fibres

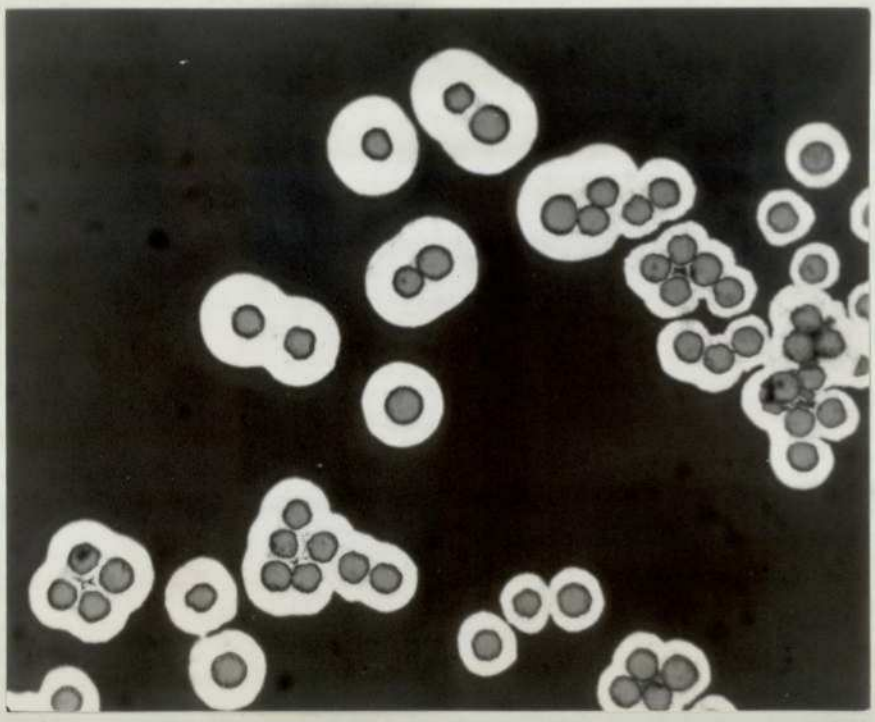
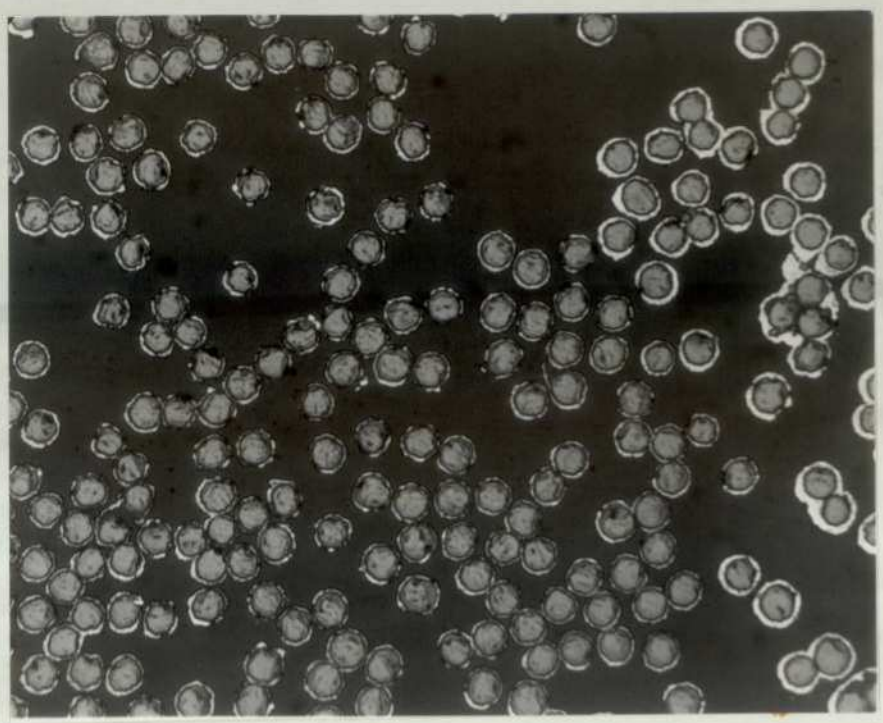


Fig. 73 Distribution of Cu on plated tow 45°C, 0.2 A/10^{-2} m^2, 60M. Average volume fraction - 0.39. X500.

a. Centre fibres

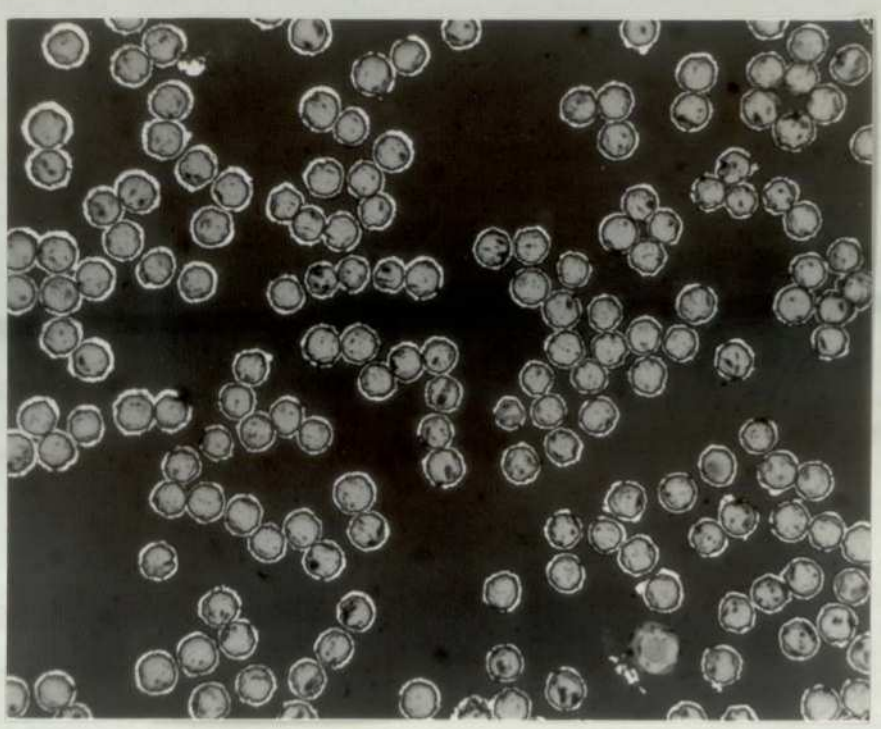


b. Outer fibres



Fig. 74 Distribution of Cu on plated tow 45°C, 0.4 A/10^{-2} m^2, 60M, Average volume fraction - 0.24. X500.

a. Centre fibres



b. Outer fibres

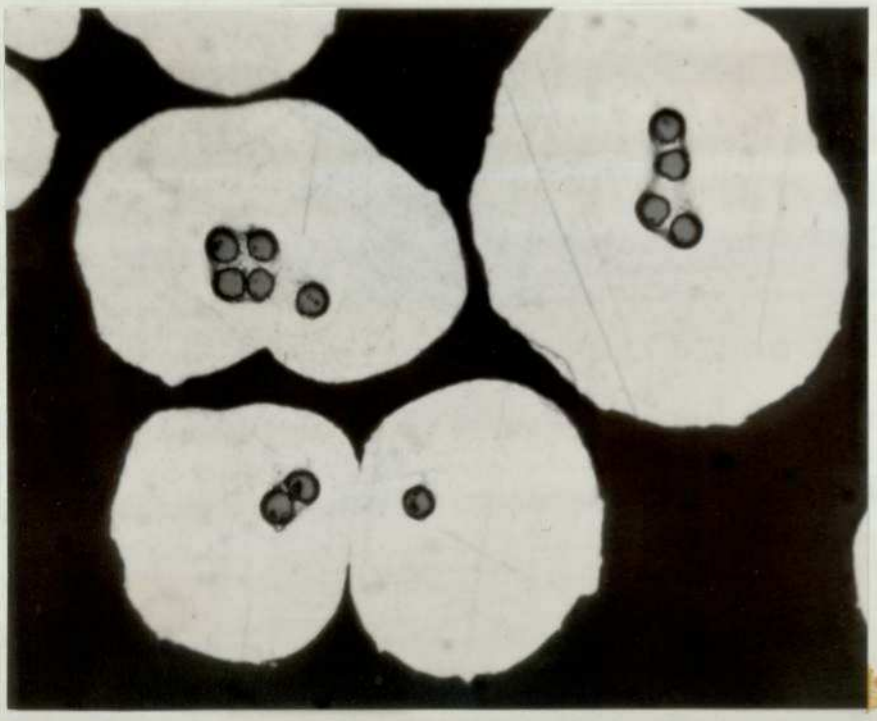
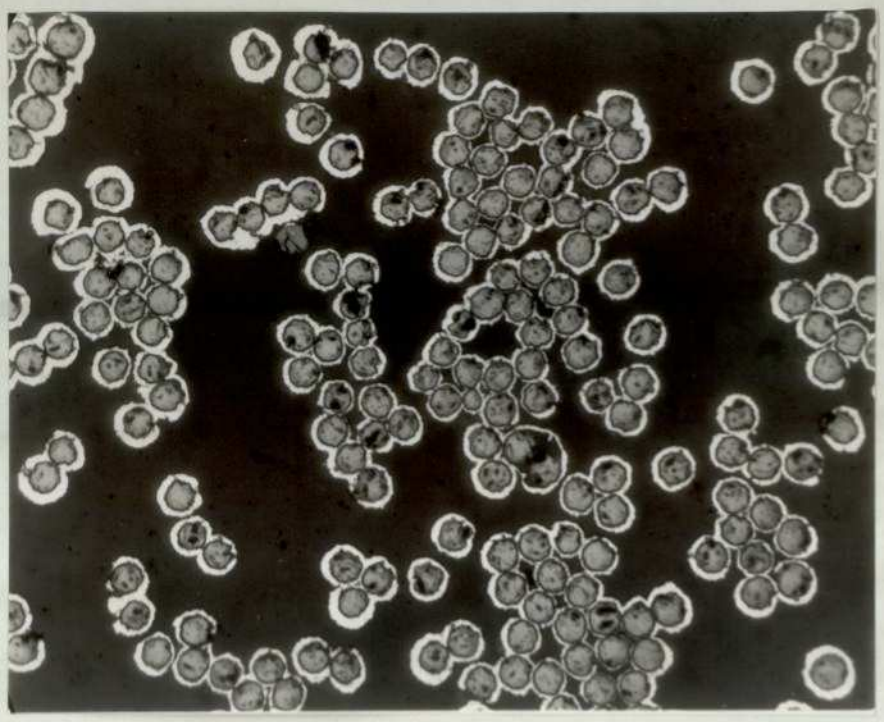


Fig. 75 Distribution of Cu on plated tow 45°C, 0.6 A/10^{-2} m^2, 60M. Average volume fraction - 0.21. X500.

a. Centre fibres



b. Outer fibres

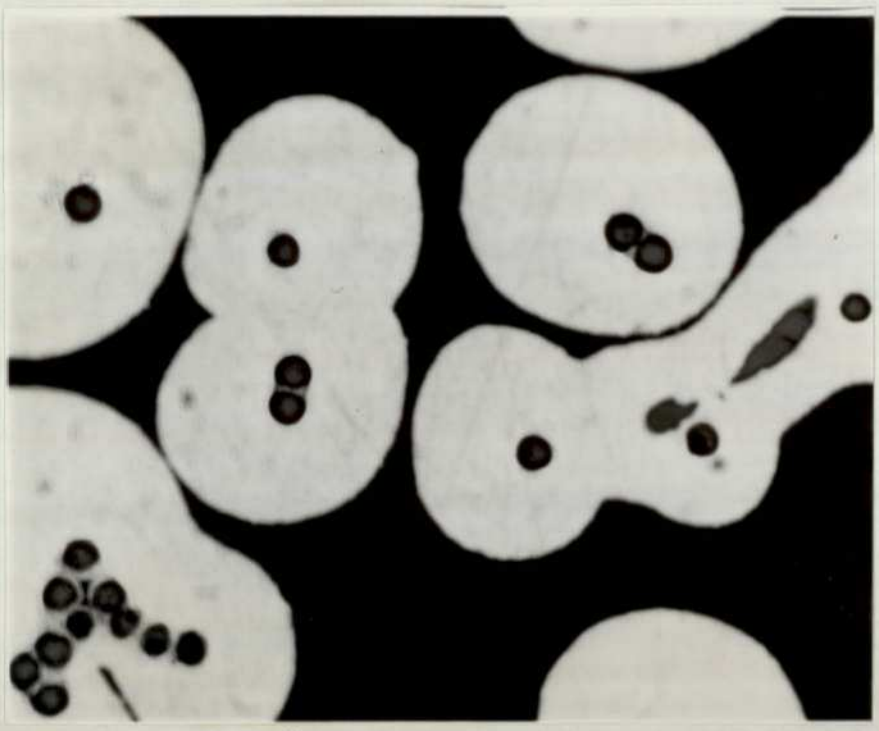


Fig. 76 Distribution of Cu on plated tow 45°C, 0.8 A/10^{-2} m^2, 60 M. Average volume fraction - 0.12. X500.

6.6 Identification of blue compound formed at low free cyanide concentrations

The blue colouration of the solution formed during electrodeposition of copper at low free cyanide concentrations was seen to flow from the anode and it was necessary first to identify the product and then to determine whether the reaction was solely electrolytic or chemical in nature.

A 4 hour run was made at 0.8 $A/10^{-2}m^2$ 20°C, in an electrolyte initially containing 2 g/l free cyanide. This resulted in a heavily plated tow which will be examined later. The electrolyte turned an intense blue during the plating period.

This solution was allowed to evaporate, in a current of warm air, for two days, resulting in the growth of a polycrystalline mass of small blue crystals, on the bottom of the vessel and anode surface. These crystals were washed, dried in vacuo and powdered for X-ray diffraction analysis. In parallel with this sample, sample powder patterns of malachite and azurite, both basic copper carbonates, were prepared.

Fig. 77 shows the comparison and analysis of the 'd' spacings suggests that the blue compound formed, consists approximately of a 75% azurite - 25% malachite mixture: (75%-2 $CuCO_3.Cu(OH)_2$ - 25%-$CuCO_3.Cu(OH)_2$), both of these compounds being insoluble in water but soluble in alkaline cyanide solutions.

To determine whether the blue compound had been formed as a result of electrolysis or not, a 25 ml sample of electrolyte, with and without a 10 sq.cm. sample of Cu sheet, to simulate the metallic anode condition, was allowed to stand for 72 hours, in air. After this period, the formation of an intense blue colouration was observed, but only in the sample with a dummy copper anode. Subsequent trials showed that this colouration took place without the Rochelle salt content in the electrolyte, but not without the sodium carbonate component.

Thus it has been shown that the azurite, basic copper carbonate complex can be synthesized chemically, in the presence of a source of



Fig. 77 Comparison between cyanide blue compound, malachite and azurite

cuprous ions, but that the reaction is much slower by the chemical route, than during electrolysis.

If one considers how complex the electrolyte is with the possible existence in solution of complex cyanide-copper ions such as, $Cu(CN)_2^-$, $Cu(CN)_3^{--}$ or $Cu(CN)_4^{---}$ it is not surprising that odd, unreported, results can take place from time to time, particularly when operating the electrolytic process outside the normal stable range of free cyanide concentration and with an unusually high surface area cathode for such a small volume of electrolyte.

Now Thompson[11], (1941), gives the reaction

$$Cu(CN)_4^{---} \rightleftharpoons Cu^+ + 4(CN)^- \qquad \ldots (58)$$

and deduces that the dissociation or instability constant of this reaction is:

$$K = \frac{[Cu^+][(CN)^-]^4}{Cu(CN)_4^{---}} \qquad \ldots (59)$$

$$= 5 \times 10^{-28}$$

This implies a very low concentration of cuprous ions, which can be removed from the solution mainly in two ways - electrolytically or by atmospheric oxidation and to maintain equilibrium they must, by the Le Chatelier's principle be replaced from the anode.

And so we also have removal of cuprous ions during oxidation:-

$$Cu^+ - e \rightleftharpoons Cu^{++} \qquad \ldots (60)$$

and if we accept the early work of Briggs[12], (1921), which suggests that no reaction involving the dissolution of copper can take place without the initial reaction:

$$Cu - e \rightleftharpoons Cu^{+} \qquad \ldots (61)$$

we have an increasing source of cupric ions in solution, when the $(CN)^{-}$ content decreases.

Also one must remember that since the principal site of the reaction is the anode, then as the $(CN)^{-}$ content decreases locally the probability of immediate oxidation of cuprous to cupric ions, as they leave the anode surface must increase owing to the presence of nascent oxygen forming on the anode surface and that this effect would be greater than oxidation due to dissolved oxygen in the electrolyte.

The cupric ion could then be removed by two major routes, as a tartrate or carbonate, since these two ions are also present in high concentrations.

As has been seen, however, the end product of this ionic interplay was actually the deep blue azurite/malachite, basic copper carbonate compound, found in solution, and not the pale blue tartrate. It should be noted that formation of the blue compound is most unlikely to occur under industrial conditions since the total quantity of available cyanide would never be allowed to reach the unstable range investigated here and also the copper anodes are lifted out of the electrolyte, when not in use.

6.7 Summary of results

The importance of free cyanide concentration of the electrolyte on the Faraday efficiency and thickness of deposit, was confirmed and the dependence of plating quality on this variable was delineated.

Results from the standard experimental block of 5x5 plating runs showed the overall experimental accuracy and that tensile strengths, in general, were largely a function of deposit thickness or volume fraction of carbon fibre in the composite, variations in temperature and current density being auxiliary to this, provided that deposits were chosen from the normal plating zones. The subsequent analysis of these results serves to emphasize these points, and shows that results from whole tow work must, of

necessity be taken from general means and not individual runs.

Lastly, the blue compound formed whilst plating in the unstable < 2 g/l free cyanide zone was isolated, identified and synthesized chemically - the compound proving to be a mixture of about 75% azurite - 25% malachite, the basic carbonates of copper.

References 6

6.1 Graham, A., and Read, H. J., Metal Industry, Pt.I, 559, Nov. 1937

6.2 Ibid Pt. II, 617, Dec. 1937

6.3 Ibid Pt.III, 15, Jan. 1938

6.4 Ibid Pt. IV, 77, Feb. 1938

6.5 Ibid Pt. V, 120, Mar. 1938

6.6 Ibid Pt. VI, 169, Apr. 1938

6.7 Thompson, M. R., Monthly Review, Am. Electroplaters Soc. 18, 31, May, 1931.

6.8 McDowell, R. G., A.E.R.E. Private Communication, 1969.

6.9 Bennett, M. J., A.E.R.E. Private Communication, 1970.

6.10 Lowenheim, F. A., Ed. "Modern Electroplating", John Wiley, 1942.

6.11 Thompson, M. R., Trans. Amer. Electrochem. Soc. 417, Vol. 79, 1941.

6.12 Briggs, T. R., Trans. Amer. Electrochem. Soc. 231, Vol. XL, 1921.

CHAPTER 7

Effect of Surface Treatments and Annealing on Final Strength

7.1 Introduction - surface treatments

During manufacture, carbon fibre becomes covered with a powdery but adherent form of soot. Various commercially classified treatments exist designed to remove this and one based on the oxidizing properties of hypochlorite solutions is now in vogue. The properties of Type II fibre, treated in this way to remove soot, might well have a different strength after plating.

In the same vein, other surface treatments might have similar effects. Of these, three come to mind at once, i.e. a pre-dip to wet the surface in the alkaline electrolyte, surface activation and pre-dripping in an organic wetting agent.

The surface activation treatment chosen for this work came from the art of plating babyshoes and silvering mirrors. This pre-treatment consists of a pre-dip in a stannous chloride/hydrochloric acid solution, followed by a wash in distilled water. Little is known as to the mechanisms involved with this treatment but the fact remains, it does provide a surface ready to accept and adhere to depositing metal ions. One possible explanation of the effect a $SnCl_2$ dip has, on say a carbon surface, could be as shown in Fig. 78 where Cl^- ions are attracted to the positive carbon surface to recombine with Sn^{++} ions in situ and provide a more electronegative potential than that of carbon.

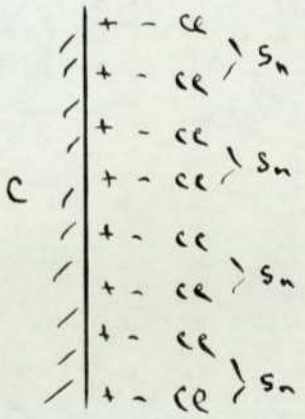


Fig. 78

Finally an electrically neutral wetting agent was chosen as a pre-dip, namely Lubrol W, a non-ionic fatty alcohol ethylene oxide condensate.

Table 14 Effect of surface pre-treatments on U.T.S. of Cu plated fibre.

Pre-treatment	0.1 A/10^{-2} m^2				0.2 A/10^{-2} m^2				0.4 A/10^{-2} m^2				0.6 A/10^{-2} m^2				0.8 A/10^{-2} m^2			
	No.	U.T.S (psi x 10^6)	t (μm)	F_s	No.	U.T.S (psi x 10^6)	t (μm)	F_s	No.	U.T.S (psi x 10^6)	t (μm)	F_s	No.	U.T.S (psi x 10^6)	t (μm)	F_s	No.	U.T.S (psi x 10^6)	t (μm)	F_s
Type II, untreated	230	0.0831	2.0	0.44	233	0.0588	2.6	0.35	236	0.0489	4.3	0.24	239	0.0396	4.7	0.21	242	–		
Standard	231	0.0844	2.0	0.44	234	0.0539	2.7	0.36	237	0.0464	4.6	0.22	240	0.0327	5.6	0.18	243	0.0339	6.6	0.15
45°C run.	232	–			235	0.0671	2.6	0.37	238	0.0479	4.9	0.20	241	–			244	0.0330	6.3	0.15
Arithmetic Mean		0.0837	2.0	0.44		0.0599	2.6	0.36		0.0477	4.7	0.23		0.0389	5.2	0.19		0.0334	6.5	0.15
Standard Deviation		656psi.	%S.D. = 0.8			5450psi.	%S.D. = 9.1			1020psi.	%S.D = 2.1			3049psi.	%S.D. = 7.8			447psi	%S.D. = 1.3	
Type II, untreated, Soak in CuCN electrolyte.	304	0.0751	2.0	0.44	307	0.0589	3.1	0.32	310	0.0458	4.1	0.25	312	0.0350	5.3	0.19	316	0.0385	7.0	0.13
	305	0.0561	1.8	0.48	308	0.0516	3.0	0.33	311	0.0434	4.4	0.23	314	0.0437	5.2	0.19	317	0.0285	7.1	0.13
	306	0.0592	1.8	0.48	309	0.0518	2.9	0.34	312	0.0401	5.0	0.20	315	0.0399	5.6	0.18	318	0.0298	7.1	0.13
A.M.		0.0635	1.9	0.47		0.0551	3.0	0.33		0.0431	4.5	0.23		0.0395	5.4	0.19		0.0323	7.1	0.13
S.D.		8323.	%S.D = 13.1			3540.	%S.D. = 6.4			2337.	%S.D. = 5.4			3561.	%S.D. = 9.0			4440.	%S.D. = 13.7	
Type II, treated, Soak in CuCN electrolyte.	319	0.0655	2.2	0.42	322	0.0618	3.2	0.31	325	0.0416	5.3	0.19	328	0.0497	5.2	0.19	331	0.0440	6.7	0.14
	320	0.0644	2.2	0.42	323	0.0492	3.2	0.31	326	0.0438	4.9	0.20	329	0.0506	5.2	0.19	332	0.0324	6.3	0.15
	321	0.0478	2.3	0.41	324	0.0543	3.2	0.31	327	0.0485	4.2	0.24	330	0.0436	6.1	0.16	333	0.0300	7.1	0.13
A.M.		0.0592	2.2	0.41		0.0551	3.2	0.31		0.0446	4.8	0.23		0.0480	5.5	0.18		0.0355	6.7	0.14
S.D.		8098.	%S.D = 13.7			5175.	%S.D. = 9.4			2878.	%S.D. = 6.5			3110.	%S.D. = 6.5			6113.	%S.D = 17.2	
Type II, untreated, Soak in Lubrol W.	334	0.0621	1.8	0.48	337	0.0504	3.0	0.33	340	0.0365	4.6	0.22	343	0.0366	5.3	0.19	346	0.0261	6.9	0.14
	335	0.0682	1.9	0.47	338	0.0530	2.9	0.34	341	0.0455	4.5	0.22	344	0.0361	5.3	0.19	347	0.0262	6.9	0.14
	336	0.0605	1.9	0.46	339	0.0493	3.1	0.32	342	0.0456	4.1	0.24	345	0.0377	5.3	0.19	348	0.0323	6.6	0.14
A.M.		0.0636	1.9	0.47		0.0509	3.0	0.33		0.0425	4.4	0.23		0.0368	5.3	0.19		0.0282	6.8	0.14
S.D.		3323.	%S.D. = 5.2			1553.	%S.D = 3.1			4243.	%S.D. = 10.0			671.	%S.D. = 1.8			2900.	%S.D. = 10.3	
Type II, treated. Soak in Lubrol W.	349	0.0728	2.0	0.44	352	0.0581	3.3	0.30	355	0.0367	4.8	0.21	358	0.0364	6.1	0.16	361	0.0335	7.4	0.12
	350	0.0552	2.2	0.42	353	0.0533	3.5	0.28	356	0.0408	4.6	0.22	359	0.0425	7.0	0.13	362	0.0330	7.9	0.11
	351	0.0509	2.2	0.42	354	0.0599	3.4	0.29	357	0.0404	4.7	0.21	360	0.0428	6.9	0.14	363	0.0280	7.8	0.12
A.M.		0.0596	2.2	0.43		0.0571	3.4	0.29		0.0393	4.7	0.22		0.0406	6.4	0.15		0.0315	7.7	0.12
S.D.		9474.	%S.D. = 15.9			2496.	%S.D. = 4.4			1846.	%S.D. = 4.7			2949.	%S.D = 7.3			2484.	%S.D = 7.9	

Table 14 Effect of surface pre-treatments on U.T.S. of Cu plated fibre.

	0.1 A/10^{-2} m^2				0.2 A/10^{-2} m^2				0.4 A/10^{-2} m^2				0.6 A/10^{-2} m^2				0.8 A/10^{-2} m^2			
Pre-treatment.	No.	U.T.S (psi x 10^6)	t (μm)	F_s	No.	U.T.S (psi x 10^6)	t (μm)	F_s	No.	U.T.S (psi x 10^6)	t (μm)	F_s	No.	U.T.S (psi x 10^6)	t (μm)	F_s	No.	U.T.S (psi x 10^6)	t (μm)	F_s
Type II, untreated	230	0.0831	2.0	0.44	233	0.0588	2.6	0.35	236	0.0489	4.3	0.24	239	0.0396	4.7	0.21	242	–		
Standard	231	0.0844	2.0	0.44	234	0.0539	2.7	0.36	237	0.0464	4.6	0.22	240	0.0327	5.6	0.18	243	0.0339	6.6	0.15
45°C run.	232	–			235	0.0671	2.6	0.37	238	0.0479	4.9	0.20	241	–			244	0.0330	6.3	0.15
Arithmetic Mean		0.0837	2.0	0.44		0.0599	2.6	0.36		0.0477	4.7	0.23		0.0389	5.2	0.19		0.0334	6.5	0.15
Standard Deviation		656 psi.	% S.D. = 0.8			5450 psi.	% S.D. = 9.1			1020 psi.	% S.D = 2.1			3049 psi.	% S.D. = 7.8			447 psi	% S.D. = 1.3	
Type II, untreated,	304	0.0751	2.0	0.44	307	0.0589	3.1	0.32	310	0.0458	4.1	0.25	312	0.0350	5.3	0.19	316	0.0385	7.0	0.13
Soak in CuCN	305	0.0561	1.8	0.48	308	0.0516	3.0	0.33	311	0.0434	4.4	0.23	314	0.0437	5.2	0.19	317	0.0285	7.1	0.13
electrolyte.	306	0.0592	1.8	0.48	309	0.0518	2.9	0.34	312	0.0401	5.0	0.20	315	0.0399	5.6	0.18	318	0.0298	7.1	0.13
A.M.		0.0635	1.9	0.47		0.0551	3.0	0.33		0.0431	4.5	0.23		0.0395	5.4	0.19		0.0323	7.1	0.13
S.D.		8323.	% S.D. = 13.1			3540.	% S.D. = 6.4			2337.	% S.D. = 5.4			3561.	% S.D. = 9.0			4440.	% S.D. = 13.7	
Type II, treated,	319	0.0655	2.2	0.42	322	0.0618	3.2	0.31	325	0.0416	5.3	0.19	328	0.0497	5.2	0.19	331	0.0440	6.7	0.14
Soak in CuCN	320	0.0644	2.2	0.42	323	0.0492	3.2	0.31	326	0.0438	4.9	0.20	329	0.0506	5.2	0.19	332	0.0324	6.3	0.15
electrolyte.	321	0.0478	2.3	0.41	324	0.0543	3.2	0.31	327	0.0485	4.2	0.24	330	0.0436	6.1	0.16	333	0.0300	7.1	0.13
A.M.		0.0592	2.2	0.41		0.0551	3.2	0.31		0.0446	4.8	0.23		0.0480	5.5	0.18		0.0355	6.7	0.14
S.D.		8098.	% S.D. = 13.7			5175.	% S.D. = 9.4			2878.	% S.D. = 6.5			3110.	% S.D. = 6.5			6113.	% S.D = 17.2	
Type II, untreated	334	0.0621	1.8	0.48	337	0.0504	3.0	0.33	340	0.0365	4.6	0.22	343	0.0366	5.3	0.19	346	0.0261	6.9	0.14
Soak in	335	0.0682	1.9	0.47	338	0.0530	2.9	0.34	341	0.0455	4.5	0.22	344	0.0361	5.3	0.19	347	0.0262	6.9	0.14
Lubrol W.	336	0.0605	1.9	0.46	339	0.0493	3.1	0.32	342	0.0456	4.1	0.24	345	0.0377	5.3	0.19	348	0.0323	6.6	0.14
A.M.		0.0636	1.9	0.47		0.0509	3.0	0.33		0.0425	4.4	0.23		0.0368	5.3	0.19		0.0282	6.8	0.14
S.D.		3323.	% S.D. = 5.2			1553.	% S.D. = 3.1			4243.	% S.D. = 10.0			671.	% S.D. = 1.8			2900.	% S.D. = 10.3	
Type II, treated.	349	0.0728	2.0	0.44	352	0.0581	3.3	0.30	355	0.0367	4.8	0.21	358	0.0364	6.1	0.16	361	0.0335	7.4	0.12
Soak in	350	0.0552	2.2	0.42	353	0.0533	3.5	0.28	356	0.0408	4.6	0.22	359	0.0425	7.0	0.13	362	0.0330	7.9	0.11
Lubrol W.	351	0.0509	2.2	0.42	354	0.0599	3.4	0.29	357	0.0404	4.7	0.21	360	0.0428	6.9	0.14	363	0.0280	7.8	0.12
A.M.		0.0596	2.2	0.43		0.0571	3.4	0.29		0.0393	4.7	0.22		0.0406	6.4	0.15		0.0315	7.7	0.12
S.D.		9474.	% S.D. = 15.9			2496.	% S.D. = 4.4			1846.	% S.D. = 4.7			2949.	% S.D. = 7.3			2484.	% S.D. = 7.9	

Table 15

Variations in experimental control as a result of surface treatment

Treatment	% deviation of UTS from mean without the treatment
Standard run, 45°C, Type II, untreated	4.2
Hypochlorite dip, Type II treated	6.0
Stannous chloride activation, Type II, untreated	7.3
10 min soak in electrolyte, Type II, untreated	9.5
Type II, treated	10.7
10 min soak in Lubrol W, Type II, untreated	6.1
Type II, treated	8.0

7.2 Experimental detail

For this work a comparative set of plated finishes were produced using the five current densities, at 45°C, employed in the experimental test block described in Chapter 6, (Table 11). This range was prepared with Type II fibre either treated to remove surface soot, or untreated, followed by:

a. Activating dip in 10% stannous chloride -5% hydrochloric acid solution, followed by a distilled water wash. The hydrochloric acid was added to prevent the formation of a white precipitate of stannous oxychloride, 2 $Sn(OH)Cl.H_2O$.

b. Pre-plating soak in cyanide electrolyte for 10 minutes, at room temperature.

c. A pre-plating dip in 0.1% Lubrol W for 10 minutes, at room temperature.

After plating, tows were dried, weighed and tensile tested as described in Chapter 6.

7.3 Surface treatment results

Comparisons between the standard 45°C run and hypochlorite treated Type II fibre can be made from the data in Table 13, also the effect of stannous chloride activation can be evaluated, but the general result was a decrease in experimental control introduced by the extra handling associated with the various treatments.

For example the per cent deviation from the mean, for the standard run was 4.2%; for the hypochlorite treated material, 6.0% and for the stannous chloride activation treatment, 7.3%. A slight reduction in final strength of the pre-treated plated tows was also observed.

Table 14 shows similar results but here the "handling effect" was more marked, as can better be seen from the analysis of the per cent deviations from the mean, given in Table 15, for all the treatments.

Pre-treatments and their effect on U.T.S.

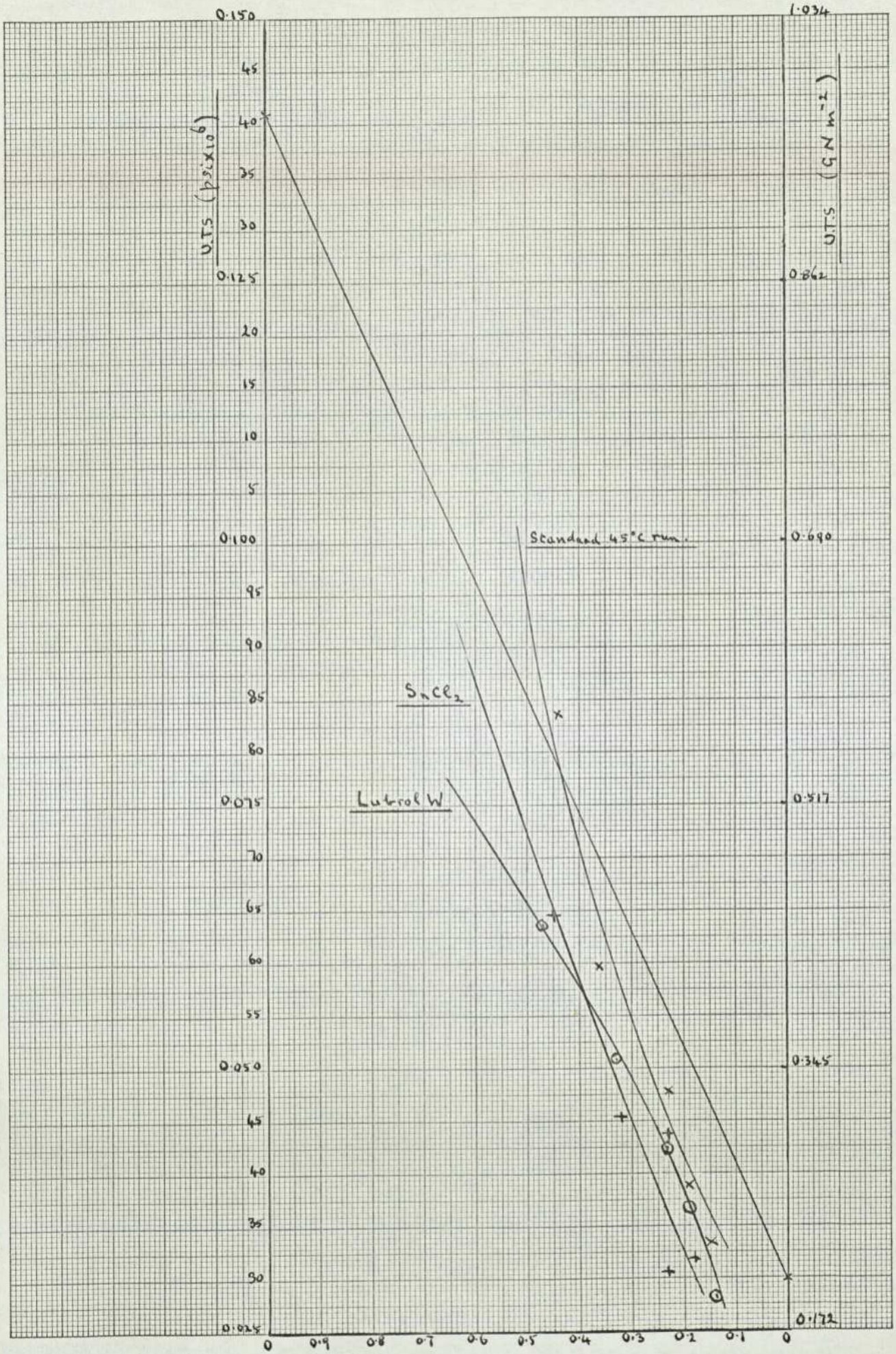


Fig. 79 Vol. fraction of C fibre in Cu plated tow

Showing increase in U.T.S due to copper plating, at 45°C.

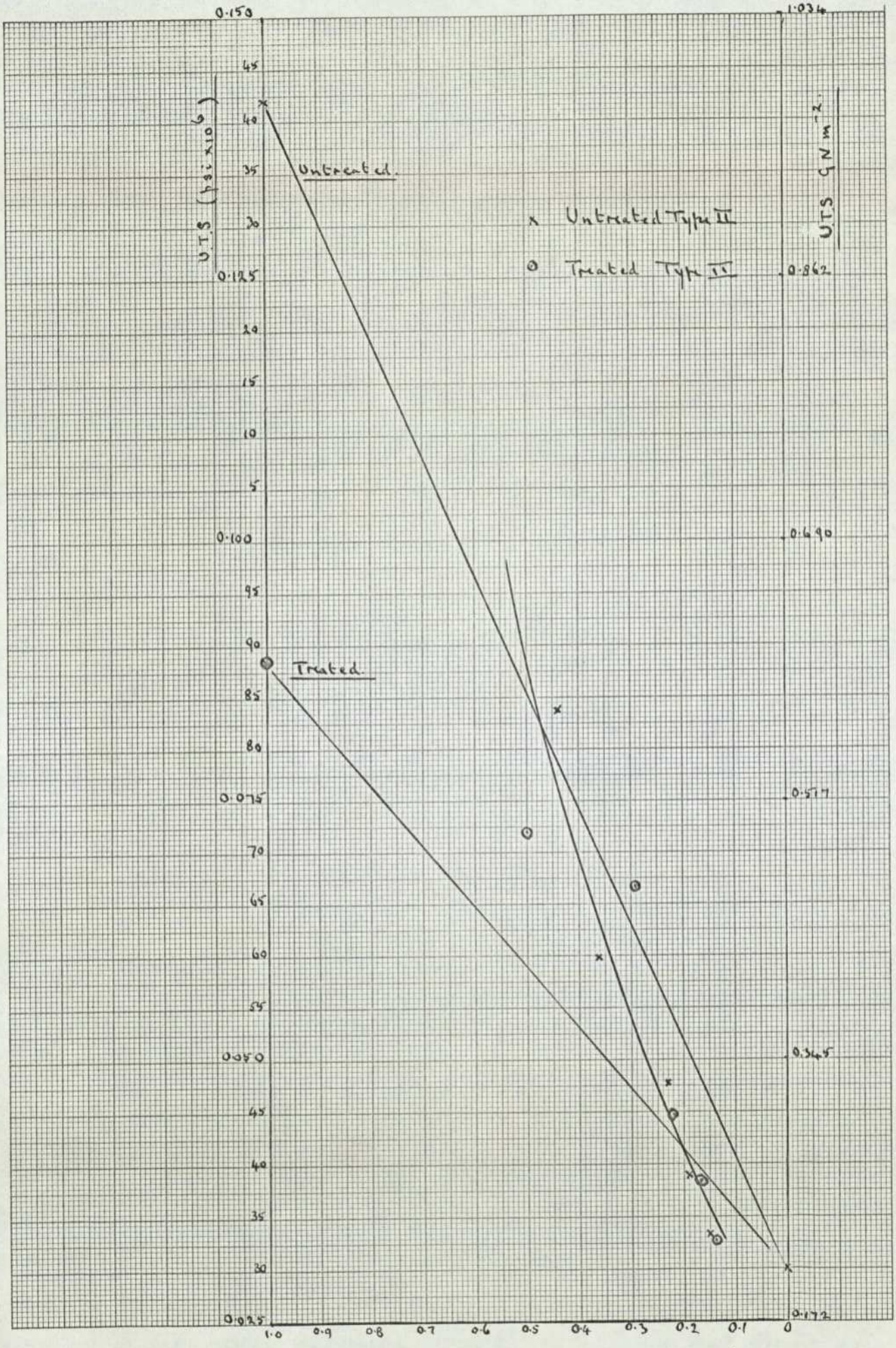


Fig. 80 Vol. fraction of C fibre in Cu plated tow

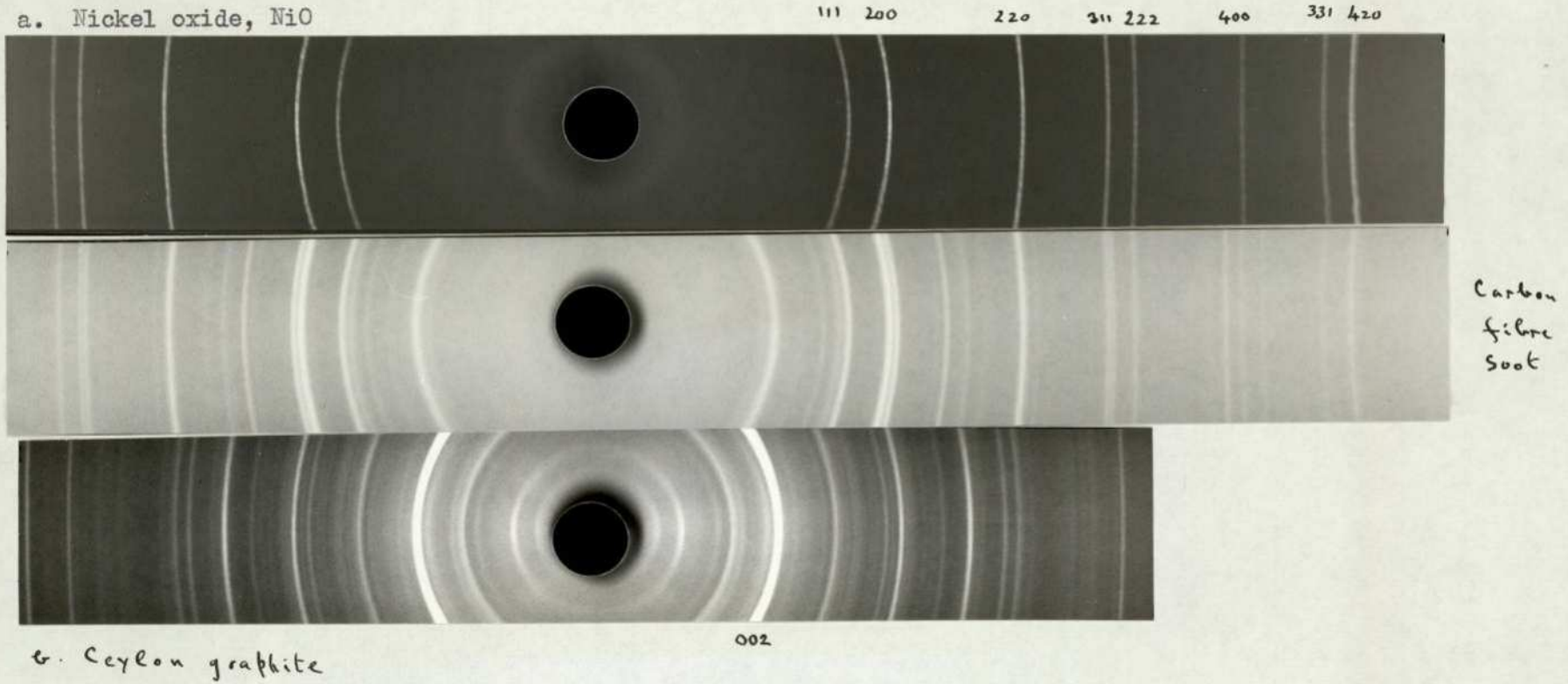


Fig. 81. Identification of major impurity in carbon fibre soot

A comparison between the standard, stannous chloride activation and non-ionic wetting agent pre-treatments is made in Fig. 79 where it can be seen that both treatments produced tows with strengths significantly below those of the standard run. This effect was almost certainly due to the poor penetration of Cu throughout the tow which was also observed with all the wetting pre-treatments, which caused the fibres to stick together, thus removing the "ballooning", introduced during racking of the fibre tow, and preventing gas separation during plating.

A comparison is also made in Fig. 80 of the standard run at 45°C in which Type II untreated fibre was used as precursor and Type II material from another fibre batch, hypochlorite treated to remove soot. No significant difference was found between the average tensile strengths of the two materials, apart from the "handling effect". But it is of interest to note that the hypochlorite treated material had the initial very low strength of about 87,000 psi and thus plating this quality fibre effectively improved the strength, to very nearly that found in the much stronger untreated fibre (142,000), after plating. Such an improvement might arise from a decrease in Griffith crack concentration due to "bridging" by the copper-deposit.

7.4 Identification of carbon fibre soot

An X-ray diffraction powder pattern photograph of the soot formed on fibre surfaces during manufacture and isolated by shaking sooty, untreated Type II fibre in a cellophane bag, gave the pattern shown in Fig. 81. This, when compared with the pattern for graphite, b, gave positive identification of many lines from the graphite structure, as might be expected but this comparison left a family of unidentified lines with a strong suggestion of cubic structure. These were identified, line by line, with those of the black nickel oxide, NiO, or bunsenite cubic pattern, also shown in Fig. 81, a. Several faint lines

of the Fe_2O_3 pattern are present in this pattern too, the comparison being made by "d" spacing measurements from an Fe_2O_3 powder pattern produced with a nickel filter and copper target. From line intensities one might assume that nickel oxide was the major impurity in the soot and present at 50% of the material examined. To appreciate X-ray powder analysis it is necessary to know the concentration identification limits, which are usually not less than 5%, in a mixture, for positive identification.

The presence of nickel oxide in carbon fibre soot is quite unexpected. However, if one postulates the formation of CO as well as the reported evolution of HCN and NH_3, (Shindo, (1.17) 1961) during the preliminary oxidation, at 220°C, of PAN fibre, then this gas would diffuse through the furnace space and react with any nickel rich surface, such as the nichrome furnace winding, with the formation of nickel carbonyl, $Ni(CO)_4$, which might very well be reduced on the carbon fibre surface, to form part of the soot found, during the higher temperature exothermic phase of the oxidation process. Iron carbonyls might also form under these conditions.

Dissolution of this nickel oxide component of the soot, during the cold hypochlorite dip cleaning process, would explain the efficacy of such a treatment, since one would not expect carbon alone to be removed by dipping in this medium.

7.5 Effect of annealing treatments on copper plated tows

a. Experimental detail

Again taking the 5 current densities at 45°C as the comparative standard, one duplicate set of fibre tows was prepared for subsequent heat treatment at 500°C. Another set of 16 tows, plated at 0.4 $A/10^{-2}$ m^2, 45°C, was prepared to study the effect of several heat treatments, starting at 300°C and rising by 100° intervals to 800°C.

Table 16 Effect of annealing on final strength of Cu plated carbon fibre.

Treatment.	0·1A/10^{-2} m^{2} No.	U.T.S (psi x10^{5})	t (mm)	F_f	0·2 A/10^{-2} m^{2} No.	U.T.S (psi x10^{6})	t (mm)	F_f	0·4A/10^{-2} m^{2} No.	U.T.S (psi x10^{6})	t (mm)	F_f	0·6A/10^{-2} m^{2} No.	U.T.S (psi x10^{6})	t (mm)	F_f	0·8A/10^{-2} m^{2} No.	U.T.S (psi x10^{6})	t (mm)	F_f
Type II, untreated	230	0·0831	2·0	0·44	233	0·0588	2·6	0·35	236	0·0489	4·3	0·24	239	0·0396	4·7	0·21	242	—		
Standard	231	0·0844	2·0	0·44	234	0·0539	2·7	0·36	237	0·0464	4·6	0·22	240	0·0327	5·6	0·18	243	0·0339	6·6	0·15
45°C run.	232	—			235	0·0671	2·6	0·37	238	0·0479	4·9	0·20	241	—			244	0·0330	6·3	0·15
Arithmetic Mean		0·0837	2·0	0·44		0·0599	2·6	0·36		0·0477	4·7	0·23		0·0389	5·2	0·19		0·0334	6·5	0·15
Standard Deviation		656 psi.	% S.D. =	0·8		5450 psi.	% S.D. =	9·1		1020 psi.	% S.D. =	2·1		3049 psi.	% S.D. =	7·8		447 psi.	% S.D. =	1·3
Annealed at 400°C	371	0·0804	1·8	0·48	374	0·0639	2·8	0·35	377	—			380	0·0382	5·3	0·19	383	0·0315	7·5	0·12
for comparison	372	0·0723	1·5	0·54	375	0·0651	2·7	0·36	378	0·0470	4·2	0·24	381	0·0477	5·2	0·19	384	0·0274	6·8	0·14
with standard run	373	0·0803	1·5	0·53	376	0·0634	2·8	0·35	379	0·0487	4·1	0·24	382	0·0395	5·0	0·20	385	0·0369	6·3	0·15
A.M.		0·0777	1·6	0·55		0·0641	2·8	0·36		0·0478	4·2	0·24		0·0415	5·2	0·20		0·0319	6·9	0·14
S.D.		3795 psi	% S.D. =	4·9		876 psi	% S.D. =	1·4		640 psi.	% S.D. =	1·3		4410 psi	% S.D. =	10·6		3819 psi	% S.D. =	12·2

All specimens plated under conditions of standard run.

	300°C No.	U.T.S (psi x10^{5})	t (mm)	F_f	400°C No.	U.T.S (psi x10^{6})	t (mm)	F_f	500°C No.	U.T.S (psi x10^{6})	t (mm)	F_f	600°C No.	U.T.S (psi x10^{6})	t (mm)	F_f	700°C No.	U.T.S (psi x10^{6})	t (mm)	F_f
Full annealing	386	0·0457	4·7	0·21	389	0·0484	5·5	0·18	392	0·0429	5·1	0·20	395	0·0422	4·7	0·21	398	0·0451	4·8	0·21
range for	387	0·0474	4·8	0·21	390	0·0476	4·8	0·21	393	0·0454	5·0	0·20	396	0·0419	4·6	0·22	399	0·0473	4·8	0·21
Type II fibre	388	0·0589	4·7	0·21	391	0·0484	5·1	0·19	394	0·0419	5·1	0·19	397	0·0454	4·3	0·24	400	0·0423	5·2	0·19
A.M.		0·0506	4·8	0·21		0·0481	5·5	0·20		0·0434	5·1	0·20		0·0431	4·6	0·23		0·0449	5·1	0·21
S.D.		5863 psi.	% S.D. =	11·6		378 psi.	% S.D. =	0·8		1473 psi.	% S.D. =	3·4		1597 psi.	% S.D. =	3·7		2047 psi.	% S.D. =	4·6

800°C No.	U.T.S (psi x10^{6})	t (mm)	F_f
401	0·0367	4·9	0·20
402	0·0334	5·2	0·19
403	0·0420	4·8	0·21
A.M.	0·0374	5·1	0·21
S.D.	3625 psi.	% S.D. =	9·7

All annealing was carried out in a stream of hydrogen, purified by passage through a Baker platinum deoxidizer, which removes oxygen impurity in the hydrogen stream by catalytic combination, on a platinum black surface, to form water, which was removed by a drying column.

Specimens were individually wrapped in copper foil to avoid contact and held at temperature for 4 hours, being subsequently furnace cooled, in vacuo.

7.6 Annealing results

Table 16 shows a comparison between the standard plating sets, before and after heat treatment at 400°C and apart from the "handling effect" on experimental control, of 6.1% deviation from the mean, compared with 4.2% for the standard, no significant difference in strength was observed. The same result was shown by all the annealing runs from 300°-700°C, with material of substantially constant volume fraction of fibre. After the 800°C run however, it was seen that sintering of individual fibres, to each other and to the protective Cu sheath, had taken place, and a significant drop in tensile strength of about 10,000 psi, was recorded.

Such mass transfer of Cu from fibre to fibre is an example of surface tension sintering, as described by Herring[2], (1951), which readily takes place with copper on a completely "non-wetting" surface such as graphite, as shown by Mortimer and Nicholas[3], (1969), in their work on the "wetting" of graphite by copper and copper alloys. Milner and Totte[4], (1964), also showed the effect, on a UO_2 surface, in their work on metal bonding.

A similar effect was reported by Flint[5], (1964), in work on metal plated uranium oxide spheres, another example of a "non-wetting" system. Here the copper films, heated to 750°C, parted due to plastic flow and micro-sectioning revealed a "cog-wheel" effect. This was on spheres of particle size 160-250μ (1 micron ≡ 10^{-6}m) and such mass transfer would be

expected to be even more pronounced on Cu plated carbon fibres of only 8μ diameter. The full results are described in Appendix 5, for convenience.

7.7 Summary of results

With the introduction of further processes in the chain leading to plated carbon fibre, a decrease in experimental control was observed coupled with a slight reduction in tensile strength. This result was contrary to expectations since it was thought that true "wetting" would lead to maximum adhesion and therefore improved tensile strength. The "handling effect" was observed no matter which pre-treatment was involved, together with poor penetration of the Cu deposit.

The carbon fibre soot which such pre-treatments would help to remove was identified as an approximately equal mixture of graphite and black nickel oxide. This result could be of considerable interest to those investigating the nickel plating of carbon fibres.

With regard to the heat treatment of tows after plating, results suggest that any annealing above 700°C will be deleterious and lead to considerable loss in strength, due to a surface tension-sintering effect.

7.8 A specification covering the electrodeposition of Cu on to carbon fibres.

At this stage, sufficient is known from the work described in the previous Chapters, concerning the behaviour of carbon fibres, for a detailed plating specification to be drawn up.

It has been shown that a normal Rochelle salt-cyanide copper plating solution, with very close control of the free cyanide content, will produce copper plated carbon fibre tows with reproducible thicknesses of good quality copper deposit, leading to a composite fibre which follows closely the predicted "law of mixtures" value of tensile strength which depends on the initial strength of the original fibres and the deposited

TABLE 17

Carbon Fibre Copper Plating Specification

	Chemical	Concentration g/l	Working Limits g/l
Electrolyte	Copper cyanide, CuCN	22.0	20-25
	Sodium cyanide, NaCN, (total)	30.0	-
	Free cyanide, NaCN	6.0	4-8
	Rochelle salt, $COOK(CH.OH)_2COONa.4H_2O$	50.0	40-60
	Sodium carbonate, $Na_2CO_3.1\ OH_2O$	25.0	20-40
pH control	Sodium hydroxide, NaOH, to pH 12.6 (12.2-12.8)		
Agitation	Mechanical stirring		
Anode/Cathode ratio	2:1		
Anode material	Electrolytic copper sheet		
Electrode spacing	Not less than 10 cms		
Recommended Current Density	$0.4A/10^{-2}m^1$. At this current density, bath control is simple		
Pre-treatment	None		
Temperature	40-45°C. At this temperature instability due to "blueing" of the electrolyte is avoided, with proper "free cyanide control"		
Plating Time	60 minutes. A slow penetration, further into tow, at recommended current density.		
Ageing of solution	None		
Control	Free cyanide titration after each run, followed by accurate make-up of concentration, and solution level		
Finish	Wash in distilled water, as the final rinse, and vacuum dry.		
Heat treatment	None		

copper, and of course the volume fraction of fibre present in the composite. This fact indicates that a good bond between metal and fibre is obtained.

Also as a general rule it has been shown that the thicker the deposit, the weaker the fibre composite produced. All this being true only when plating conditions are maintained well within the limits described in Chapter 6.

In addition the work has demonstrated that only Type II untreated carbon fibre gives the highest tensile strengths and only then when plated in a stable cyanide solution. Type I fibres and acid copper sulphate electrolytes gave poor tensile results and little adhesion of deposits.

As final points it should be borne in mind that low rates of deposition improve penetration of the copper through the tow, since slow plating does not give rise to encapsulation of the bundle before coverage, and a final heat treatment of the plated material does not appear to be of any benefit, whilst being definitely bad if carried out above 700°C.

The specification drawn up with these points in mind appears in Table 17. Of course plating current densities can be varied to change the volume fraction of fibre in the composite but for maximum coverage, and hence maximum tensile strength, low deposition rates must be strictly maintained.

REFERENCES 7

7.1 Shindo, A., 1961, See Ref. 1.26.

7.2 Herring, C., Physics of Powder Metallurgy, McGraw-Hill, 1951.

7.3 Mortimer, D.A., and Nicholas, M., A.E.R.E. R-6025, 1969.

7.4 Milner, A., and Tottle, C.R. J. Inst. Met. 93,2, 48, 1964.

7.5 Flint, O., A.E.R.E., M-1508, 1964.

CHAPTER 8

Carbon fibre/copper composites

8.1 Introduction

When considering the tensile testing of a simple composite, a single copper plated carbon fibre, (in Section 4.4b,) use was made of an elementary "law of mixtures", (Mellor[1], 1946), for the calculation of composite densities etc., viz:

$$R_{(Cu+f)} = aR_f + bR_{Cu} \qquad \ldots (45)$$

where R was the symbol for density and 'a' and 'b' the respective volume fractions. The concept was also employed by Dietz and Heyser[2], (1954), in their work on tensile strengths of fibre glass reinforced plastics.

Later McDanels et al[3], (1960), expanded equation (45) to fit the circumstances controlling strengths of metal/metal composites. They considered the case of ductile, pure, copper strengthened by tungsten fibres, and they argued that when tungsten fibres carried the major load, P, the equation should be:

$$P = \sigma_c A_c = \sigma_F A_F + \sigma_M^* A_M \qquad \ldots (62)$$

where P = load carried by composite

σ_c = tensile strength of composite

A_c = cross-sectional area of composite (=1)

σ_F = tensile strength of tungsten fibre

A_F = fraction of cross-sectional area of composite occupied by fibre

σ_M^* = stress on copper matrix

and A_M = fraction of cross-sectional area of composite occupied by matrix [= $(1-A_F)$].

They also emphasized that the stress on the copper, σ_M^*, was not the ultimate tensile strength of copper in the composite but a stress selected from the stress/strain diagram for pure annealed copper, at the final elongation of 1.5%, that is to say, stressed to about 8000 psi and well below the U.T.S. of about 30,000 psi.

This treatment was extended by Cottrell[4], (1964) and Kelly[5], (1964), to the now familiar equation for composite tensile strength:

$$\sigma_c = \sigma_f V_f + \sigma_m' (1-V_f) > \sigma_u \qquad \ldots (63)$$

where σ_c = tensile strength of composite

σ_f = tensile strength of fibres

V_f = volume fraction of fibres

σ_m' = average stress on the matrix, at the breaking strain of the fibres.

and σ_u = ultimate tensile stress of the matrix,

which can be taken as the UTS of the matrix if the presence of the broken fibres produce no change in the work hardening characteristics of the matrix, in which they are embedded.

Since the maximum elongation for stressed, unplated, carbon fibre is about 1% and that for annealed tungsten wire 8%, or for fully hard wire, about 4%, one might expect composites made from both materials, with copper as a matrix, to behave in a similar manner.

Kelly and Tyson[6], (1965), for copper/tungsten composites obtained a linear relationship between V_f = 0.1 and 1.0, showing that the relationship in Eqn. (63) was obeyed over a wide range of values of V_f, in the case of metal/metal composites, of this type.

It must be emphasized here that for the case of a Cu/W composite a continuous, uniaxially aligned system of fibres, in a metal matrix, can actually almost be obtained experimentally, such that the deformation

behaviour is one of isostrain, that is to say the strains in the matrix and fibre are equal and hence equal to the composite strain. Thus at low strains both fibre and matrix would deform elastically and on reaching the yield strain of the copper, this metal would deform plastically but the tungsten fibres, having a higher yield strength, would remain elastic. When the strain on the composite reached the yield strain of the W fibres, both the fibres and the matrix would deform plastically, to the limit of the elongation of the tungsten. On fibre fracture the composite itself fails by rupture, so long as the fibre content is greater by some minimum value.

The composite system described above is practically an ideal one but in practice the tungsten fibres, in the matrix, would not all be perfectly parallel and hence not all of identical length and fibre fracture leading to rupture would be more of a cascade type, than instantaneous. This state of affairs, would of course occur to a much greater extent in a Cu/Cf composite where it is, at present, an experimental impossibility to align such ultra thin fibres parallel and uniaxial and even if one could they would fracture and disarrange, to an unknown extent, during hot pressing.

It was felt however that this method of composite assessment would at least indicate the degree of bonding and/or damage taking place during composite manufacture.

8.2 Composite manufacture - experimental detail

Previous attempts to manufacture copper-carbon fibre composites, using the available 50 ton hydraulic press, had shown that a temperature of about 850°C was necessary to produce machinable compacts at a pressure low enough to keep fibre damage to a minimum, and that this was only possible if the 6" diameter ram and die were surrounded by an inert gas envelope. It was realised that the temperature throughout the high pressure zone was uneven and that the surrounding argon atmosphere was not

oxygen free. Proper control of these factors, however, would require an entirely new design of hydraulic press, which was beyond the scope of this work.

It was decided, therefore, to employ the orthodox compacting procedure and correlate the tensile results with those observed with uncompacted plated fibres, even though previous work had shown that annealing of the plated fibres, above 700°C, resulted in loss of strength.

In order to make useful sized test pieces from copper/carbon fibre blocks one must prepare a considerable quantity of copper plated fibre, and as the work involved was multidisciplinary in that plating, pressing, machining, testing and assessing would not all be done by one man as a continuous effort, tests were designed to cover as wide a field as possible, bearing in mind the fixed high temperature restriction.

Some 12 feet of Type II, 14", untreated carbon fibre was copper plated, in short lengths,for one hour at various current densities to give various volume fractions of fibre under laboratory conditions. A further 12 ft. of the same material was plated to give a range of volume fractions, under production conditions, which involved shorter plating times at higher current densities and lower bath temperatures, with the essential difference that production practice during plating, involved mechanical teasing of the fibre tow with a glass paddle. Finally another 12 feet of continuous carbon fibre was continuously plated, under production conditions, involving the slow passage of a length of fibre through a long tank, in a manner similar to industrial coating of wires etc.

From these three varieties of plated fibre, ten 2" lengths were cut and placed horizontal and parallel in a graphite lined die, maintained in a flowing argon atmosphere. The composite was hot pressed at 850°C, at 2-3 tons/sq.in. (1 ton per sq.in. ≡ 15.44 MNm^{-2}) no further improvement in compact quality being obtained with higher pressures. Compacts were cooled in the die, after pressing and were then machined into "dog-bone" shaped test pieces.

For universal comparison of tensile tests it has been decided, on an empirical basis, (Timoshenko[7], 1950), that cylindrical and rectangular test pieces should have standard shape and dimensions; $5.65\sqrt{A_o}$ for short specimens and $11.3\sqrt{A_o}$, for long ones, where A_o, in Fig. 82, is the cross-

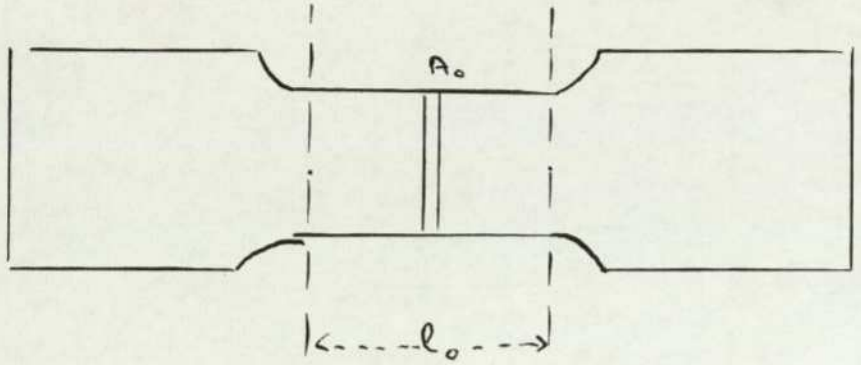
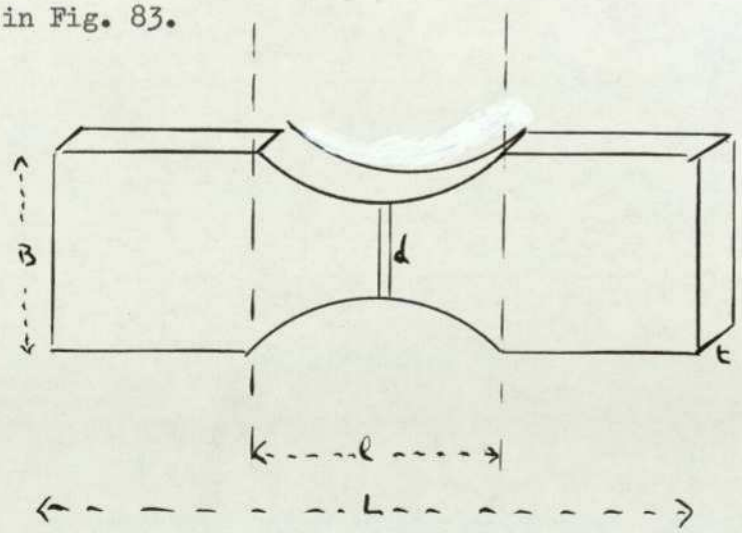


Fig. 82

sectional area of the specimen, and l_o, the gauge length. With the carbon fibre work, however, too little material was available for either type of test piece and therefore a simple "continuous neck" specimen was made so that fracture is forced to occur in the test area and the specimen has no gauge length, per se, other than 'l' the length of the effective test area, as shown in Fig. 83.



t = 0.32 cms
d = 0.25 cms
L = 5 cms
B = 2 cms
l = 2.5 cms

Fig. 83

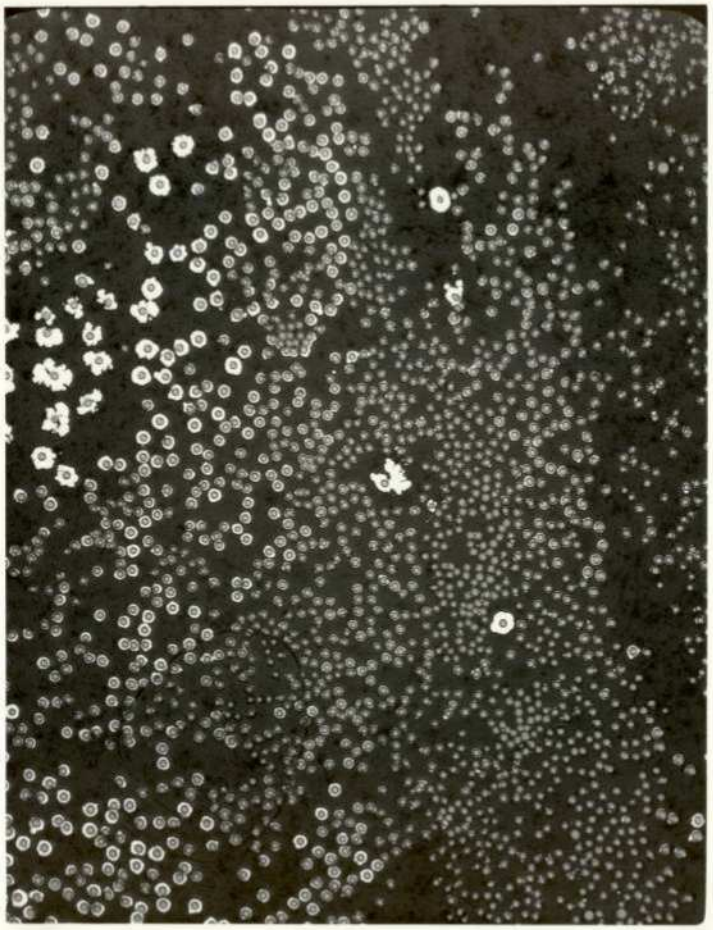


Fig. 84 Distribution of Cu in a production plated carbon fibre tow. X100.

Strength of Cu/carbon fibre composites in relation to volume fraction of fibre

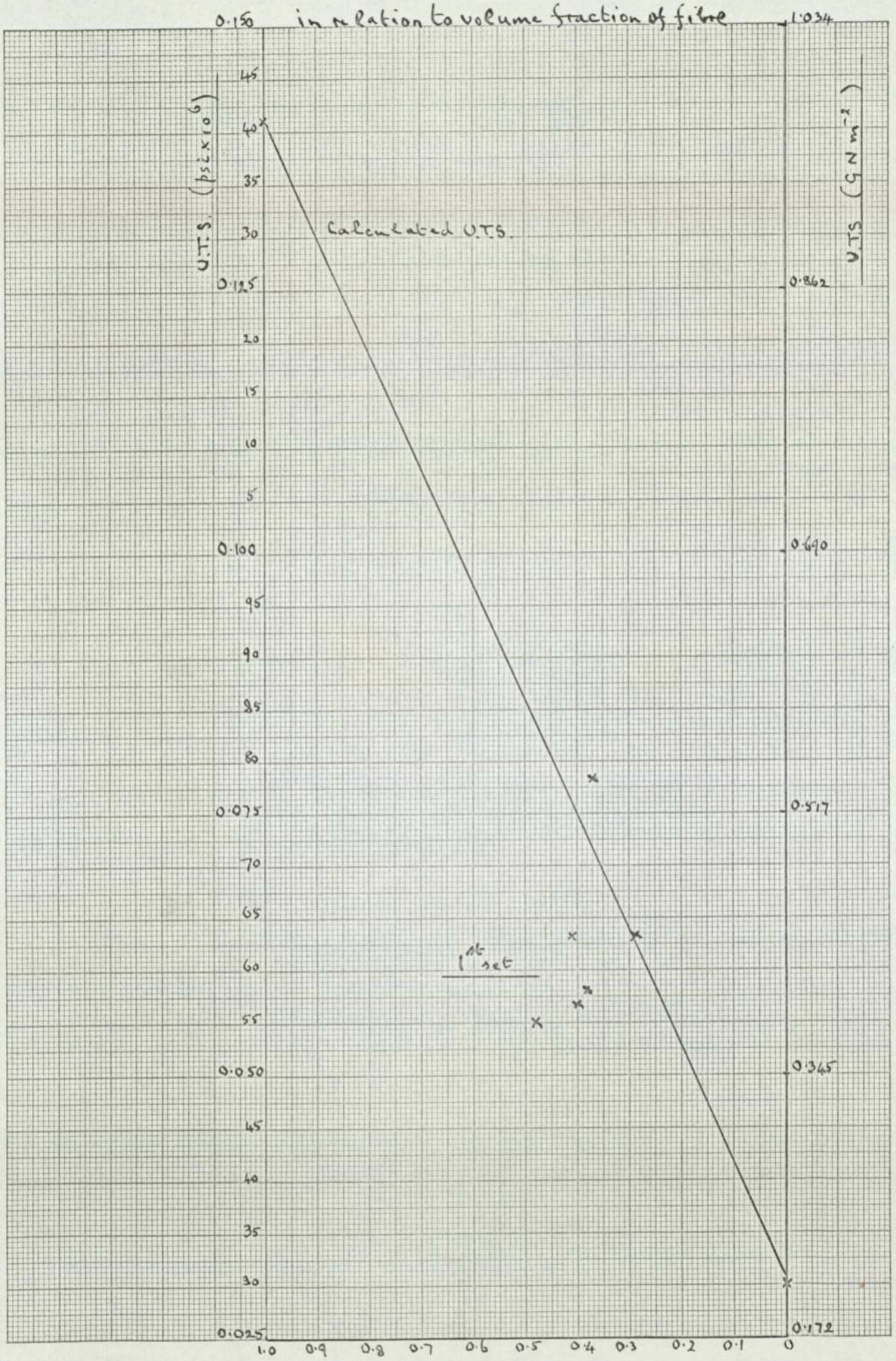


Fig 85 Vol. fraction of C fibre in composite

These specimens were then tensile tested in an Instron Universal Testing machine, in the manner described, composites being taken in two batches, the first batch including static plated fibres and the second continuously plated material.

8.3 Cu/Cf composite tensile results

As a check on the plating procedure test samples of similar volume fraction of 0.32 fibre, were tensile tested before compaction. The plated tensile strength of both laboratory and production runs, showed no significant difference, giving an average figure of 0.0549×10^6 psi, (from an unplated fibre strength of 142,000 psi). This result, although slightly lower, compares favourably with 0.0556×10^6 psi for similar samples from the standard 5x5 experimental test set of samples, but it must be remembered that accurate matching of results is not to be expected between laboratory and production methods.

Samples of continuously plated continuous tow gave a mean tensile strength of 0.0643×10^6 psi, from an unplated tensile of 335,000 psi. Such a large drop in strength after plating was probably due to the excessive handling inherent in initial runs associated with any new continuous plating process.

A micro-section of a production plating tow was made and is shown in Fig. 84. It can be seen that mechanical agitation of the tow during deposition, results in a more even distribution of fibres with different thicknesses of copper deposit, than that shown in Figs. 72-76, (Chapter 6) of static tow plating.

Tensile test results of the first batch of Cu/Cf composites are shown in Fig. 85 compared with those calculated by the "law of mixtures". The cluster of points about the calculated line indicates some reinforcement effect, tailing off with increase in fibre volume fraction. A decrease in strength with increase of carbon fibre content was not expected since

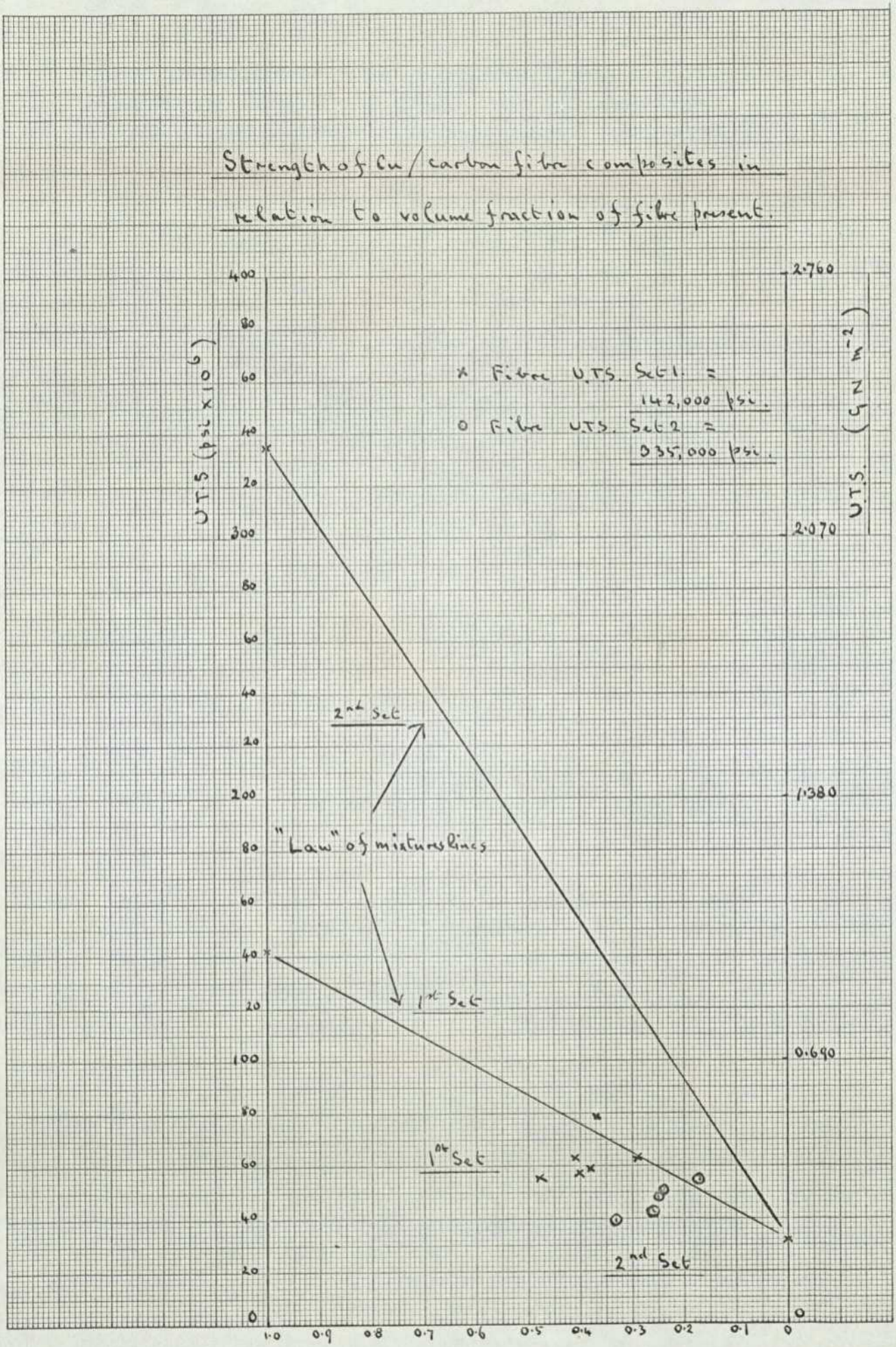


Fig 86 Vol. fraction of C fibre in composite

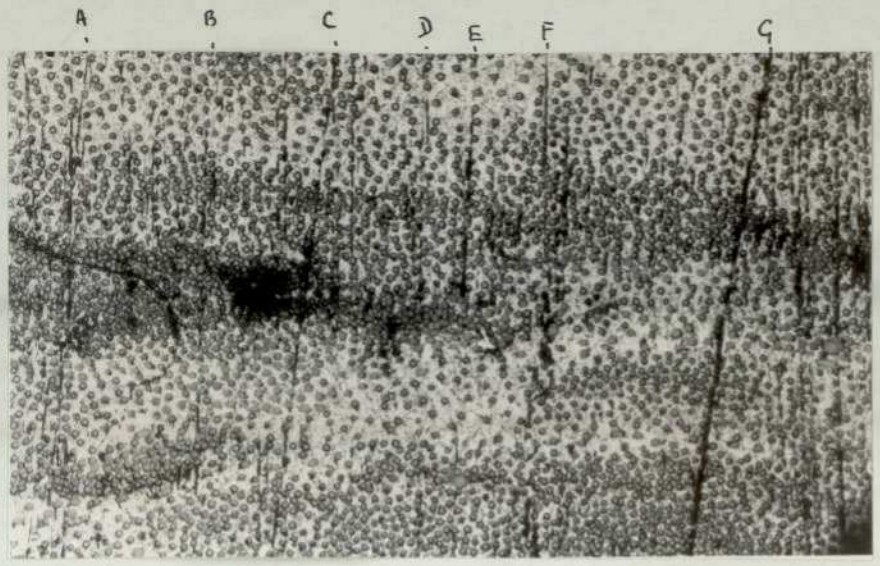


Fig. 87 Cu/Cf composite X100.

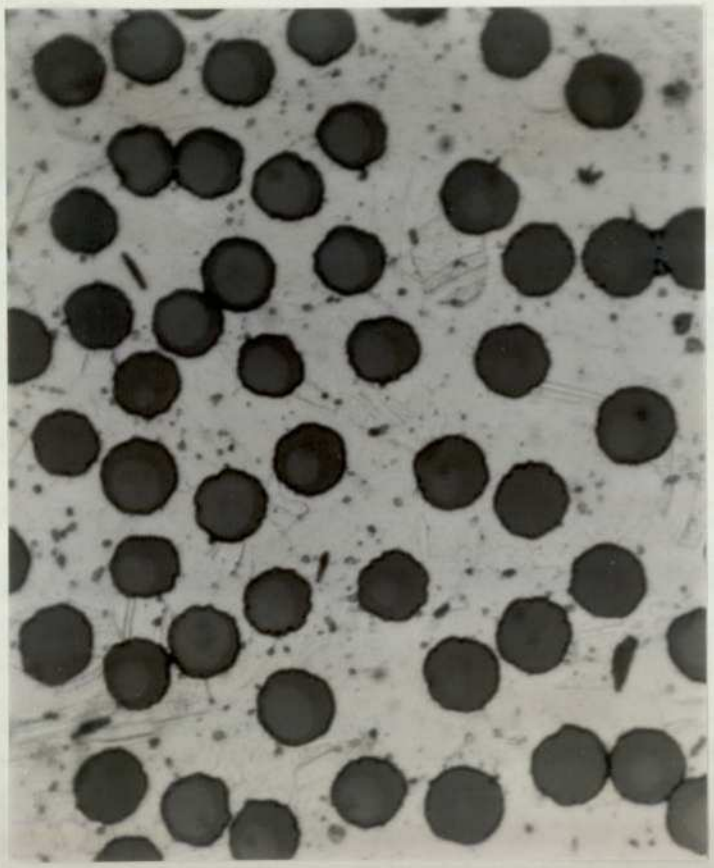


Fig. 88 Detail of fibre separation in composite. X1000.

uncompacted plated fibre results show the exact reverse, but such a result could be a reflection of increased fibre damage during the pressing process, as reported by Howlett et al[8], (1970).

Results of the second batch, prepared from continuous fibre, continuously plated, are shown compared with the first batch in Fig. 86. The family of points are well removed from their respective calculated "law of mixtures" line, indicating little or no reinforcement.

It is not known why such poor results were shown by the continuously plated materials but the parameters involved in the hot pressing of any plated carbon fibre material are not well known - much further work being needed in this field. Fig. 87 is of a microsection of a copper composite and lines A-G etc., which do not go through individual fibres and cannot therefore be scratches, may well indicate poor bonding, from bundle to bundle, in the die. The separation of the fibres, as seen in Fig. 88 is very good.

8.4 Quantitative analysis of copper on continuous tow, continuously plated

Because the tensile results from composites, made with continuously plated, continuous fibre, were so low it was felt that some of the deposit may have been detached from the tow during extra mechanical handling inherent in a continuous plating process, and it was therefore decided to analyse for total copper on unit length of fibre.

The copper on a length of tow was estimated volumetrically, via the sodium thiosulphate/starch iodide route, a method due to Haën and Low[9], (1854), subsequently re-examined by Gooch and Heath[10], (1867), based on the reaction:

$$2\ Cu^{++} + 4\ I^{-} \rightleftharpoons Cu_2I_2 + I_2 \qquad \ldots (64)$$

The copper was dissolved in a few mls of dilute nitric acid, fibres filtered off, filtrate precipitated with Na_2CO_3 and re-acidified with acetic acid,

TABLE 18

Analysis of Copper Deposit on Plated Tows

4" of continuously plated, continuous tow, taken for each sample.

Average weight of 4" unplated tow = 0.1130 gms
≡ 0.0282 gms/1"

SAMPLE 1

W, (gm)	∴ Wt. of Cu (gm)	Wt./cm. of plated fibre	t (microns)	Vol. fraction %
0.9903 T.R.	0.8773 I 1.4	0.1081	3.35 T.R.	29.6 II 1.4

∴ Copper content = 1.4 x 0.00636 x 100
= 0.8904 gms/4"

Weight of tow after Cu removal
= 0.0934 0.0234 gm/1"

∴ Actual wt. of deposit = 0.8969 gm.

∴ % Cu in deposit = 99.3%

∴ New vol. fraction = 30.0%

SAMPLE 2

0.9123 T.R.	0.7993 I 1.3	0.0995	3.15 T.R.	31.3 II 1.25

∴ Copper content = 0.8109 gm

Wt. of tow after Cu removal
= 0.0998 ≡ 0.0249 gms/inch

∴ Actual wt. of deposit = 0.8674 gm.

∴ % Cu in deposit = 99.8%

∴ New vol. fraction = 31.7%

thus removing free mineral acid, and then the solution was made up to 1 litre; 10 ml aliquots used.

A few gms of KI were added to test sample and the liberated iodine in solution titrated with N/10 $Na_2S_2O_3$ until a faint straw colour. Starch solution was then added and the whole titrated until colourless.

Then

$$TR \times 0.00636 \times 100 = g/l\ Cu,$$

(T.R. = titration reading)

since 1 ml N/10 $Na_2S_2O_3 \equiv 0.00636$ gms Cu. The results are given in Table 18 and provide no obvious reason for loss in tensile strength due to copper loss during production.

8.5 Discussion of Cu composite results

The results obtained do not indicate any high degree of reinforcement of Cu plated carbon fibre tows, on compaction. Whatever the cause, it is certain that some fibre damage occurs, may be in several ways, during hot pressing.

Let this degree of overall damage = k, then equation (63)

$$\sigma_c = \sigma_f V_f + \sigma_m' (1-V_f)$$

when modified to include a damage factor, k, should be:

$$\sigma_c = k [\sigma_f V_f + \sigma_m' (1-V_f)] \qquad \ldots (65)$$

or

$$k = \frac{\sigma_c}{[\sigma_f V_f + \sigma_m' (1-V_f)]} \qquad \ldots (66)$$

$$= \frac{\text{Observed u.t.s.}}{\text{Calculated u.t.s.}}$$

Assessment of Cu/carbon fibre composites –
Damage factor.

$$k = \frac{\text{Observed U.T.S.}}{\text{Calculated U.T.S.}}$$

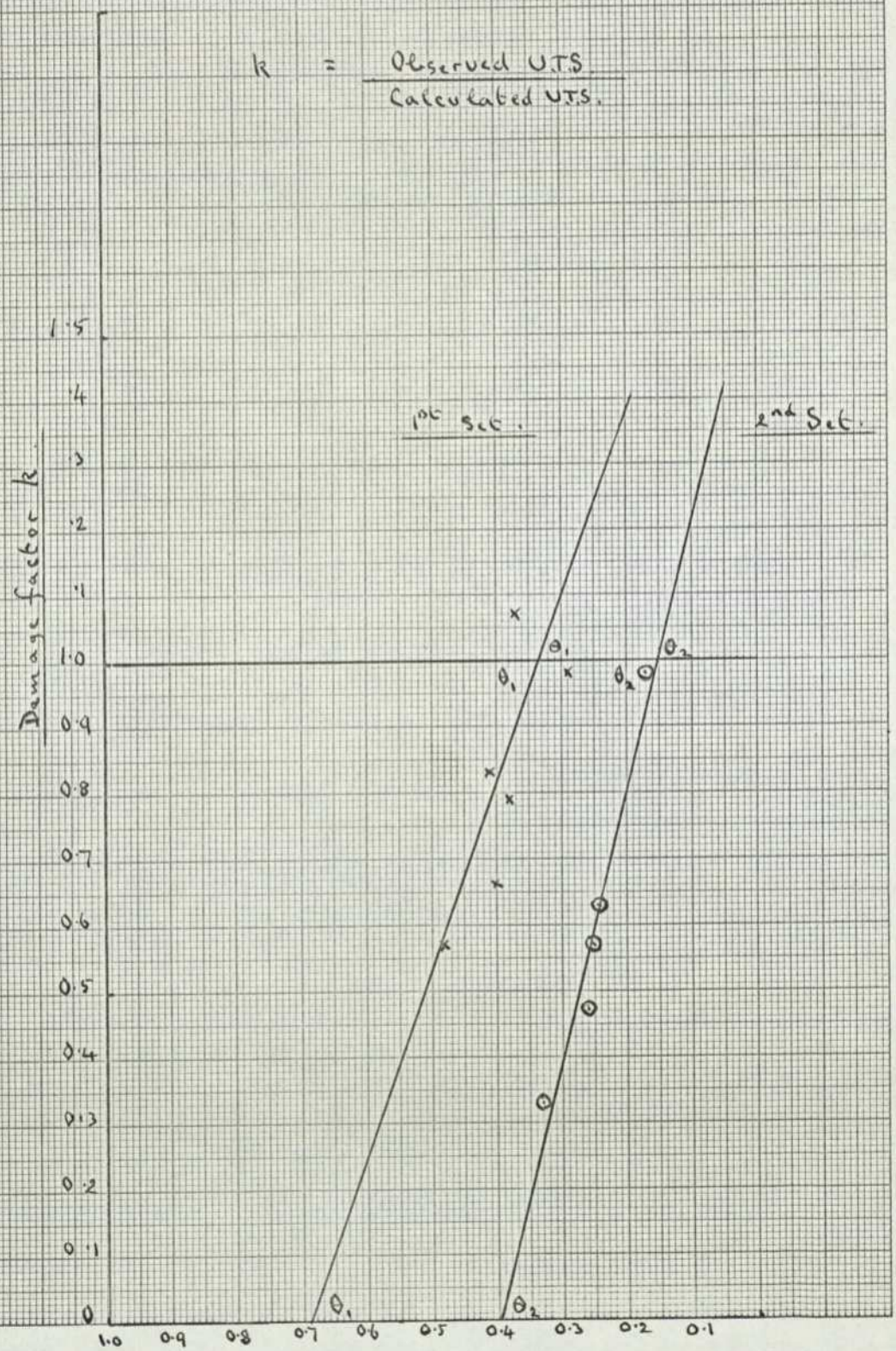


Fig. 89 Vol. fraction of C fibre in composite.

Here k = damage factor

σ_c = observed composite strength

$$= \frac{\text{Load}}{\text{Area of cross section of test piece}}$$

σ_f = U.T.S. of unplated fibres

V_f = vol. fraction of fibre

and σ'_m = Proof stress of Cu at 2% elongation, from curves of fully annealed Cu ≡ 32,400 psi, determined experimentally.

Values of k for both batches of copper compact are plotted against vol. fraction of fibre in Fig. 89. The angles θ_1 and θ_2 these lines make with a horizontal line through unit damage factor k, that is to say through a value of k for an ideal, damage free, compact, are an indication of the degree of reinforcement any given batch of compacts has attained, since when $\theta = 0$ we have the ideal state. It can be seen from this analysis that we have a long way to go before reaching perfection, although θ, at 70.8°, indicates a lower damage factor than that shown by θ_2, at 76.2°, a fact which adds weight to the results shown in Fig. 85, and also suggests that 1st batch was better.

Apart from damage during hot pressing, causing loss of strength, fibre mis-orientation can lead to a drastic short-fall in compact tensile strengths. Bhattacharyya and Parikh[11], (1970), report that a 10° misalignment in any epoxy-resin fibre glass composite would reduce its strength by 80%, similarly drastic reductions of up to 40%, in tensile strength, are reported, at misalignments of 20°, for his silver/tungsten composites. These results are confirmed, to a lesser degree, by those of Morris[12], (1970), in his work on the effect of fibre mis-orientation on the Young's modulus of carbon fibre/epoxy resin composites, where he reports that a short-fall of 15%, with Type II fibre, can occur with only 5% mis-orientation.

It must be pointed out that for the Cu/Cf compacts examined in this

work, the degree of fibre mis-orientation was an unknown factor, but fibre spacing in Fig. 88 indicates that it must be a variable, both parallel to the fibre axis at any one point, and along the length of the compact.

A further point for consideration is the temperature of 850°C chosen for hot compaction of the plated fibre. The hot pressing temperature was selected from previous experience of powder compaction etc., and might not necessarily be ideal for copper/carbon fibre work, and indeed the significant loss in tensile strength of plated fibres, annealed at 800°C, as reported in Section 7.6, makes it plain that much more work is needed in this field.

References 8

8.1 Mellor, 1946, See ref. 4.6.

8.2 Dietz, A. G. H. and Heyser, A. S., pp. 175-180 of Fibre Glass Reinforced Plastics, Ed., Sonneborn, R. H., Reinhold Press, 1954.

8.3 McDanels, et al, 1960, See ref. 1.43.

8.4 Cottrell, 1964, See ref. 1.45.

8.5 Kelly, 1964, See ref. 1.44.

8.6 Kelly, A. and Tyson, W. R., High Strength Materials, pp. 578, Wiley, New York, 1965.

8.7 Timoshenko, S., Strength of Materials, Pt. II, pp. 396, Van Nostrand, 1950.

8.8 Howlett, B. W., Minty, D. C., and Old, C. F., A.E.R.E. R-6577, 1970.

8.9 Haën and Low, A. H., Ann. Chem. Pharm., 91, 237, 1854.

8.10 Gooch, F. A. and Heath, F. H., Am. J. Sci., 4, 25, 1867.

8.11 Bhattacharyya and Parikh, N. M., See ref. 1.47.

8.12 Morris, J. B., A.E.R.E. H.C.F.W.P.(70)P.12, 1970.

CHAPTER 9

General Assessment of Results

9.1 Major variables affecting strength of PAN and unplated carbon fibre

When assessing the real value of any work on carbon fibre and its PAN precursor we have to consider the interplay of the many variables associated with what is, in reality, a multicomponent system, and try to isolate first order causes and effects from the many and confusing second order phenomena.

Starting then with PAN fibre, apart from the more obvious physical and geometrical variations such as occur in the density and diameter, from fibre to fibre and along the length etc., we have the loss in tensile strength caused by internal and external flaws in the polymer. Johnson and Thorne[1], (1969), have assessed the importance of the internal/surface flaw frequency by etching the fibre, when an increase in strength was accompanied by an increase in the frequency of internal flaw failures to a value of F (internal)/F (internal and surface) of 0.54, which, they say, is a value close to the predicted probability of internal flaw occurrence of 0.60. They also measured flaws in single fibres of from 1-4μ width, as elongated voids, parallel to the fibre axis with a 60% chance of finding such a flaw in any 3 cm length of fibre chosen at random.

Coming to the carbon fibre we have several main causes for variation in Young's modulus and tensile strength, as shown in Fig. 90, taken from the work of Moreton et al[2], (1967), such as variations introduced in the pre-oxidation stage due to the exothermic reaction, the degree of tension in the fibre, furnace residence time at the high or low temperature stage, resulting in a variable degree of graphitization, together with many other secondary effects.

We also have the initial flaws in the raw PAN and probably many flaws

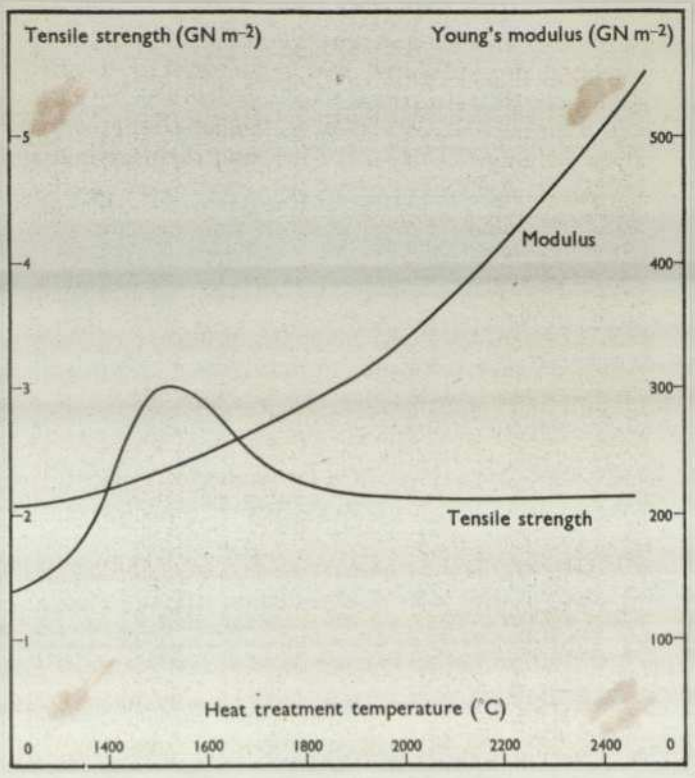


Fig. 90. Effect of heat treatment on mechanical properties of fibres (After Moreton(2), 1967).

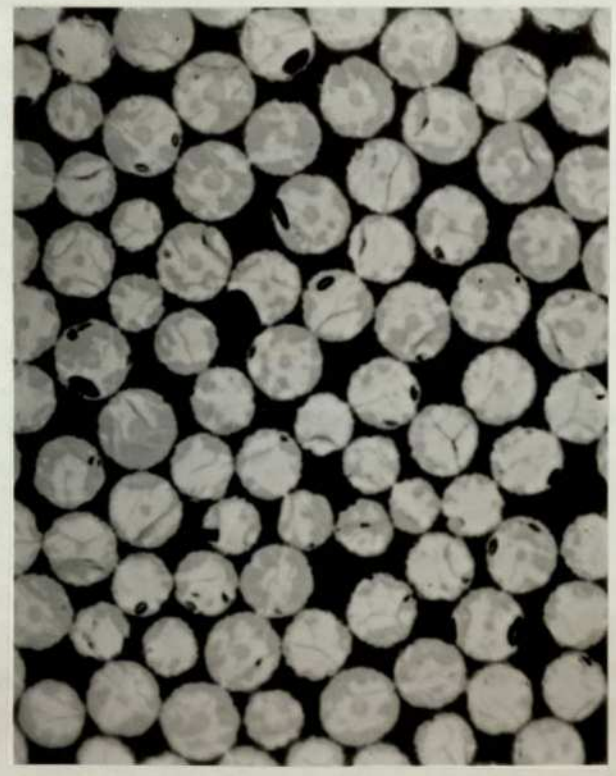


Fig. 91. Two-phase structure of carbon fibre. (After Macphail,(5), 1969) x1000.

produced during the evolution of hydrocyanic acid gas and ammonia during pyrolysis, leading to variable roughness of fibre surface and the two phase structure postulated by Shindo[3], (1961), observed under polarized light by Knibbs[4], (1969), and photographed from a micro-section, shown in Fig. 91, by Macphail[5], (1969).

As a matter of some importance it is worth noting that the hump shown in the tensile strength curve, in Fig.90, at about 1500°C is not reproduced in the modulus curve, since tensile strength is affected by surface flaws such as nicks and Griffith cracks etc. which have little effect on the modulus. Taking the experimentally observed tensile strength of unplated Type II fibre it is possible to work out the limiting depth of a surface crack leading to fibre rupture, using the relationship given by Griffith[6], (1924).

He stated that the condition for rupture was of the form:

$$R = \sqrt{\frac{2ET}{\pi c}} \qquad \ldots (67)$$

assuming the crack to have a surface which had the form of an elliptic cylinder and that c was the half length of the focal line also that:

E = Young's modulus

T = surface energy

and R = the component of the applied edge traction, normal to the direction of crack.

This equation, restated is:

$$R = m\, c^{-\frac{1}{2}} \qquad \ldots (68)$$

where 'm' is the constant of the material, which will of course change with preparation and subsequent handling.

The value of T for carbon fibre is not known, but to a first approximation, T for carbon is about 4.2 Joules/m^2, (Reynolds[7], 1971), R for the case under consideration, experimentally was 0.1069×10^{11} dynes/cm^2

and $E = 0.22 \times 10^{13}$ dynes/cm^2. Substituting these values in equation (67), with appropriate conversions, gives a value for $c = 0.5145 \times 10^{-4}$ cms = the half length of the focal line $\therefore 2c = 1.029$ microns or the length of the crack at condition for rupture, that is to say, about $\frac{1}{10}$ the diameter of the fibre (8).

Since such cracks are a function of the degree of handling experienced by carbon fibre, they become a major variable in relation to the tensile strength, and as stated by Cottrell[8], (1964), ideal strengths, σ_i, for solids, of the order $\frac{E}{10}$, are rarely reached, because brittle solids break prematurely at Griffith's cracks and stress concentrators, experimental results often being two orders of magnitude less than σ_i. The "handling effect" leading to poorer experimental control and lower tensile results was demonstrated in the surface treatment work described in Chapter 7.

The failure of Type I, high temperature fibre at such low and irreproducible tensile strengths could also well be due to a high concentration of Griffith's cracks, in the fibre surface, a phenomenon to be expected in a fibre with a much higher degree of graphitization than that found in Type II material.

9.2 Major variables affecting strength and quality of copper plated carbon fibre

The early plating work quickly showed that copper plating from the acid sulphate both gave deposits of low tensile strength well below the calculated "law of mixtures" line and some explanation is needed for this unexpected result.

During work on the electroplating of non-conductors, whose surfaces had been rendered conducting by a film of alcohol DAG, (Defloculated Acheson Graphite) it was noticed that surface coverage was slow at low current densities and that nucleation occurred in scattered patches which subsequently coalesced. Nystrom[9], (1969), using electron microscopy

and metallographic techniques, has demonstrated that initially copper deposition on polished graphite surfaces consisted of clusters of grains, randomly distributed over the surface which developed projections growing out into the electrolyte, complete surface coverage being eventually achieved through combination of cluster growth and additional nucleation. Such a mode of growth would lead to a columnar structure with preferred orientation at right angles to the fibre surface which would, in shear, provide a weaker bond than would a layer of copper deposited in laminar structure parallel to the fibre axis, similar to the small grain sized copper deposit which forms in the cyanide electrolyte. The growth mode described may also be a function of complete non-wetting of carbon by the acid electrolyte, but the addition of wetting agents such as Perminal BX or WA, which are stable to acids and metallic salts, produces bright brittle deposits, with poor strength.

Coming to fibres plated in the cyanide electrolyte, the factors affecting the strength of the copper/carbon fibre simple composite can be broadly divided into two fields, electrochemical and physical. Results described in Chapter 6 show that the most important parameter controlling quality of deposit is the free cyanide content and that the concentration should be kept between the excessive gassing/low metal deposition zone of high free cyanide (>10 g/l) and the blue/dendritic deposit zone of low free cyanide, (< 2 g/l), for best copper deposits. The work also showed that measurement of Faraday efficiency only served as a guide to solution control butnot to quality of deposit, since high efficiency often produced powdery deposits.

This work also showed that the tensile strength of the composite was a function of thickness or volume fraction of the deposit and that variations of factors such as temperature, current density etc., were largely revealed only by changes in thickness of deposit, expressed as

an average throughout the tow. To illustrate the relationship of tensile strength with thickness consider Equation (35), once more:

$$\sigma^2 = \frac{2A_x E R}{W l} \qquad \ldots (35)$$

Now

$$W = \frac{RV}{l} \qquad \ldots (69)$$

where R = density of composite

V = total volume of fibre

Thus

$$W = \frac{Ra\,l}{l} \qquad \ldots (70)$$

where a = cross sectional area of composite.

Therefore

$$\sigma = \sqrt{\frac{2A_x E R}{Ra\,l}} \qquad \ldots (71)$$

and since $a = \pi r^2$ where $r = \frac{d+2t}{2} = \frac{d}{2} + t$, where 'd' is fibre diameter and 't' the plating thickness, we have

$$\sigma = \sqrt{\frac{2A_x E}{\pi l}} \cdot \left[\frac{1}{(d/2+t)}\right] \qquad \ldots (72)$$

Thus the tensile strength is inversely proportional to the plating thickness, all other variables remaining constant. In general, therefore, the lower the volume fraction of copper in the composite the stronger the plated tow.

From the analysis of whole tow testing given in Chapter 4 we have seen that the Instron results can also be analysed in other ways by equation (35) where

$$\sigma = \sqrt{\frac{2A_x E R}{W l}}$$

and σ is a function of composite modulus, E, composite density, R, and

Variation of observed result with fibre diameter (calculated).

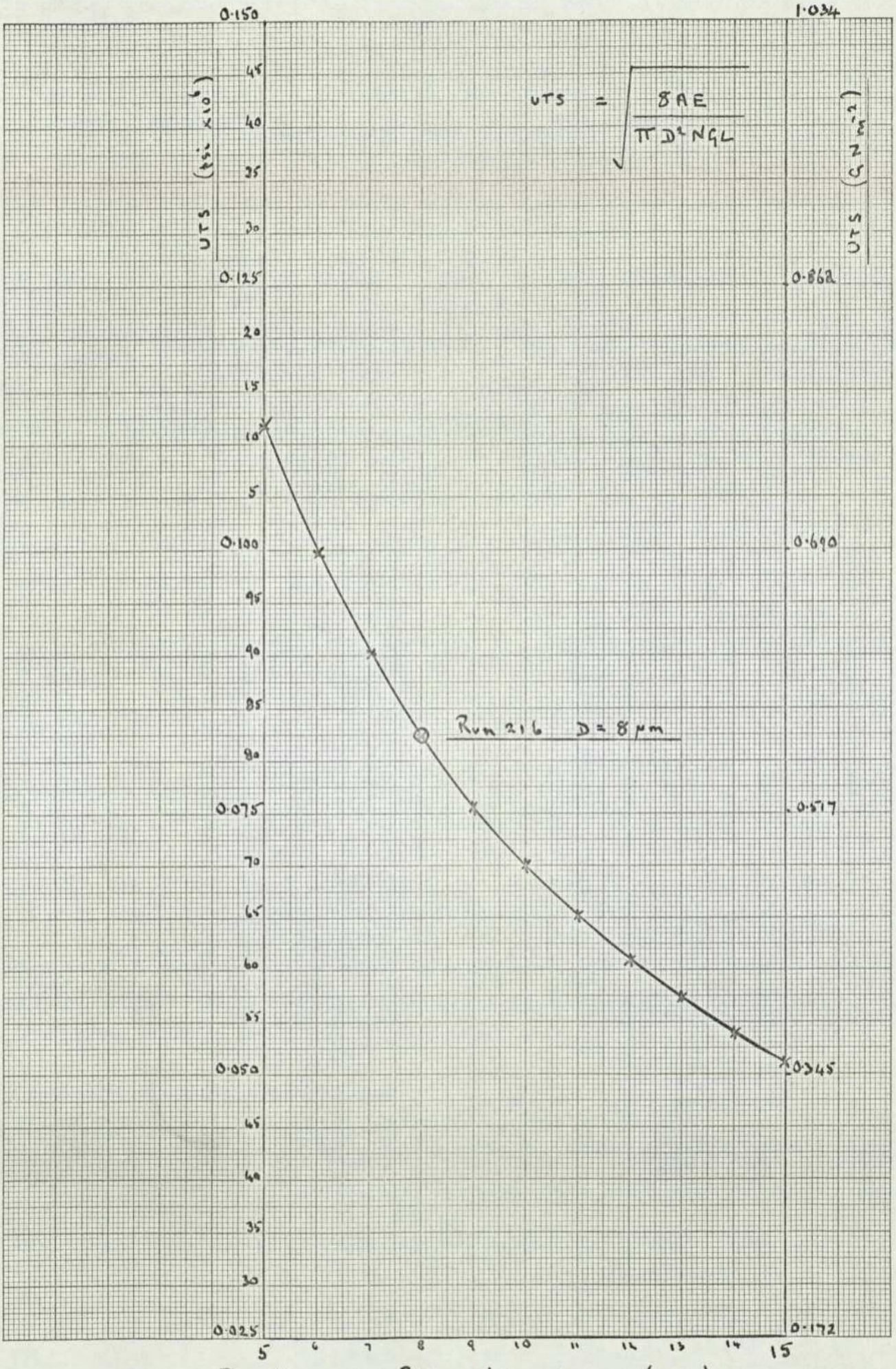


Fig. 92

Variation of U.T.S. of an observed result, with number of fibres in tow (Calculated)

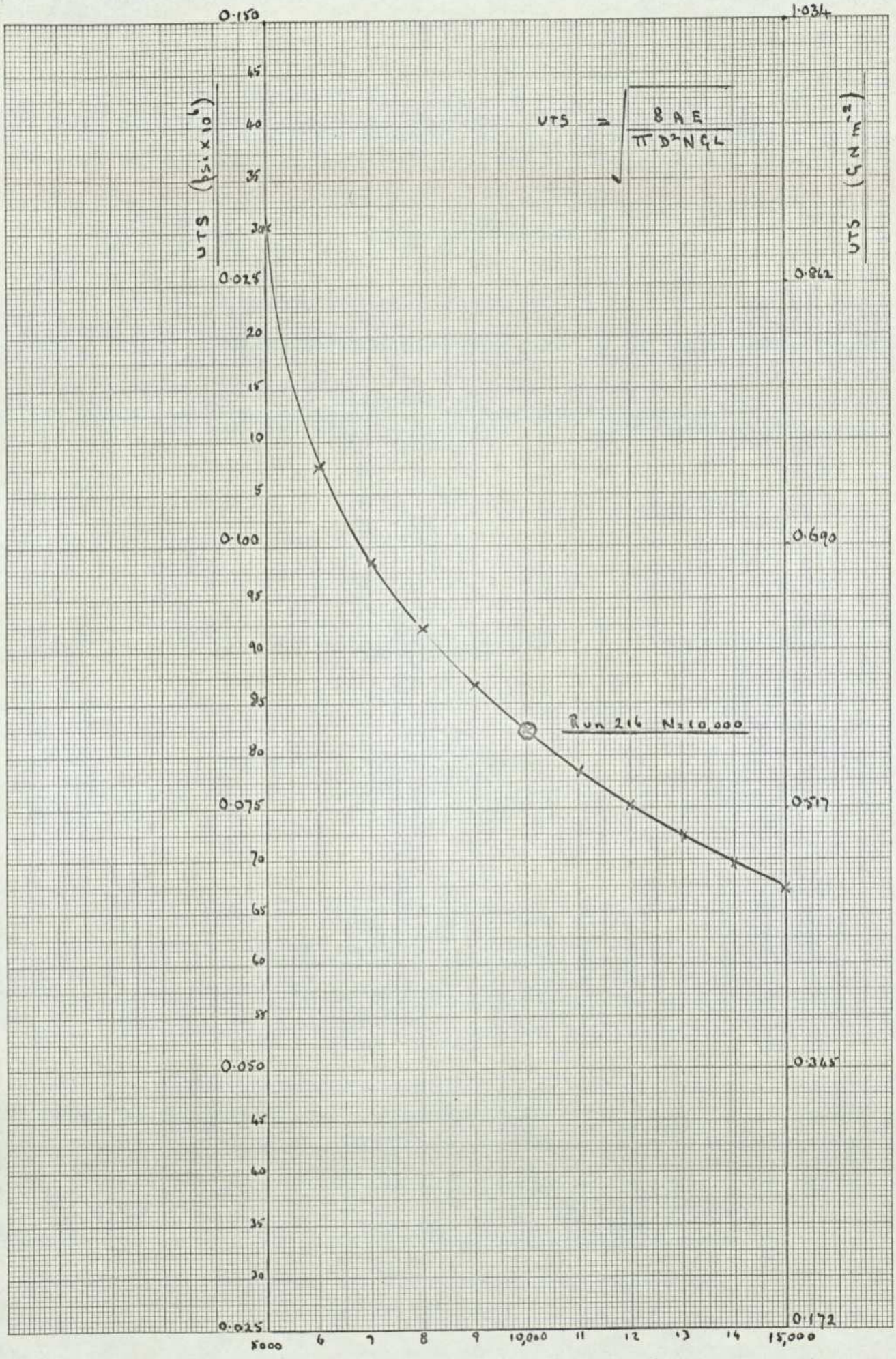


Fig. 93 N-the number of fibres per tow.

Variation of observed result with Young's Modulus.

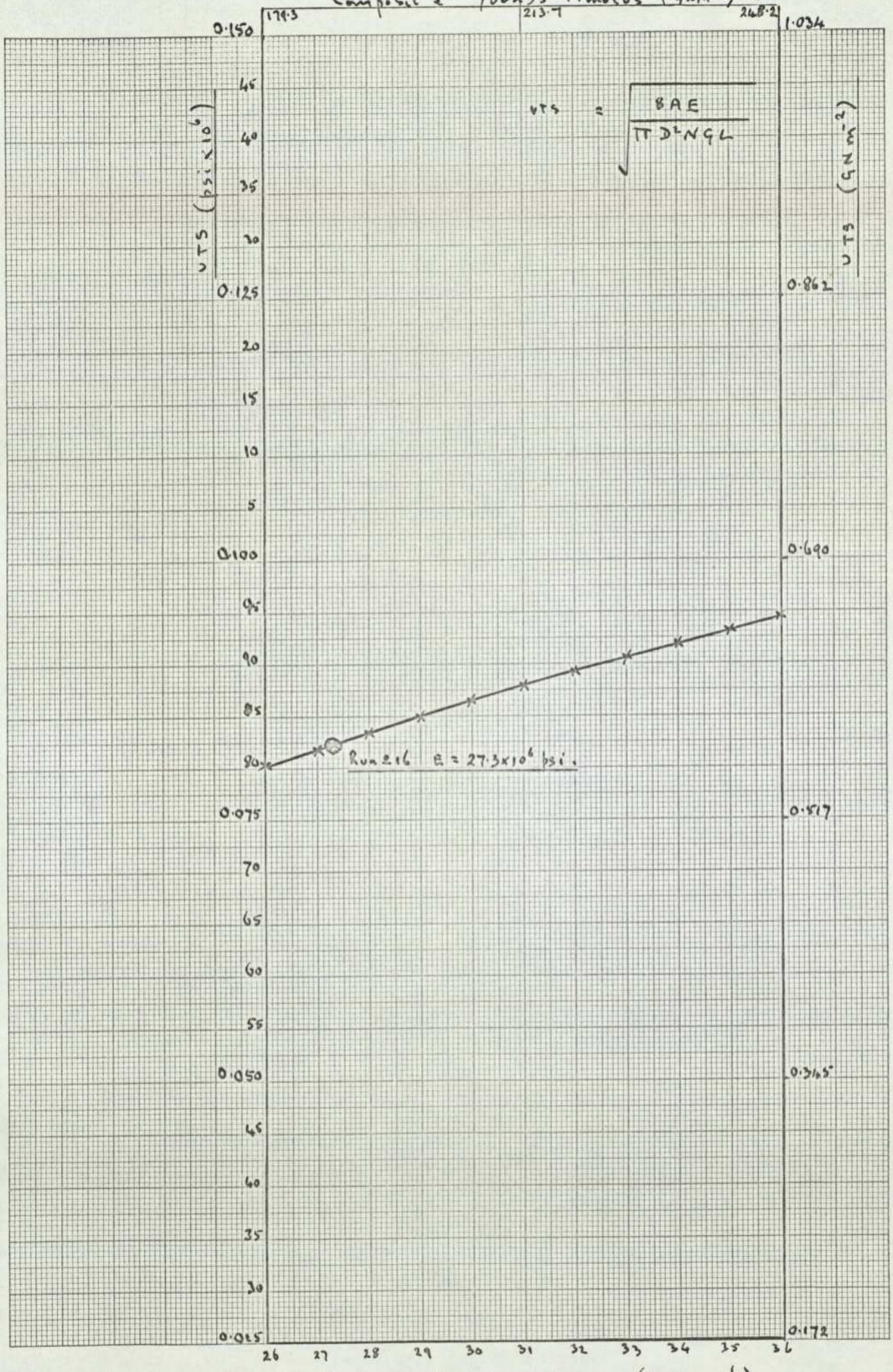


Fig. 94 Composite Young's Modulus (psi x10⁶)

Table 19 Variation of U.T.S of Cu plated Type II fibre with various parameters, calculated by deposit thickness route.

	0·1 A/10^{-2} m^2				0·2 A/10^{-2} m^2				0·4 A/10^{-2} m^2				0·6 A/10^{-2} m^2				0·8 A/10^{-2} m^2			
Deposition Temperature	No.	U.T.S (psi x 10^6)	t (μm)	F_f	No.	U.T.S (psi x 10^6)	t (μm)	F_f	No.	U.T.S (psi x 10^6)	t (μm)	F_f	No.	U.T.S (psi x 10^6)	t (μm)	F_f	No.	U.T.S (psi x 10^6)	t (μm)	F_f
20°C	197	–			200	0·0753	2·0	0·44	203	–										
	198	0·0936	1·5	0·53	201	–			204	0·0583	3·0	0·33	95	0·0436	3·5	0·24	96	0·0331	4·0	0·16
	199	0·1047	1·4	0·56	202	0·0675	2·1	0·44	205	0·0529	3·0	0·33								
Arithmetic Mean		0·0991	1·5	0·55		0·0714	2·1	0·44		0·0556	3·0	0·33								
Standard Deviation		5518 psi.	%S.D. = 5·6			3900 psi.	%S.D. = 5·5			2700 psi.	%S.D. = 4·9									
30°C	185	0·1001	1·5	0·53	209	0·0583	2·6	0·37	212	0·0534	3·9	0·26								
	207	0·0975	1·6	0·51	210	0·0580	2·5	0·38	213	–										
	208	–			211	0·0679	2·5	0·39	214	0·0514	4·3	0·23								
A.M		0·0988	1·6	0·52		0·0614	2·5	0·38		0·0524	4·1	0·25								
S.D.		1300.	%S.D. = 1·3			4600.	%S.D. = 7·5			1000.	%S.D. = 1·9									
40°C	215	–			218	0·0719	2·6	0·37	221	0·0471	4·3	0·24	224	0·0434	5·4	0·18	227	0·0422	7·3	0·13
	216	0·0897	1·7	0·49	219	0·0669	2·8	0·35	222	0·0463	4·1	0·24	225	0·0362	5·4	0·18	228	0·0418	6·6	0·14
	217	0·0963	1·8	0·48	220	0·0733	2·9	0·34	223	0·0523	4·6	0·23	226	–			229	0·0477	5·6	0·17
A.M		0·0930	1·8	0·49		0·0707	2·8	0·35		0·0486	4·2	0·24		0·0398	5·4	0·18		0·0439	6·8	0·15
S.D.		3300.	%S.D. = 3·5			2750.	%S.D. = 3·4			2661.	%S.D. = 3·8			3600	%S.D. = 9·1			2693.	%S.D. = 6·1	
45°C	230	0·0831	2·0	0·44	233	0·0588	2·6	0·35	236	0·0489	4·3	0·24	239	0·0420	4·7	0·21	242	–		
	231	0·0844	2·0	0·44	234	0·0539	2·7	0·36	237	0·0464	4·6	0·22	240	0·0358	5·6	0·18	243	0·0339	6·6	0·15
	232	–			235	0·0671	2·6	0·37	238	0·0479	4·9	0·20	241	–			244	0·0330	6·3	0·15
A.M.		0·0837	2·0	0·44		0·0599	2·6	0·36		0·0477	4·7	0·23		0·0389	5·1	0·19		0·0334	6·5	0·15
S.D.		656.	%S.D. = 0·8			5450.	%S.D. = 9·1			1020.	%S.D. = 2·1			3049.	%S.D. = 7·8			447.	%S.D. = 1·3	
50°C	245	0·0720	2·3	0·41	248	0·0516	3·1	0·32	251	0·0449	5·1	0·20	254	0·0397	6·0	0·16	257	0·0311	7·6	0·11
	246	0·0787	2·1	0·44	249	0·0562	2·9	0·34	252	0·0404	4·8	0·21	255	0·0369	6·0	0·16	258	0·0324	7·5	0·12
	247	0·0764	2·2	0·42	250	0·0542	3·0	0·33	253	0·0426	4·7	0·21	256	0·0339	6·5	0·15	259	0·0312	7·4	0·12
A.M.		0·0757	2·2	0·43		0·0540	3·0	0·33		0·0426	4·9	0·21		0·0368	6·2	0·16		0·0315	7·5	0·12
S.D.		4889.	%S.D. = 6·5			1884.	%S.D. = 3·5			1839.	%S.D. = 4·3			2369.	%S.D. = 6·4			592.	%S.D. = 1·9	

U.T.S. Calculation by
direct and indirect routes.

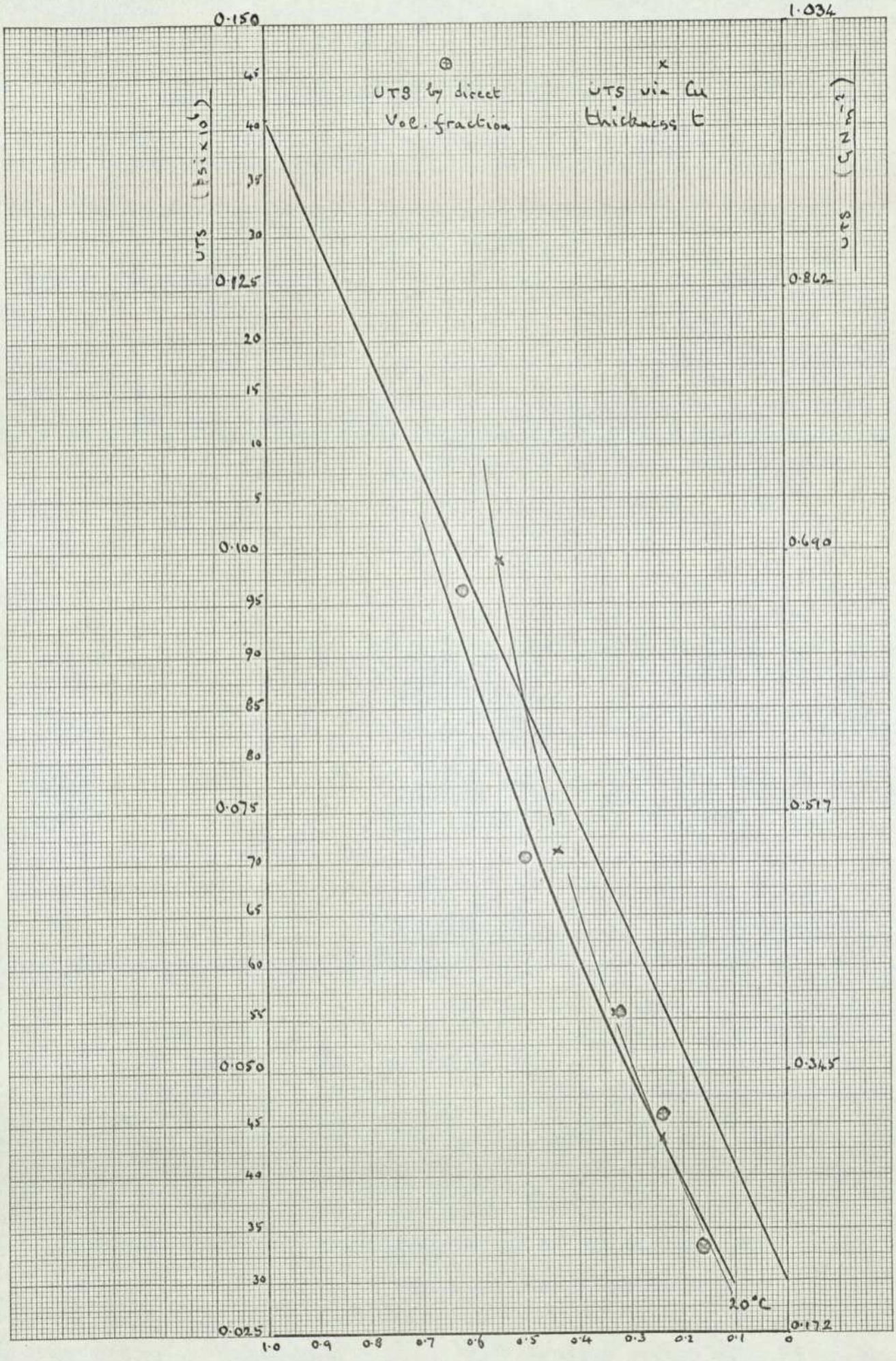


Fig. 95 Vol. fraction of C fibre in Cu plated tows.

weight per unit length, W., or from equn (30), where

$$\sigma = \sqrt{\frac{8A_x E}{\pi D^2 N l}},$$

where the result is a function of the composite Young's modulus E, the fibre diameter D and the number of fibres per tow.

To demonstrate the effect of any variation of the parameters in eqn. (30) on the value of σ, an experimental run, (No. 216), has been taken at random and variations of the observed tensile strength due to variations of E, D and N, have been calculated. Fig. 92, showing the calculated effect of variation of fibre diameter, from the nominal 8μ of the fibre used, indicates that an increase in diameter would lead to a sharp fall in tensile strength and a decrease would give rise to a sharp increase in σ. A variation in σ would be expected from Eqn. (30) but this treatment provides an idea of the magnitude of the variation produced by choice of incorrect values of E, D and N. Similarly Fig. 93, shows the effect on σ of variations of N, the number of fibres per tow, a value which is never known with accuracy. The variation from the observed result of σ, for run 216, is of the same order as that produced by the calculated variation of diameter. Fig. 94, shows a similar plot of the effect of variation of the composite modulus on σ and here the value of σ is least sensitive to variations of E.

One can also calculate the tensile strength of the plated fibre from the thickness of copper deposited, as has been shown. Table 19 shows the results of the standard experimental 5 x 5 test block of plated fibres, calculated in this way.

The difference in σ calculated from thickness and those values given in Table 11, (Chapter 6), calculated from direct weights, is not significant, except for results produced at 20°C, as shown in Fig. 95 where σ from direct weight is slightly lower.

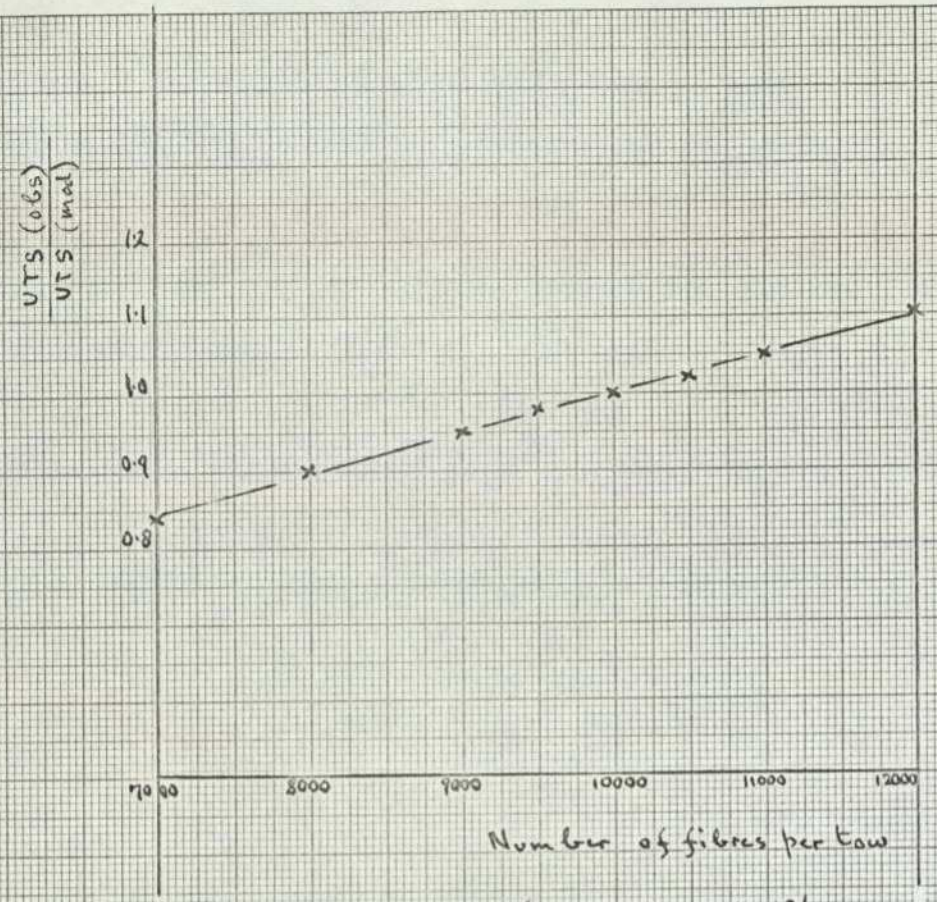


Fig 96 Adjustment curve for variations in N.

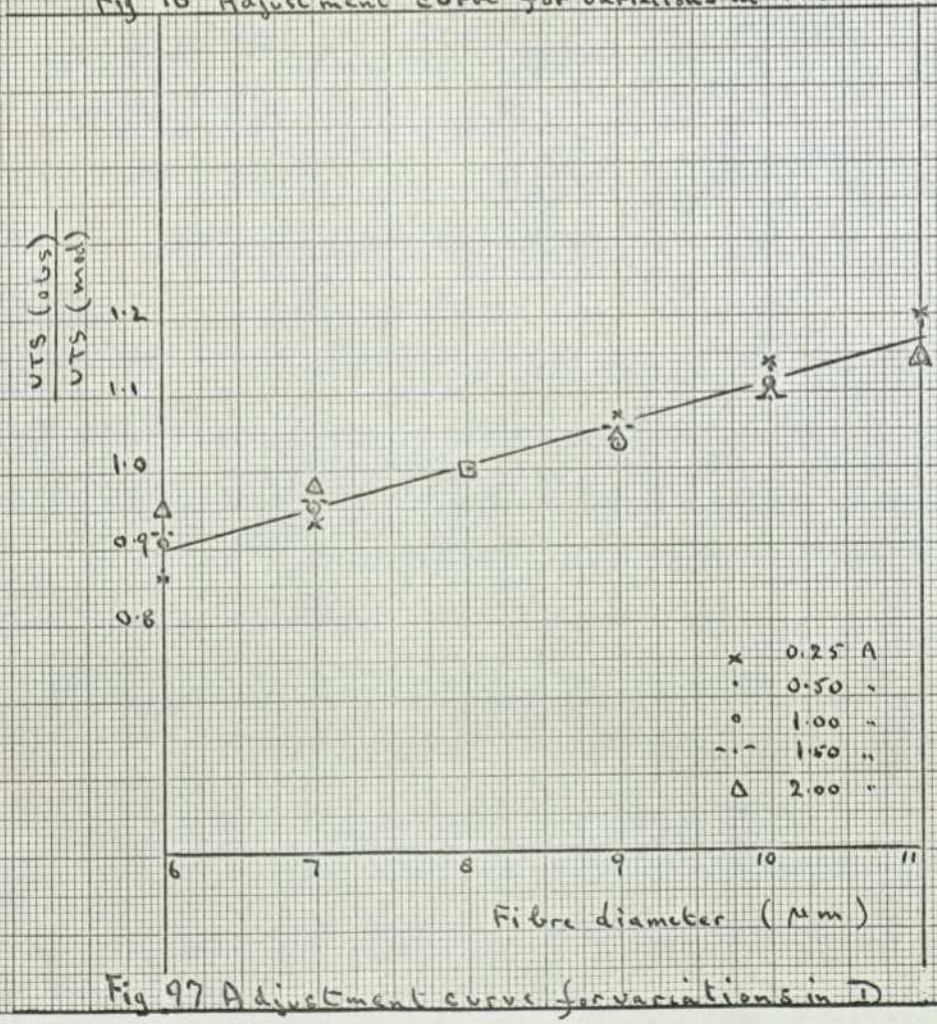


Fig 97 Adjustment curve for variations in D

Adjustment curves covering variations of major parameters.

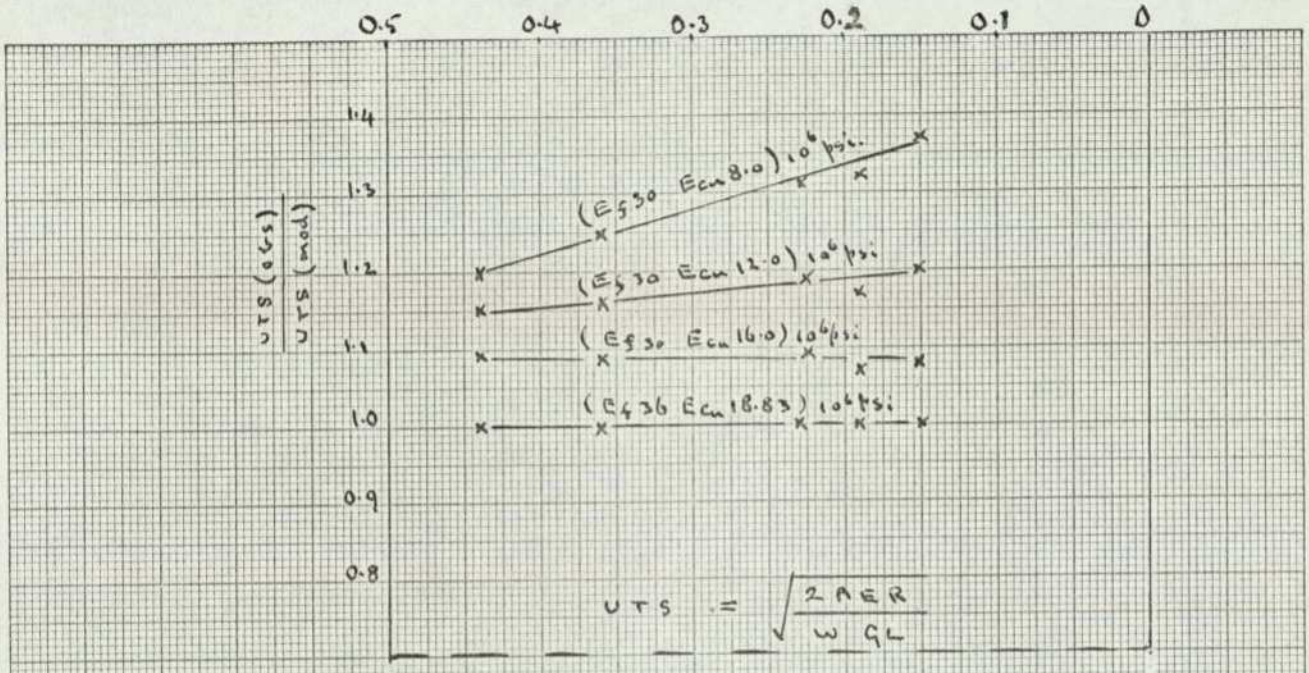


Fig 98 Variations in Young's Modulus at 45°C.

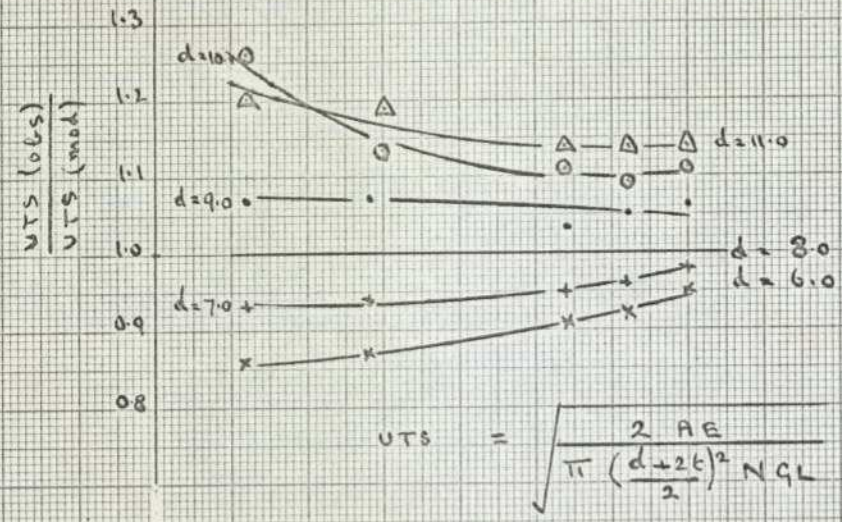


Fig 99 Variations in fibre diameter.

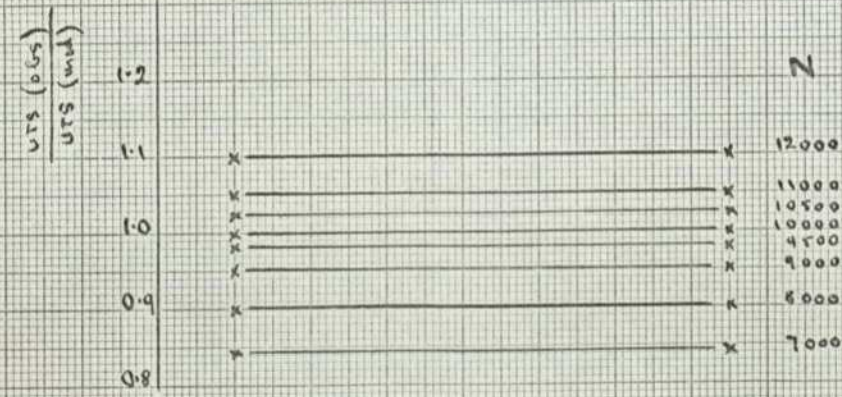


Fig. 100 Variations in number of fibres per tow

0.5 0.4 0.3 0.2 0.1 0

V.f. fraction of C fibre in Cu plated tow.



Fig. 101. 4 hr deposit at $0.8/10^{-2}m^2$, 20°C. x1½



Fig. 102. Gas cups on heavy deposit x6

Finally, if it is thought, when assessing results, that the observer has chosen an incorrect value for N or D in any published results, correction factors from the adjustment curves shown in Figs. 96 and 97, can be chosen to round up or down any given result; similarly should the results express σ as a function of volume fraction of fibre present, then factors from Figs. 98, 99 and 100 can be chosen.

A further primary variation affecting the observed tensile strength is of course the type of copper deposit on the fibre. As an exaggerated example, Fig. 101 shows a heavy deposit of powdery Cu on a carbon fibre tow. From the detail in Fig. 102, a formation similar to acorn cups can be seen on the deposit. These are due to clinging hydrogen bubbles and should they be built over by the growing deposit, would result in internal flaws.

In this analysis one must also consider those specimens of plated fibre which fail under stress, well before the value of σ calculated by the "law of mixtures", assuming, in the first place, that the fibre substrate was not initially of poor quality.

Now a plated fibre can be considered as a cylinder of carbon in a copper tube and Bridgmann[10], (1952), in his studies of plastic flow, considered the case of the deformation of a tube to fracture. He said, in explanation of the more complex behaviour exhibited by tubes that:

> "... we are here concerned with a two dimensional instability instead of a one dimensional instability, corresponding to necking along the radius and the circumference".

Experimentally he showed that inward radial flow of the tube took place sufficient to cause binding on the ram-rod of the apparatus, unless appropriate precautions were taken and also that the wall thickness decreased. Fracture started at a single point and travelled round the circumference and under no circumstances did the fracture show a cup and cone type of break but the surfaces of the fracture were shearing surfaces,

inclined at roughly 45° to the tube axis.

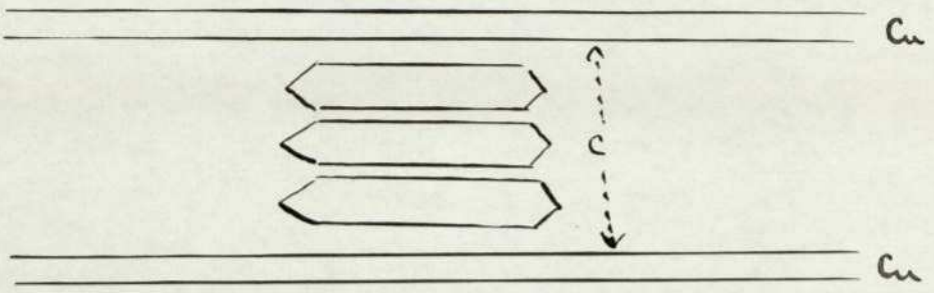
Now the above mentioned facts would explain nothing in the case of the plated fibre if the deposit were of even thickness around the circumference, but if this thickness varied, then unequal forces would arise at right angles to the fibre surface, and at the site of a Griffith crack, such a state of shear would lead to premature rupture. Even the presence of a surface flaw would not be strictly necessary since the tensile strength of carbon fibre at right angles to the fibre axis is only about 3000 p.s.i. or approximately 100 times less than the strength measured parallel to the fibre, (Reynolds[11], 1968).

An interesting corollary to the above is the behaviour of de-plated carbon fibre. It has been observed in this work that no matter how weak a plated fibre tow proved to be on test, similar tows, with the copper removed, were restored to approximately original strength. This has also been reported by Calow and Moore[12], (1971), in their work on copper plated single fibres, and proves among other things, that the cyanide plating process has very little effect on carbon fibre, as was thought in the early days. It appears to show that removal of stress concentrators prevents premature rupture. A similar result has been reported by Johnson and Thorne[13], (1969), after etching carbon fibre surfaces, where removal of surface flaws leads to improved tensile strength and by Griffith[14], (1921), in his work on rupture of solids.

Finally, one must consider the overall low strength recorded for hot-pressed copper/carbon fibre compacts. Apart from the phenomena, noted in Section 8.5, as possible causes, such as mechnical damage during pressing and fibre mis-orientation etc., the effect of thermal stress must be examined.

If one imagines an ideal copper plated carbon fibre, then all the graphite crystallites would be oriented in stacks, with basal planes

parallel to the fibre axis, as in Fig. 103, below:



and the thermal expansion of the fibre in the direction of the 'c' axis, perpendicular to the basal plane, would be approximately 28.3 x 10^{-6} cms per ^{o}C and approximately -1.5 x 10^{-6} per ^{o}C, between 0-150^{o}C and +0.9 x 10^{-6} per ^{o}C, between 600-800^{o}C, in the direction of the 'a' axis, that is parallel to the fibre axis. The copper deposit, which can again be regarded as a copper tube in this argument, with an internal diameter d, would only expand 17.8 x 10^{-6} cms per ^{o}C, that is 10.5 x 10^{-6} cms/^{o}C less than the carbon fibre and therefore the degree of mechanical adhesion of the deposit would increase considerably.

Thermal expansion along the fibre axis would however result in little increase in length of the fibre whilst the heat bonded copper could only extend to the elastic limit of the fibre and beyond this would therefore be put in a state of compression with, of course, corresponding tension in the fibre.

At 850^{o}C, the hot pressing temperature, 1 cm of Cu would become

$$l_t = 1\ (1 + 0.0000178 \times 850)$$

$$= 1.01513 \text{ cms}$$

$$\equiv 1.51\% \text{ elongation.}$$

Now the elongation to fracture of carbon fibre, as has been said, is of

the order of 1% and therefore one could argue that the significantly low tensile strengths recorded for hot pressed copper compacts was due to a combination of factors, a major one being thermal stress. Supporting evidence for this view is provided by the significant decrease in tensile strength observed in uncompacted copper plated tows, annealed to 800°C, (fibre damage taking place during the process).

9.3 General conclusions

Type II carbon fibre can be copper plated, with advantage, under the conditions described in the plating specification, given in Section 7.8 Because the tensile strength of coated fibre is inversely proportional to the thickness of copper deposited and roughly obeys the "law of mixtures", it should be possible to make hot-pressed copper/carbon fibre compacts, of near theoretical strength but these have not been produced, as yet, due to fibre mis-orientation, poor fibre management, mechanical damage during hot-pressing, thermal stress and many other secondary contributory factors.

In particular much more work is needed before the art of fibre management is mastered, and reproducible control of the 10,000 odd, 8 micron fibres attained. Much could be learnt from the spinning and weaving industries since, after all, at this stage, it is a textile problem. The problem is further aggravated by the very low tensile strength at right angles to the fibre axis, since this rigorously dictates parallel alignment of the plated fibres before compaction and introduces a new design philosophy when incorporating in a structure any carbon fibre composite, as described in the work of Pearce[15], (1969).

A further limitation of the use of Cu/Cf composites is the loss in strength which occurs at temperatures above 700°C, due, it is thought, to thermal stress. The work of McKee[16], (1969), showed that oxidation, at this temperature in air, would be accelerated. He found that the

oxidation of graphite was catalysed by the presence of copper, and copper oxide particles, of 1-5μ size, moved rapidly on the basal plane of graphite crystals, cutting irregular channels in the surface. Such phenomena could not be tolerated with carbon fibres since the end result could only be drastic loss in strength.

In view of these restricting circumstances, the use of Cu/C composites may be confined to contact-breakers generator brushes, electric overhead rail shoes, etc.

It is felt that the work described in this report may well act as a guide to the coating of carbon fibre with other metals, pointing out, as it does, the many variations in the raw materials, the important zones needing close control and weaknesses to be avoided.

As to the future, work along the lines of Fink and Prince[17], (1928), on the co-deposition of copper and graphite could well lead to important results, if modified to suit the requirements of chopped fibre compaction. They were able to co-deposit 42 per cent by volume of graphite in the copper composite which formed on the cathode, from a simple copper sulphate electrolyte, stabilized with gelatin.

Finally, I would like to quote a rhyme as an apologia, to cover the many instances when, for the sake of clarity, pounds per square inch etc., instead of S.I. units have been used. The rhyme was sung at the Metropolitan Red Lion Club of Church St., London, in 1839, soon after the French had invited us to "go metric", in 1790.

"Some talk of millimetres and some of kilo-grams,
And some of decilitres to measure beer and drams:
But I'm a British workman too old to go to school,
So by pounds I'll eat,
By quarts I'll drink,
And I'll work by my three-foot rule!"

REFERENCES 9

9.1 Johnson, J.W. and Thorne, D.J. Carbon, No. 6, Vol. 7, p.659-661, 1969.

9.2 Moreton, R, Watt, W., and Johnson, W., Nature, Lond., 213, 690, 1967.

9.3 Shindo, 1961, See ref. 1.17.

9.4 Knibbs, 1969, See ref. 1.28.

9.5 Macphail, I., A.E.R.E., R-6168, 1969

9.6 Griffith, A.A., Proc. Int. Congr. Applied Mechanics, Delft, 1924.

9.7 Reynolds, W.N., Private communication, 197,

9.8 Cottrell, 1964, See ref. 1.45.

9.9 Nystrom, W.A., Plating, Vol. 56, No. 3. pp.285, 1969.

9.10 Bridgman, P.W., Studies in Large Plastic Flow and Fracture, McGraw-Hill, 1st Ed. 1952.

9.11 Reynolds, W.N., Physical Properties of Graphite, 55 et. seq. Elsevier, 1968.

9.12 Calow, C and Moore, A., A.W.R.E. Private Communication, 1970.

9.13 Johnson and Thorne, 1969, See ref. 9.1.

9.14 Griffith, A.A., see ref. 1.21.

9.15 Pearce, D.G., A.E.R.E., M-2137, 1969.

9.16 McKee, D.W. Carbon, Vol. 8, No. 2, pp.131-139, 1970.

9.17 Fink, C.G. and Prince, J.D., Trans. Amer. Electrochem. Soc., pp.315, Vol. LIV, 1928.

APPENDIX 1

The denier system of fibre classification

APPENDIX 1

The Denier System of Fibre Classification

The system of fibre classification based on the denier is a very loose one and many interpretations or mis-interpretations are possible. A few of the definitions are given below to emphasize this point.

Ref. 1. The denier system

> "The system used in the 'counting' of silk and rayon yarns; designated by the weight in grams of 9000 metres of yarn, the unit of length. Originally, in 1839, a unit of weight equal to about $8\frac{1}{5}$ tray grains, ($\equiv$0.533 gms), by which silk yarn is weighed and its fineness estimated. Hence the French verb, denier, to ascertain the fineness of (silk) yarns, in deniers".

Here we see that the unit was originally used in the silk industry, for a material which presumably has a constant density, but this fact is often forgotten, viz:

Ref. 2. The denier

> "The weight of 9000 metres of yarn, the unit of length. 1 gram = 1 denier".

Here, if $W = \rho V$, we have

$$1 = \rho \times 9000 \times 100 \times \pi r^2$$

This gives two unknowns, an impressive definition. The next definition is even further removed from reality:

Ref. 3. The denier

> "The denier unit is applied to silk of such a fineness that 4,464,531 yards of thread would weigh exactly one pound".

In the next definition we have:

Ref. 4. The denier

> "A denier rayon yarn means that 9000 metres weighs 65 gms. And 150/36 yarn means 36 filaments of 150 denier".

The latest system for fibre classification is given in:

Ref. 5. Yarn count or yarn number

> "In the Western hemisphere, the unit used is the "drex", which gives the mass in grams of 10,000 metres length of yarn. In

TABLE 20

Fibre Classification

Direct, (mass per unit length)			
Name	Unit of mass	Unit of length	Value = 20 tex
denier	gram	9000 metres	180
drex	"	10000 metres	200
(Western hemisphere)		(the International denier)	
poumer	pound	10^6 yds	40.3
-	grain	100 yds	28.2
-	"	120 yds	33.9
tex			
(Eastern hemisphere)	gram	1000 metres	20
Indirect (length per unit mass)			
American run	ounce	100 yds	15.5
Cotton	pound	840 yds (hand)	29.5
Linen	"	300 yds (lea)	82.7
metric	kg	1000 metres	50
typp	pound	1000 yds	24.8
Worsted	pound	560 yds	44.3

> the Eastern hemisphere, the unit is the tex, which is the mass in grams of 1000 metres. All other units are technically obsolete, but it will be a very long time before they go completely out of use. Thus the denier is still widely used".

Again, in the above definition, the density of the material is not mentioned. For easy reference, units used at present are given in Table 20.

It will be of interest to try to evaluate from a quoted number of deniers, the diameter of the PAN precursor used in the manufacture of carbon fibres. In a recent review Bailey and Clarke,[6] (1970), give for PAN precursor a density of 1.15 kg/m^3 and a fibre diameter of 14μm, for a material of $1\frac{1}{2}$ denier per filament, with 10,000 filaments per tow.

Now from $W = \rho V$, we have

$$1.5 = 1.15 \times \frac{22}{7} \times 9000 \times 100 \times \frac{D^2}{4}$$

assuming 9000 metres of PAN weighs 1.5 gms. Hence

$$D^2 = \frac{1.5 \times 7 \times 4}{1.15 \times 22 \times 9000 \times 100}$$

and $D = 9.054 \times 10^{-4}$μm or roughly 9 microns, which does not tally with their quoted value of 14μm for fibre diameter!

From these remarks it is obvious that the use of the system of fibre classification, incorporating the denier, cannot be used, in a meaningful way, by those outside the textile industry, unless both the material and its density are specified correctly, as a matter of course.

REFERENCES - APPENDIX 2

1. The Shorter Oxford English Dictionary, 3rd ed., 1964.

2. Chambers Technical Dictionary, 3rd ed., 1967.

3. Encyclopaedia Brittanica, Vol. 20, 666b, 1964.

4. Thorpe's Dictionary of Applied Chemistry, 4th ed., 1956.

5. A Dictionary of Scientific Units, Jerrard, H.G. and McNeill, D.B., 2nd ed., 1964.

6. Bailey, J.E., and Clarke, A.J., Chemistry in Britain, Vol. 6, No. 11, pp 484, Nov. 1970.

APPENDIX 2

Calibration of Instron universal Testing machine

APPENDIX 2

Calibration of Instron Universal Testing Machine

Apart from the daily load cell test recommended by the makers, the Instron must be calibrated to allow for slackness in the cross-head screws, bowing of beams under stress, load cell error, jaw errors and other variables. Also because the machine reacts to a different degree with different materials, of variable geometry, it's characteristics must be determined before a long run of any new type of test piece. Needless to say, any correction factor obtained on calibration would only be specific to the machine under test.

As an example of this general machine slackness, the Young's modulus of a $\frac{1}{2}$" diameter mild steel bar, when tested on the Instron used for carbon fibre work, gave from the slope of the curve on the chart, a value of 9.785×10^6 psi, about a factor of 3 less than the value of 27×10^6 psi, quoted for this material.

To calibrate for the "softness factor" of the machine, by the method of Goggin[1], (1969), sets of six lengths of tungsten rod were cut for each gauge length tested, from 1-10 inches. Tungsten rod of 0.040" diameter, having a cross-sectional area of 0.001 sq. ins. approximately equal to the integrated cross-sectional area of a carbon fibre tow, was used because tungsten has a similar elongation to fracture as has carbon fibre, (4-8% compared with 1%). These rods were mounted and pulled at a cross-head speed of 0.005"/minute, with a chart speed of one inch a minute, to a full scale deflection, (F.S.D.), of 100 lbs. Now true extension of tungsten is

$$\frac{\text{Load} \times l}{A \times E} \qquad \ldots (73)$$

where l = gauge length

A = cross-sectional area

E = Young's modulus

Calibration of Instron Tensile Testing Machine. 1st Stage.

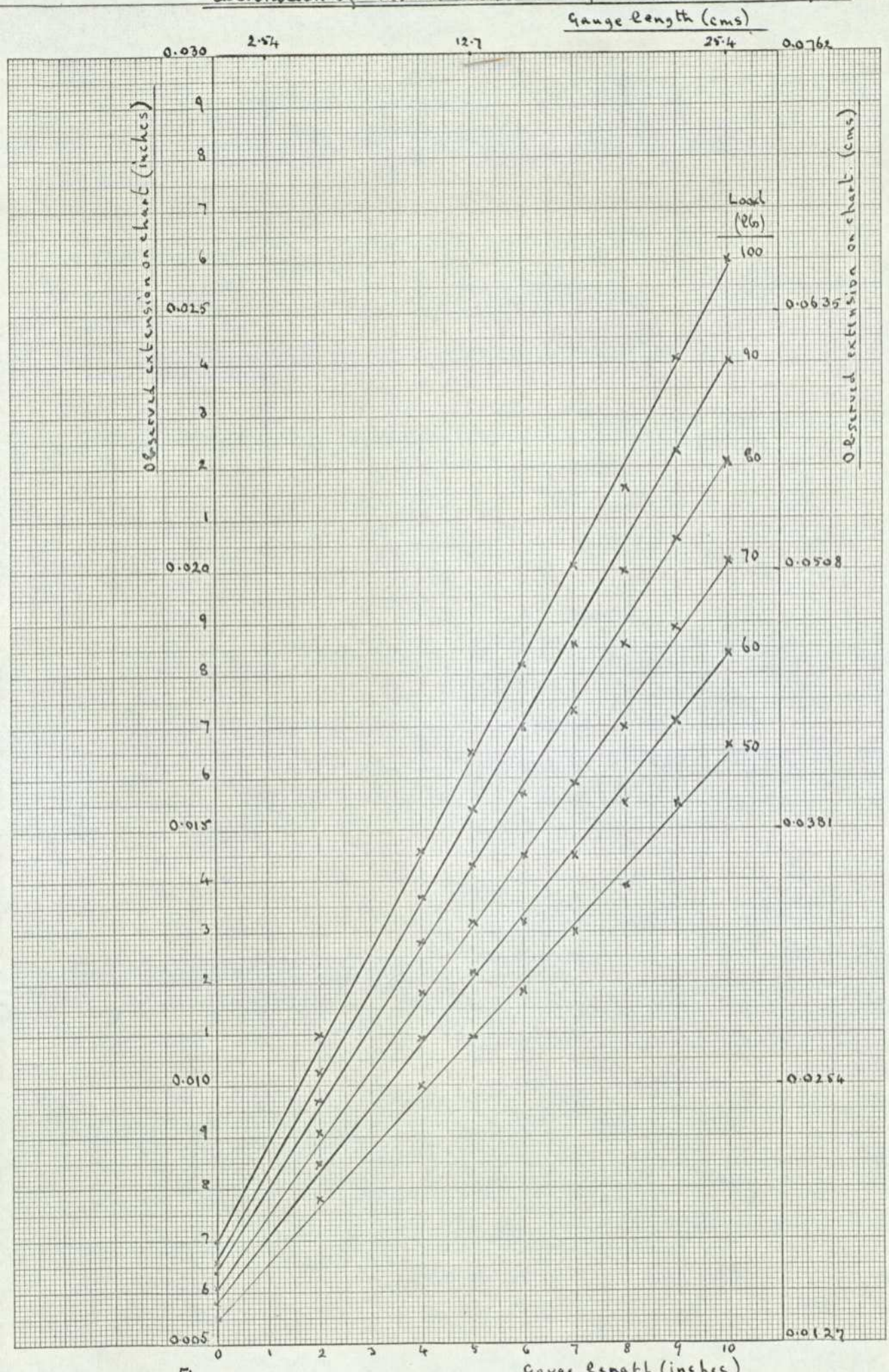


Fig. 103

Calibration of Instron Tensile Testing Machine 2nd Stage

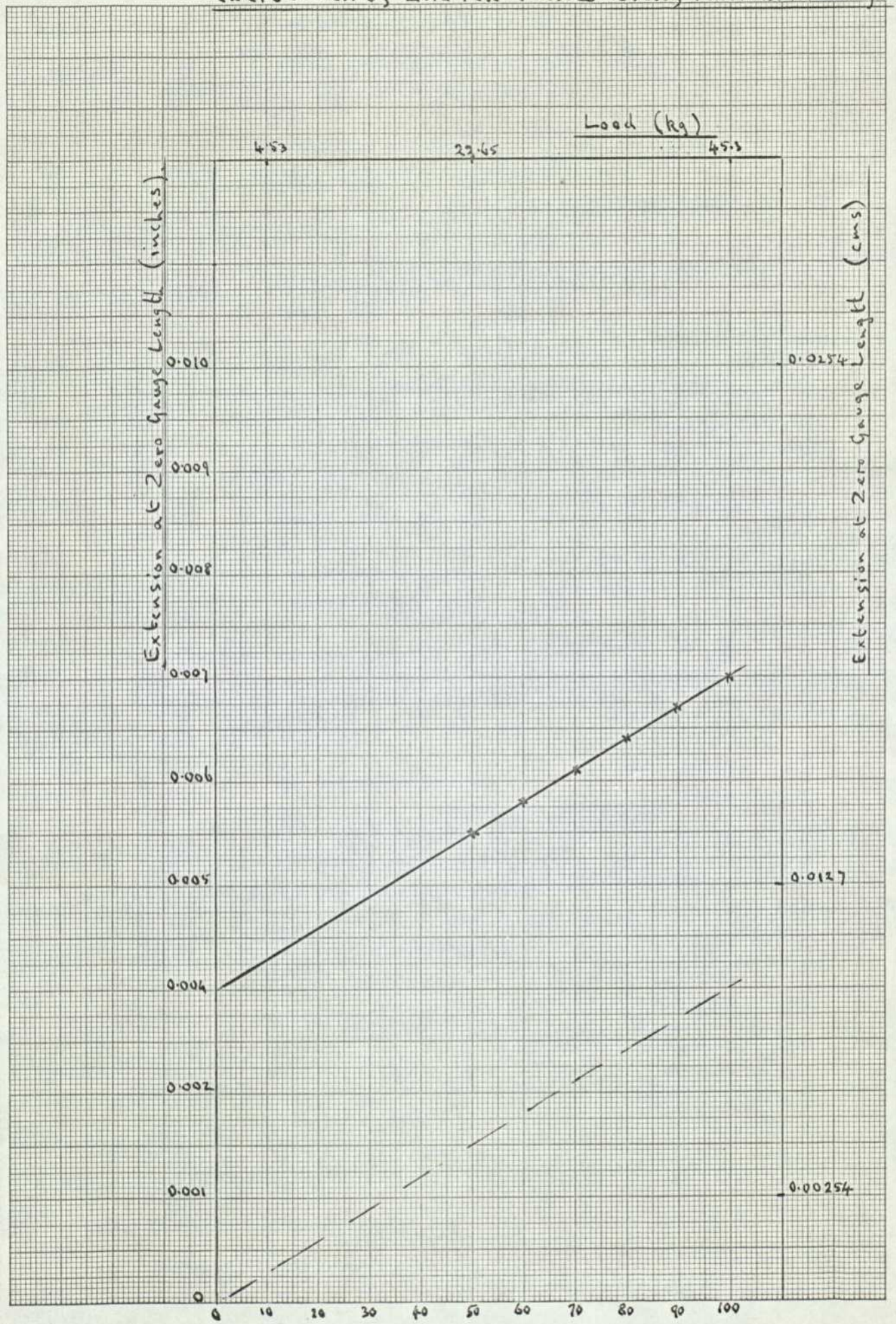


Fig. 104

The observed extension on the chart is

$$\frac{\text{Load} \times l}{A \times E} + \text{S.F.M.} \times \text{Load} \qquad \ldots (74)$$

where S.F.M. = "softness factor" of machine

= general slackness factor +

load cell error + etc.

Since Young's modulus for tungsten is the same whatever the gauge length, A is constant, l is known and Load, (F), is known, we have

Observed extension = const. x l + const. F

which is of the form $y = mx + c$.

Thus if we plot the observed extension, on the chart, against gauge length, as in Fig. 103, for each 10 lb. increase in load, we can, from the plot, measure the observed extension for each 10 lb. load, at zero gauge length. Then plotting observed extension, when l = 0, against load we have, as in Fig. 104, a line whose slope is "m" the S.F.M. or "softness factor" of the machine, since:

Observed extension on chart = S.F.M. x Load,

at zero gauge length ... (75)

The curve does not pass through the origin because of load cell error, etc.

From Fig. 104 we have, at zero gauge length, an observed extension of:

0.003" per 100 lb. load

$\therefore$ correction of extension for the machine

$$mF = \frac{0.003}{100} \times 100 = 0.003"$$

This, in inches of chart movement is

$$\frac{0.003}{0.005} \equiv 0.6" \text{ plus a load}$$

cell error etc., of 0.004" $\equiv$ 0.80" of chart movement, making a total deduction of 1.40" from chart length δl.

Table 21

Calibration of Instron

Nominal Gauge length (inches)	Gauge length corrected for jaw chamfer (inches)	Young's modulus, E, x 10^6 psi
2	2.24	50.8
3	3.24	43.3
4	4.24	47.4
5	5.24	46.7
6	6.24	46.8
7	7.24	46.2
8	8.24	47.2
9	9.24	46.4
10	10.24	44.6
		Mean Value:
		46.1

The calculated values of the Young's modulus for tungsten, using the total machine correction factor of 1.40", together with the 0.24" increased gauge length to accommodate the jaw chamfer correction, as mentioned in Section 4.2, are given in Table 21. The mean value, 46.1 x 10^6 psi is on the low side but an experimental check on the density of tungsten rod employed gave approximately 85% of theoretical and hence:

$$E = \frac{46.1}{100} \times 115 \times 10^6$$

$$= 53.0 \times 10^6 \text{ psi}$$

This agrees well with Northcott's[2] (1961), value for tungsten of E = 52 x 10^6 psi, and so the Instron can be calibrated in the manner described, to correct for "softness factor", to give an accurate value for the modulus of a material.

This correction factor will, however, be applicable to rigid systems, having a similar geometry.

In the case of plated carbon fibre tows, in addition to the machine "slackness factor" we have each tow with a different degree of slackness in the bundle, therefore a direct comparison of the observed slope of many runs with the value of E, calculated from the "law of mixtures", must be made to arrive at a mean S.F.M. Fig. 105 shows a typical run and here AB = δl = 2.6 inches is the observed chart movement for a load of 94 lbs. and BC is the combined carbon fibre tow slackness, S.F.M. and load cell error, etc.

It can be seen that if the curve of the test in Fig. 105, had been from a poor quality plated tow, as in Fig. 106;

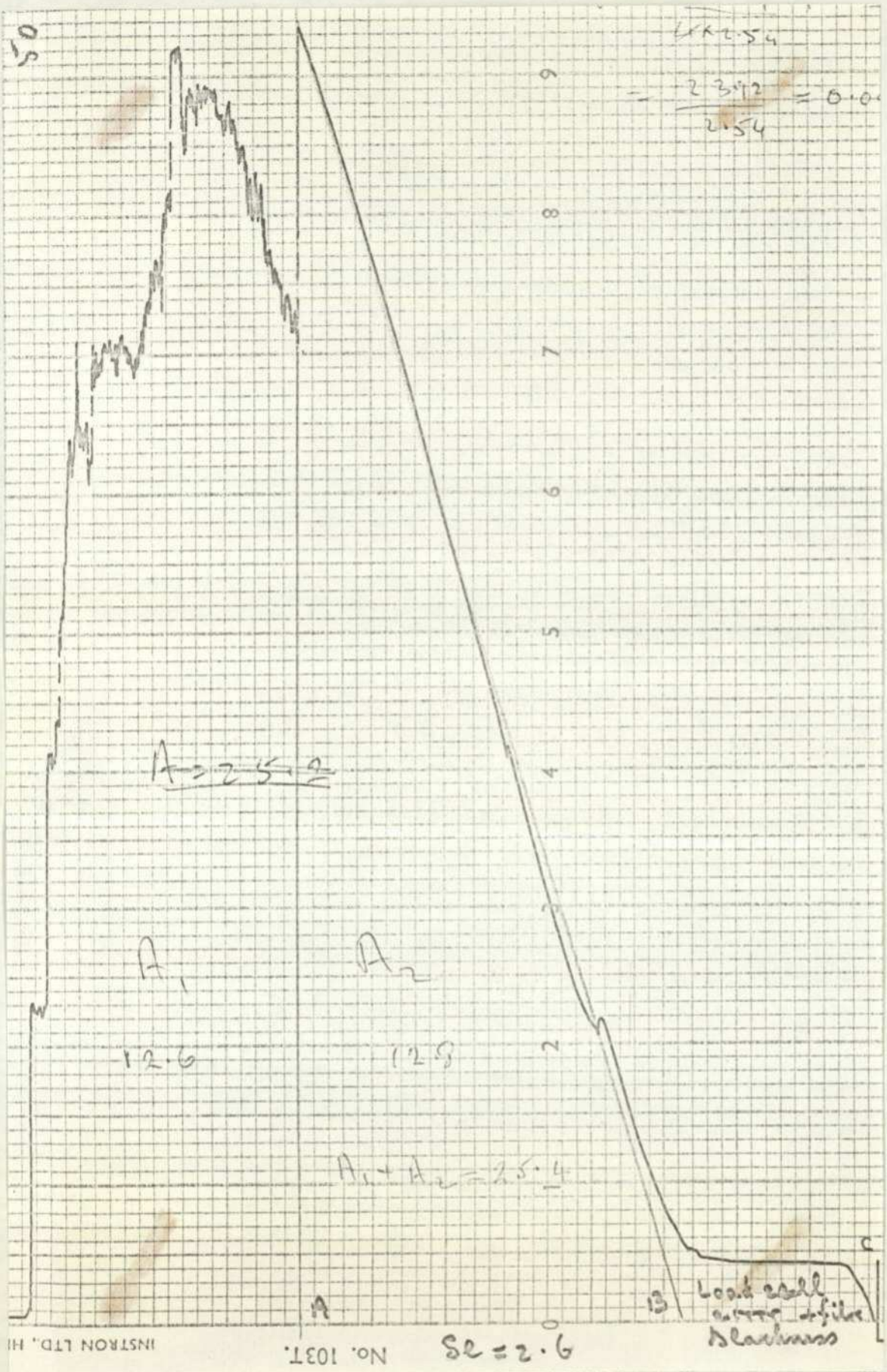


Fig. 105. Instron calibration for fibre tows.

Table 22

Instron and Copper Plated Carbon Fibre Tow

slackness calibration

Run	Temperature °C	Volume fraction	δl (inches)	E Observed	E, law of mixtures	$\frac{E(\text{Mixtures})}{E(\text{observed})}$
202	20	0.44	3.30	2.79	26.3	9.43
207	30	0.51	5.48	2.39	27.6	11.55
211	"	0.39	3.80	2.65	25.4	9.60
212	"	0.26	3.20	2.21	23.2	10.51
218	40	0.37	3.90	2.41	25.1	10.40
219	"	0.35	3.50	2.54	24.8	9.90
220	"	0.34	3.30	2.63	24.6	9.35
221	"	0.24	2.80	2.30	22.9	9.94
222	"	0.24	3.05	2.05	23.0	11.00
223	"	0.23	3.90	1.49	22.8	15.30
236	45	0.24	2.80	2.15	22.9	10.40
237	"	0.22	3.00	1.84	22.5	12.30
239	"	0.21	2.40	2.28	22.5	9.80
		Mean of $\frac{E(\text{mixtures})}{E(\text{observed})}$ = 10.60				

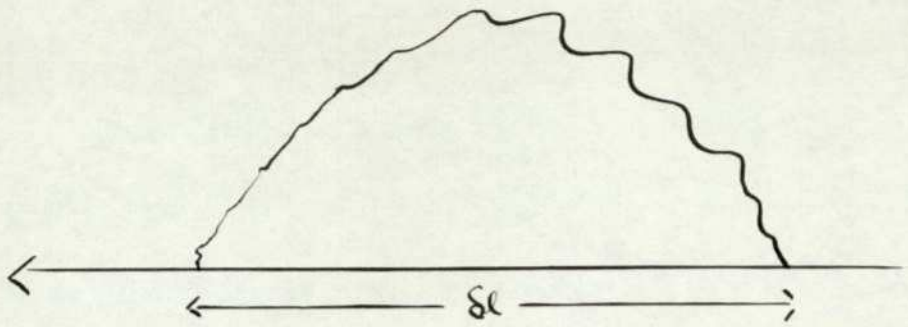


Fig. 106. Diagram of poor quality tow test result

no evaluation of the slope could be made and any direct correction of δl, as made in tungsten runs, would be meaningless. Table 22 gives the tensile results of a series of plated carbon fibre tows.

From the calculated mean value of the difference between the observed and "law of mixtures" values of E, the calculation of the tensile strength of the plated carbon fibre tow, by the method given in Chapter 4.

$$\sigma = \sqrt{\frac{2A_x E_{(Cu+f)} R_{(Cu+f)}}{Wl}} \qquad \ldots (35)$$

gives too high a value, since $E_{(Cu+f)}$ is the "law of mixtures" value which must be adjusted, by means of the slackness factor 10.6 to suit the other data in the equation.

Thus the observed tensile strength would be

$$\sigma_{obs} = \frac{\sigma}{\sqrt{10.6}} = \frac{\sigma}{3.256} \qquad \ldots (76)$$

REFERENCES - APPENDIX 2

1. Goggin, P.R., Private Communication, 1969.

2. Northcott, L., Papers on Fe, Nb, Ta, Mo and W. Conference at Sheffield, Ed. Quarrell, A.G., Elsevier, 1961.

APPENDIX 3

X-Ray Diffraction Techniques

APPENDIX 1

Catalogue of Powder Pattern Library

(Those items marked with an asterisk have been identified in industrial scales)

Name	Mineral	Formula	Structure
*Aluminium		Al	f.c.c.
*Aluminium oxide	Böehmite	α-$Al_2O(OH)_2$	Orthorhombic
*Calcium carbonate	Aragonite	$CaCO_3$	Orthorhombic
*Calcium carbonate	Calcite	$CaCO_3$	Hexagonal
*Hydrated basic Calcium chloride	-	$CaCl_2Ca(OH)_2.H_2O$	-
Calcium hypochlorite tetra hydrate	-	$Ca(ClO)_2.4H_2O$	-
*Calcium sulphate	Anhydrite	β-$CaSO_4$	Orthorhombic
*Calcium sulphate		γ-$CaSO_4$	Hexagonal or Triclinic
*Calcium sulphate hemi-hydrate	Bassanite Plaster of Paris	$CaSO_4.\frac{1}{2}H_2O$	Hexagonal
*Hydrated calcium sulphate	Gypsum	$CaSO_2.2H_2O$	Monoclinic
Copper	-	Cu	f.c.c.
Copper chloride	-	$CuCl_2$	Monoclinic
Basic copper chloride	-	$Cu_2(OH)_3Cl$	Monoclinic
*Basic copper chloride	Atacamite	$Cu_2(OH)_3Cl.$ $\frac{1}{2}(CuCl_2.3CuO.H_2O)$	-
Copper hydroxide	-	$Cu(OH)_2$	-
Copper I oxide	Cuprite	Cu_2O	Cubic
Copper II oxide	-	CuO	Monoclinic
Copper I, II, oxide	-	$(Cu''_{16-2x}Cu'_{2x})_{16}O_{16-x}$	Tetragonal
Iron	-	α-Fe	Cubic
Iron carbide	-	FeC	-
Iron carbide	-	Fe_3C	Orthorhombic
Iron bi-carbonate	-	$Fe(HCO_3)_2$	-
*Iron carbonate	Siderite	$FeO.CO_2$	Rhombohedral
Ferrous II fluoride (3 forms)	-	FeF_2	-
Iron III fluoride	-	FeF_3	Hexagonal

Name	Mineral	Formula	Structure
β Iron III fluoride tri-hydrate	-	β-FeF_3-$3H_2O$	-
Iron II ortho phosphate octa hydrate	-	$Fe_3(PO_4)_2.8H_2O$	-
Iron (ous) oxide	-	FeO at 90°K	Rhombohedral
Iron II oxide	Wüstite	FeO	Cubic
α-Iron oxide	Hematite	α-Fe_2O_3	Rhombohedral
γ-Iron oxide	Maghemite	γ-Fe_2O_3	-
Iron oxide	Magnetite	Fe_3O_4	Cubic
α-Basic iron oxide	-	α-FeO(OH)	Orthorhombic
δ-iron oxide	-	δ-Fe_2O_3	Hexagonal
α-iron oxide hydrate	Göethite	α-$Fe_2O_3.H_2O$	Orthorhombic
β-iron oxide hydrate	-	β-$Fe_2O_3.H_2O$	-
γ-iron oxide hydrate	Lepidocrocite	γ-$Fe_2O_3.H_2O$	Orthorhombic
Iron II sulphate mono-hydrate	-	$FeSO_4.H_2O$	-
Iron sulphate tetra hydrate	-	$FeSO_4.4H_2O$	Monoclinic
Iron sulphate hepta hydrate	-	$FeSO_4.7H_2O$	Monoclinic
Magnesium	-	Mg	c.p.h.
Magnesium carbonate	Nesquehonite	$MgCO_3.3H_2O$	Orthorhombic
Magnesium carbonate hydrate	-	$5MgO.4CO_2 5H_2O$	Monoclinic
Basic magnesium chloride	-	$Mg_2(OH)_3Cl.4H_2O$	Tri clinic
*Basic magnesium oxy chloride	-	$MgCl_2.9Mg(OH)_2.5H_2O$	Monoclinic
Magnesium oxide	Periclase	MgO	f.c.c.
*Magnesium hydroxide	Brucite	$Mg(OH)_2$	Hexagonal
Magnesium sulphate	Epsoms Salts	$MgSO_4.7H_2O$	-
Nickel	-	β-Ni	f.c.c.
Nickel oxide	Bunsenite	NiO	Cubic
Potassium bromide	-	KBr	Cubic
Potassium chloride	Sylvite	KCl	Cubic

Name	Mineral	Formula	Structure
*Sodium chloride	Halite	NaCl	Cubic
Sodium fluoride	Villiaumite	NaF	Cubic
Sodium hydrogen fluoride	-	$NaHF_2$	-
α-sodium sulphite	-	αNa_2SO_4	-
Sodium sulphate, form I	Meta thenardite	Na_2SO_4	-
Acid sodium sulphate (hydrated)	-	$NaHSO_4.H_2O$	-
Acid sodium sulphate	-	$NaHSO_4$	-
Acid sodium sulphate	-	$Na_3H(SO_4)_2$	-
Sodium sulphate	Thenardite	Na_2SO_4	-
Sodium sulphate deca hydrate	-	$Na_2SO_4.10H_2O$	-
Silica	Quartz sand α-Cristobalite	SiO_2	Tetragonal
Silica IV	α-quartz	SiO_2	-
Silica (Synthetic)	Coesite	SiO_2	Monoclinic
Silica	β-quartz	SiO_2	Hexagonal
Silica	β-cristobalite	SiO_2	Cubic
Silica	Tridymite	SiO_2	Orthorhombic
Silica	Tridymite (Low form)	SiO_2	"

Table I

Artificial Sea Water

(Lyman and Fleming, 1940)

Salt	Concentration (g/kg)
NaCl	23.476
$MgCl_2$	4.981
Na_2SO_4	3.917
$CaCl_2$	1.102
KCl	0.664
$NaHCO_3$	0.192
KBr	0.096
H_3BO_3	0.026
$SrCl_2$	0.024
NaF	0.003
Total	34.481 salinity

Water to 1000 cc.

This yields a solution of 19‰ chlorinity, proper allowance being made for water of crystallization in any of the salts. After aeration the solution has a pH of 7.9 - 8.3.

Ref. Harvey (1963)

Note:

Chlorinity is expressed as grams per 20° litre.

Chlorosity is obtained by multiplying the chlorinity of a water sample by its density at $20^{\circ}C$.

Normal water is sea water whose chlorinity has been adjusted to about 19.4‰ and accurately determined by direct or indirect comparisons with the original 1902 standard

Sverdrup's 'The Oceans' (1946).

Table II

Evaporation and Distillation Products of Sea Water

Slow Evaporation (Top to bottom of salt deposit)		Distillation (Order of appearance of scale)	
Compound	Mineral	Compound	Mineral
$KCl.MgCl_2$	Carnalite	$CaCO_3$ (67-77°C)	Calcite[1]
$MgSO_4$	Kieserite	$Mg(OH)_2$ (77-88°C)	Brucite[1]
$K_2SO_4.MgSO_4CaSO_4.2H_2O$	Polyhalite		
NaCl	Halite (Rock salt)	$CaSO_4.2H_2O$ (88-128°C)	Gypsum[2]
Ground Layers		$CaSO_4.\frac{1}{2}H_2O$ (128-163°C)	Bassanite[2] (Plaster of Paris)
$CaSO_4.2H_2O$	Gypsum		
$CaSO_4$	Anhydrite	$CaSO_4$ (163° onwards)	Anhydrite[2]
$MgCO_3.CaCo_3$	Dolomite	Brine	
$CaCO_3$	Calcite		

Rutley's (1962)

Stassfurt Salt Deposits.

(1) H. Hillier (1952)

(2) Mellor (1946)

Table III

Solubility of Scale Constituents in Water
(gm/100 cc)

Compound	Mineral	Cold Water 20°C	Hot Water 100°C
$CaCO_3$	Calcite	0.0014	0.0018
$Mg(OH)_2$	Brucite	0.0009	0.004
$CaSO_4 \cdot 2H_2O$	Gypsum	0.241	0.222
$CaSO_4 \cdot \frac{1}{2}H_2O$	Bassanite	0.3	-
$CaSO_4$	Anhydrite	0.209	0.162

Handbook of Chemistry, 39th Ed.

Chem. Rub. Pub. Co. (1958).

Table IV

Powder Pattern Data for Sea Water Halides

CuKα

KBr			KCl			NaCl			NaF		
Cubic			Sylvite Cubic			Halite Cubic			Villiaumite Cubic		
~~hkl~~ dÅ	I/I_1	Miller Indices	~~hkl~~ dÅ	I/I_1	Miller Indices	~~hkl~~ dÅ	I/I_1	Miller Indices	~~hkl~~ dÅ	I/I_1	Miller Indices
3.80	15	(111)	3.146	100	200	3.258	13	(111)	2.680	3	111
3.292	100	(200)	2.224	59	220	2.821	100	(200)	2.319	100	200
2.333	57	220	1.816	23	222	1.994	55	220	1.639	60	220
1.989	7	(311)	1.573	8	400	1.701	2	(311)	1.399	2	311
1.905	16	(222)	1.407	20	420	1.628	15	(222)	1.338	17	222
1.649	10	400	1.284	13	422	1.410	6	400	1.1588	7	400
1.514	2	(331)	1.1126	2	440	1.294	1	(331)	1.0633	<1	331
1.475	17	(420)	1.0490	6	600	1.261	11	(420)	1.0363	12	420
1.346	8	422	0.9951	2	620	1.1515	7	422	0.9458	8	422
1.269	2	511	0.9486	3	622	1.0855	1	511	0.8920	1	511
1.1666	3	440	0.9083	1	444	0.9969	2	440	0.8192	3	440
1.0987	5	600	0.8727	2	640	0.9533	1	(531)			
1.0436	4	620	0.8410	6	642	0.9401	3	(600)			
0.9947	4	622				0.8917	4	620			
0.9148	2	640				0.8601	1	(533)			
0.8814	3	642				0.8503	3	(622)			
						0.8141	2	444			

Table V

Powder Pattern Data for $CaCO_3$ and Na_2SO_4 Structures

CuKα

$CaCO_3$		$CaCO_3$		Na_2SO_4		$Na_2SO_4 10H_2O$	
Aragonite Orthorhombic		Calcite Hexagonal		Thenardite		MoKα	
~~hkl~~ d Å	I/I_1	~~hkl~~ d Å	I/I_1	~~hkl~~ d Å	I/I_1	~~hkl~~ d Å	I/I_1
4.212	2	3.86	12	4.66	73	6.3	3
3.396	100	3.035	100	3.84	18	5.5	100
3.273	52	2.845	3	3.178	51	4.8	42
2.871	4	2.495	14	3.075	47	4.33	13
2.730	9	2.285	18	2.783	100	3.82	27
2.700	46	2.095	18	2.646	48	3.60	7
2.481	33	1.927	5	2.329	21	3.40	7
2.409	14	1.913	17	2.211	5	3.22	50
2.372	38	1.875	17	1.919	4	3.10	50
2.341	31	1.626	4	1.891	4	2.93	7
2.328	6	1.604	8	1.864	31	2.80	27
2.188	11	1.587	2	1.841	6	2.70	10
2.106	23	1.525	2	1.798	4	2.56	7
1.977	65	1.518	4	1.680	12	2.52	27
1.882	32	1.510	3	1.662	8	2.44	10
1.877	25	1.473	2	1.605	5	2.37	7
1.814	23	1.440	5	1.589	3	2.29	7
1.759	4	1.422	3	1.553	10	2.19	7
1.742	25	1.356	1	1.537	< 1	2.10	20
1.728	15	1.339	2	1.512	2	2.03	7
1.698	3	1.297	2	1.497	5	1.97	7
1.557	4					1.92	17
1.535	2	Plus 18 lines		Plus 13 lines		1.83	3
1.499	4	to 0.9655		to 1.1345		1.79	10
1.475	3					1.74	7
1.466	5					1.71	7
1.411	5					1.66	10
1.404	3					1.53	3
1.365	3					1.46	3
1.358	3					1.37	7
1.328	2					1.31	7
1.261	6					1.26	3
1.240	7						
1.224	5						
Plus 4 lines to 1.1599							

Table VI

Powder Pattern Data for Magnesium Salts

CuKα

MgO		$Mg(OH)_2$		$Mg(OH)_3Cl.4H_2O$		$MgCl_2 9Mg(OH)_2.5H_2O$	
Periclase		Brucite					
Cubic		Hexagonal		Triclinic		Monoclinic	
~~hkl~~ d Å	I/I_1	~~hkl~~ d Å	I/I_1	~~hkl~~ d Å	I/I_1	~~hkl~~ d Å	I/I_1
2.431	10	4.77	90	8.14	100	11.06	23
2.106	100	2.725	6	7.11	20	7.93	100
1.489	52	2.365	100	5.97	30	7.27	54
1.270	4	1.794	56	4.28	3	5.87	20
1.216	12	1.573	36	4.07	35	4.11	29
1.0533	5	1.494	18	3.87	68	4.03	26
0.9665	2	1.373	16	3.56	26	3.68	6
0.9419	17	1.363	2	3.44	2	3.63	19
0.8600	15	1.310	11	3.27	4	3.48	3
0.8109	3	1.192	2	3.06	5	3.08	4
		1.183	9	3.05	5	3.07	4
		1.118	1	2.967	4	2.788	1
		1.092	3	2.900		2.758	4
		1.034	5	2.876	2	2.636	23
		1.030	1	2.833		2.629	3
		1.0067	7	2.750		2.531	4
		0.9543	1	2.715	26	2.484	12
		0.9503	5	2.627	5	2.436	10
		0.9455	8	2.613	10	2.404	89
		0.9085	3	2.533	3	2.344	4
		0.9001	<1	2.455	51	2.261	58
		0.8974	1	2.411	18	2.144	13
		0.8923	2	2.250	8	1.977	1
		0.8643	5	2.169	1	1.888	1
		0.8156	3	2.130	2	1.866	3
		0.7865	3	1.979	9	1.852	1
				1.955	2	1.840	1
				1.861	10	1.800	1
				1.845	1	1.724	3
				1.646	3	1.709	7
				1.637	3	1.696	9
				1.567	13	1.626	1
				1.490	8	1.590	17
				1.360	5	1.575	1
				Plus 4 lines		1.565	36
				to 1.209		1.537	11
						1.529	8
						1.523	15
						Plus 16 lines	
						to 1.189	

Table VII

Powder Pattern Data for Calcium Sulphate Structures

CuKα

β - $CaSo_4$		γ - $CaSo_4$		$CaSO_4\frac{1}{2}H_2O$		$CaSO_4.2H_2O$		
Anhydrite Orthorhombic		Hexagonal or Triclinic		Bassanite Hemihydrate Plaster of Paris Hexagonal		Gypsum Monoclinic		
~~hkl~~ d Å	I/I_1	d Å ~~hkl~~	I/I_1	d Å ~~hkl~~	I/I_1	d Å ~~hkl~~	I/I_1	
3.87	6	6.05	100	5.98	90	7.56	100	I/I_1 =
3.498	100	3.48	60	4.35	20	4.27	51	
3.118	3	3.01	90	3.45	80	3.79	21	intensity of
2.849	33	2.80	90	2.98	100	3.163	3	line with
2.797	4	2.70	10	2.78	100	3.059	57	reference to
2.473	8	2.33	20	2.69	30	2.867	27	intensity of
2.328	22	2.17	10	2.33	40	2.786	5	strongest
2.208	20	2.14	5	2.26	20	2.679	28	line
2.183	8	2.09	10	2.20	20	2.591	4	
2.086	9	2.00	10	2.12	80	2.530	< 1	
1.993	6	1.91	20	1.99	30	2.495	6	
1.938	4	1.85	60	1.89	60	2.450	4	
1.869	15	1.74	20	1.84	90	2.400	4	
1.852	4	1.69	40	1.72	40	2.216	6	
1.749	11	1.54	5	1.69	80	2.139	1	
1.748	10	1.51	5	1.65	60	2.080	10	
1.648	14	1.48	20	1.60	20	2.073	8	
1.594	3	1.44	10	1.53	30	1.990	4	
1.564	5	1.39	5	1.47	40	1.953	2	
1.525	4	1.35	5	1.44	30	1.898	16	
1.515	1	1.30	30	1.35	30	1.879	10	
1.490	5	1.26	20	1.29	70	1.864	4	
1.424	3	1.24	20	1.26	60	1.843	1	
1.418	1	1.21	20	1.24	60	1.812	10	
1.398	3	1.16	5	1.21	20	1.796	4	
1.396	2	1.14	30	1.17	20	1.778	10	
1.365	1	1.09	5	1.15	30	1.711	1	
1.319	4	1.05	5	1.13	20	1.684	1	
1.296	2	1.04	10	1.12	20	1.664	4	
1.277	5	1.02	5	1.11	20	1.645	2	
1.237	2	1.00	10	1.09	20	1.621	6	
1.216	4	0.992	10	1.08	30	1.599	< 1	
1.1993	2					1.584	2	
1.1781	< 1					1.532	1	
1.1663	4					1.522	1	
1.1651	1							
1.1483	1					Plus 16 other lines to 1.190		
1.1062	5							
1.1044	4							
1.0785	2							

Table VIII

Powder Pattern Data for Iron Oxides

CoKα

FeO		$\alpha-Fe_2O_3$		$\gamma-Fe_2O_3$		Fe_3O_4	
Wustite Cubic		Haematite Rhombohedral		Maghemite		Magnetite Cubic	
~~hkl~~ d Å	I/I_1	~~hkl~~ d Å	I/I_1	~~hkl~~ d Å	I/I_1	~~hkl~~ d Å	I/I_1
2.486	80	3.68	70	5.90	2	4.86	30
2.153	100	2.69	100	4.82	5	2.97	60
1.523	60	2.51	80	4.18	1	2.53	100
1.299	25	2.20	70	3.73	5	2.425	10
1.243	15	2.07	10	3.41	2	2.097	50
1.077	15	1.837	70	2.95	34	1.714	40
0.988	10	1.691	80	2.78	19	1.615	60
0.9631	15	1.634	10	2.64	-	1.484	70
		1.596	40	2.52	100	1.326	10
		1.484	70	2.41	1	1.279	30
		1.451	80	2.32	6	1.266	10
		1.348	20	2.23	0.5	1.209	20
		1.309	40	2.08	24	1.120	20
		1.255	30	1.87	0.5	1.091	50
		1.224	10	1.70	12	1.048	20
		1.205	10	1.61	33	0.988	10
		1.187	30	1.55	0.5	0.968	40
		1.160	30	1.53	1	0.938	30
		1.137	40	1.48	53		
		1.100	40	1.27	11		
				1.09	19		

Table IX

Powder Pattern Data for Hydrated Iron Oxides

CoKα

α-FeO(OH)		α-$Fe_2O_3.H_2O$		β-$Fe_2O_3.H_2O$		γ-$Fe_2O_3.H_2O$	
Goethite Orthorhombic		Goethite Orthorhombic				Lepidocrocite Orthorhombic	
~~hkl~~ d Å	I/I_1	~~hkl~~ d Å	I/I_1	~~hkl~~ d Å	I/I_1	~~hkl~~ d Å	I/I_1
4.97	60	5.0	20	7.45	80	6.26	100
4.18	100	4.21	100	5.26	80	3.29	90
3.36	60	3.37	20	3.32	100	2.79	10
2.69	70	2.69	80	2.64	40	2.47	80
2.58	55	2.57	20	2.54	100	2.36	20
2.48	40	2.51	10	2.43	20	2.09	20
2.44	80	2.48	20	2.36	10	1.937	70
2.30	10	2.44	70	2.28	80	1.848	20
2.25	60	2.25	20	2.10	20	1.732	40
2.18	60	2.18	40	2.06	10	1.566	20
2.14	10	2.09	5	1.94	40	1.535	20
2.09	15	2.00	10	1.85	10	1.524	40
2.01	20	1.92	10	1.75	40	1.496	10
1.92	40	1.83	20	1.71	10	1.449	10
1.80	50	1.774	5	1.63	100	1.433	20
1.77	30	1.719	50	1.55	10	1.418	10
1.72	70	1.689	20	1.51	50	1.389	10
1.69	50	1.660	10	1.48	40	1.367	30
1.66	40	1.602	20	1.44	60	1.261	10
1.63	10	1.563	30	1.38	60	1.213	10
1.60	50	1.507	20	1.31	40	1.196	20
1.56	65	1.468	10	1.14	60	1.189	20
1.51	60	1.456	5			1.10	20B
1.46	40	1.452	20			1.075	40
1.45	60	1.420	5				
1.42	50	1.392	10				
1.39	50	1.360	10				
1.37	40	1.347	5				
1.36	50	1.318	20				
1.35	20	1.293	5				
1.32	60	1.263	10				
1.29	40	1.239	10				
		1.197	10				
		Plus 14 lines to 0.996.					

Table X

Powder Pattern Data for Miscellaneous Compounds

CuKα CoKα

$Cu_2(OH)_3Cl.\frac{1}{2}(CuCl_2.3CuO.H_2O)$		SiO_2		$FeO.CO_2$		$FeSO_4.4H_2O$	
Atacamite		α – Cristobalite Tetragonal		Siderite Rhombohedral		Monoclinic	
hkl d Å°	I/I_o	hkl d Å°	I/I_o	hkl d Å°	I/I_1	hkl d Å°	I/I_1
5.4	100	4.04	100	3.59	60	6.9	38
5.0	100	3.138	12	2.79	100	5.5	100
2.82	100	2.845	14	2.56	10	4.49	100
2.75	100	2.489	18	2.35	50	3.99	75
2.62	20	2.468	6	2.13	60	3.60	3
2.52	40	2.342	< 1	1.963	60	3.40	50
2.26	100	2.121	4	1.795	50	3.24	50
2.19	40	2.024	3	1.734	80	2.97	75
2.13	60	1.932	4	1.527	20	2.75	20
2.03	20	1.874	4	1.505	60	2.58	38
1.95	40	1.756	1	1.426	50	2.43	38
1.82	80	1.736	1	1.395	40	2.36	38
1.78	40	1.692	3	1.381	20	2.27	38
1.74	60	1.642	1	1.373	20	2.18	3
1.71	40	1.612	5	1.354	60	2.11	8
1.67	40	1.604	2	1.281	40	2.04	3
1.60	80	1.574	1	1.258	20	1.97	38
1.56	80	1.535	2	1.229	40	1.89	20
1.50	20	1.495	3	1.198	50	1.80	18
1.47	20	1.432	2	1.172	20	1.76	8
1.44	20	1.423	1	1.147	10	1.72	10
1.41	60	1.401	1	1.124	40	1.67	10
1.39	20	1.368	1	1.114	10	1.63	8
1.37	20	1.353	1	1.086	40	1.59	3
1.35	20	1.345	1	1.081	60	1.57	3
1.32	20	1.336	1	1.066	50	1.55	3
1.29	20	1.301	2	1.034	10	1.51	10
1.25	40	1.282	2	1.006	20	1.49	3
1.19	20	1.235	< 1	0.9815	50	1.45	13
1.13	20	1.224	< 1	0.9717	60	1.40	10
1.10	20	1.207	1	0.9666	20	1.37	10
1.06	20	1.1842	2	0.9392	20	1.29	15
1.05	20	1.1762	1	0.9352	40	1.23	3
1.02	20	1.1659	1	0.9305	70	1.20	5
0.96	20	1.1556	< 1	0.9248	50	1.14	3
		1.1112	1	0.9086	10		
		1.0989	3	0.9054	60		

Table XI

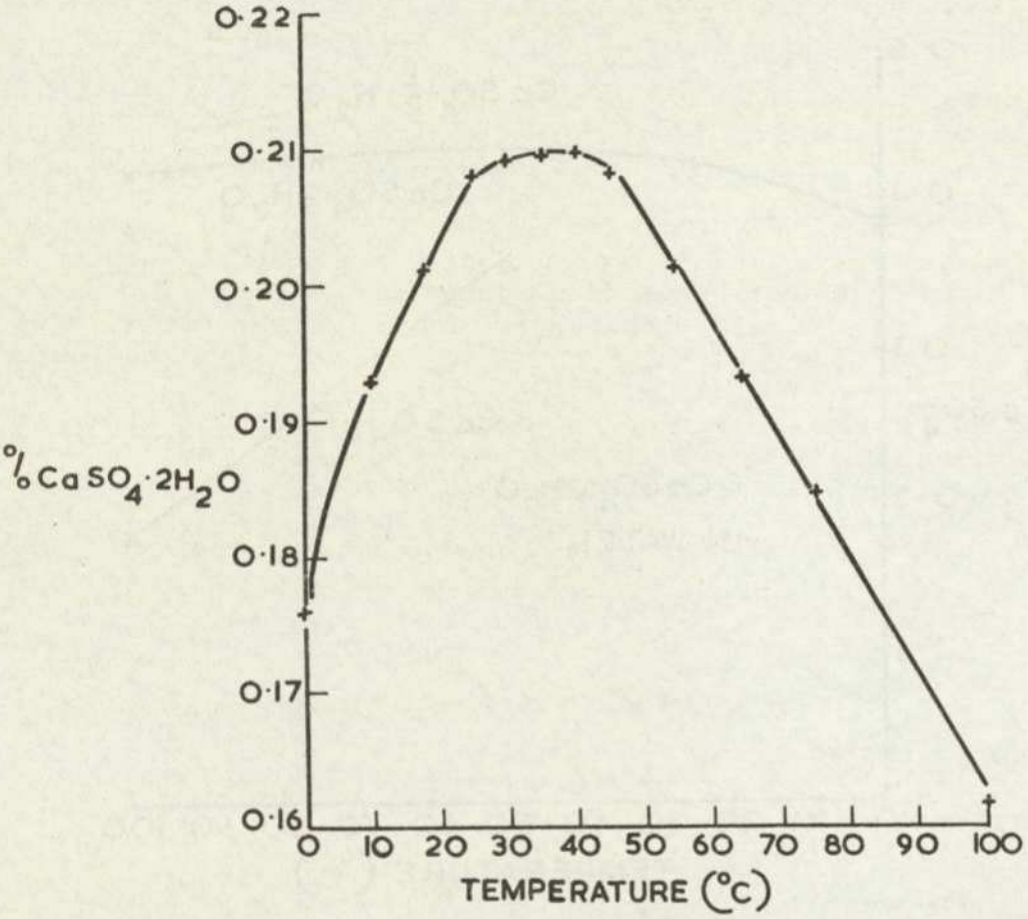
Galvanic Series of Metals in Sea Water

Metals Handbook (1961)

Anodic End

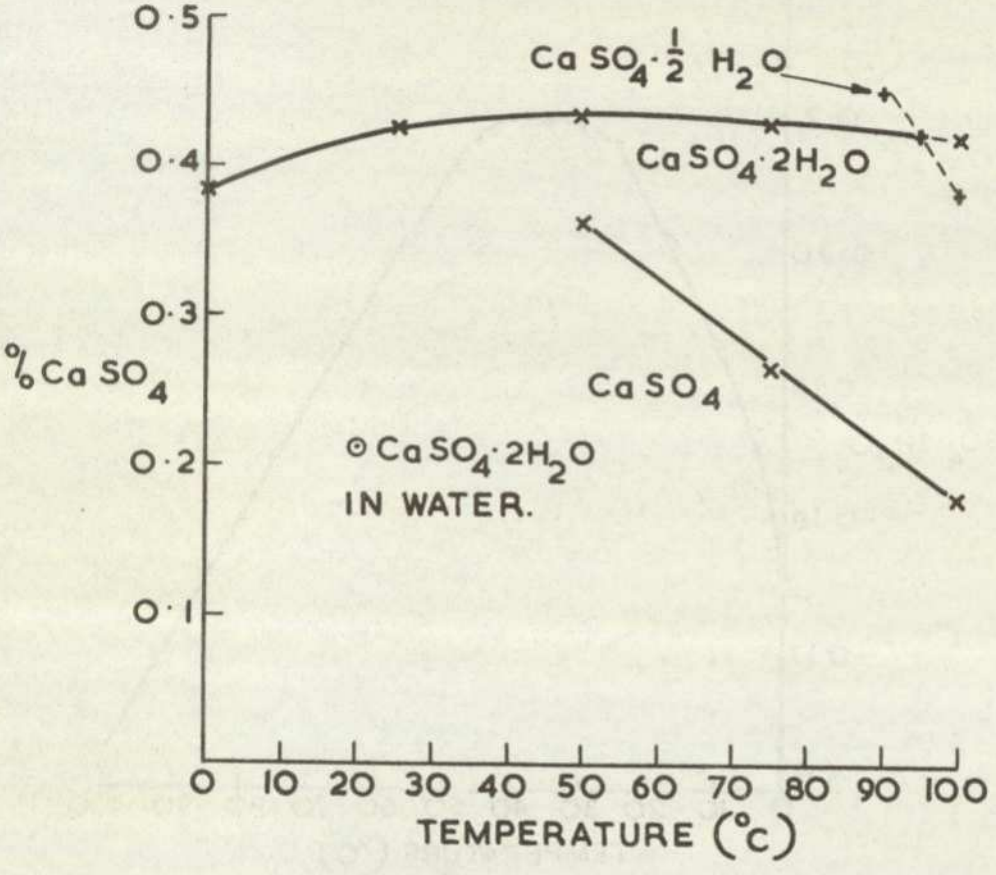
Order		Order	
1.	Magnesium (most active)	19.	Manganese bronze
2.	Magnesium alloys	20.	Naval brass
3.	Zinc	21.	Nickel (active)
4.	Galvanised steel	22.	Inconel (active)
5.	Aluminium (5052 H)	23.	Cartridge brass
6.	Alclad	24.	Admiralty brass
7.	Cadmium	25.	Aluminium bronze
8.	Mild steel	26.	Red brass
9.	Wrought iron	27.	Copper
10.	Cast iron	28.	Silicon bronze
11.	Nickel	29.	30% Cupro-nickel
12.	13% Chromium stainless steel	30.	Nickel (passive)
13.	50-50 lead/tin solder	31.	Inconel (passive)
14.	18-8 stainless steel	32.	Monel
15.	18-8-3 stainless steel	33.	18-8 stainless steel (passive)
16.	Lead	34.	Silver
17.	Tin	35.	Gold
18.	Muntz Metal	36.	Platinum

Cathodic End

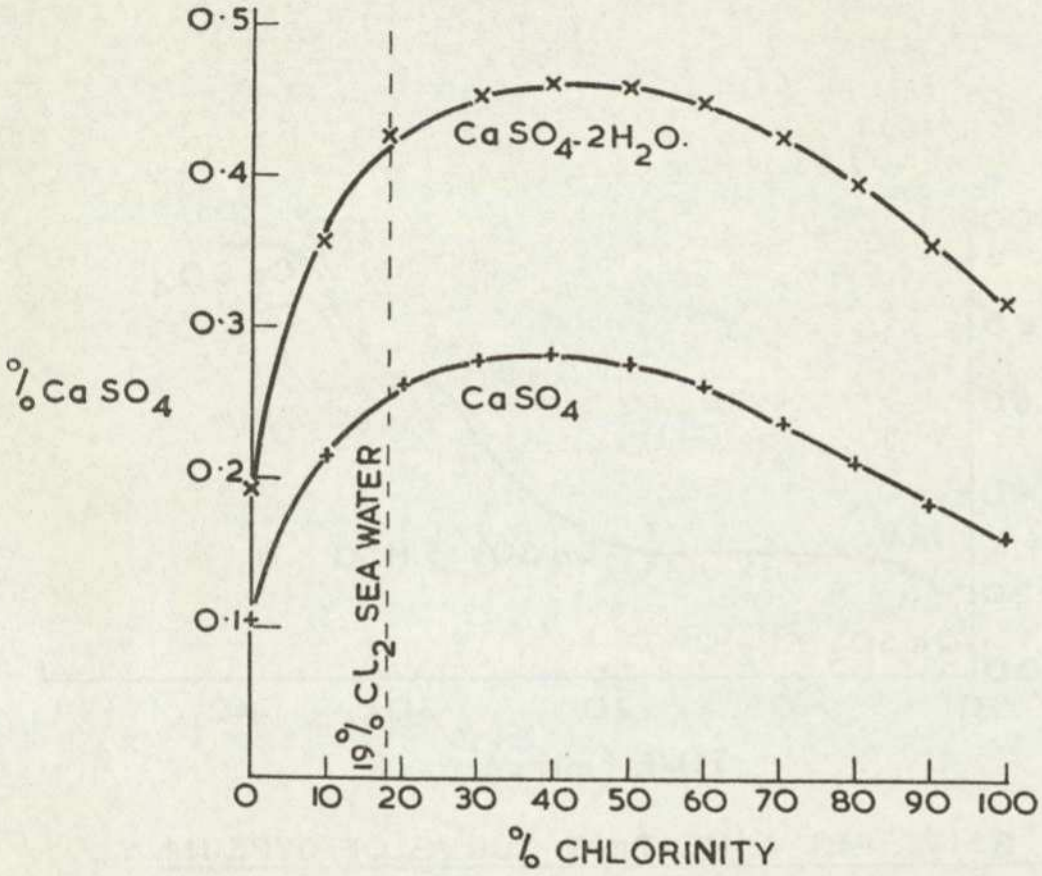


AERE R5171. FIG. 1. SOLUBILITY OF GYPSUM IN FRESH WATER

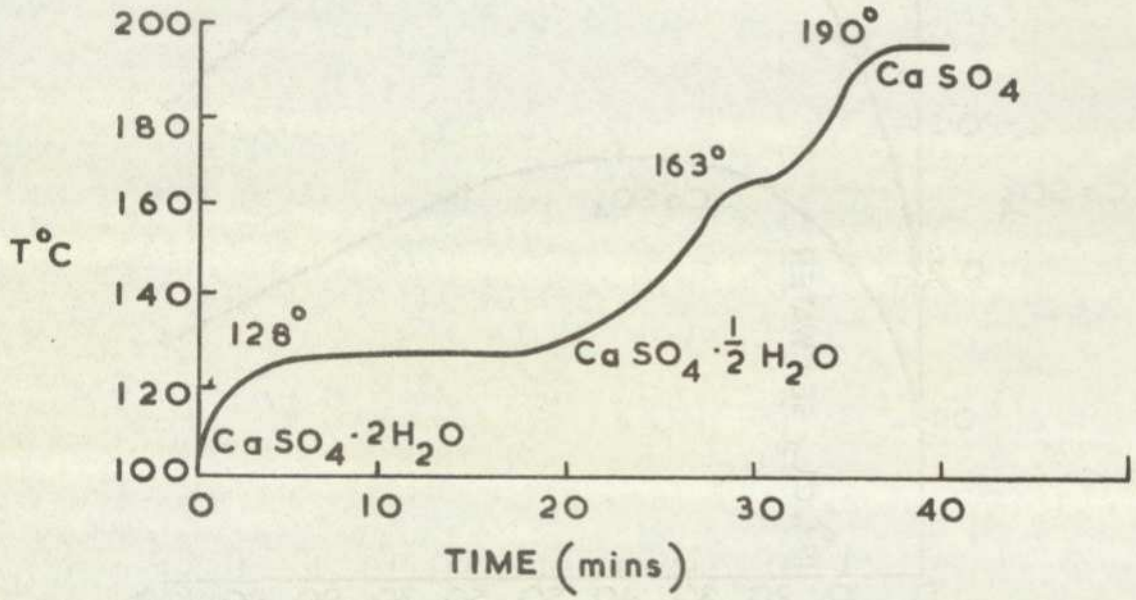
(AFTER HULETT AND ALLEN.)



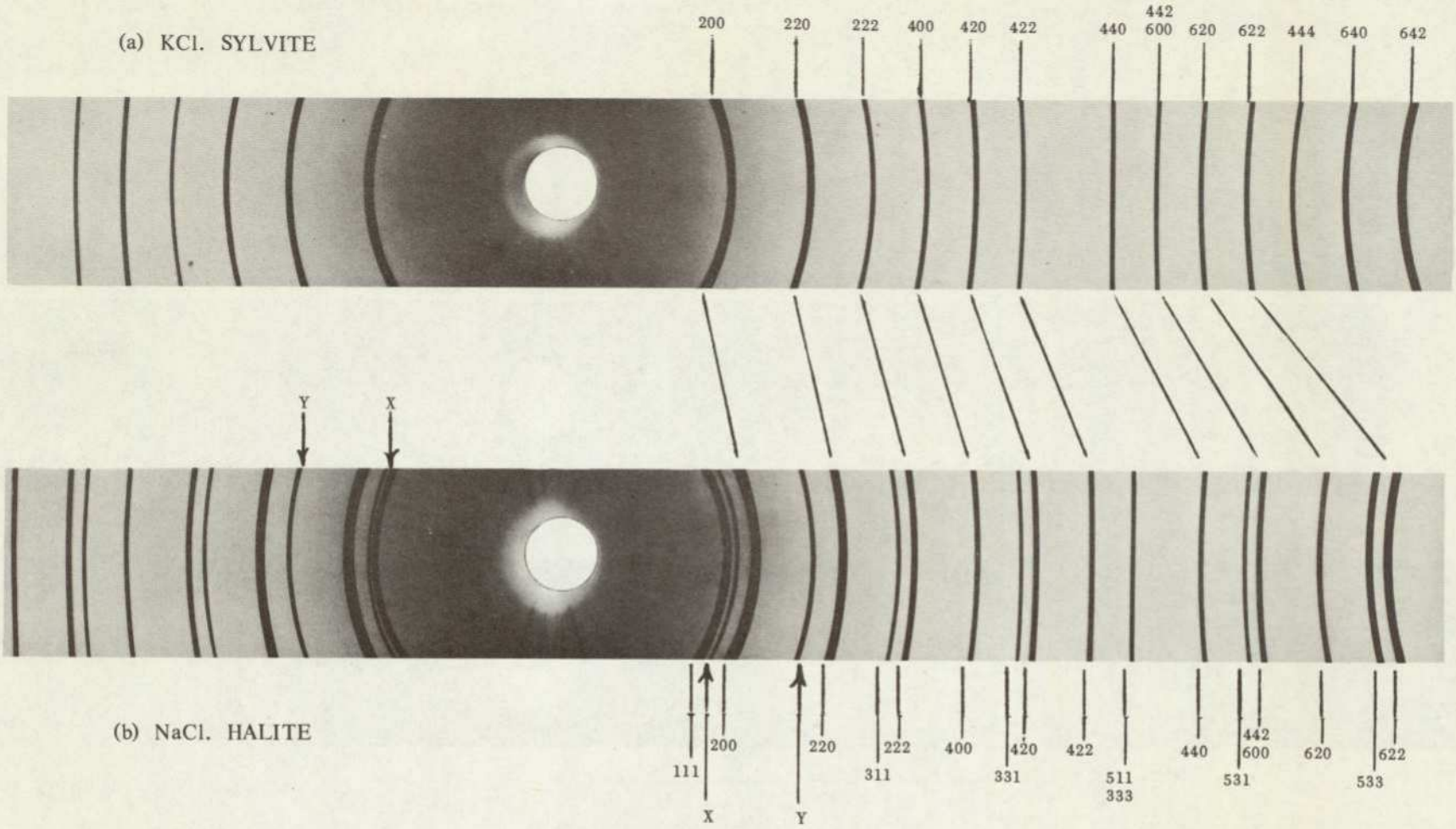
AERE R5171. FIG. 2 SOLUBILITY OF FORMS OF $CaSO_4$ IN SEA WATER (20% CHLORINITY) (AFTER T. TORIUMI et al., Y. TANAKA et al.)



AERE R5171. FIG. 3. SOLUBILITY OF $CaSO_4$ VERSUS BRINE CONCENTRATION AT 75°C (AFTER Y. TANAKA et al.)

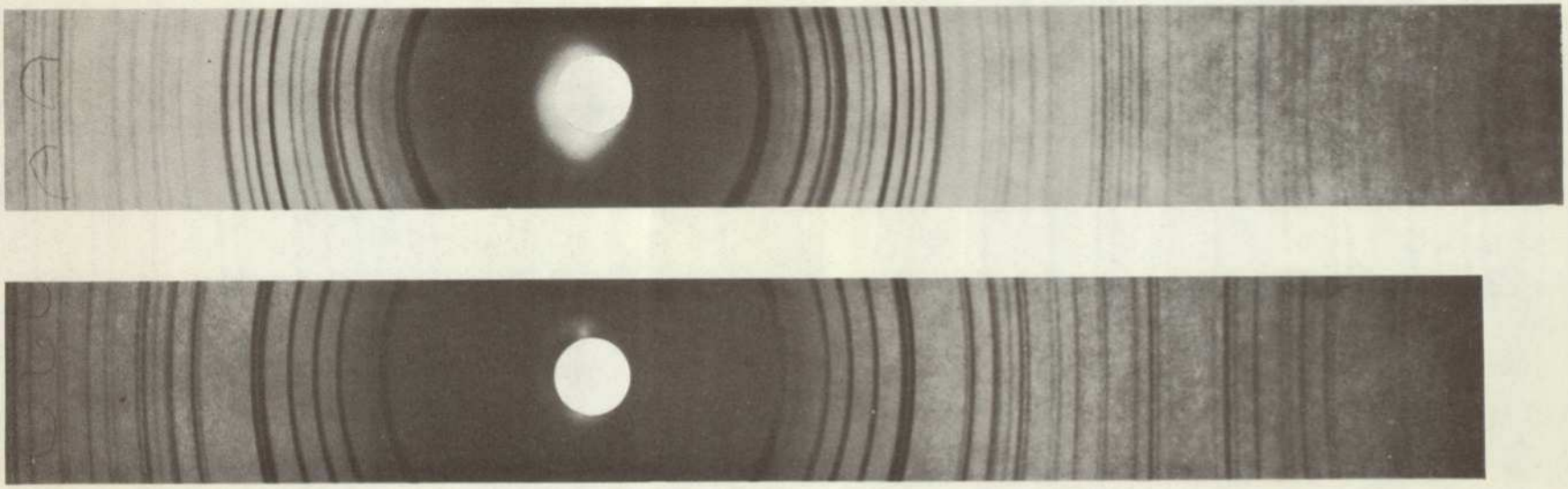


AERE R5171. FIG. 4. HEATING CURVE OF GYPSUM. IN AIR (LE CHATELIER)



AERE - R 5171 Fig. 5
Comparison of KCl and NaCl Powder Patterns (After Bunn, 1961)

(a) Kettle fur

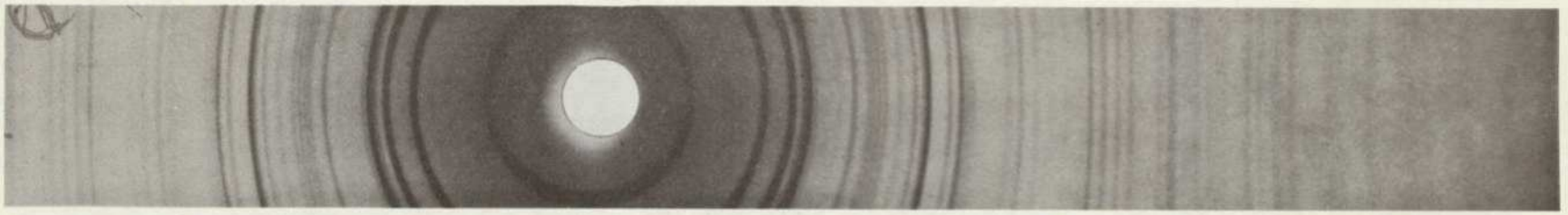


(b) Calcite, $CaCO_3$

AERE - R 5171 Fig. 6
Powder Pattern of Domestic Kettle Fur Compared with Calcite

(a) β-$CaSO_4$. Anhydrite

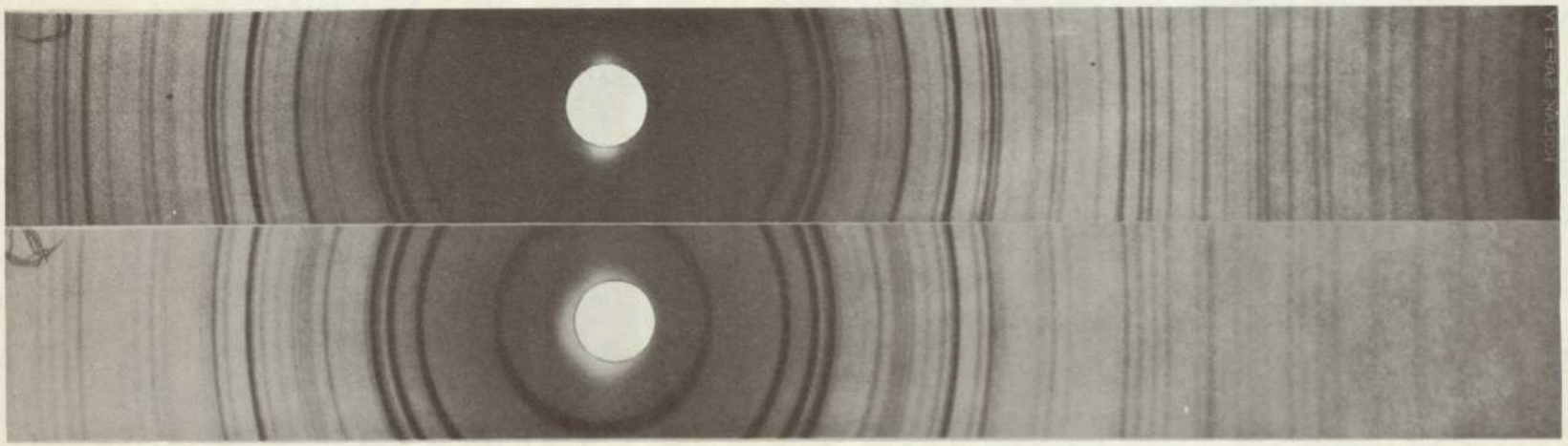




(b) γ-$CaSO_4$

AERE - R 5171 Fig. 7
Comparison of β-$CaSO_4$ and γ-$CaSO_4$ Powder Patterns

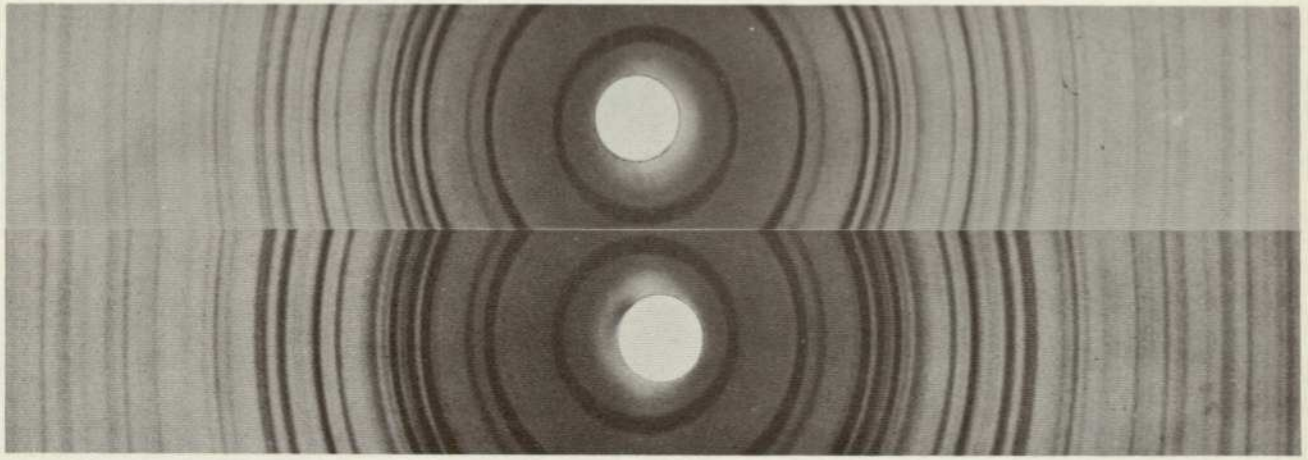
(a) $CaSO_4 . \frac{1}{2} H_2O$



(b) $CaSO_4$. γ form

AERE - R 5171 Fig. 8
Comparison of hemi-hydrate with γ-$CaSO_4$ Powder Pattern

(a) Heavy Scale



(b) Gypsum, $CaSO_4 . 2 H_2O$

AERE - R 5171 Fig. 9
Comparison of Heavy Scale with Standard Gypsum Powder Pattern

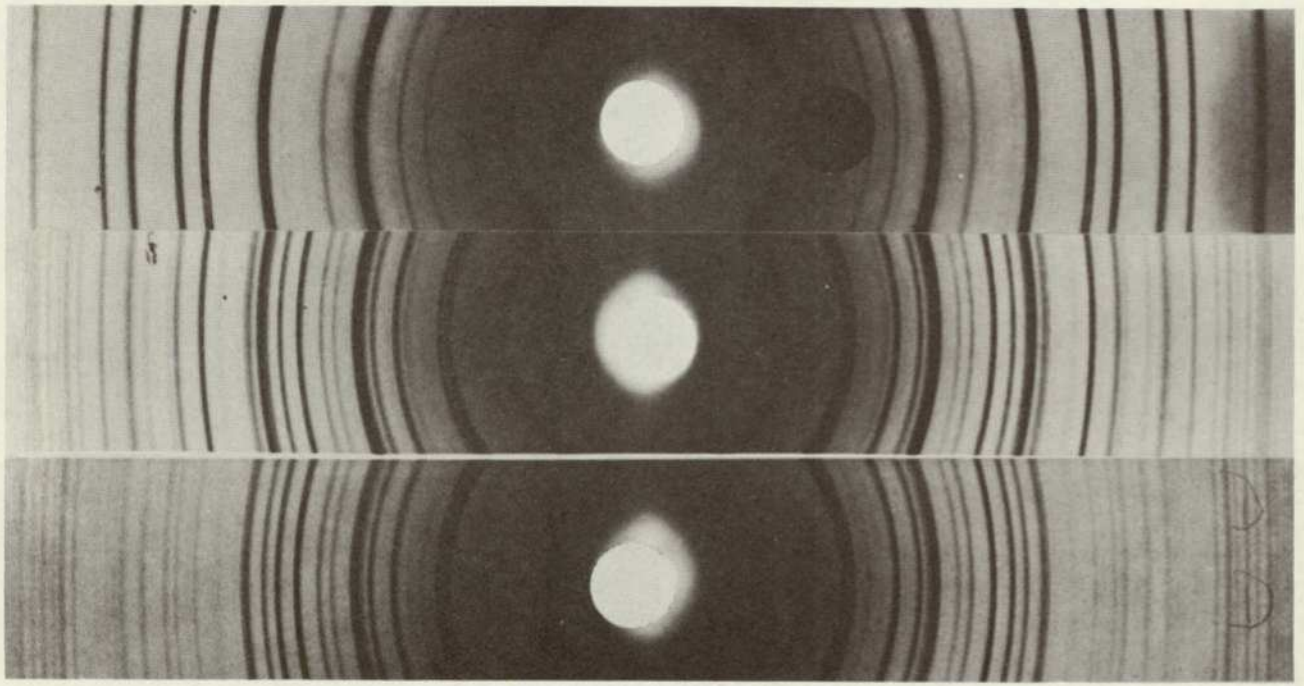
(a) β-$CaSO_4$. Cu$K\alpha$



(b) β-$CaSO_4$. Co$K\alpha$

AERE - R 5171 Fig. 10
Powder Patterns of β-$CaSO_4$ with Cu$K\alpha$ and Co$K\alpha$ Radiation

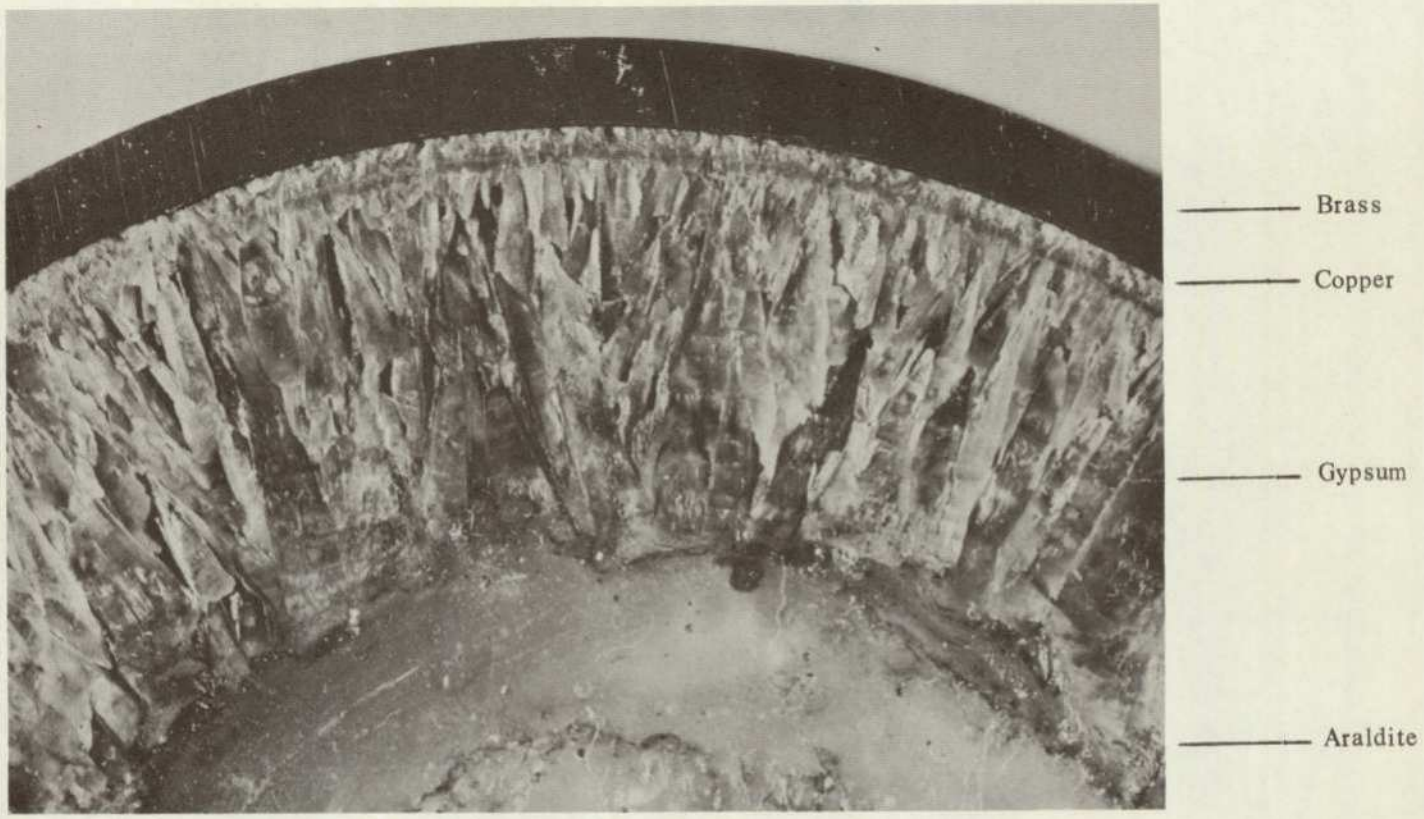
(a) Brucite, $Mg(OH)_2$



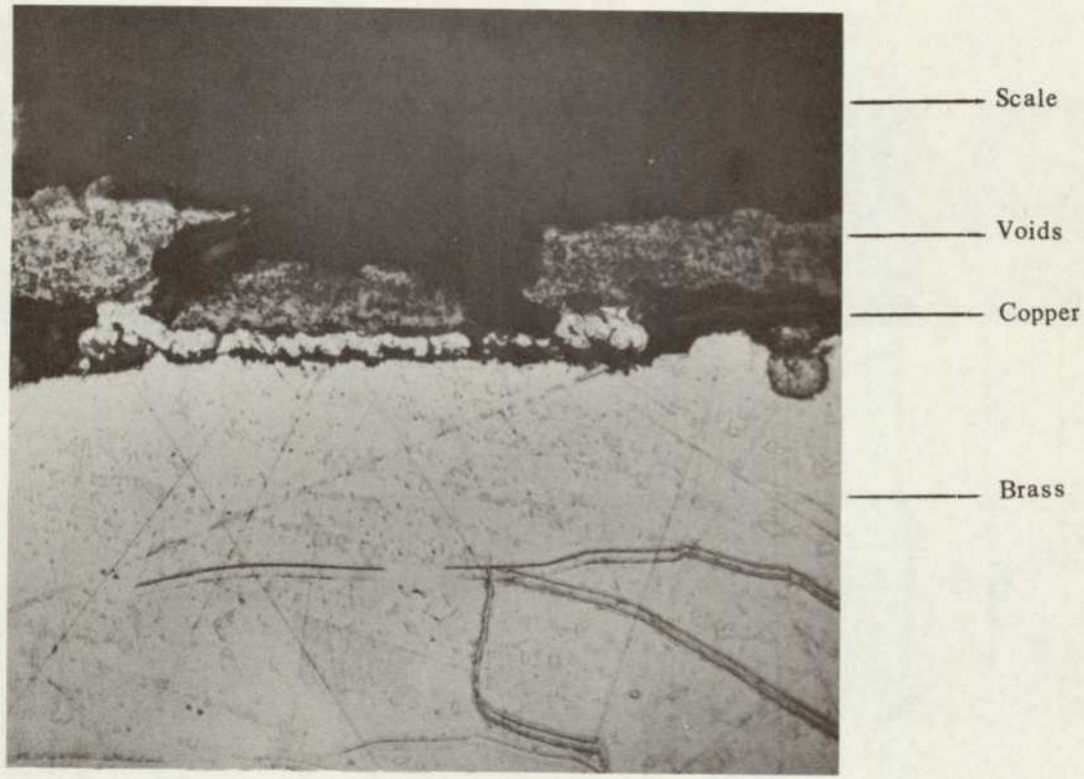
(b) Ocean vessel scale

(c) Kettle fur, Aragonite, $CaCO_3$ + Impurity

AERE - R 5171 Fig. 11
Brucite, Ocean Vessel Scale and Kettle Fur Patterns Compared

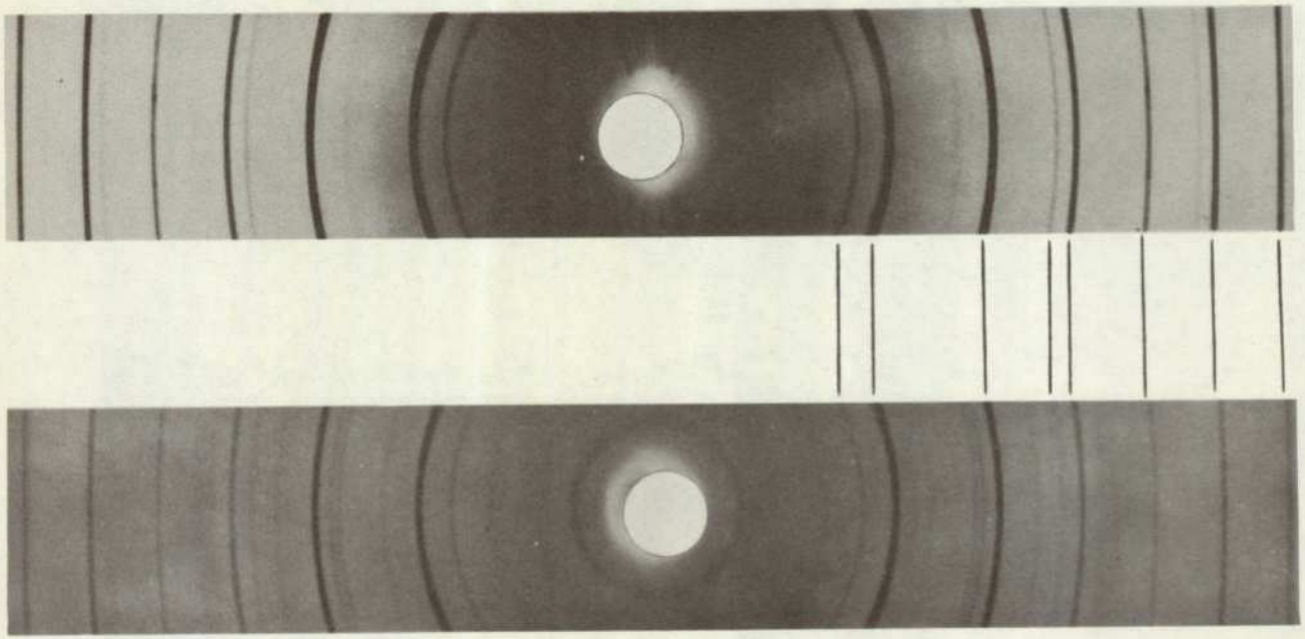


AERE - R 5171 Fig. 12 x 6
Macrocrystalline Structure of Heavy Gypsum Scale



AERE - R 5171 Fig. 13 x 500
Corrosion of Brass Tube Showing Free Copper at Tube/Scale Interface

(a) NaCl

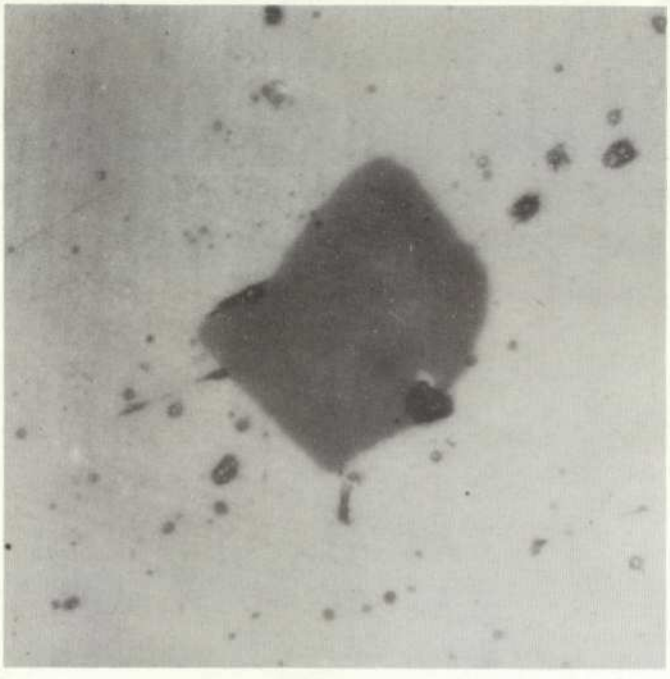


(b) Industrial scale

AERE - R 5171 Fig. 14
Identification of NaCl in Industrial Scale

APPENDIX 4

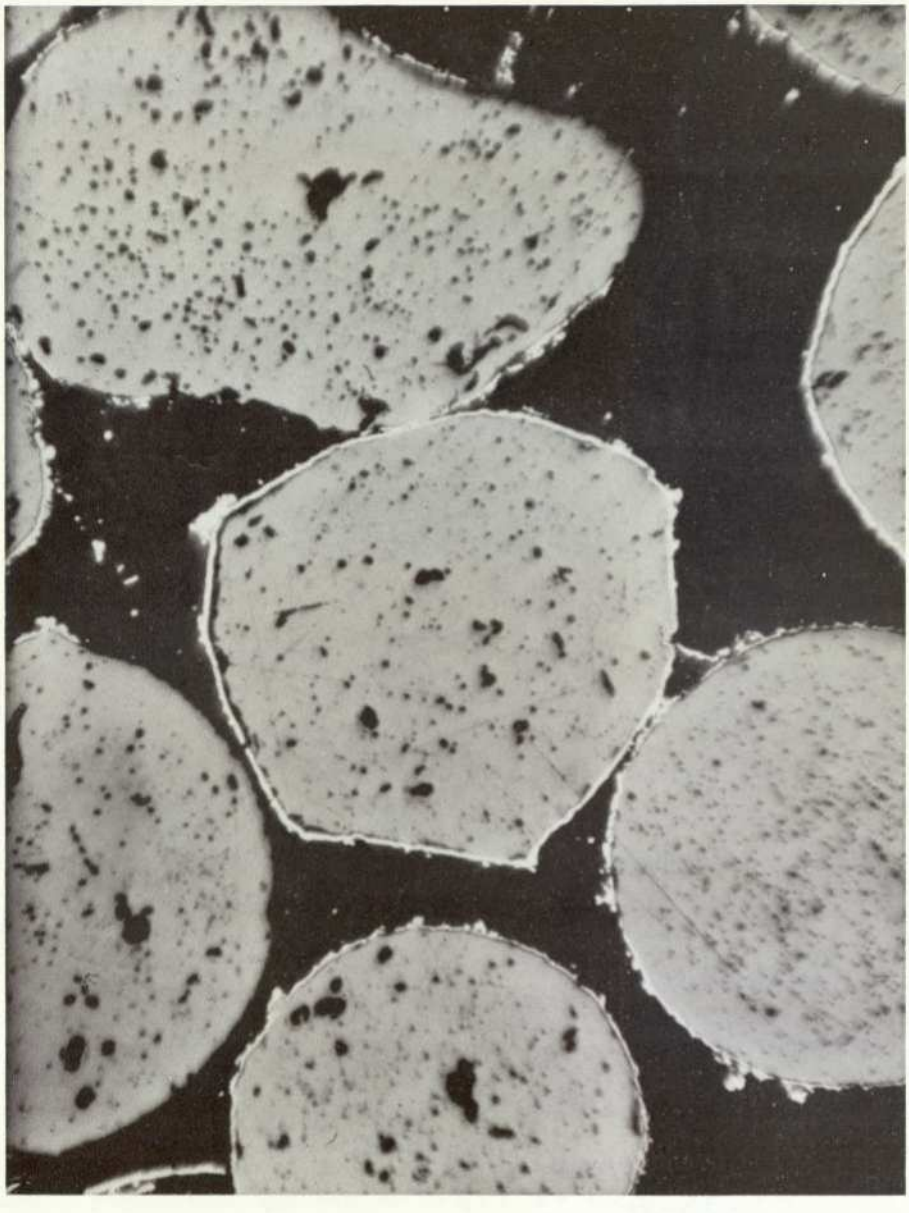
A Powder Pattern Scanner



AERE - M 1508 Fig. 1 x 1000
Cuboid inclusion in UO_2.

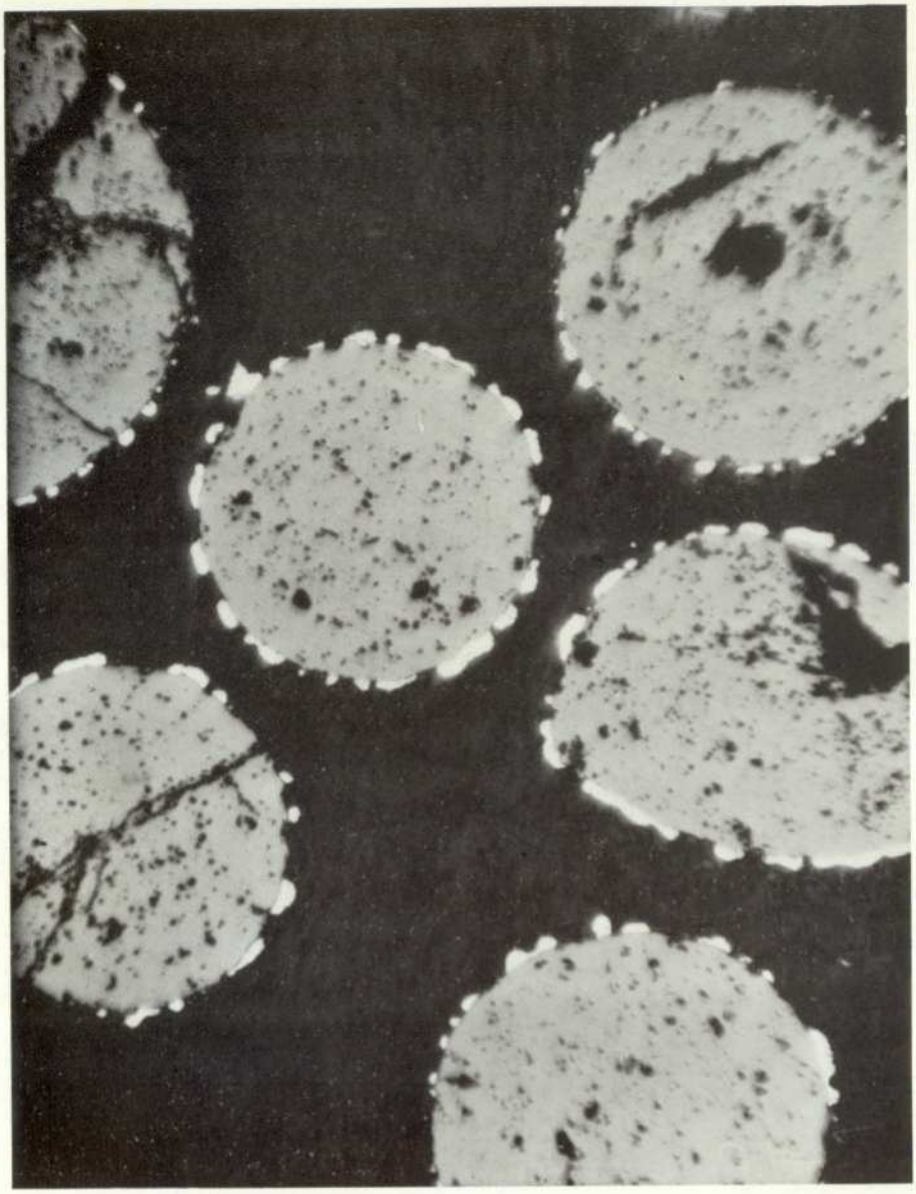


AERE - M 1508 Fig. 2 x 500
Powdery Cu deposit, from Rochelle salt solution, on UO_2 sphere.

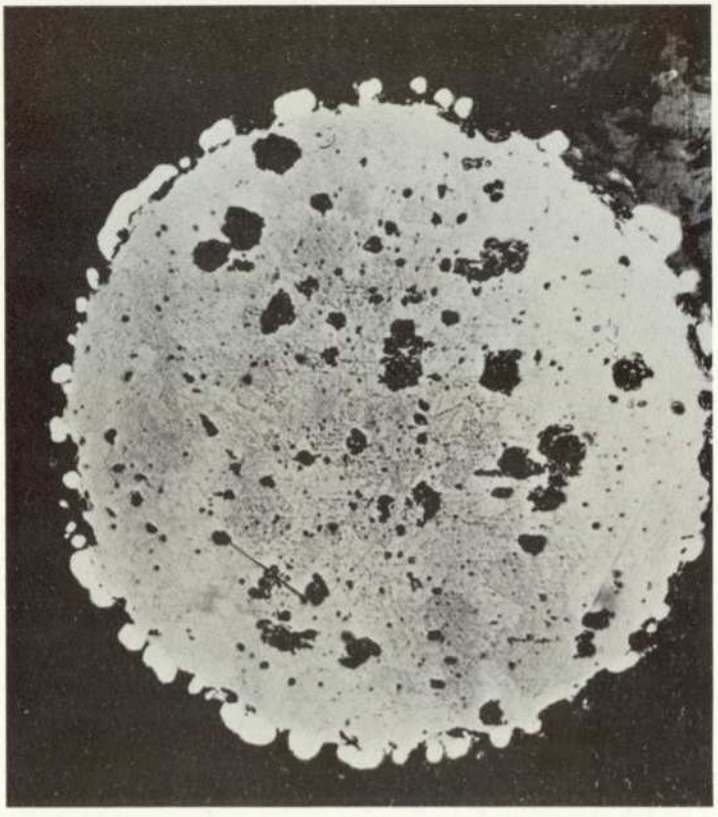


AERE - M 1508 Fig. 3 x 500

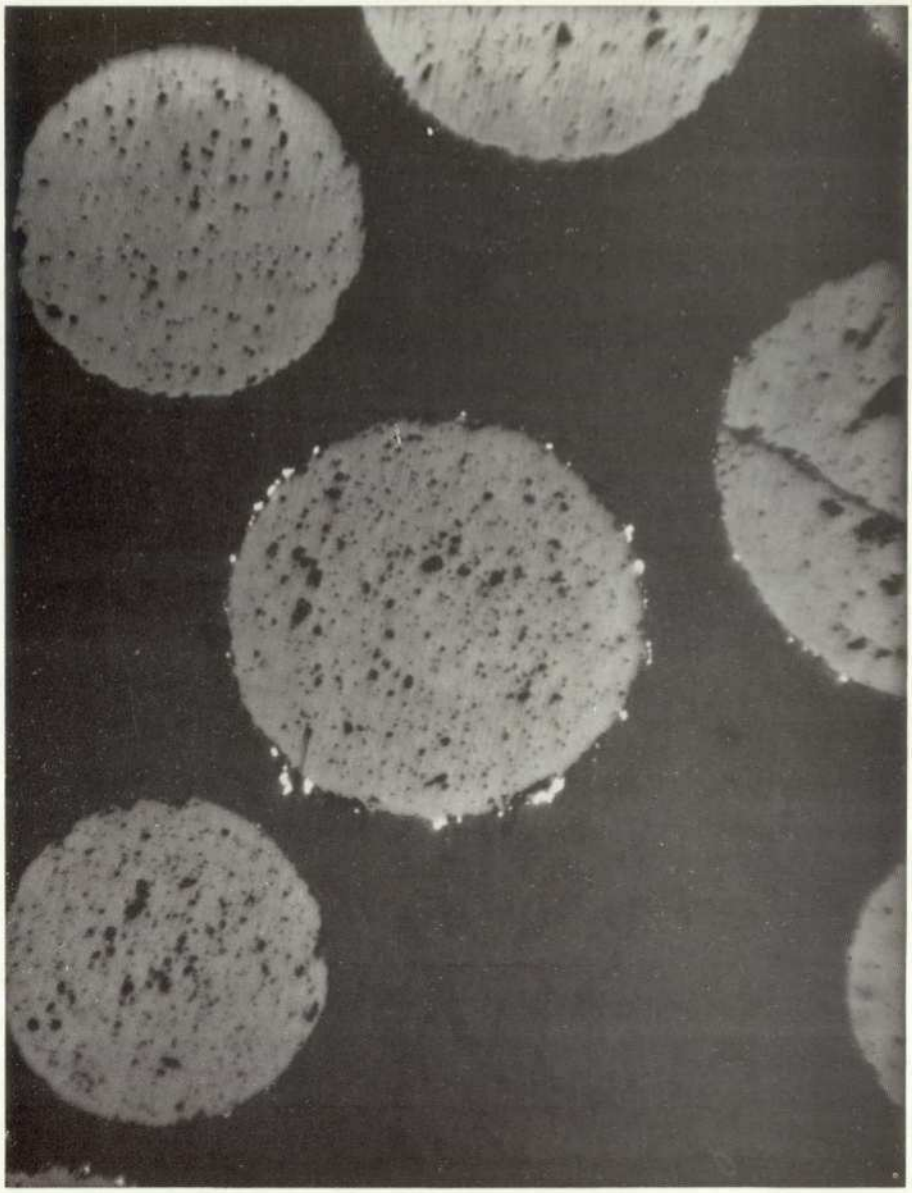
Electroless 8% phosphorus/nickel, deposit from acid solution, on UO_2 spheres.



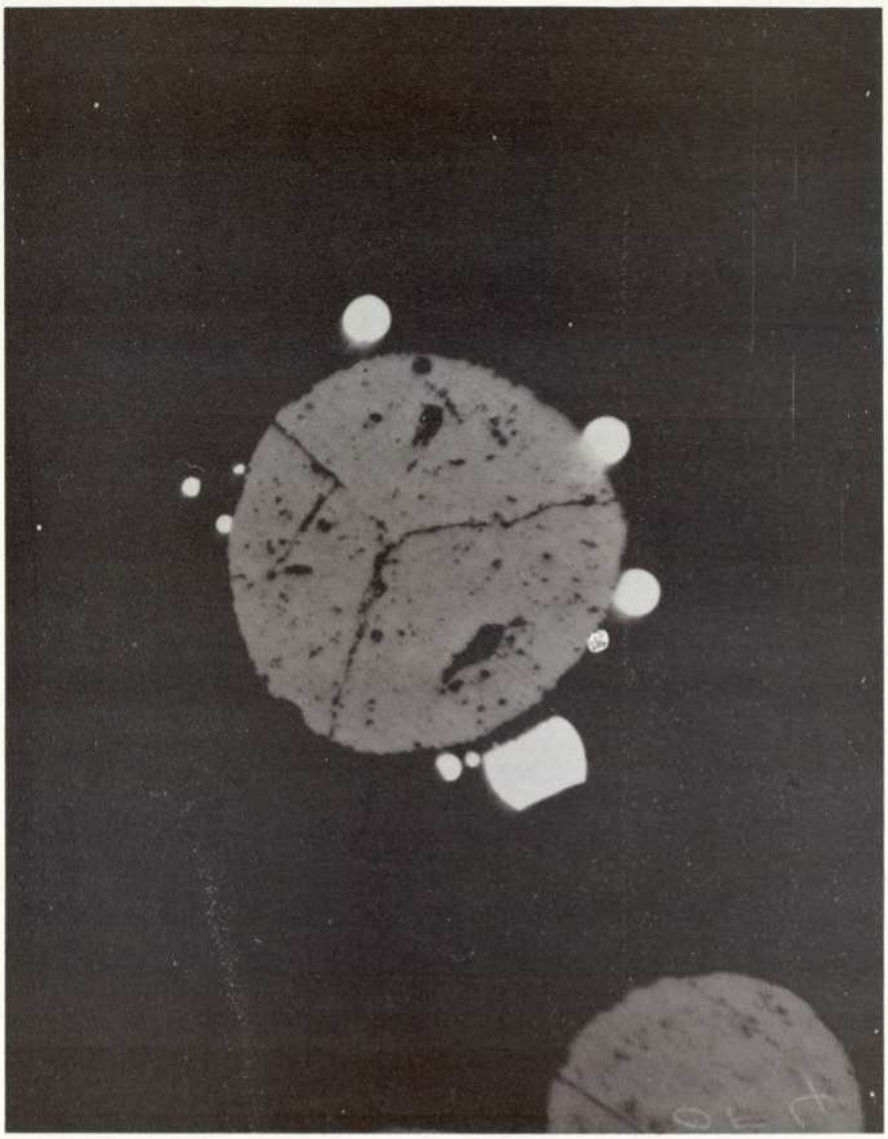
AERE - M 1508 Fig. 4 The "Cog Wheel" Effect. x 500
Copper deposit on UO_2 after 5 hrs. vacuum anneal at 750°C.



AERE - M 1508 Fig. 5 x 1000
Detail of Cu deposit on UO_2.



AERE - M 1508 Fig. 6 x 500
Ag deposit on UO_2 after 5 hrs. vacuum anneal at 800°C.



AERE - M 1508 Fig. 7 x 500

Exaggerated "Cog Wheel" effect shown by 8% P/Ni deposit on UO_2 after 5 hrs. vacuum anneal at 1000°C.

> the Eastern hemisphere, the unit is the tex, which is the mass in grams of 1000 metres. All other units are technically obsolete, but it will be a very long time before they go completely out of use. Thus the denier is still widely used".

Again, in the above definition, the density of the material is not mentioned. For easy reference, units used at present are given in Table 20.

It will be of interest to try to evaluate from a quoted number of deniers, the diameter of the PAN precursor used in the manufacture of carbon fibres. In a recent review Bailey and Clarke,[6] (1970), give for PAN precursor a density of 1.15 kg/m^3 and a fibre diameter of 14μm, for a material of $1\frac{1}{2}$ denier per filament, with 10,000 filaments per tow.

Now from $W = \rho V$, we have

$$1.5 = 1.15 \times \frac{22}{7} \times 9000 \times 100 \times \frac{D^2}{4}$$

assuming 9000 metres of PAN weighs 1.5 gms. Hence

$$D^2 = \frac{1.5 \times 7 \times 4}{1.15 \times 22 \times 9000 \times 100}$$

and $D = 9.054 \times 10^{-4}$μm or roughly 9 microns, which does not tally with their quoted value of 14μm for fibre diameter!

From these remarks it is obvious that the use of the system of fibre classification, incorporating the denier, cannot be used, in a meaningful way, by those outside the textile industry, unless both the material and its density are specified correctly, as a matter of course.

TABLE 20

Fibre Classification

Direct, (mass per unit length)			
Name	Unit of mass	Unit of length	Value = 20 tex
denier	gram	9000 metres	180
drex	"	10000 metres	200
(Western hemisphere)		(the International denier)	
poumer	pound	10^6 yds	40.3
-	grain	100 yds	28.2
-	"	120 yds	33.9
tex			
(Eastern hemisphere)	gram	1000 metres	20
Indirect (length per unit mass)			
American run	ounce	100 yds	15.5
Cotton	pound	840 yds (hand)	29.5
Linen	"	300 yds (lea)	82.7
metric	kg	1000 metres	50
typp	pound	1000 yds	24.8
Worsted	pound	560 yds	44.3

REFERENCES - APPENDIX 2

1. The Shorter Oxford English Dictionary, 3rd ed., 1964.

2. Chambers Technical Dictionary, 3rd ed., 1967.

3. Encyclopaedia Brittanica, Vol. 20, 666b, 1964.

4. Thorpe's Dictionary of Applied Chemistry, 4th ed., 1956.

5. A Dictionary of Scientific Units, Jerrard, H.G. and McNeill, D.B., 2nd ed., 1964.

6. Bailey, J.E., and Clarke, A.J., Chemistry in Britain, Vol. 6, No. 11, pp 484, Nov. 1970.

APPENDIX 2

Calibration of Instron universal Testing machine

APPENDIX 2

Calibration of Instron Universal Testing Machine

Apart from the daily load cell test recommended by the makers, the Instron must be calibrated to allow for slackness in the cross-head screws, bowing of beams under stress, load cell error, jaw errors and other variables. Also because the machine reacts to a different degree with different materials, of variable geometry, it's characteristics must be determined before a long run of any new type of test piece. Needless to say, any correction factor obtained on calibration would only be specific to the machine under test.

As an example of this general machine slackness, the Young's modulus of a $\frac{1}{2}$" diameter mild steel bar, when tested on the Instron used for carbon fibre work, gave from the slope of the curve on the chart, a value of 9.785×10^6 psi, about a factor of 3 less than the value of 27×10^6 psi, quoted for this material.

To calibrate for the "softness factor" of the machine, by the method of Goggin[1], (1969), sets of six lengths of tungsten rod were cut for each gauge length tested, from 1-10 inches. Tungsten rod of 0.040" diameter, having a cross-sectional area of 0.001 sq. ins. approximately equal to the integrated cross-sectional area of a carbon fibre tow, was used because tungsten has a similar elongation to fracture as has carbon fibre, (4-8% compared with 1%). These rods were mounted and pulled at a cross-head speed of 0.005"/minute, with a chart speed of one inch a minute, to a full scale deflection, (F.S.D.), of 100 lbs. Now true extension of tungsten is

$$\frac{\text{Load} \times l}{A \times E} \qquad \ldots (73)$$

where l = gauge length

A = cross-sectional area

E = Young's modulus

Calibration of Instron Tensile Testing Machine. 1st Stage.

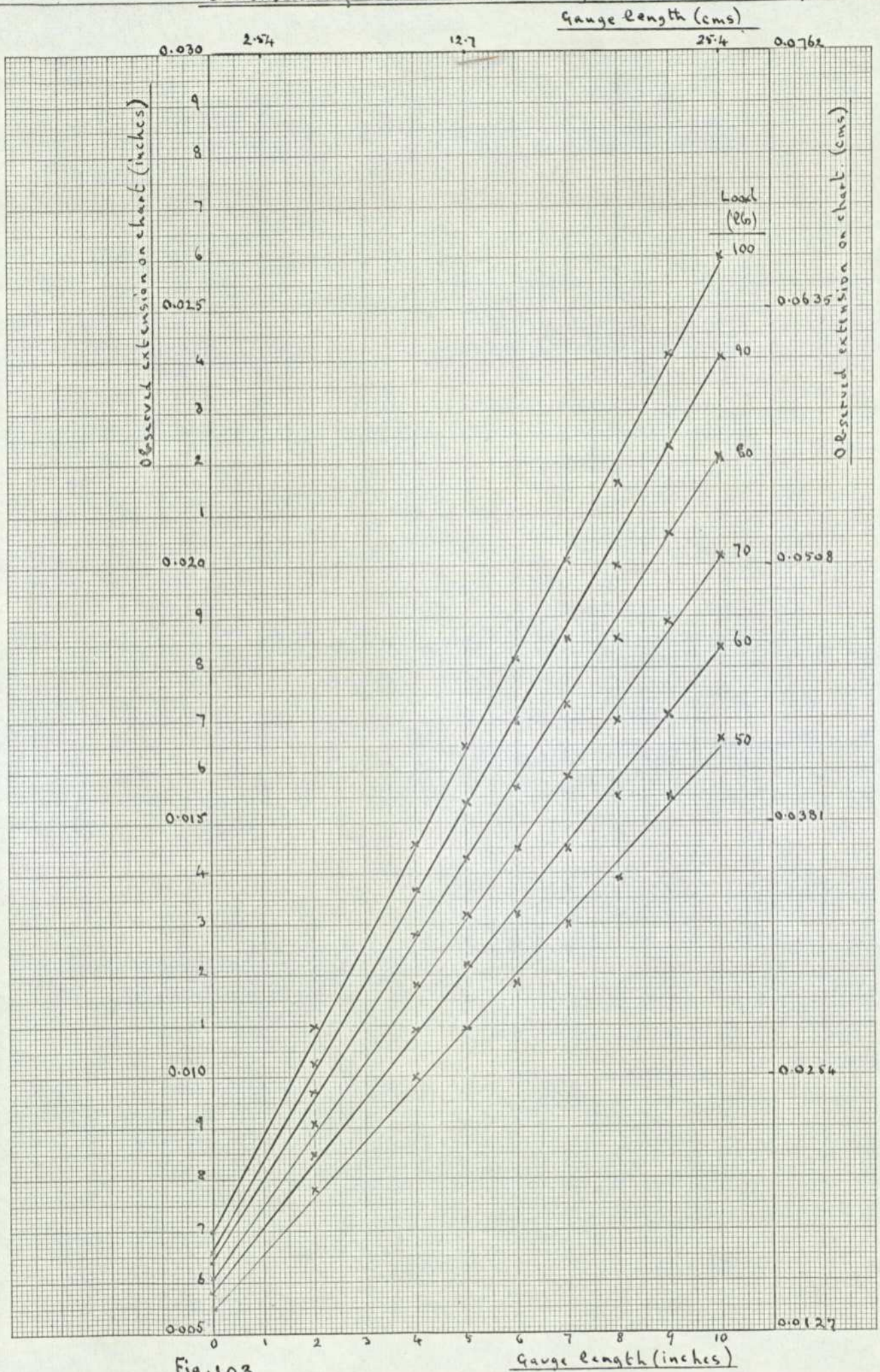


Fig. 103

Calibration of Instron Tensile Testing Machine 2nd Stage

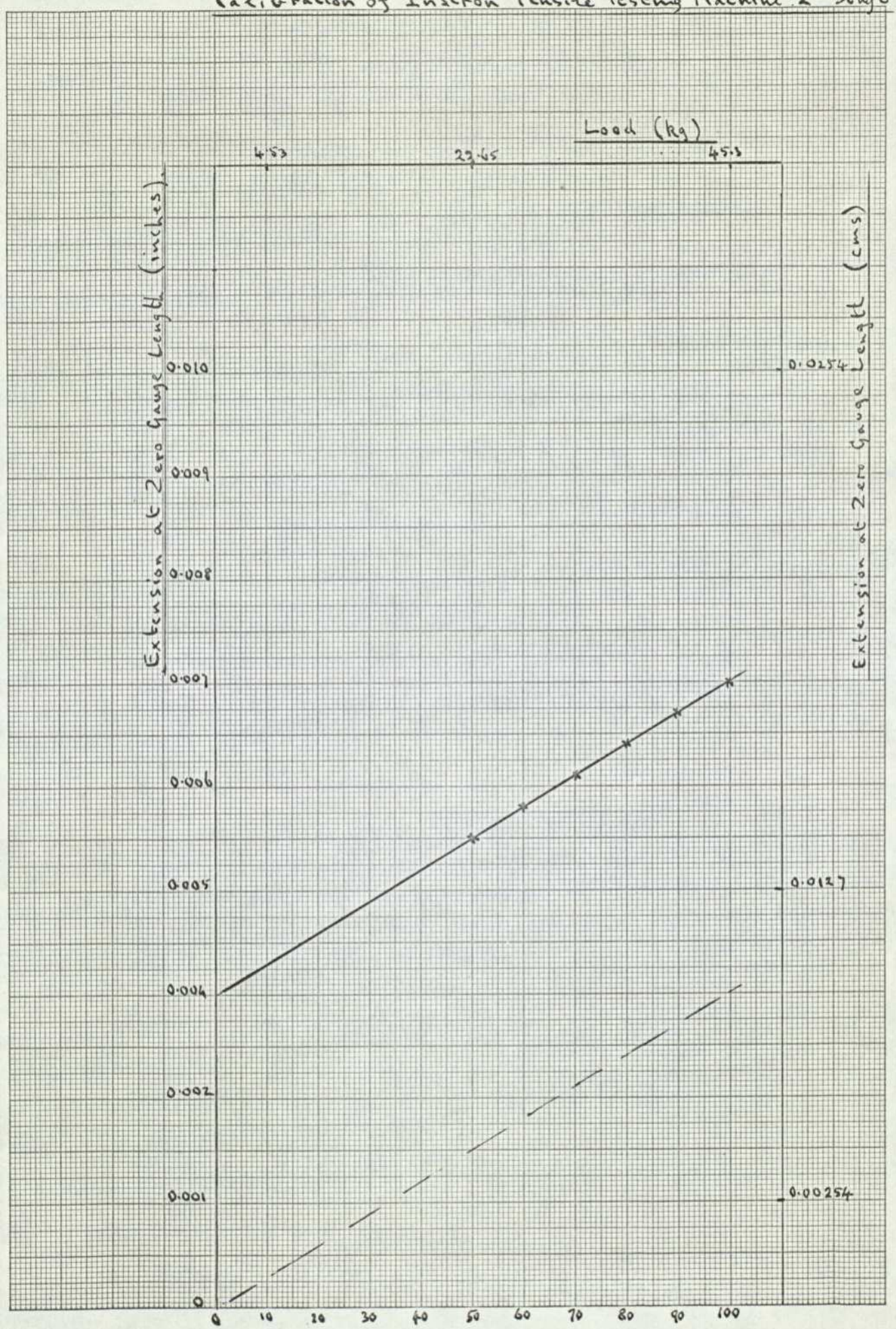


Fig. 104

The observed extension on the chart is

$$\frac{\text{Load} \times l}{A \times E} + \text{S.F.M.} \times \text{Load} \qquad \ldots (74)$$

where S.F.M. = "softness factor" of machine

= general slackness factor +

load cell error + etc.

Since Young's modulus for tungsten is the same whatever the gauge length, A is constant, l is known and Load, (F), is known, we have

Observed extension = const. x l + const. F

which is of the form $y = mx + c$.

Thus if we plot the observed extension, on the chart, against gauge length, as in Fig. 103, for each 10 lb. increase in load, we can, from the plot, measure the observed extension for each 10 lb. load, at zero gauge length. Then plotting observed extension, when l = 0, against load we have, as in Fig. 104, a line whose slope is "m" the S.F.M. or "softness factor" of the machine, since:

Observed extension on chart = S.F.M. x Load,

at zero gauge length ... (75)

The curve does not pass through the origin because of load cell error, etc.

From Fig. 104 we have, at zero gauge length, an observed extension of:

0.003" per 100 lb. load

$\therefore$ correction of extension for the machine

$$mF = \frac{0.003}{100} \times 100 = 0.003"$$

This, in inches of chart movement is

$$\frac{0.003}{0.005} \equiv 0.6" \text{ plus a load}$$

cell error etc., of 0.004" $\equiv$ 0.80" of chart movement, making a total deduction of 1.40" from chart length δl.

Table 21

Calibration of Instron

Nominal Gauge length (inches)	Gauge length corrected for jaw chamfer (inches)	Young's modulus, E, x 10^6 psi
2	2.24	50.8
3	3.24	43.3
4	4.24	47.4
5	5.24	46.7
6	6.24	46.8
7	7.24	46.2
8	8.24	47.2
9	9.24	46.4
10	10.24	44.6
		Mean Value:
		46.1

The calculated values of the Young's modulus for tungsten, using the total machine correction factor of 1.40", together with the 0.24" increased gauge length to accommodate the jaw chamfer correction, as mentioned in Section 4.2, are given in Table 21. The mean value, 46.1 x 10^6 psi is on the low side but an experimental check on the density of tungsten rod employed gave approximately 85% of theoretical and hence:

$$E = \frac{46.1}{100} \times 115 \times 10^6$$

$$= 53.0 \times 10^6 \text{ psi}$$

This agrees well with Northcott's[2] (1961), value for tungsten of E = 52 x 10^6 psi, and so the Instron can be calibrated in the manner described, to correct for "softness factor", to give an accurate value for the modulus of a material.

This correction factor will, however, be applicable to rigid systems, having a similar geometry.

In the case of plated carbon fibre tows, in addition to the machine "slackness factor" we have each tow with a different degree of slackness in the bundle, therefore a direct comparison of the observed slope of many runs with the value of E, calculated from the "law of mixtures", must be made to arrive at a mean S.F.M. Fig. 105 shows a typical run and here AB = δl = 2.6 inches is the observed chart movement for a load of 94 lbs. and BC is the combined carbon fibre tow slackness, S.F.M. and load cell error, etc.

It can be seen that if the curve of the test in Fig. 105, had been from a poor quality plated tow, as in Fig. 106;

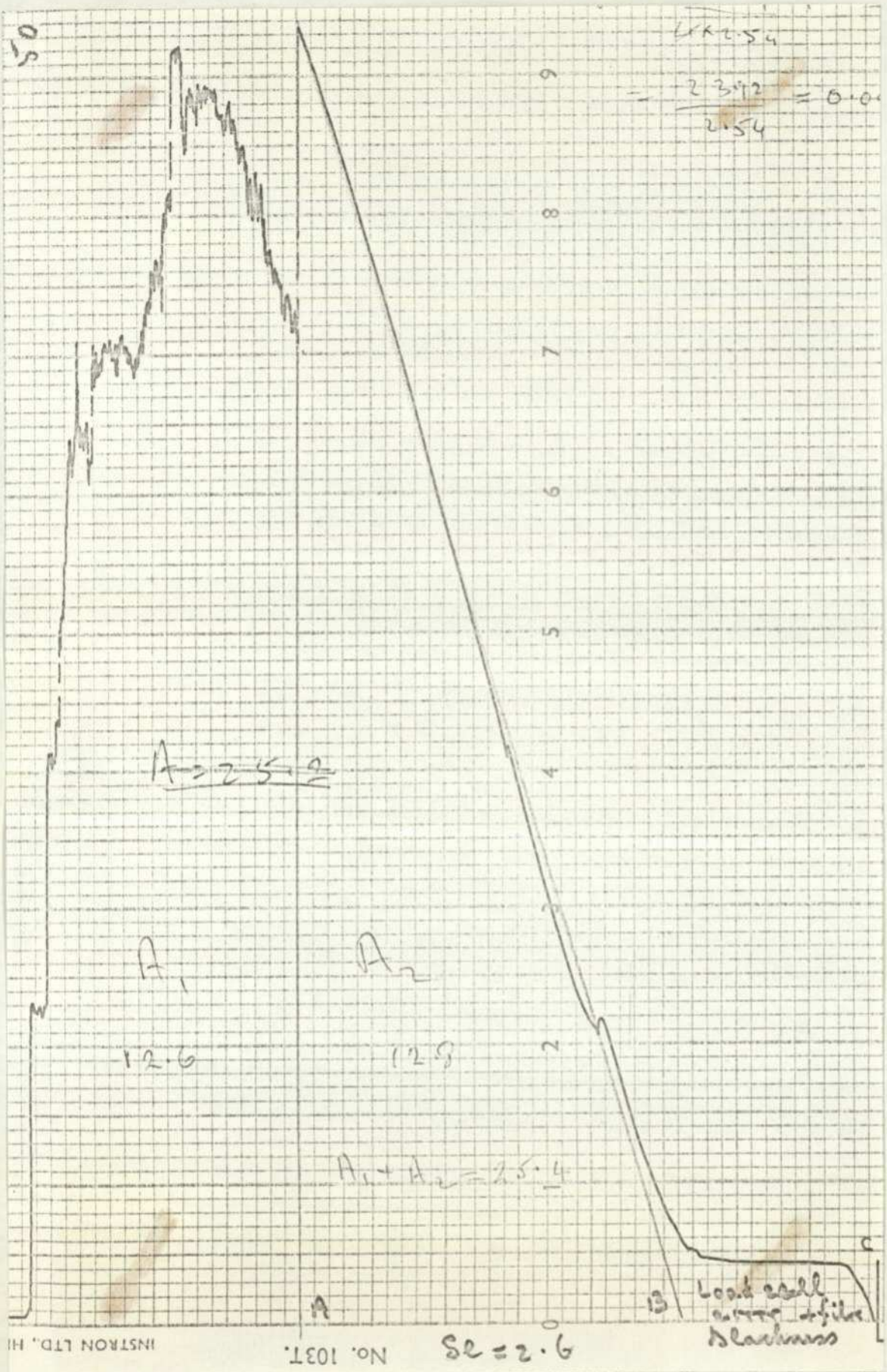


Fig. 105. Instron calibration for fibre tows.

Table 22

Instron and Copper Plated Carbon Fibre Tow

slackness calibration

Run	Temperature °C	Volume fraction	δl (inches)	E Observed	E, law of mixtures	$\frac{E(\text{Mixtures})}{E(\text{observed})}$
202	20	0.44	3.30	2.79	26.3	9.43
207	30	0.51	5.48	2.39	27.6	11.55
211	"	0.39	3.80	2.65	25.4	9.60
212	"	0.26	3.20	2.21	23.2	10.51
218	40	0.37	3.90	2.41	25.1	10.40
219	"	0.35	3.50	2.54	24.8	9.90
220	"	0.34	3.30	2.63	24.6	9.35
221	"	0.24	2.80	2.30	22.9	9.94
222	"	0.24	3.05	2.05	23.0	11.00
223	"	0.23	3.90	1.49	22.8	15.30
236	45	0.24	2.80	2.15	22.9	10.40
237	"	0.22	3.00	1.84	22.5	12.30
239	"	0.21	2.40	2.28	22.5	9.80
		Mean of $\frac{E(\text{mixtures})}{E(\text{observed})}$ = 10.60				

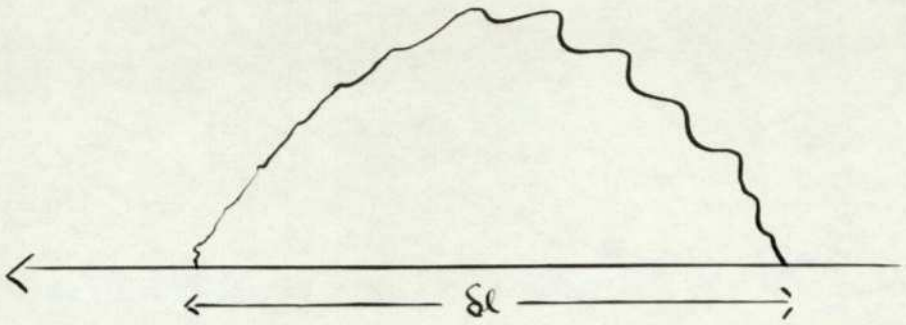


Fig. 106. Diagram of poor quality tow test result

no evaluation of the slope could be made and any direct correction of δl, as made in tungsten runs, would be meaningless. Table 22 gives the tensile results of a series of plated carbon fibre tows.

From the calculated mean value of the difference between the observed and "law of mixtures" values of E, the calculation of the tensile strength of the plated carbon fibre tow, by the method given in Chapter 4.

$$\sigma = \sqrt{\frac{2A_x E_{(Cu+f)} R_{(Cu+f)}}{Wl}} \qquad \ldots (35)$$

gives too high a value, since $E_{(Cu+f)}$ is the "law of mixtures" value which must be adjusted, by means of the slackness factor 10.6 to suit the other data in the equation.

Thus the observed tensile strength would be

$$\sigma_{obs} = \frac{\sigma}{\sqrt{10.6}} = \frac{\sigma}{3.256} \qquad \ldots (76)$$

REFERENCES - APPENDIX 2

1. Goggin, P.R., Private Communication, 1969.

2. Northcott, L., Papers on Fe, Nb, Ta, Mo and W. Conference at Sheffield, Ed. Quarrell, A.G., Elsevier, 1961.

APPENDIX 3

X-Ray Diffraction Techniques



AERE - M 1508 Fig. 1 x 1000
Cuboid inclusion in UO_2.

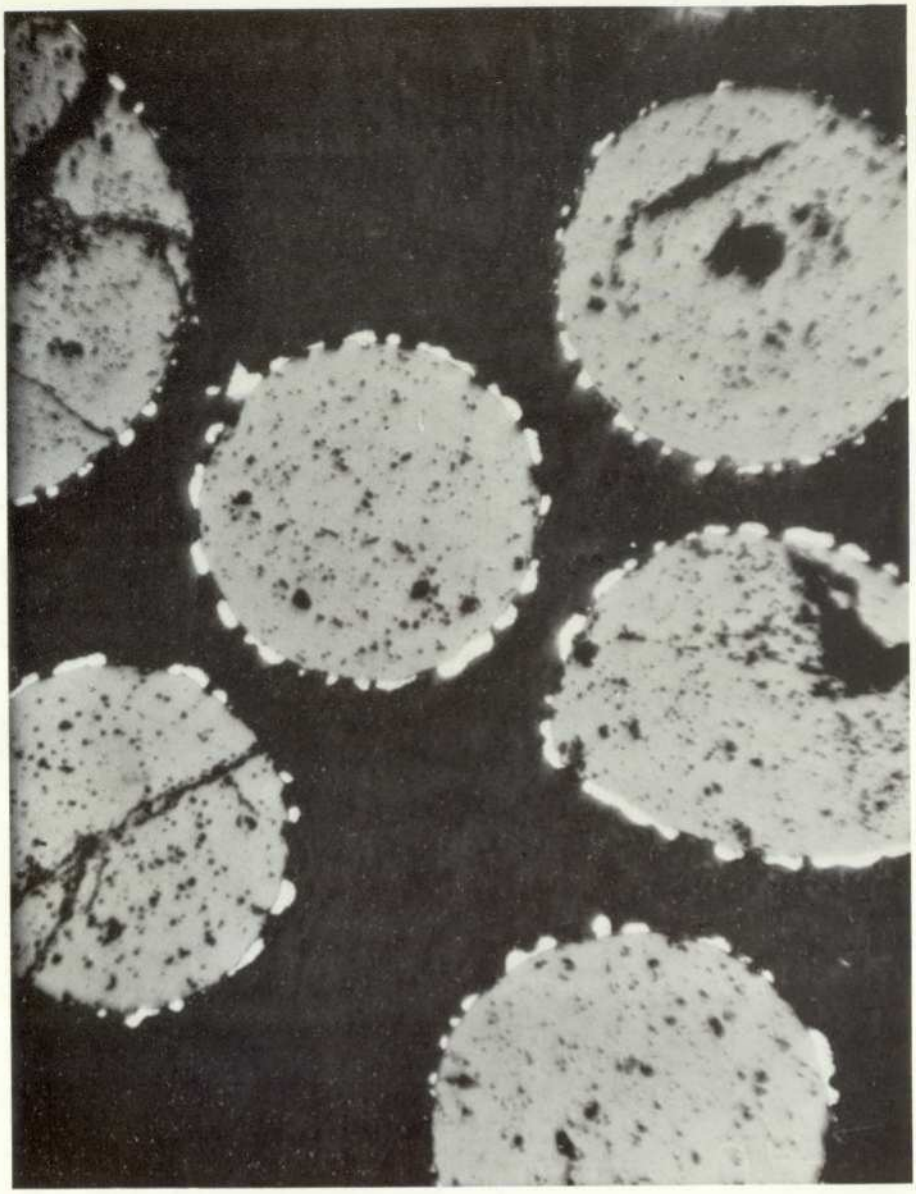


AERE - M 1508 Fig. 2 x 500
Powdery Cu deposit, from Rochelle salt solution, on UO_2 sphere.

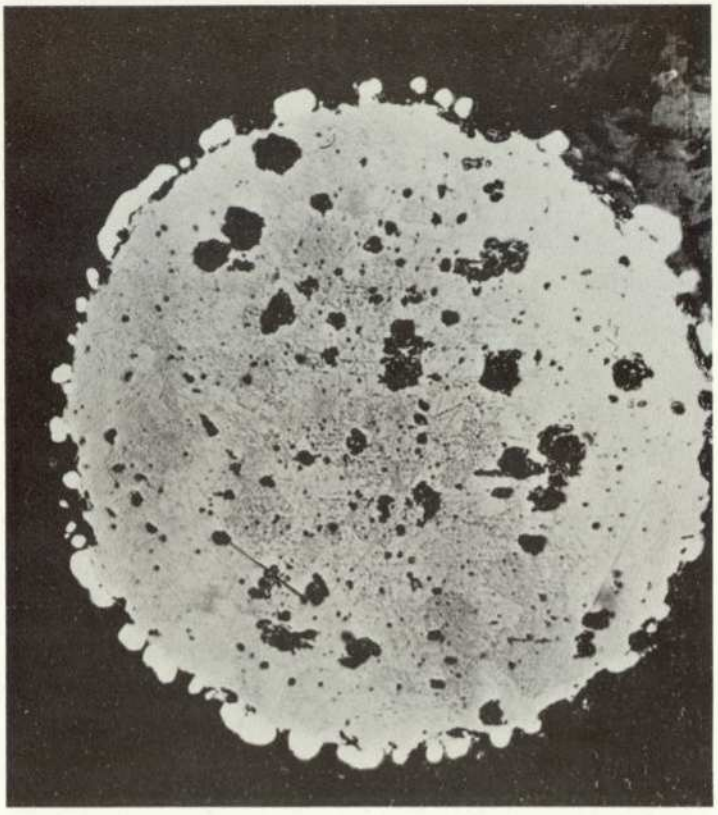


AERE - M 1508 Fig. 3 x 500

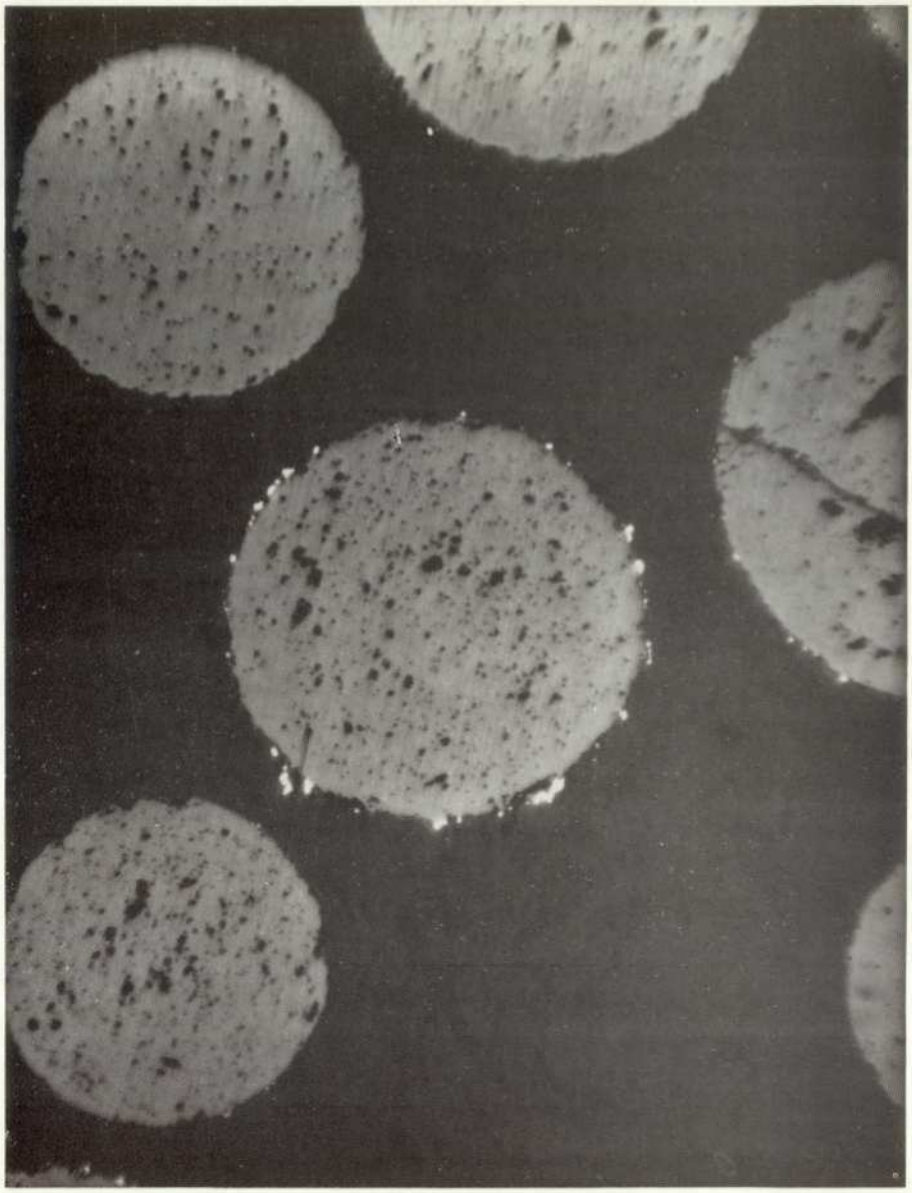
Electroless 8% phosphorus/nickel, deposit from acid solution, on UO_2 spheres.



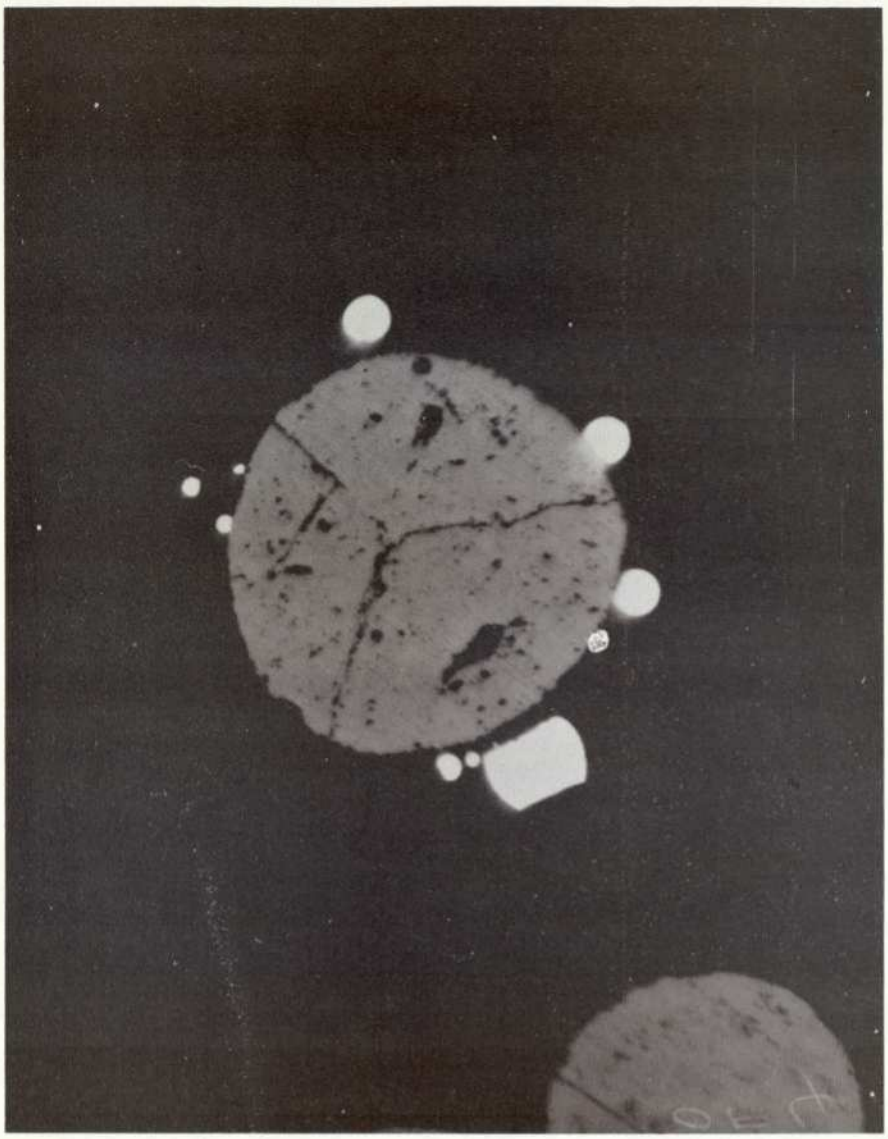
AERE - M 1508 Fig. 4 The "Cog Wheel" Effect. x 500
Copper deposit on UO_2 after 5 hrs. vacuum anneal at 750°C.



AERE - M 1508 Fig. 5 x 1000
Detail of Cu deposit on UO_2.



AERE - M 1508 Fig. 6 x 500
Ag deposit on UO_2 after 5 hrs. vacuum anneal at 800°C.



AERE - M 1508 Fig. 7 x 500

Exaggerated "Cog Wheel" effect shown by 8% P/Ni deposit on UO_2 after 5 hrs. vacuum anneal at 1000°C.